PURIFICATION OF PROGENITOR PHOTORECEPTORS DERIVED FROM THE DIRECTED DIFFERENTIATION OF HUMAN PLURIPOTENT STEM CELLS

A Thesis Presented to University College London in Candidacy for the Degree of

Doctor of Engineering

by

Benjamin David Weil (MRes, MEng Hons.)

September 2016

The Advanced Centre for Biochemical Engineering

Department of Biochemical Engineering

University College London

Statement of Originality

I, Benjamin David Weil, confirm that the work presented in this thesis is my own. Where information has been derived from other sources or through a collaborative means, I confirm that this has been indicated in the thesis.

Print: Ben Weil

Date: September 2016

In memory of Christine Weil

Abstract

Cell therapy has the potential to treat a wide variety of unmet therapeutic indications that affect a growing number of people globally. Many of these therapies require purification steps to separate specific cell types from heterogeneous populations. This thesis investigates current affinity purification platforms to isolate human pluripotent stem cell-derived progenitor photoreceptors for the treatment of retinal dystrophies, and introduces a novel purification technology which possess bioprocessing and clinical advantages over current techniques.

Successful production of progenitors was achieved using both induced pluripotent stem cells (iPSC) and human embryonic stem cells (hESC). By controlling the cell aggregation step and other iterative improvements to the retinal differentiation, 35.7% of cells generated expressed Cone-Rod Homeobox (CRX)-positive – a key marker to define progenitor photoreceptors. The critical performance metrics of fluorescent-activated cell sorting (FACS) and magnetic-activated cell sorting (MACS) were then derived through experimentation. Sort purity, progenitor yield and viable cell recovery of CD73-positive cell populations – a surface marker shown to co-express with CRX - were measured, and demonstrated that high purity separations above 90% were attained. However, both methods suffered from low cell recoveries with over 30 or 40% of cells (for FACS and MACS respectively) lost through the numerous processing steps involved in labelling cells with either a fluorescent or paramagnetic tag, washing and sorting samples. Cell labelling also leaves the product with a bound cellular label, complicating additional processing and potentially causing toxic clinical affects.

A novel purification technology was assessed with SpheriTech affinity beads that possess bioprocess and clinical advantages over current purification methods. Cells are unmodified through isolation, with the positively selected cell type remaining label-free after processing. Consequently, cells experience minimal process steps so the time, risk, cost burden of purification and cell loss is reduced. Comparable purity with all separations was observed, however progenitor yield was noted to be lower with SpheriTech affinity beads than for FACS and MACS. To assess the impact different purification technologies have upon the complete

bioprocess in an iPSC-derived therapy, an economic cost-modelling tool was created. By inputting experimentally-derived data into an integrated model, the cost of goods (COG) per dose was evaluated when using each of the three affinity purification methods. FACS was found to be economically favourable only at small production scales due to throughout limitations, with MACS presenting the most cost effective technology at all other scales. However, if progenitor yield could be increased to improve process yields through further process development, SpheriTech would compete with MACS across all scales tested.

Acknowledgements

To everyone in microfluidics who helped me hugely. Prof Nicolas Szita, Ya-Yu, Nikolay, Rys, Pia and Anand. To Sam Ranasinghe and his multiphoton confocal training, and the team at the Rockefeller for their microscopy help. Thank you to Beattie for her help with the Mastersizer.

I want to thank Krisztina Kovacs-Schreine for her help with the Akta – I forgot to acknowledge her in my 1st year presentation, never again.

A huge thank you to Jamie Evans and especially Tomas Adejumo for their patience in teaching my flow cytometry and FACS. To Dr Lara Bogart who gave so much of her precious time to help me, and also Richard Jackson at the Royal Institution. To Mark Turmaine for his SEM help.

Of just as significant note, thank you to everyone who has helped me stay sane and on course the past few years from a non-academic standpoint. Stefan, James and Rubi to name a small handful.

Finally, I want to thank Prof Mark Lowdell for his support and understanding during my thesis write-up, and everyone else at the Royal Free for all the small and not-so-small things you have done to help me.

Table of contents

Table of figures

Chapter 4

Chapter 5

Chapter 6

Chapter 7

List of tables

Chapter 1

Chapter 2

Chapter 3

Chapter 5

Chapter 6

Chapter 7

List of acronyms

AAV - adeno-associated virus

ACLSCT - autologous cultured limbal stem cells transplantation

ADP - adenosine monophosphate

AMD - age-related macular degeneration

APS - average particle size

ASCAT - autologous stem cells in achilles tendinopathy

ATMP - advanced therapy medicinal products

bFGF - basic fibroblast growth factor

BMP - bone morphogenetic protein

CAR - chimeric antigen receptor

CD - cluster of differentiation

CMFDA - 5-chloromethylfluorescein diacetate

CNS - central nervous system

COG - cost of goods

CRX - cone-rod homeobox

CV - coefficient of variation

DAPI - 4',6-diamidino-2-phenylindole

DAPT - N-[N-(3,5-difluorophenacetyl)-L-alanyl]-S-phenylglycine t-butyl ester

DPBS - Dulbecco's phosphate-buffered saline

D.P.C. - days post coitum

DCM - dichloromethane

Dkk-1 - dickkopf -1

DMEM - dulbecco's modified eagle medium

DNA - deoxyribonucleic acid

DPBS - dulbecco's phosphate-buffered saline

EB - embryoid body

EBA - expanded bed chromatography

EDCI - 1-Ethyl-3-(3-dimethylaminopropyl)carbodiimide

EDTA - ethylenediaminetetraacetic acid

EM - electron microscopy

EMA - european medicines agency

EMEM - eagle's minimal essential medium

ESC - embryonic stem cell

FACS - fluorescent activated cell sorting

GFP - green fluorescent protein

GPI - glycosylphosphatidylinositol

GvHD - graft versus host disease

HCL - hydrochloric acid

hESC - human embryonic stem cells

hESCRPE - human Embryonic Stem Cell Derived Retinal Pigmented Epithelial

hFGF2 - human fibroblast growth factor 2

HLA - human leukocyte antigen

ICM - inner cell masses

IGF-1 - insulin-like growth factor-1

iPSC - induced pluripotent stem cells

ISCT - international society for cellular therapy

IVF - in vitro fertilisation

KLF4 - Kruppel-like factor 4

KOSR - knockout serum replacement

MACS - magnetic activated cell sorting

MEF - mouse embryonic fibroblast

MHC - major histocompatibility complex

MHRA - medicines & healthcare products regulatory agency

MRI - magnetic resonance imaging

MSC - mesenchymal stem/stromal cells

NEAA - non-essential amino acids

NHS - n-hydroxysulfosuccinimide

NMM - n-methylmorpholine

NRL - neural retina leucine zipper

NT5E - ecto-5'-nucleotidase

OCT - optimal cutting temperature

Oct4 - octamer-binding transcription factor 4

ONL - outer nuclear layer

OTX2 - orthodenticle homeobox 2

PAX - paired box 6

PBS - phosphate-buffered saline

PFA - paraformaldehyde

PMMA - poly(methyl methacrylate)

qPCR - quantitative polymerase chain reaction

RA - retinoic acid

rd1 - retinal degeneration 1

RFU - relative fluorescence units

RNA - ribonucleic acid

ROCK - rho kinase inhibiter

ROI - region of interest

RP - retinitis pigmentosa

RPE - retinal pigment epithelium

RPM - revolutions per minute

s - second

SCID - severe combined immunodeficiency

SD - standard deviation

SEM - scanning electron microscope

Shh - sonic hedgehog

SMD - stargardt's macular dystrophy

SOX2 - (sex determining region Y)-box 2

SSEA1 - stage-specific embryonic antigen 1

SSEA4 - stage-specific embryonic antigen 4

SQUID - superconducting quantum interference device

STR - stirred tank reactor

T/E - trypsin/EDTA

T3 - triiodo-l-thyronine

TRA - tumour-recognition antigens

UCL - university college london

VBA - visual basic for applications

zFGF2 - recombinant zebrafish Fibroblast growth factor 2

Chapter 1: Introduction

1.1 Thesis Overview

This thesis is centred on the purification of specific cell populations that are indistinguishable by physical means. The principle aim was to develop a new technology to overcome many of the technical challenges associated with current state-of-the-art affinity purifications techniques. A secondary aim was to assess the economic impact such a technology could make compared with the current gold standards.

In order to accomplish this, a study was carried out to separate progenitor photoreceptors, derived from human pluripotent stem cells, for the treatment of photoreceptor dystrophies. Purification was critically evaluated for purity, progenitor yield and viable cell recovery. Using the experimental data generated, an economic appraisal was carried out. A novel affinity separation with SpheriTech beads was then examined due to the numerous technical benefits offered.

1.2 Cell therapy

Cell therapy encompasses any treatment involving living cells, independent of the mode of action or indication. Therapies can range from cell transplantation (e.g. Hemacord by New York Blood Center, Inc) to bioaesthetic applications (e.g. LaViv by Fibrocell Technologies) or tissue regeneration (e.g. Carticel by Genzyme). An annual global revenue over 7 billion USD is estimated, with new companies and translational research rapidly creating an expanding, lucrative field (Mason *et al.*, 2012).

Although the majority of commercially approved products use somatic cells, stem cell-derived therapies are currently dominant in clinical development, with a move towards more ambitious indications such as cardiovascular, neuro-regenerative or autoimmune diseases (Webster, 2011). A few clinical trials of interest in the UK are:

- The phase I/II multicentre trial involving the transplantation of human Embryonic Stem Cell-Derived Retinal Pigmented Epithelial (hESCRPE) cells for Stargardt's Macular Dystrophy (SMD) (NCT01469832) by Ocata Therapeutics;

- the phase II clinical trial Autologous Stem Cells in Achilles Tendinopathy (ASCAT) (NCT02064062), run by University College London (UCL) using autologous, ex vivo expanded mesenchymal stem/stromal cells (MSCs) to promote healing;

- the phase I trial involving implantation of human Embryonic Stem Cell (hESC)-derived Retinal Pigment Epithelium (RPE) cells for patients with acute wet Age-related Macular Degeneration (AMD) (NCT01691261), sponsored by Pfizer in collaboration with UCL.

The regulatory landscape for Advanced Therapy Medicinal Products (ATMPs) - which comprise of gene therapy, somatic cell and tissue-engineering products - has changed dramatically over the past decade. Regulation instigated by the European Medicines Agency (EMA) for ATMPs has resulted in biological products being governed by pharmaceutical legislation. As a result, cell therapy regulation in the UK must now comply to both the Medicines & Healthcare products Regulatory Agency (MHRA) and EMA, which presents a significant burden.

The first EMA approved stem cell-based (ATMPs), Holoclar by Holostem Advanced Therapies, has now received a conditional marketing authorisation for the treatment of limbal stem cell deficiency with autologous cultured limbal stem cell transplantation (ACLSCT) (EMEA/H/C/002450/0000). Prochymal by Osiris Therapeutics, now TEMCELL by Mesoblast, has also been approved as an 'off-the-shelf' stem cell treatment of graft versus host disease (GvHD) in Japan.

1.3 Cell purification

Due to the increasing demand and development of new cell therapies across a wide range of indications, one of the major challenges facing the industry is the translation of therapies to meet commercial manufacture scales and regulatory demands, while reducing production costs.

Currently, cell purification is mostly conducted by crude apheresis devices, with the removal of contaminants largely addressed by upfront validation of cGMP materials, reagents and

consumables (Weil and Veraitch, 2014). However, although many clinical trials have shown very promising safety data with no adverse effects and negligible toxicity after administration (Lalu *et al.*, 2012), stem cell products have suffered from a limited efficacy and lack of understanding regarding the underlying mechanisms of actions. One such example of limited efficacy is MultiStem by Athersys, a treatment for stroke which failed to show significant improvement against their phase II placebo control group (Athersys Inc., 2015). Similar efficacious concerns have been noted across other stem cell and chimeric antigen receptor (CAR)-T cell therapies (Mastri, Lin and Lee, 2014; Chen *et al.*, 2015; Sommermeyer *et al.*, 2015; Oh *et al.*, 2016; Wang *et al.*, 2016).

In part, the lack of statistically relevant efficacy data in the clinic has been due to a lack of characterisation and definition of the cellular product. There is a need for tighter selection criteria in clinical trials (Harrop *et al.*, 2012), and with increasing numbers of cell therapies reaching this stage, a stricter product definition to fulfil more demanding ATMP regulation is expected (Weil and Veraitch, 2014).

However, there is still a lack of consensus over an optimal strategy for a scalable purification platform. As such, attention given to the identification and isolation of target cells for therapeutics is rapidly increasing. Technical improvements must be made to increase the efficiency of clinical cell sorting (Bersenev, 2016).

1.4 Affinity purification

Cell purification is critical, not only for selecting the correct, efficacious target population, but also to remove unwanted and potentially dangerous impurities. For this, affinity purification is the gold standard technique (Wognum and Eaves, 2003; Wobus and Boheler, 2005). Many therapies such as the engraftment of CD34-positive cells for cancer (Boccaccio, 1999; Richel *et al.*, 2000; Siena *et al.*, 2000; Vogel *et al.*, 2000), the isolation of antigen-specific B cells (Kodituwakku *et al.*, 2003), TCR-engineered T cells or CD3 (T-lymphocyte) depletion (Dykes *et al.*, 2007; Govers *et al.*, 2012) for peripheral blood progenitor cell (PBPC) transplantation use an affinity purification step.

There has been a lot of attention lately given to CAR-T immunotherapies, with many large pharmaceutical companies striking up partnerships to target cancers: Novartis and the University of Pennsylvania (Schuster *et al.*, 2015), Merck and Intrexon (Intrexon Corporation 2015), Juno with AstraZeneca and Celgene (Lawrence, 2016), Kite and Amgen (Amgen, 2015) as well as Pfizer and Cellectis (Pfizer, 2014). Following the crude separation of an apheresis product, these bioprocesses all involve affinity purification steps to isolate T-cells which can then be modified, expanded and infused into a patient.

However, cell enrichment and depletion is particularly important for the purification of stem cell-derived therapies, where the target cell population is separated from a very heterogeneous culture with potentially tumourigeneic cells present. Although to date only one study from transplanted stem cell-derived material has shown the induction of a tumour, the potential for teratoma formation is still a serious safety concern and increases the purification burden significantly (Arnhold *et al.*, 2004).

1.4.1 Antibody-dependent purification

Affinity purification is an immunoseparation technique that uses the specificity of antibody selection to identify and bind 'tissue specific' cells. Novel experimental methods to characterise cells, such as using microarrays to test thousands of different samples at once, have simplified the search for genetic markers to define specific cell types. There are currently over 400 surface molecules, or clusters of differentiation (CD), that characterise the structure and function of cells (Clark *et al.*, 2016). These have benefited antibody-dependent purification techniques by enabling specific CD molecules to be targeted that can identify, and sort target cell populations.

Fluorescent-Activated Cell Sorting (FACS) is the most establish affinity purification technology, with functional studies dating back to the 1970s (Bonner *et al.*, 1972; Julius, Masuda and Herzenberg, 1972). For clinical affinity purification, Magnetic-Activated Cell Sorting (MACS) is the gold standard technique, with CliniMACS by Miltenyi Biotec being the system of choice.

Both FACS and MACS rely on the identification of target cells by attaching a cellular label; FACS uses a fluorescent tag, whilst MACS uses paramagnetic nanobeads. Once the target

cells have been labelled, they can be separated into an alternative fluidic path (with FACS), or retained within a magnetic field if paramagnetic microbeads are bound (with MACS). No removal of fluorophores or nanobeads is possible after the purification step.

1.4.2 Limitations of current technology

Current affinity purification techniques possess several technical challenges to their use in cell therapies. For FACS, fluorescent-bound material could impact vision after the transplantation; especially in postmitotic cells. The configuration of aseptic FACS instruments for clinical use may also require further development (Jayasinghe *et al.*, 2006). Extensive cleaning of the fluidics to validate the process and prevent sample contamination is necessary, as well as complications with aerosol generation and potential contamination during the instrument's setup (Mcintyre, Flyg and Fong, 2010).

In regard to MACS, nanobeads can be internalised by cells (Chen *et al.*, 2011; Bannunah *et al.*, 2014) and produce cytotoxic effects that inhibit cell growth (Singh and Nalwa, 2007) or detrimentally alter cell morphology (Neubert *et al.*, 2015). Optimal uptake into non-phagocytic cells was observed at nanoparticle diameters of 50nm, which corresponds exactly to the size of MACS beads (Kettler *et al.*, 2014). Iron, also present in MACS beads, has the potential to contribute to retinal degeneration through the generation of hydroxyl free radicals (He *et al.*, 2007).

Many studies have demonstrated that exposure to nanoparticles can lead to translocation through the lungs towards the kidneys, liver, spleen and brain (Oberdörster, 2001; Nemmar *et al.*, 2002; Borm and Kreyling, 2004; Semmler *et al.*, 2004; Elder and Oberdörster, 2006; L'azou *et al.*, 2008). However, nanoparticle toxicity through drug delivery, such as with cell transplantation, has received less attention.

Thus, the retention of cellular labels limit the use of FACS and MACS for clinical applications, and as a result, highlight the need for novel development within the field. The bioprocess, technical, and economic considerations of FACS and MACS purification will be evaluated in

more depth in this thesis. Additionally, a novel affinity method will be assessed using SpheriTech's macro-polymer beads that leave no cellular label after purification.

1.5 SpheriTech beads

SpheriTech is a small laboratory and consultancy company who specialise in polymers, particle design and chromatography. Their proprietary products revolve around the properties of poly-Ɛ-lysine to create different polymer structures; from hydrogels in contact lenses (Gallagher *et al.*, 2016) to biocatalysis and regenerative medicine fields. Antibody immobilised SpheriTech beads could provide a label-free, high resolution affinity purification method which is economically competitive and very favourable in a clinical setting.

1.5.1 Poly-Ɛ-lysine

Poly-Ɛ-lysine is a naturally occurring polyamine chain which comprises of a lysine amino acid bound between the carboxyl and epsilon amino group. The polymer has anti-microbial properties (Hyldgaard *et al.*, 2014), is biodegradable and metabolises into all naturally occurring amino acids. Manufacture is conducted by large scale Streptomyces bacterial fermentation due to its use as a food preservative, and as a result, is commercially available with a ready supply at minimal cost (Shima and Sakai, 1977).

Poly-Ɛ-lysine can be cross-linked by an aliphatic compound, such as an amino acid or peptide, to form insoluble polymeric supports. Polymeric supports are used in a variety of chemical and physical processes which require substrate interaction, such as chromatography (Liang, Svec and Fréchet, 1995), cell culture scaffolds (Dhandayuthapani *et al.*, 2011), biocatalysis (Gandini, 2010) and solid phase extraction (Majors, 2008). Cross-linking amide bonds allow the creation of polymer structures such as sheets, fibres or particles. Depending on the cross-linker used and the level of cross-linking desired, the physical and chemical reactivity of the final polymer can be controlled. For example, a high level of cross-linked bonds will yield a rigid, macroporous material; fewer cross-links will increase elasticity, allowing microporous structures while keeping amine functionality high.

1.5.2 Polymer beads

Macro-polymer beads have a wide range of applications across many industries, from water treatment to being mixed with Ammonium Nitrate Fuel Oil (ANFO) for explosive mining. In the biopharmaceutical and biotechnology industry, polymer beads are often used as the stationary phase in chromatography purification--predominantly made from cross-linked polystyrene. For other purification applications, the material, bead diameter and characteristics vary considerably depending on the manufacturer (Table 6.1).

Table 1.1 *Composition and features of macrobeads found within the biotechnology and cell therapy industry*

Company	Material	Size (µm)	Buoyancy	Magnetism	Application
Bangs Laboratories, Inc.	PS-/PMMA	0.02-200	X	X	Affinity binding systems
Iontosorb	Cellulose	30-100	X	✓	Protein
Spherotech	Polysytrene	<13	X	✓	Cell separation
Advanced BioMatrix	Collagen	100-400	X	X	Suspension culture
GE Healthcare	Agarose	100-300	X	X	Capture step in viscous feeds
CellCap	Polymer	50-200	X	✓	Cell separation
Sterogene	Agarose	20-1000	X	X	Protein
Qiagen	Agarose	20-70	X	✓	Protein
GE	Polymer	200-500	X	X	Cell separation

Healthcare					
Fresenius Hemocare	Polyacrylamide	120-180	X	X	Cell separation
Bio-World	Alginate	100-500	X	✓	Cell/enzyme immobilisation
Cube Biotech	Agarose	300-500	X	X	Protein

1.5.3 Affinity beads

Affinity bead purification systems work through the irreversible attachment of proteins or antibodies to the surface of beads. Immobilised beads can then be incubated with heterogeneous populations, and permit only target cells expressing a specific surface molecule to bind. Due to the high specificity of antibodies, precise sub-populations of cells can be targeted that otherwise possess similar physiological properties such as cell size, density, surface charge or structure.

Once target cells are bound to beads, several physical characteristics can be exploited to capture the beads, whilst eluting unbound cellular impurities. SpheriTech beads are manufactured to contain iron oxide which, similar to MACS beads, enables manipulation in a magnetic field. Due to their size, a significantly lower magnetic field strength if required for the capture of SpheriTech beads. This simplifies process scale up by dramatically increasing the distance beads can be held from a magnetic source, whilst still inducing paramagnetism.

Alternatively, due to the physical dimensions of SpheriTech beads, bead capture could occur through the physical constraint of beads while allowing unbound material to be eluted. Through the addition of hollow microballoons during manufacture, the density of beads can also be altered. By controlling the buoyancy and paramagnetic characteristics of beads, different purification systems could be developed in order to find optimal conditions for cell binding.

Unlike MACS and FACS, after the positive selection of target cells, the mechanism to identify and isolate target cells can then be detached. Cells can be detached from macro-polymer beads by altering the pH (Bryan *et al.*, 2013), osmolality, or by enzymatic dissociation, leaving the cellular product free from any label or tag.

The following body of work will focus on affinity purification to target precise sub-populations of cells. To evaluate the impact FACS, MACS and SpheriTech beads have, a suitable bioprocess must be chosen. The requirements were:

a) A process requiring isolation of a rare sub-type cell population via affinity purification.
b) A therapeutic indication with unmet need that can highlight the clinical advantages and limitations of purification technologies.
c) A bioprocess that has shown preliminary success, but requires further technical improvement for clinical translation.

These requirements were met by the production of progenitor photoreceptors, derived from the directed differentiation of human pluripotent stem cells for the treatment of photoreceptor dystrophies.

1.6 Photoreceptors dystrophies

1.6.1 Photoreceptors

Once fully developed, the mammalian retina is comprised of 55 individual cell types which enable the processing of visual information (Masland, 2001). Photoreceptors are specified neuronal cells which convert light into electrical impulses via a process known as phototransduction (Hubbell and Bownds, 1979). They are derived through the ectoderm lineage and are located in the outer nuclear layer (ONL) of the retina.

Photoreceptors comprise of three classes: rods, cones and (more recently discovered) photosensitive ganglion cells. Cones are located within the macula, concentrated inside the

fovea, and allow the perception of trichromatic colour. Around 4.6 million cones are present here, with a density of 200,000 cones per mm (O'Brien, Schulte and Hendrickson, 2003). Rod cells are less sensitive to colour, but instead provide motion detection and sight in scotopic conditions. They outnumber cones at a ratio of 20:1 and are located across most of the retina to improve peripheral vision (Sugita, Suzuki and Tasaki, 1989). The third class of photoreceptors, recently discovered within ganglion cells, was found to mediate circadian rhythms of day/night cycles, control the pupil's response to light and regulate melatonin levels (Berson, Dunn and Takao, 2002).

1.6.2 Photoreceptor dystrophies

Retinal dystrophies incorporate a wide range of disorders affecting photoreceptors (i.e. photoreceptor dystrophies) and/or RPE cells (Ruether and Kellner, 1998). Late stages of these diseases usually result in visual impairment or blindness through photoreceptor malfunction or degeneration. Inherited autosomal dominant mutations are a common cause (Churchill *et al.*, 2013) that prevent the translation of integral proteins for phototransduction, metabolism or photoreceptor structural development (Valle, Erkkilä and Raitta, 1981). One such genetic degradation has been noted within the cone-rod homeobox (CRX) gene, which results in cone-rod dystrophy (Freund *et al.*, 1997).

CRX is a photoreceptor-specific transcription factor that has been linked to several retinal diseases (Chen *et al.*, 1997), however, many separate genetic sites have been associated with photoreceptor dystrophies and more are being discovered regularly (Retina International, 2014). The most prevalent group of inherited retinal disease is Retinitis Pigmentosa (RP), linked to mutations in over 250 genes with around 4500 different causative mutations, most with unknown inheritance methods (Haim, 2008; Sorrentino *et al.*, 2016).

1.6.3 Current treatment for Retinitis Pigmentosa

RP is characterised by the progressive apoptosis of rod photoreceptors leading to the early onset of night blindness, then degeneration of the visual field (Van Soest *et al.*, 1999). One in every 4000 people worldwide are affected (Bundey and Crews, 1984).

There is no current cure or treatment for RP and other associated photoreceptor dystrophies, only attempts to slow progression of the disease. Retinyl palmitate (synthetic vitamin A) has shown some potential to slow retinal degeneration, but teratogenic effects are possible in pregnant women and long term intake will increase the risk of osteoporosis (Fahim, Daiger and Weleber, 1993). Alternatively, preserving photoreceptors by administering growth factors direct to the eye by injection (LaVail *et al.*, 1998), gene therapy (Liang *et al.*, 2001; Sanftner *et al.*, 2001) or by transplantation of cells which produce retinal growth factors (Keegan *et al.*, 2003; Lawrence *et al.*, 2004) have also been trialled, but with limited success.

Although significant improvements have been made regarding diagnosis, treatments that slow, halt, or restore vision are required. RP has been shown to have a significant effect on mobility, leading to suffers being five times more likely to have a mobility incident than normal sighted subjects (Geruschat, Turano and Stahl, 1998). To estimate the annual patient cost of RP upon healthcare services in the United States, retrospective claims of 2990 patients were examined with regard to hospital admissions, inpatient and outpatient visits, prescription and other medical costs. Patients with RP had significantly higher health care expenditure, totalling to more than $7000 per patient per year higher than non-RP counterparts (Frick *et al.*, 2012). Consequently, a 'cure' would have a significant impact both financially, and to patient quality of life.

1.7 Photoreceptor transplantation

The replacement of photoreceptors is a challenging, but necessary prospect for the restoration of visual acuity. Due to the irreversible loss of connectivity between neurons, transplantation of healthy photoreceptors is one of few options for regeneration.

1.7.1 Process development

A pioneering study by Gouras et al. transplanted photoreceptors from neonatal transgenic mice into the sub-retinal space of (2 to 3 month old) retinal degeneration (rd) mice mutants (Gouras *et al.*, 1992). Transplanted cells were shown to survive effectively for 9 months after surgery, without rejection or initiating any immune response (Gouras *et al.*, 1994). By transplanting high

enough numbers of cells, sufficient integration into the host retina was noted to perform a simple light-dark discrimination test (Kwan, Wang and Lund, 1999).

The next significant development occurred in a study by MacLaren et al., which demonstrated that donor cells, taken during peak rod genesis (Young, 1985), integrate into an adult or degenerating retina to form functional, subcortical synaptic connections - effectively restoring vision (MacLaren *et al.*, 2006). The post-mitotic, rod progenitor photoreceptors for transplantation were defined by expression of the transcription factor neural retina leucine zipper (NRL). They were genetically tagged with green fluorescent protein (GFP)(Akimoto *et al.*, 2006) which allowed NRL-positive cells to be purified, transplanted, and then tracked within a donor retina. These findings defined a population of non-proliferating cells, which had the potential to integrate into the ONL of damaged retinas, and mature into functional photoreceptors. However, as low integration efficiencies of cells were still observed, defining the 'regenerative' population that restore vision may still require stricter characterisation (West *et al.*, 2012).

1.7.2 Surface marker

Affinity purification has become a core step in many therapies across a wide range of cell types and indications, owing to its ability to identify and sort specific cell types from heterogeneous populations. Progenitor photoreceptors, however, have predominantly been characterised by the transcription factor CRX (Furukawa, Morrow and Cepko, 1997; O'Brien, Schulte and Hendrickson, 2003; Jomary and Jones, 2008) or NRL (Rehemtulla *et al.*, 1996; Mitton *et al.*, 2000). Both intracellular markers have been used for cell sorting in a research setting by genetically modifying a cell line to co-express a fluorescent protein with CRX (Decembrini *et al.*, 2014) or NRL (MacLaren *et al.*, 2006). For a clinical setting, genetically altering a patient's progenitor cells to fluoresce is impractical and adds significant cost and regulatory complication to the bioprocess. Consequently, a surface antigen is needed to identify progenitor photoreceptors. The surface antigen CD73 has shown initial success to differentially identify NRL/CRX-positive cells from other cellular impurities (Koso *et al.*, 2009). Furthermore, CD73-

enriched heterogeneous populations have shown increased integration and photoreceptor formation following transplantations into damaged retinas (Eberle *et al.*, 2011).

This thesis will forward these studies with CD73, and validate it as an antigen for cell sorting across different affinity purification technologies.

1.8 Pluripotent cell source

A critical problem with transplantation is finding an appropriate cell source. For pre-clinical work, progenitor photoreceptors were derived from postnatal day 1 cells, however a corresponding human equivalent would involve retinal cells from second-trimester foetuses. Given the prohibitive ethical and supply limitations, this is not feasible for clinical development.

As a result, alternative sources of cells have been tested. Potential sources include the induction of photoreceptors from adult retinal cells (Akagi *et al.*, 2004; Jomary and Jones, 2008), iris tissue (Haruta *et al.*, 2001) adult neural retina (MacNeil *et al.*, 2007; Kokkinopoulos *et al.*, 2008), or by deriving photoreceptors from human pluripotent stem cells.

Pluripotent cells possess the capacity to form derivatives of all three embryonic germ layers, and can proliferate indefinitely with asymmetric cell division (i.e. producing two daughter cells which have independent cellular fates) (Evans and Kaufman, 1981; Amit *et al.*, 2000). They are characterised to assess karyotypic normality, expression of cell surface antigens relating to pluripotency (van den Engh, Trask and Visser, 1981) and the capacity for spontaneous differentiation to form endoderm, mesoderm and ectoderm germ layers (Thomson and Marshall, 1998). A more complete characterisation, however, includes transplanting cells into an early stage embryo to permit the formation of a teratoma which can retrospectively be studied and trace to the cell line (Wobus *et al.*, 1984).

1.8.1 Embryonic stem cells

Embryonic stem cell development dates back to the 1960/70s, when embryonic carcinoma cells from germ line tumours, teratocaricomas (Stevens, 1967), were cultured as cell lines (Kahan

and Ephrussi, 1970; Jakob *et al.*, 1973). The first isolation of embryonic pluripotent stem cell lines were from the inner cell masses (ICM) of mouse blastocysts in 1981 (Martin, 1981). However, a characterised human line was not created until 1998 by Thomson et al. (Thomson *et al.,* 1998).

hESC are derived from ethically approved surplus in vitro fertilised embryos, originally donated for in vitro fertilisation (IVF) treatment. The ICM is isolated from the blastocyst and co-cultured with mouse embryonic fibroblasts (MEFs) (Thomson *et al.*, 1998). These mouse cells are referred to as "feeders" due to the mix of growth factors and proteins they naturally provide embryonic stem cells to maintain pluripotency. However, conditioned medias now exist which eliminate the need for feeders, preventing the risk of cross-contamination (Xu *et al.*, 2001). Additionally, several improvements have been made since this initial derivation method, creating cGMP cell lines (Crook *et al.*, 2007) and deriving hESC without destruction of the embryo (Chung *et al.*, 2008).

Embryonic stem cells provide an allogeneic stem cell source, meaning they have the capacity to treat many patients from a single embryo (Gearhart *et al.*, 1998). Using a pluripotent stem cell source permits progenitor photoreceptors to be manufactured without the limitation of donor material. After more than three decades of research into pluripotent cells, clinical products are now being tested with promising phase I/II safety data (ClinicalTrials.gov identifiers: NCT01344993, NCT01345006, NCT01469832, NCT01625559, NCT01674829, NCT01691261 and NCT02286089). It is important to note that no immunological responses have been observed, suggesting immunosuppression may not be required for hESC-derived graft survival (Hambright *et al.*, 2012).

However, hESC remain an ethically controversial source of stem cells (McLaren, 2001). Informed consent is required for any donation involving clinical or research purposes, however, with the potential for immortal stem cell lines to be derived, providing information regarding the intended uses of donated material is complicated. Scientific advancement often presents new avenues of research previously unpredicted, so ensuring the donor is 'informed' can be a challenge.

1.8.2 Induced pluripotent stem cells

Due to recent technical and biological advances in understanding the molecular pathways involved in pluripotency, it is now possible to reprogramme somatic (adult) cells into possessing pluripotent characteristics. Induced pluripotent stem cells (iPSCs) were first created by transfecting a combination of four transcription factors, required for pluripotency (see Table 1.1), with a retroviral vector. This was performed in three independent studies using adult human fibroblasts that were reprogrammed to create human iPSCs (Takahashi *et al.*, 2007; Yu *et al.*, 2007; Park *et al.*, 2008).

Table 1.2 Transcription factors involved in creation of the first iPSC cell lines (Takahashi et al., 2007; Yu et al., 2007; Park et al., 2008).

Study	Transcription Factors
Takahashi et al.	Oct-4, SOX2, KLF4, c-Myc
Yu et al.	Oct-4, SOX2, NANOG, LIN28
Park et al.	Oct-4, SOX2, KLF4, Myc

iPSCs possess analogous features of pluripotency to hESC. They express the same panel of surface 'stem cell' markers, proliferate indefinitely with asymmetric cell division, can form all three embryonic germ layers in vitro and form teratomas upon transplantation into immunocompromised donors (Yu *et al.*, 2007; Park *et al.*, 2008). The full extent of their similarity/differences, however, is still very limited, as is the impact of different reprogramming methods (Feng *et al.*, 2010). Variable yields of iPSC-derived mouse neuronal cells have been observed (Hu *et al.*, 2010), although this is likely due to differences in the potency of reprogramming murine fibroblasts (Boland *et al.*, 2009; Kang *et al.*, 2009; Zhao *et al.*, 2009). Premature senescence (Feng *et al.*, 2010) and some residual epigenetic memory of original cell type has also been noted (Kim *et al.*, 2010). Importantly, both hESCs and iPSCs have been used to derive retinal cells which are capable of transmitting action potentials (Riazifar *et al.*, 2014), providing an alternative to progenitor photoreceptor donation. Additionally, comparative

transplantations of hESC and iPSC-derived cells for retinal dystrophies have shown survival, migration and integration of cells to produce a functional response to light stimuli (Riera *et al.*, 2016).

As with hESC, the derivation of iPSC lines has seen improvements too. The use of retroviral transduction to reprogramme cells, as used in the initial creation of cells lines, may result in the addition of transgenes leading to oncogenesis (Cattoglio *et al.*, 2007). Consequently, other gene delivery systems have been developed without viral vectors that are more clinically friendly. This was first accomplished in mouse iPSC using two plasmids, one with c-Myc cDNA and one with Oct-4, SOX2 and KLF4, which do not integrate viral genes into the host genome (Okita *et al.*, 2008). Although this technique suffers from a low reprogramming efficiency, more recent developments with plasmids (Si-Tayeb *et al.*, 2010) or adeno-associated virus (AAV) vectors (Zhou and Freed, 2009; Khan *et al.*, 2010) have shown greater success. Additionally, novel iPSC technology now exists that relies on the delivery of proteins, rather than transcription factors, for reprogramming (Kim *et al.*, 2009). This mitigates the risk from DNA transfection, as well as potentially mutagenic molecules or viral involvement.

The tumourigenicity of transplanted iPSC-derived RPE has been examined in mice (N=65), and no tumours found during 15 months of monitoring (Kanemura *et al.*, 2014). This suggests negligible tumourigenic potential, and indicates preliminary longer-term safety. cGMP compliant iPSC lines are also now available, permitting clinical-grade patient-specific clones (Ohmine *et al.*, 2011).

Unlike hESC, iPSC could present a 'personalised' medicine with autologous therapies. This means donor tissue can be biopsied from a patient, reprogrammed and expanded in vitro, before transplantation back into the same patient. Although this approach still presents major logistical and financial complications, the possibility of immune rejection and GvHD is greatly diminished in comparison to allogeneic material. However, it is also possible to generate an iPSC bank for human leukocyte antigen (HLA)-matched transplantation. HLA genes help the immune system to distinguish between foreign pathogens and the body's own tissue; known as the major histocompatibility complex (MHC) for non-human species. By matching HLA types for

transplantation, allograft rejection can be greatly decreased (Taylor and Dyer, 1995). Although there are more than 200 genes which permit a huge variation in genotypes, by carefully selecting individuals with homozygous HLA types, the number of donors required to create a cell bank capable of treating a high proportion of the populous is significantly minimised (Taylor *et al.*, 2005). By selecting 150 HLA-typed volunteers, it is predicted an iPSC bank could be generated which could treat 93% of the UK's population (Taylor *et al.*, 2012), greatly increasing the therapeutic potential.

Beyond their capacity as a pluripotent cell source, iPSCs have been used to increase our understanding of the causation and response to different drugs for retinal diseases. A drug screening platform has been created from RP patient-derived iPSCs, that enables cells to be genetically manipulated to explore the role of specific mutations and find novel therapeutic approaches (Jin *et al.*, 2012; Yoshida *et al.*, 2014). From genomic screening, it is possible to learn more about RP pathogenesis (Welsbie *et al.*, 2013), as well as conduct high throughput drug or small molecule experiments to optimise retinal differentiation or find novel disease pathways (Ferrer *et al.*, 2014).

1.9 Retinal differentiation

Differentiation is the process of cells developing into a more specialised cell type. Pluripotent stem cells can spontaneously differentiate into all three germ layers, however it is also possible to control their differentiation towards a certain pathway or genetic lineage.

In vitro directed differentiation strategies usually aim to replicate the microenvironment in vivo through the addition of growth factors. As a result, it is important to understand how progenitor photoreceptors develop in foetal retinas.

1.9.1 In vivo ocular development

The formation of retinal tissue in embryo development is dependent upon the inhibition of two signalling pathways: the bone morphogenetic protein (BMP) and Wnt signalling pathways (Glinka *et al.*, 1998; Muñoz-Sanjuán and Brivanlou, 2002), which result in forebrain and frontal

eye fields. Two key antagonists, Noggin and Dickkopf-1 (Dkk-1), are involved in this. Noggin is an endogenous growth factor which inhibits the BMP pathway, whilst Dkk-1 is a secreted protein that antagonises the Wnt signalling pathway (Glinka *et al.*, 1998; Mukhopadhyay *et al.*, 2001).

Once the eye fields have been specified, the growth of mesodermal tissue leads to formation of an optic cup and lens vesicle (Pei and Rhodin, 1970). From this, the retina and associated epithelium, photoreceptors and neuro-ectodermal tissue will form (O'Rahilly, 1975; Beebe, 1986).

Several different protocols exist to differentiate hESC into retinal progenitors; all using related combinations of growth factors, but with different durations and outcomes (Lamba *et al.*, 2006; Osakada, Ikeda, *et al.*, 2009).

1.9.2 Lamba et al. protocol

The Lamba et al. protocol was the first published method to describe the generation of retinal progenitors through direct differentiation of hESC (Lamba *et al.*, 2006). The H-1 stem cell line (WiCell Research Institute, Inc.) was cultured on MEFS, before dissociating with collagenase to form cell aggregates, or embryoid bodies (EBs), in suspension for 3 days.

Many differentiation protocols use EBs to create concentration gradients through the different layers of dense aggregates, which forms heterogeneous cell populations (Van Winkle, Gates and Kallos, 2012). EBs have been used to assess pluripotency due to their potential generation of all three germ layers (Sheridan, Surampudi and Rao, 2012), as observed with the derivation of dopaminergic neurons – ectoderm (Chambers *et al.*, 2009), insulin-secreting pancreatic islet cells - endoderm (Lumelsky *et al.*, 2001) and cardiomyocytes - mesoderm (Xu *et al.*, 2002).

During aggregation, hESC were initially directed towards a retinal fate through the antagonistic growth factors Dkk-1, Noggin and IGF-1. Studies have shown Wnt or BMP antagonism produce neural tissues of the anterior central nervous system (CNS) (Itsykson *et al.*, 2005; Watanabe *et al.*, 2005), but IGF-1 appears to specifically direct cells towards a retinal progenitor identity (Lamba *et al.*, 2006).

On the fourth day, EBs were cultured adherently on poly-D-lysine/Matrigel coated plates, and the concentration of growth factors increased 10-fold for 21 days to expedite differentiation. Interestingly, after only 1 or 2 weeks, differentiation cultures begin to show neural retina characteristics of the optic cup.

After 3 weeks, up to 80% of cells were observed to express retinal progenitor markers, but only 12% of cells expressed CRX and 5% NRL. The directed differentiation was also validated using iPSC (iPSC-MHF2 c1 and c2) and multiple other hESC (Hues6, Hues14, Hues16, Mel1 and Mel2) lines (Lamba *et al.*, 2010).

1.9.3 Osakada et al. protocol

The Osakada et al. protocol defines an alternative method to induce photoreceptor differentiation (Osakada, Ikeda et al. 2009). hESC are dissociated to small clumps of around 5 to 10 cells, using an enzymatic bulk-passaging technique which selectively harvests stem cell colonies (Suemori *et al.*, 2006). hESC are then cultured for 21 days in suspension with Dkk-1 and Lefty-A. Lefty-A is an antagonist to the Nodal signalling pathway, also linked with early embryonic development (Sakuma *et al.*, 2002). Rho kinase inhibiter (ROCK), Y-27632, is added for the first 15 days to improve cell viability in suspension (Watanabe *et al.*, 2007).

Cell aggregates are then plated onto fibronectin, laminin and poly-D-lysine coated dishes. Around day 90, the media is treated with 100 nM retinoic acid (RA) and 100 M taurine. Both RA and taurine have been shown to promote rod genesis by activating NRL expression in serum-deprived cultures (Levine, Fuhrmann and Reh, 2000; Khanna *et al.*, 2006).

After 120 and 170 days, 11.3% and 19.6% of hESC-derived cells respectively were observed to express CRX (Osakada *et al.*, 2008). The protocol has since been validated in iPSC lines (201B6, 201B7 and 253G1)(Hirami *et al.*, 2009), and successfully replicated by an independent research group (Nistor *et al.*, 2010).

In addition, Osakada et al. reported an in vitro directed differentiation protocol using small-molecules instead of a dependence upon recombinant proteins (Osakada, Jin, *et al.*, 2009). hESC and iPSC-derived retinal progenitors were produced using the small molecules CKI-7 and

SB-431542 which block the Wnt and Nodal signalling pathways respectively. The use of small molecules provides a significant advantage over growth factors by minimising cross contamination through the removal of animal derived components, reduced batch-to-batch variability, and are much more economically feasible. Comparable efficiencies to Dkk-1 and Lefty-A induced retinal progenitors were noted with the xeno-free protocol (Osakada, Jin, *et al.*, 2009), however, overall differentiation efficiency may be impacted, as noted with the 170 day period to produce CRX-positive cells.

1.9.4 Mellough et al. protocol

The Mellough et al. protocol uses a three-step process for the directed differentiation of hESC (H9) and iPSC (hiPSC-NHDF) towards a photoreceptor fate (Mellough *et al.*, 2012). Pluripotent cultures were dissociated with collagenase and cultured in suspension supplemented with Noggin, Dkk-1, IFG-1, Lefty-A, human Sonic Hedgehog (Shh) and Triiodo-L-thyronine (t3) to form EBs for 30 days and trigger anterior neural specification. On day 30, the suspension culture is plated onto poly-L-ornithine and laminin coated plates for another 30 days of culture for retinal determination. Additional supplements are added at day 37 that commence the final step - photoreceptor maturation, which include RA, basic fibroblast growth factor (bFGF), T3 and Shh. The concentration of Noggin, Dkk-1 and IGF is increased by 10-fold, similar to the Lamba et al. protocol. During day 37 to 41, media was supplemented with human activing-A, shown to initiate rod photoreceptor differentiation in embryonic retinal cultures (Davis, Matzuk and Reh, 2000).

The combination of growth factors used to induce differentiation was derived through a combination of the two previously described protocols. The addition of Shh and T3 has been previously shown to promote retinal progenitor and cone photoreceptor induction in foetal development (Kelley, Turner and Reh, 1995). Peak CRX-expression was noted at day 45 with 16% of the cell population expressing CRX (Mellough *et al.*, 2012), however expression in iPSC-derived populations were very variable.

Importantly, Mellough et al. have shown that differentiation is segmented into three developmental stages. The initiation of the neuronal forebrain pathway, retinal determination

then photoreceptor maturation. By focussing on the production of progenitor photoreceptors, with this greater understanding of signalling pathways that affect cell fate, it may be possible to optimise the conditions for CRX-positive cell production.

1.10 Summary of retinal differentiation strategies

Pluripotent stem cells provide a theoretically limitless supply of cellular material for progenitor transplantation, however improvements must still be made to the differentiation efficiency and standardisation over culture length. Key developments have been made with the use of animal-free, small molecule components and by increased understanding of the signalling pathways involved. However, there is a high degree of variability within the differentiation harvest.

Detailing the three currently published retinal progenitor differentiation protocols highlights the heterogeneity found within processing, and within the final culture's composition. Although differentiation can be optimised, owing to this inherent variability, purification will be pivotal for the success of pluripotent stem cell-derived products. Translation will require greater characterisation over the target cellular product, along with technical advancements in purification techniques to separate these cells for safe transplantation.

For more information on cell transplantation strategies for retinal repair, several review papers have been published which encompass the field to date (West *et al.*, 2009; Jayakody *et al.*, 2015).

1.11 Overview of bioprocess

Although autologous cell transplantation of iPSC-derived progenitor photoreceptors still presents many technical challenges, it may well be technical feasible in the near future. Autologous transplantation of iPSC-derived cells has been demonstrated to repair damaged tissue (Hanna *et al.*, 2007), and genes can be successfully corrected in human iPSCs from patients with blood disorders (Simara, Motl and Kaufman, 2013). A recent clinical study has demonstrated that vision can be improved in a blind patient through stimulation of the outer

nuclear layer (Zrenner *et al.*, 2011), and neural retina and optic cup formation can be generated through human pluripotent cells (Nakano *et al.*, 2012).

The bioprocess examined here (as summarised in Figure 1.1) involves reprogramming of a patient biopsy to form iPSC, followed by expansion and differentiation in vitro (Cramer and MacLaren, 2013; Wright *et al.*, 2014). The regenerative photoreceptor population must then be purified to produce a final cellular product, capable of integrating and restoring vision in damaged retinas.
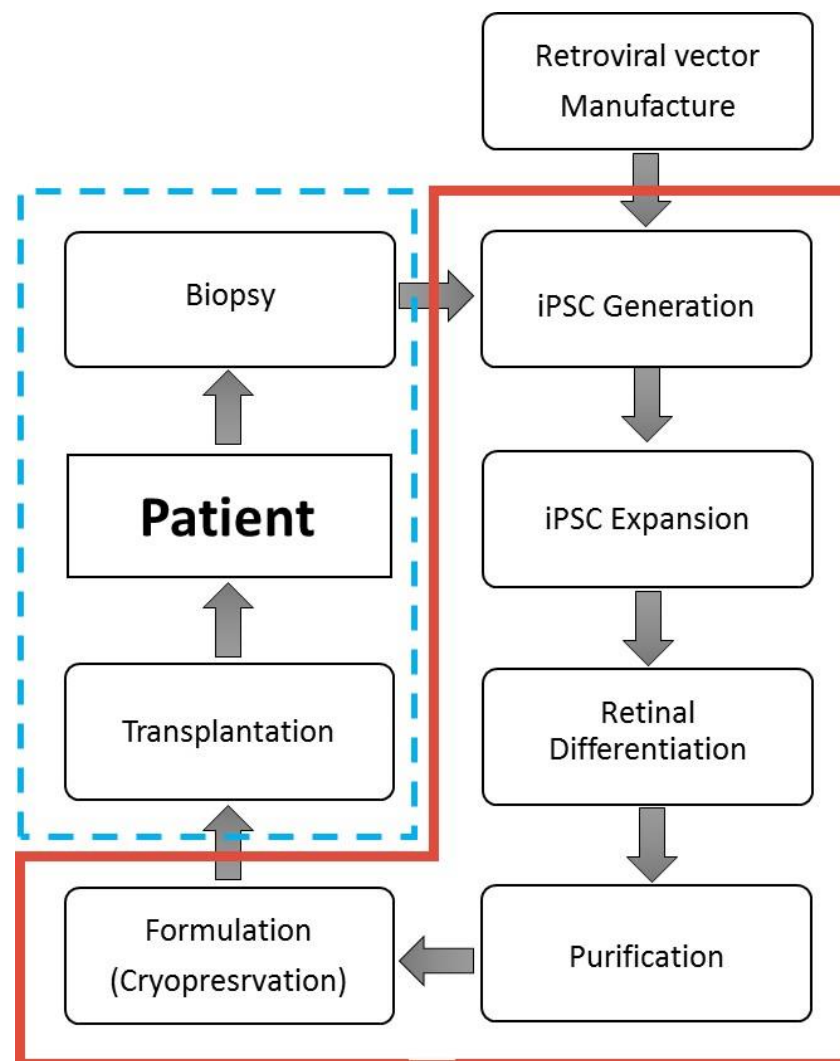
Figure 1.1 *Flow sheet for autologous iPSC-derived progenitor photoreceptor cell therapy for the treatment of retinal dystrophy. The red box indicates the bioprocess unit operations carried out at the site of manufacture; the dotted blue box indicates operations carried out at a hospital or clinic.*

1.12 Commercial significance

The development of novel purification technology is more important than ever with the increasing growth and demand for cell therapies. With the introduction of tighter ATMP legislation, regulation has become a bigger hurdle for translation, and purification presents a key factor for product safety and efficacy.

Affinity purification is used across a wide range of bioprocesses to positively separate specific cell sub-types and remove unwanted impurities. Currently, there are 113 clinical studies in progress treating 319 conditions across the United States and Europe; predominantly requiring haematopoietic progenitor cell enrichment (with T or B cell depletion) for the treatment of haematological malignancies (data collected from https://ClinicalTrials.gov on the 2nd of March 2016). All these therapies are dependent upon affinity purification techniques, demonstrating the growing demand for clinical translation.

Cell therapy as a therapeutic platform to treat retinal disease was chosen due to the rapid development towards clinically feasible products in this field. Progenitor photoreceptor transplantation still faces significant technical challenges, but presents an achievable goal to meet the therapeutic need (Zheng, Li and Tsang, 2015). This thesis will evaluate the technical, processing and economic characteristics of current affinity purification, allowing the requirement for a successful new commercial technology to be assessed.

1.13 Thesis hypothesis

There is a need for novel purification technology that delivers scalable, highly specific isolation of target cells, while operating with sufficient cell recovery and a cost per dose to be economically favourable due to current cell purification technology being insufficient to match the increasing technical and regulatory demands, the required scale of production, and economic pressure from the burgeoning field of cell therapy.

Chapter 2: Materials and methods

2.1 Cell culture

2.1.1 Isolation of mouse embryonic fibroblasts

Female mouse embryos 13 days post coitum (d.p.c.) were obtained and separated from the placenta using sterile tweezers. Surgical scissors were then used to cut the embryo sac and remove the brain and other organs, before the remaining embryo was minced and incubated (Sanyo, MC0-18AIC, Leicestershire, UK) with 2ml 0.25% Trypsin/EDTA (T/E) (Invitrogen, Poole, UK) for 15 minutes at 37°C. Subsequently the material was resuspended in 2ml mouse embryonic fibroblast (MEF) media, consisting of Dulbecco's modified Eagle's medium (DMEM) with L-glutamine (4500mg/ml glucose; Lonza-Bio-Whittaker, Wokingham, UK), 10% (v/v) foetal bovine serum and 1% non-essential amino acids (NEAA) (both Gibco Invitrogen, Paisley, UK). The suspension was centrifuged for three minutes at 300g before the supernatant was aspirated and the pellet resuspended in fresh MEF media. The MEF suspension was then transferred into T75 tissue culture flasks (Nunc, Safford, UK) and named passage zero, before being frozen in cryovials two days later.

2.1.2 Expansion and inactivaton of mouse embryonic fibroblasts

Primary MEFS were thawed, washed and then resuspended in fresh media. The cell suspension was then transferred into T75 flasks and named P1. When MEF confluency reached 70 to 80%, they were inactivated with 9ml Mytomycin-C (1mg/ml, Sigma-Aldrich, Poole, UK) for 2 hours at 37°C. Following incubation, the cells were washed 3 times in 5ml PBS before 5ml (0.1 w/v) T/E was added. The cells were incubated for 3 minutes at 37°C before enzyme neutralisation with MEF media and centrifugation at 300g. The supernatant was aspirated and the pellet resuspended in 20ml of MEF media for counting via haemocytometry. Inactivated MEFS were seeded into T25 flasks at a density of 250,000 cells/cm^3.

To continue culturing, 5ml of T/E was added to some MEF flasks not treated with Mytomycin, and incubated for three minutes at 37°C. After washing the cells with Dulbecco"s modified phosphate-buffered saline (DPBS) (Sigma-Aldrich), the MEFs were resuspended and seeded into new T75 flasks (split at a ratio between 1:5 and 1:3).

2.1.3 Culture of human induced pluripotent stem cells

Cell line: MSU-001 induced pluripotent stem cells (iPSCs) were acquired from the Spanish Stem Cell Bank for use in retinal differentiation experiments. The human iPSCs were derived from IMR90; IMR90 is an ethically approved fibroblast line, derived from a 16 week-gestation age female. Both the fibroblast and resulting iPSC line were found to have identical normal karyotypes.

iPSC derivation: Faetal IMR90 fibroblasts were obtained from ATCC, before infection with high-titre lentiviral vectors which encoded for the reprogramming factors Oct4, Sox2, Nanog, and Lin28. Infected IMR90 cells were cultured in human embryonic stem cell (hESC) medium supplemented with 100ng/ml recombinant zebrafish Fibroblast growth factor 2 (zFGF2) for approximately day 21-post infection. hESC-like colonies were passaged, and expanded on a feeder layer of MEF until stable colonies were noted. With increased passage number, zFGF2 was switched to human Fibroblast growth factor 2 (hFGF2) at 5-20ng/ml. hESC media contains KO-DMEM supplemented with 20% Knockout serum replacement (KOSR), 2mmol/l glutamine, 0.05% beta-mercaptoethanol, 1% NEAA, 0.5% pen-strep and 100ng/ml zFGF2 or 5-20ng/ml hFGF2 (all reagents from Gibco Invitrogen). iPSC colonies were passaged mechanically by manually selection, and split 1:3 onto flasks containing inactivated MEFs.

Validation: Pluripotency of the cell bank was validated through phenotyping, differentiation into ectoderm, endoderm and mesoderm cell lineages and in vivo teratoma formation in severe combined immunodeficiency (SCID) mice.

Cell culture: Human induced pluripotent stem cells (MSU-001 iPSCs (Spanish Stem Cell Bank)) were cultured with 250,000 inactivated MEFS on 0.1% gelatin (Sigma-Aldrich) coated T25 flasks (ThermoFisher Scientific, Leicestershire, UK) with 7ml media comprised of DMEM,

20% (v/v) KOSR, 1% NEAA, 1mM L-glutamine, 100mM beta-Mercaptoethanol and 4ng/mL bFGF (all Gibco Invitrogen, Paisley, UK). iPSCs were incubated at 37°C and 5% (v/v) CO_2 with media exchanged daily. Every three or four days, iPSCs were manually transferred to new Mitomycin inactivated MEF flasks by surgical microdissection with a fine tip mini pastette (Alpha Laboratories, Hampshire, UK), then transferred to new Mitomycin inactivated MEF flasks at a 1:3 ratio. Passage numbers between p50 and p70 were used, and regularly tested for pluripotency.

2.1.4 Culture of human embryonic stem cells

Cell line: Shef3 Human embryonic stem cells were acquired from the UK Stem cell bank for use in retinal differentiation experiments. hESC were derived from an ethically approved thawed eight-cell embryo on day 3 of culture.

Cell culture: hESC were grown on 250,000 mitomycin inactivated MEFS on 0.1% gelatin coated T25 flasks with 7ml media with DMEM, 20% (v/v) KOSR, 1% NEAA, 1mM L-glutamine, 100mM ß-Mercaptoethanol and 4ng/mL basic fibroblast growth factor. Shef3 were incubated at 37°C and 5% (v/v) CO_2 with media exchanged daily. Every three to four days, T25 flasks were manually passaged onto new inactivated feeder flasks at a 1:3 ratio. Passage number 66 to 68 was used, and tested for pluripotency.

2.1.5 Culture of human lung fibroblasts

Cell line: MRC-5 human lung fibroblasts acquired from the ATCC (Catalogue No. CCL-171).

Cell culture: MRC-5 fibroblasts were cultured in Nunc T175 flasks (ThermoFisher Scientific) for a maximum of 40 populations doublings in Eagle's Minimum Essential Medium (EMEM, M5650 Sigma-Aldrich) with 10% Foetal Bovine Serum (FBS, Seralab UK), 1% Glutamine and 1% NEAA.

2.2 Cell counts

Cell counts were conducted using a Neubauer-improved haemocytometer (Marienfeld-Superior, Germany) with trypan blue (Sigma-Aldrich). Additional cell counts were also performed with the Vi-CELL Cell Viability Analyser (Beckman Coulter, UK) where 500ul of cell suspension was counted with 40 images taken to determine cell concentration and viability.

2.3 Retinal differentiation

An initial retinal differentiation protocol was first tested on human pluripotent stem cells. This was then improved to produce a higher yield of CRX-positive cells. Both protocols are detailed below.

2.3.1 Initial differentiation protocol

Pluripotent stem cells were directed towards a retinal lineage as detailed in a previous thesis (Bae, 2011). Undifferentiated iPSC or hESCs were manually dissected into small clumps using a fine tip mini pastette and aggregated as a suspension in 3ml retinal induction media to form embryoid bodies (EBs) in 30mm non-adherent bacterial-grade dishes (Sterilin, Caerphilly, UK). DMEM/F12 media (Gibco) supplemented with 10% (v/v) KOSR, 1ng/ml human recombinant DKK-1 (Cambridge Bioscience, Cambridge, UK), 1ng/ml human recombinant noggin (R&D Systems, Minneapolis, US), 5ng/ml human recombinant IGF-1 (Miltenyi Biotec, Surrey, UK), 1% (v/v) N-2 supplement (PAA Laboratories Ltd, Yeovil, UK) was used as induction media.

On day 4, 30 EBs per well were plated into each well of a 6 well plate (Sigma-Aldrich), coated in Matrigel (BD Bioscience, San Diego, CA). Retinal differentiation media containing DMEM/F12, 10ng/ml human recombinant DKK-1, 10ng/ml human recombinant Noggin, 10ng/ml human recombinant IGF-1 and 5ng/ml bFGF was used; media was changed every other day.

 On day 21, media was changed to the late retinal differentiation composition containing DMEM/F12, 100nM Taurine (Sigma-Aldrich), 10μm DAPT (Cambridge Bioscience), 10μm Retinoic acid (Alfa Aesar, Lancashire, UK) and 100U/ml N-2 supplement.

2.3.2 Initial dissociation

On day 31, retinal differentiation cultures were dissociated using 0.25% Trypsin/EDTA for 10 to 20 minutes at 37°C.

2.3.3 Improved differentiation protocol

Pluripotent stem cells were directed towards a retinal lineage via a modified, Lamba differentiation protocol (Lamba *et al.,* 2006). Undifferentiated stem cells were enzymatically dissociated with 2ml Tryple (Invitrogen, Paisley, UK) for 5 to 10 minutes at 37°C. Cells were aggregated into EBs in AggreWell 400EX Plates (STEMCELL Technologies, Grenoble, France) according to manufacturer's guidelines, with 4.7×10^6 cells seeded per well to form 4700 EBs with 1000 cells per EB. EB media comprised of DMEM/F12, 10% (v/v) KOSR, 1ng/ml human recombinant DKK-1 (PeproTech, NJ, USA), 1ng/ml human recombinant Noggin (PeproTech), 5ng/ml human recombinant IGF-1, 1% (v/v) N-2 supplement.

On day four, EBs were transferred into a 12-well plate coated in Matrigel at a density of 30 EBs per well. Retinal differentiation media was changed every other day for 28 days. Media comprised of DMEM/F12, 10ng/ml human recombinant DKK-1, 10ng/ml, human recombinant Noggin, 10ng/ml human recombinant IGF-1, 1% (v/v) N-2 Supplement, 2% (v/v) B27 supplement (PAA Laboratories) and 5ng/ml bFGF.

2.3.4 Improved dissociation

On day 31, retinal differentiation cultures were dissociated using a combination of pre-warmed TrypLE (ThermoFisher Scientific) for 10-20 minutes at 37°C, and manual scraping with a fine tip mini pastette (Alpha Laboratories).

2.4 Immunocytochemistry

Experimental cultures were treated with 4% paraformaldehyde (PFA) for 20 minutes to fix cells in-situ. Cells were then permeabilised in 0.25% (v/v) Triton X-100 (both Sigma-Aldrich) dilute in DPBS (ThermoFisher Scientific) for 10 minutes at room temperature, and incubated for 30 minutes in blocking solution (5 % (v/v) FBS in DPBS). For imaging extracellular markers, the

permeablisation step was omitted to prevent damage of cell membranes. Samples were then incubated for one hour with 500µL of primary antibody diluted in blocking solution comprising of 5 % (v/v) FBS in Dulbecco's phosphate-buffered saline (DPBS) (ThermoFisher Scientific). After three wash steps with DPBS, samples were incubated in the secondary diluted antibody for one hour in the dark at room temperature. The sample was then washed three times before 500µL of 4,6- diamidino-2-phenylindole (DAPI) (Invitrogen), diluted to a concentration of 1:1000, was added and incubated for five minutes at room temperature. Secondary only samples were used as negative control samples, with the same concentration as primary antibodies always used. Samples were analysed using a fluorescence microscope (Nikon Eclipse TE2000-U) with NIS-element software.

Table 2.1 *List of primary antibodies used for immunocytochemistry. Antibodies were supplied by ThermoFisher Scientific, Miltenyi Biotec or Santa Cruz (Texas, US).*

Function	Target	Species	Isotype	Dilution used
Progenitor photoreceptor	CD73	Mouse	$IgG1_k$	1:100
	Crx	Mouse	IgG_{2a}	1:200
	Nrl	Rabbit	Polyclonal	1:200
Pluripotency	Oct3/4	Mouse	IgG	1:200
	SSEA1	Mouse	IgM	1:100
	SSEA4	Mouse	IgG_3	1:200
	SSEA3	Mouse	IgM	1:200
	TRA-1-60	Mouse	IgM	1:200
	TRA-1-81	Mouse	IgG	1:200
Retinal	Pax6	Mouse	IgG_1	1:300
	OTX2	Mouse	IgG	1:200
Nuclear	DAPI	n/a	n/a	1:1000
CellTracker (Red)	n/a	n/a	n/a	
CellTracker (Green)	n/a	n/a	n/a	

Table 2.2 *List of secondary antibodies used for immunocytochemistry. Secondary antibodies were supplied by ThermoFisher Scientific*

Species raised in	Target species	Isotype	Excitation
Goat	Anti-mouse	IgG	488
Goat	Anti-mouse	IgG	555
Goat	Anti-mouse	IgG	594
Goat	Anti-rabbit	IgM	555
Goat	Anti-mouse	IgM	488

2.5 Microscopy

2.5.1 Confocal microscopy

For confocal imaging, the same protocol as previous detailed for staining was used. Images were taken on the Leica TCS SPE upright confocal microscope (Leica microsystems, Milton Keynes, UK) at UCL Faculty of Medical Sciences and analysed with Leica Application Suite X (Leica microsystems).

2.5.2 Multi-photon confocal microscopy

For multiphoton images, cells were cultured on glass coverslips, otherwise the same staining protocol as immunocytochemistry was used. Images were taken on a Zeiss 510 NLO multi-photon microscope (Zeiss, Cambridge, UK) and analysed with LSM 4.2 (Zeiss). The Coherent Chameleon tuneable laser (700-1020nm) with a x10 water dipping objective was used for multi-photon images.

2.6 Flow cytometry and FACS

2.6.1 Extra-cellular

Media was aspirated and cells enzymatically dissociated with Tryple for 5 to 10 minutes at 37°C. For retinal differentiation cultures, manual scraping with a fine tip mini pastette (Alpha Laboratories) was also used. The cell suspension was filtered through a 40µm mesh, then quenched with blocking solution (5 % (v/v) FBS in DPBS) and centrifuged for 5 minutes at 300g to form a pellet. After aspirating the supernatant, the pellet was re-suspended in 100µL of antibody, diluted in blocking solution to meet the antibody manufacturer's recommended concentration. Samples were incubated for 20 minutes in the fridge, centrifuged and then re-suspended in 1ml blocking solution for flow cytometry or cell sorting.

2.6.2 FACS

Prepared samples were sorted by a fluorescent-activated cell sorter (FACSAria II, BD Bioscience) for CD73 expression.

2.6.3 Intracellular

For intra-cellular flow cytometry analysis, whether after cell sorting or straight from dissociated cell cultures, samples were fixed with 4% PFA for 20 minutes at room temperature, then permeabilsied with 0.25% Triton X-100 solution for 10 minutes at 37°C. Cells were centrifuged to form a pellet, supernatant aspirated, and then suspended in blocking solution for 30 minutes. Staining was then performed as described above for the extra-cellular protocol.

Table 2.3 *List of pre-conjugated antibodies for flow cytometry. Antibodies were supplied from Biorbyt (Cambridge, UK), Miltenyi Biotec, Bioss Antibodies (Massachusetts, US) and R&D Systems (Abingdon, UK). Flow cytometry antibodies not mentioned here were the same as previously stated for immunocytochemistry.*

Target	Species	Conjugated Fluorophore	Isotype
NRL	Anti-Rabbit	FITC	IgG
CD73	Mouse	PE	$IgG1_k$
CRX	Rabbit	647	IgG
Oct-4	Rat	405	IgG2B Clone # 240408

	Anti-Rabbit	FITC	IgG
	Anti-Mouse	PE	IgG
Controls	Anti-Rabbit	647	IgG
	Anti-Rat	405	IgG

2.6.4 Flow cytometry

Prepared samples were assessed using a flow cytometer (LSR II, 5 laser analyser, BD Bioscience or the Cyan ADP, Beckman Coulter, Wycombe, UK) and the data analysed with VenturiOne 6.0 (Applied Cytometry, Sheffield, UK). At least 50,000 events were initially gated with an unstained sampled using side scatter (SC) again forward scatter (FS) to remove debris, then pulse width or FS height against area to remove doublets. Positive expression was determined by gating the top 1% expression of an isotype or secondary-only control. A minimum of N=3 samples were run and the standard deviation calculated.

2.6.5 Statistical analysis

Three or more biological triplicates were tested for each experiment and all values shown represent the mean with standard deviation as error bars. Statistical analysis was performed using GraphPad software and P values calculated using two-tailed unpaired t tests. Significance was determined if $P \leq 0.05$ with a 95% confidence.

2.7 MACS

MACS was conducted according to the antibody manufacturer's protocol (Miltenyi Biotec) with a few exceptions. Media was aspirated and cells enzymatically dissociated with 2ml Tryple for 10 minutes at 37°C along with manual scraping using a fine tip mini pastette (Alpha Laboratories). The cell suspension was passed through a 40μm sterile filter and quenched with blocking buffer (5 % (v/v) FBS in DPBS), before being centrifuged for 5 minutes at 300g to form a pellet. The same CD73 antibody (as used for FACS) was incubated with cells for 10-20 minutes in a fridge

in the dark; 110µl per 10^7 cells in a 1:10 ratio. An MS or LS column, dependent on scale (with a maximum total cell number of $2x10^8$ or $2x10^9$ respectively), was held in the MACS Separator and rinsed with buffer. The cell suspension was applied and unlabelled cells collected. The column was then removed and placed in another collection tube, before being flushed through with buffer using the supplied plunger.

2.8 SpheriTech bead manufacture

2.8.1 Initial reactor manufacture

SpheriTech beads were manufactured following protocols in the patent owned by SpheriTech (SpheriTech 2014). 2% (w/v) of Span80 was dissolved in 500ml of dichloromethane (DCM) (both Sigma-Aldrich) in a round bottomed flask. A 50cm3 solution of 10g poly-Ɛ-lysine (Handary, Brussels, Belgium), 3g Sebaccic acid (Sigma-Aldrich) and 3g N-methylmorpholine (NMM) (ThermoFisher Scientific) was made up. For paramagnetic beads, 1g of iron oxide (Sigma-Aldrich) was added to this solution. For buoyant beads, a 1:1 solution of Expancel DEX80 hollow microspheres (Akzo Nobel, Sundsvall, Sweden) to polymer is used. The aqueous solution was then added into the round bottomed flask and left and agitated with an RS37 Digital Plus overhead stirrer (Radleys, Essex, UK) and Rushton impeller to generate droplets. 11.5g of 1-Ethyl-3-(3-dimethylaminopropyl)carbodiimide (EDCI) (Cambridge Bioscience) was added to the reactor through a funnel and incubated for 1.5 hours with agitation to allow for polymerisation.

The solvent layer was removed via filtration and particles washed in a 200µm sieve with 2% isopropylene then excess water. Beads were stored in water with sodium azide (Sigma-Aldrich).

2.8.2 Updated reactor manufacture

Various iterative improvements were made to the reactor manufacture during experimentation as detailed in chapter 5.3. The new chemicals and equipment used were toluene (Sigma-

Aldrich), iron (iii) oxide magnetic NanoArc (Alfa Aesar) instead of the and a VJ150 Viscojet impeller (VISCO JET® Rührsysteme GmbH, Germany).

2.8.3 Microfluidic system

The microfluidic system was set up as shown in Figure 6.1. 10g of poly-ε-ysine was dissolved in 30ml water in a 50ml falcon tube (Corning). Sebaccic acid (3g) and NMM (3g) was then added to 20ml of water and left on a roller. Once dissolved, the two falcons were mixed together and used to fill a glass syringe. 2% SPAN80 was then dissolved in DCM with 60mmol EDCI and used to fill a second glass syringe. Using a neMESYS syring pump (Centoni, Germany), the tubing was primed with solvent before beginning bead productive. The output tubing from the microchip fed into a beaker containing DCM with 0.1g/ml EDCI which was gently agitated using a magnetic stirrer. A range of flowrates were then tested and the bead diameters produced was assessed.

2.9 SpheriTech cell sorting

2.9.1 Antibody immobilisation

Following details in the SpheriTech patent, 1g of glutaric anhydride (Sigma-Aldrich) was added to 1ul of NMM in 2.5ml of methanol (Sigma-Alrdich). 280mg of beads was added to the vial and left on a roller for 24 hours. Polymer beads were then washed with water, before a 1 hour incubation in 170mg of N-hydroxysuccinimide (NHS) (VWR International, Leicestershire, UK) and 230mg of EDCI in pH5 solution to activate carboxyl groups. The polymer was then incubated with CD73 (Miltenyi) over-night to give a final density of approximately 4 CD73 antibodies per μm2. Immobilised beads were then washed with 5%(v/v) ethanolamine (Sigma-Aldrich) to cap remaining free carboxyls. Beads were stored in sterile PBS before use.

2.9.2 Cell sorting

Cells were suspended in PBS and incubated with CD73 immobilised beads at a density around 1×10^6 per ml for 10 to 20 minutes on a roller. The beads were then held in place with a magnet

while unbound cells were eluted and counted. Bound cells were dissociated using T/E for 5 to 10 minutes at 37°C. then counted.

2.9.3 Confocal-derived counts

Fluorescent confocal microscopy was used to visualise and count cells attached to beads. Cell suspensions were incubated with CellTracker dye (ThermoFisher Scientific) for 30 minutes at room temperature. Cell sorting was then carried out as described above and beads were imaged on an upright confocal microscope (TCS SPE confocal microscope, Leica). Cells were counted on the visible half of the bead, and then count multiplied by two to estimate cells bound over the entire bead.

2.9.4 Supernatant-derived counts

The viable cell number from dissociated retinal differentiation cultures was counted using the Vi-CELL Cell Viability Analyser (see chapter 2.2). The volume and mass of affinity beads for sorting was then determined by displacement in a fixed volume of PBS. Cell sorting was performed as described above for 10 to 20 minutes on a roller. SpheriTech beads were held in place in a magnetic field and the supernatant was eluted and cells counted using the same method. This viable cell count, as well as an average cell number lost through processing, was deducted from the starting cell number to give an estimated bound cell count.

2.10 Magnetic characterisation

2.10.1 Magnetic field measurements

To measure the magnetic field strength of magnets (Assemtech Round Magnet 6x2mm, Maplin Electronics, Rotherham, UK) used, a GM08 Gaussmeter (Hirst Magnetic Instruments Ltd., Cornwall, UK) and transverse probe (STB1X-0201 ultra thin transverse probe 0.020", Sypris F W Bell) was used. The probe was fixed in place whilst the magnet attached was precisely moved by a micro-stage with a resolution of 10 μm (Model 462 XY translation stage, Newport

Corp., USA). Reading were taken on the Gaussmeter, then experiment repeated with a piece of PDMS (2mm or 5mm thick) placed between the probe and the magnet.

2.10.2 SQUID

SQUID magnetometry measurements were performed using a Quantum Design SQUID-VSM (San Diego, USA) with a field range of ±7 T at 300 K. The magnetic moment was calibrated using a Palladium sample with known mass and susceptibility at 298 K.

Experimental samples were prepared by pipetting suspended SpheriTech beads onto filter paper and air drying for a 24 hour period. Three different manufacture batches were tested with three samples prepared for each. The solid material was added to a polycarbonate powder holder using a plastic spatula, with the mass of material measured (to 4 dp) using a Denver Instruments microbalance (NY, US).

Prior to measurement, samples were demagnetised using alternating field steps from ±7 T to 0 T. The sequence for the SQUID measurements used non-linear steps in field up to 7 T. The magnetic moment was measured five times at each field using automatic sample tracking, automatic lock-in amplifier gain and a VSM oscillation amplitude of 5 mm. The magnetic moment was corrected by removing a linear contribution to the slope, which was diamagnetic for all samples measured.

2.10.3 Mössbauer

The Mössbauer measurement set up comprised of a cobalt radioisotope gamma source (^{57}Co embedded in rhodium foil matrix) oscillated at a constant velocity of 12 mm/s. The transmitted sample was measured using a 1024 multi-channel analyser (SeeCo W202 detector). A room temperature ^{57}Fe Mössbauer spectra was recorded, then each spectrum was folded relative to the Mössbauer spectrum of a standard α-Fe foil, used as a reference material.

2.11 Bead sizing

2.11.1 Laser diffraction

Particle size measurements were carried out with a Mastersizer 2000 (Malvern Instruments Ltd, Malvern, UK) which measured a size range from 0.02 μm to 2000μm. SpheriTech beads suspended in PBS were added until the obscuration was below 15% and the weighted residual was below 3%. Fraunhofer mode was selected for approximation, assuming the beads were 2D opaque discs with refractive index having little impact at their size and opaqueness. To transform the data from a volumetric to numerical measurement, particles were assumed to be spherical and in the centre of each size band measured.

2.11.2 Microscopy

Phase contrast images of SpheriTech beads in a well plate where taken using the EVOS FL Imaging system (ThermoFisher Scientific). Using ImageJ (https://imagej.nih.gov/ij/index.html), the images were converted to Threshold images using an IJ_IsoData method to permit analysis of particle size. The ferret diameter and circularity were calculated with this software.

Circularity, how round a cross-sectional shape is in comparison to a perfect circle, was calculated by the equation:

$$circularity = \frac{4 \times \pi}{(area \times perimeter^2)}$$

where 1.0 indicates a perfect circle and 0.0 indicates an elongated polygon.

Data was collected for 268 beads, then grouped into 18 bins based off class range using the equation:

$$Class\ range = \frac{Range}{\sqrt{N}}$$

where N = the number of particles counted and Range is:

$$Range = Maximum\ particle\ size - Minimum\ particle\ size$$

This allowed the creation of a frequency histogram to compare bead sizing data to laser diffraction.

2.12 Electron Microscopy

2.12.1 SEM

Scanning electron microscopy (SEM) was conducted at the UCL Division of Biosciences Electron Microscopy facility using the Jeol 7401 high resolution Field Emission Scanning Electron Microscope.

2.12.2 Immunogold staining

For immunogold staining, SpheriTech beads were immobilised with excess CD73 antibody (Miltenyi) overnight. After washing with PBS, immobilised beads were incubated with secondary antibody 20nm colloidal gold conjugate (BioCell) at a 1:20 ratio for an hour at room temperature. A control consisting of beads without CD73 immobilised antibody was used and otherwise treated identically to the sample. Beads were washed with PBS and resuspended in ethanol for critical point drying in a pressure vessel with liquid CO_2. Samples were dried via evaporation then mounted and carbon coated for electron microscopy.

For MRC-5 testing, cell suspensions were incubate with CD73 primary antibody for an hour on ice at 1:50 ratio. Cells were fixed with 4% PFA for 10minutes at room temperature before the same secondary antibody staining procedure was utilised as for SpheriTech beads, as well as for a control cell sample without primary CD73 staining. Samples were then treated with 1% glutaraldehyde before osmication with 1% osmium for 20 minutes in the fridge. Samples were dehydrated in ethanol and then washed with HMDS (Sigma) before being mounted on a cover slip and carbon coated.

2.13 Cryosectioning

CD73 immobilised SpheriTech beads were placed into the centre of a base mould containing Optimal Cutting Temperature (OCT) compound. The mould was slowly lowered into liquid nitrogen, then fully submerged until completely frozen. A Cryotome cryostat (ThermoFisher Scientific) was pre-cooled to -20°C prior to sectioning. The embedded SpheriTech bead block

was sectioned into 5µm slices and placed onto glass slides. For immunocytochemistry, the slices were fixed with 4% PFA, then incubated with a secondary antibody to bind to CD73 for one hour at room temperature. Control beads that had been cryosectioned with no CD73 immobilisation were used as a control. After washing the slides with PBS, fluorescent microscopy was performed using the EVOS FL Imaging system.

2.14 Excitation/Emission scanning

A Tecan Safire II plate reader (Tecan, Reading, UK) was used to perform 3D wavelength scans for SpheriTech beads in suspension. The measurement parameters used are in the table below. Beads were suspended in PBS in Greiner CELLSTAR black polystryrene 96 well plate (Sigma-Aldrich) to reduce background fluorescence. A well with PBS only was used as a control.

Table 2.4 *Plate reader specification*

Parameter	Value
Measurement mode	Fluorescence Top
Wavelength scan type	3D
Excitation wavelength	230 – 550nm
Excitation step size	2nm
Emission wavelength	280 – 550nm
Emission step size	2nm
Excitation bandwidth	20nm
Emission bandwidth	20nm
Gain (manual)	20
Number of reads	20
Integration time	40µs

2.15 Bioprocess economic tool

A bioprocess economics model was created to evaluate the cost of goods (COG) associated with autologous human iPSC-derived cell therapy manufacture, when using either MACS or FACS as a positive affinity process for cell selection. Experimentally derived data for different affinity purification platforms, as detailed in Chapter 4 and Chapter 7, was fed into the tool as base case assumptions. The tool consists of a cost model with mass balance, design, sizing, resource utilisation and cost of goods equations set up in Microsoft Excel (Microsoft, WA), a database storing key data regarding different bioprocess technologies, and iterative algorithms

used during the sensitivity and scenario analysis that were developed in the Visual Basics for Applications (VBA) plug-in (Microsoft). Generation and use of the model was performed in collaboration with Michael Jenkins at UCL.

2.15.1 Deterministic model

The model was used to assess COG per dose for both purification unit operations, as well as the full bioprocess (detailed in Figure 1.1). Purification costs were calculated in the same manner as upstream processing COG, as described in Simaria et al. (2014). Briefly, purification costs per dose equal the sum of the annual material, labour and equipment depreciation costs associated with the purification operation, divided by the annual demand (or number of doses per year).

$$COG_{purification}/Dose = \frac{C_{mat}^{annual} + C_{lab}^{annual} + C_{dep}^{annual}}{demand}$$

2.15.2 Material costs

FACS and MACS rely on fixed equipment, costed through the SH800 cell sorter (Sony Biotechnology Inc.), FACSQuant Tyto (Miltenyi Biotec), and CliniMACS system (Miltenyi Biotec). Fixed equipment is supported by consumables such as disposable tubing, MACS columns, FACS sorting chips, along with antibody-based buffers and reagents. Consumable list prices were obtained from BD Biosciences and Miltenyi Biotec for FACS, and Miltenyi Biotec for the MACS platform, to give a 'price per run' for each sort ($C_{mat,r}$). The cost breakdown is in Appendix A. Material costs per dose ($C_{mat,d}$) at a given cell number, P, were calculated as follows, where u_j is the number of parallel units required to process a given cell population (according to the throughputs for a given technology given in table 8.1):

$$C_{mat,d,j} = C_{mat,r,j} \cdot u_j$$

2.15.3 Labour costs

Labour costs associated with the cell sort were calculated from assumed operator salaries. Two operators are required to handle each unit at any time for GMP processing. The labour cost per dose associated with a given purification technology, $C_{lab,d,j}$, was calculated as:

$$C_{lab,d,j} = \frac{u_j \cdot w_{ann,j}}{\text{annual demand}}$$

Where w_{ann} is the annual salary for an operator, and demand represents the annual throughput of a facility in doses/year.

2.15.4 Equipment depreciation

Equipment depreciation costs were calculated using the total cost of any fixed equipment ($C_{equipment}$) required for purification over a 10 year period (y). Multiplication factors described in Jenkins et al. (2015), were used for the tax (f_t), maintenance (f_m), and insurance (f_i) as follows:

$$C_{annual\ depreciation} = C_{equipment} * (f_m * f_t * f_i * \frac{1}{y})$$

Indirect costs associated with purification were calculated according to Simaria et al. (2014), where equipment depreciation is directly linked to handling of disposable purification technologies.

2.15.5 Bioprocess COG

Purification costs were added to expansion and differentiation costs, calculated on the basis of a cost/10^7 cells and prior work carried out at UCL's Advanced Centre for Biochemical Engineering (Jenkins et al. 2015; Weil, unpublished data). Bioprocess COGs were calculated as follows:

$$COG/_{Dose} = COG_{purification}/_{dose} + COG_{rep} + COG_{exp} + \left[\frac{P_{diff}}{10^7} (COG_{diff})\right]$$

Where COG_{rep} & COG_{exp} are the COG per dose associated with iPSC reprogramming and cell culture, P_{diff} represents the cell number required at the start of the differentiation to fulfil operation losses for a given dose size, and COG_{diff} is the COG per 10^7 cells associated with differentiation.

2.15.6 Sensitivity analysis

To determine key cost drivers associated with the bioprocess, over 20 variables were altered by ±15% from their original value to evaluate the impact on COG/dose with the best and worst case outcome. For example, the base case differentiation efficiency of 30% was varied by ± 15% to give a worst case scenario value of 25.5%, and the best case value was 34.5%.

2.15.7 Scenario analyses

The economic tool model was used to provide a detailed cost breakdown, given the base case scale and performance characteristics, when using different purification technologies. In order to assess the impact critical cost drivers had, an algorithm was developed using the Visual Basic for Applications (VBA) tool (Microsoft, WA). By assigning incremental values to the process parameters of dose size, differentiation efficiency, sort purity and purification yield, the most cost-effective, feasible technology across an array of scenarios was rapidly evaluated. The algorithm was then used to determine the purification yield at which SpheriTech beads became economically favoured, compared to FACS and MACS.

Chapter 3: Upstream Bioprocess Development

3.1 Introduction

Initial work by Lamba et al. indicated the potential for progenitor photoreceptors to be derived from a pluripotent cell source. With successful transplantation data now emerging to restore vision in visually-impaired mice models (Pearson *et al.*, 2012), there is need for an efficient, scalable bioprocess to facilitate a therapeutic endpoint. As such, the production of progenitor photoreceptors derived from pluripotent stem cells was chosen for further examination, and as a case study to test different affinity purification technologies.

3.1.1 Upstream development

An initial protocol was tested to differentiate human pluripotent stem cells towards a retinal lineage. However, due to very low progenitor photoreceptor differentiation efficiencies, upstream process development was required to improve the production output. As such, significant step improvements were required to permit the sufficient production of material for downstream analysis. This development focused on mitigating manual operations during aggregation which greatly increase variability, improving the cocktail of retinal growth factors used to direct differentiation, and changing the initial and final dissociation methodologies.

3.2 Aims and Hypotheses

3.2.1 Chapter Aim

Chapter 3 presents an overview of the characterisation and improvements made to upstream bioprocessing of the progenitor photoreceptor product. This involves the culture and differentiation of human pluripotent stem cells.

3.2.2 Hypothesis

The reproducibility of EB formation and retinal differentiation efficiency will be increased through the development of a controlled aggregation step in the differentiation process.

3.3 Stem Cell Characterisation

As stem cells have the propensity for spontaneous differentiation (Cowan *et al.*, 2004; Enver *et al.*, 2005; Mitalipova *et al.*, 2005), before commencing further experimentation, all starting material must be assessed for pluripotency. Cell morphology, immunohistochemistry and flow cytometry were selected to assess an iPSC and hESC line for suitability. A range of markers were tested based on commonly referenced pluripotency assays:

1. The transcription factor Oct-3/4 which has been shown to express in pluripotent cells in vivo and in vitro (Rosner *et al.*, 1990; Yeom *et al.*, 1996). Downregulation of Oct-3/4 results in the loss of pluripotency in embryonic stem cells (Nichols *et al.*, 1998), and as a result, is frequently targeted for identifying pluripotency.

2. Glycosphingolipid antigens Stage-Specific Embryonic Antigen (SSEA)-4 and (SSEA)-3 were also tested. SSEA-3 and SSEA-4 have been defined as markers for pluripotency (Andrews, Damjanov, *et al.*, 1984; Andrews, 1987). During differentiation, the cell surface structure of glycolipid antigens change dramatically and expression decreases (Andrews, 1987).

3. Tumour-recognition antigens (TRA)-1-81 and (TRA)-1-60 are cell surface antigens shown to express on pluripotent cells but not their derivatives or other germ line cells (Andrews, Banting, *et al.*, 1984)

These five antigens, Oct-4, SSEA-3, SSEA-4, TRA-1-81 and TRA1-60, cover the panel of cell markers most commonly tested for pluripotency (Thomson *et al.*, 1996; Carpenter, Rosler and Rao, 2003).

3.3.1 MSU001 iPSC

The iPSC line selected was generated in Jose Cibelli's lab (Michigan State University) through over-expression of Oct-4, Sox2, Nanog and Lin28 in human somatic fibroblasts with a high-titre lentiviral vector, as discussed in Chapter 2. iPSC were noted to be small, flat, and possess a

large nucleus to cytoplasm ratio in culture as expected (Takahashi *et al.*, 2007; Yu *et al.*, 2007). They were maintained on a feeder layer of inactivated mouse embryonic fibroblasts, which held stem cell colonies together as small, circular populations of around 1,000 to 10,000 cells before passaging. Every three or four days, colonies were manually dissociated into clumps and transferred to fresh T25 feeder flasks with a 1:3 seeding ratio.

Phenotyping studies were used to evaluate pluripotency before further experimentation. Firstly, immunohistochemistry was conducted to observe marker expression of Oct-4, and TRA-1-81 and TRA-1-60. These markers were expressed in all observed colonies (figure 3.1).
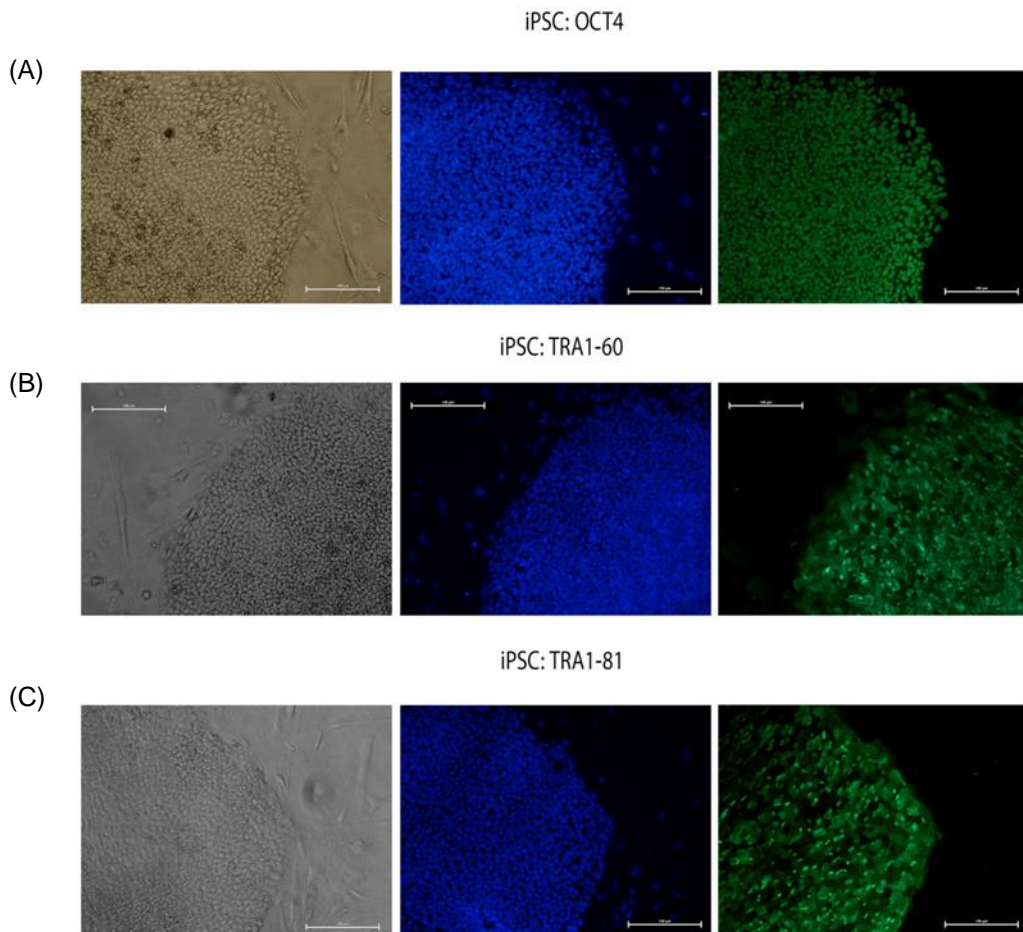
Figure 3.1 *Immunostaining of pluripotency markers (A) Oct4, (B) TRA-1-60 and (C) TRA-1-81 on human MS001 iPSC cell colonies. Phase contrast, DAPI (blue) and pluripotency marker (green) images are presented here. Scale bars = 100µm.*

Flow cytometry analysis revealed over 95% expression of key pluripotency markers (Figure 3.2). These microscopy and flow cytometry tests were carried out regularly throughout the project to ensure pluripotency was maintained at higher passages.
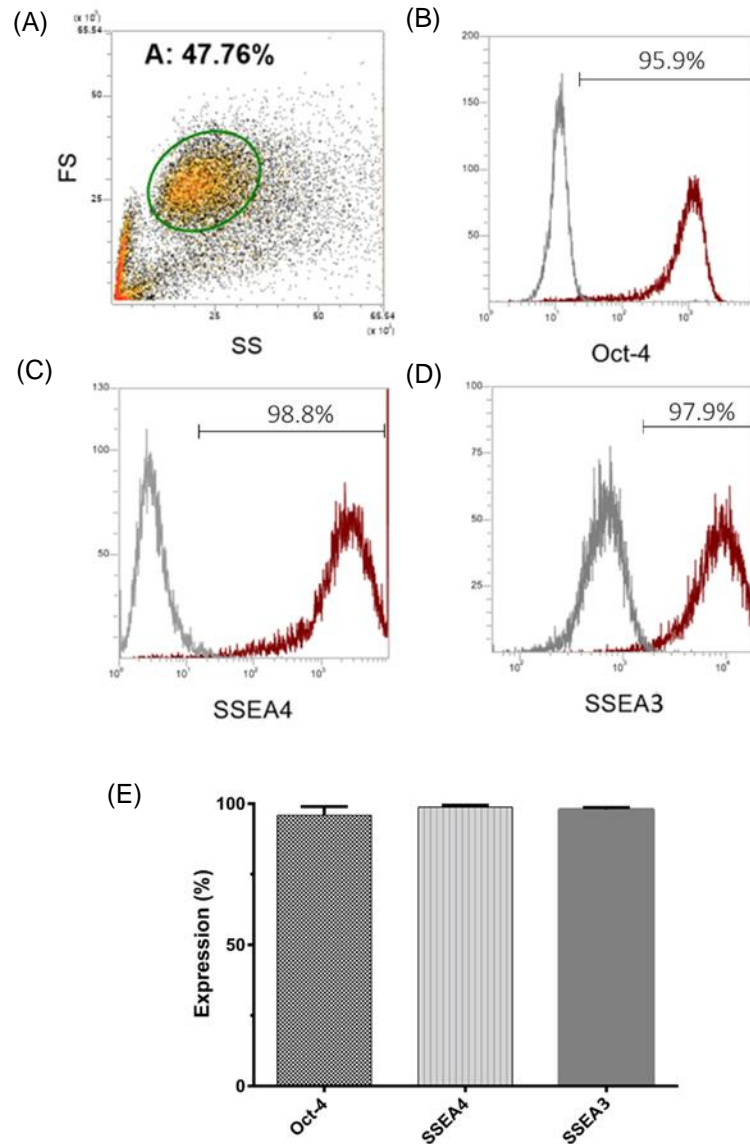
Figure 3.2 *Flow cytometry analysis of pluripotency markers Oct-4, SSEA4 and SSEA3 for human iPSC line MSU001. The gating strategy is detailed with a (A) Forward Scatter (FS) v Side Scatter (SS) dot plot (gate A) to remove debris. (B-D) Each histogram then shows the negative population stained with an isotype control (grey) and the stained sample (red) with positive expression gated from the top 1% of the isotype control. (E) Bar chart of the expression*

found from the mean positive expression with 95.9%, 98.8% and 97.9% noted respectively in N=3, ±Standard Deviation (SD).

3.3.2 Shef3 hESC

The same panel of tests were run to assess pluripotency for the second cell line tested which was the human embryonic cell line, Shef3. The cell line was derived in March 2005 following UK ethical guidelines, and is available from the UK Stem Cell Bank. Colony morphology of cells grown on a feeder layer showed features corresponding with stem cell characteristics as small, round cells with large, clear nuclei (Thomson *et al.*, 1998; Amit and Itskovitz-Eldor, 2012).

Shef 3: OCT 4

(A)

Shef 3: SSEA 4

(B)

Shef 3: TRA1-60

(C)

Shef 3: TRA1-81

(D)
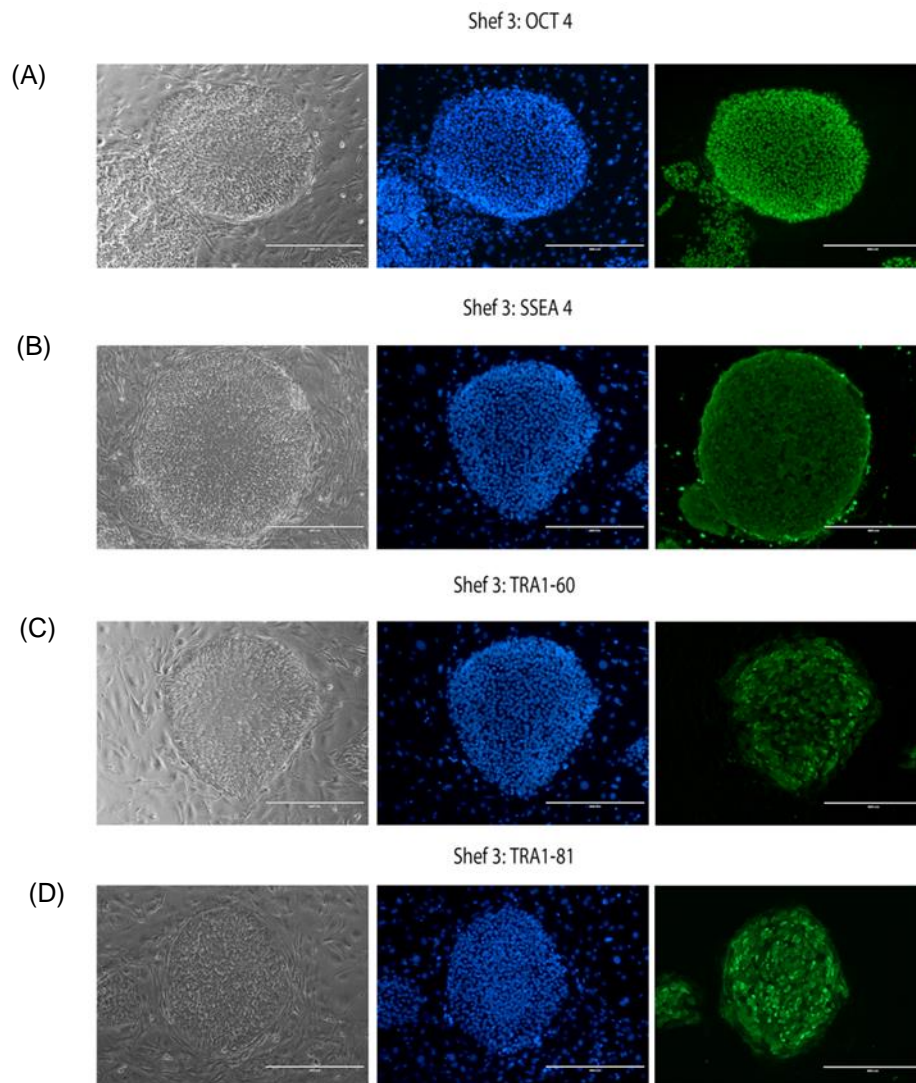
Figure 3.3 *Immunostaining of (A) Oct4, (B) SSEA4, (C) TRA-1-60 and (D) TRA-1-81 pluripotency markers for human embryonic stem cell line Shef3. Phase contrast, DAPI (blue) and pluripotent markers (green) images are presented here. Scale bars = 400µm.*

Immunohistochemistry demonstrated positive expression in the majority of colonies examined over a range of passages for a panel of common pluripotency-associated markers. These included Oct-4, SSEA4, TRA-1-60 and TRA-1-81 (Figure 3.3).

Flow cytometry quantified pluripotent expression for each marker, mirroring previously published work (Aflatoonian *et al.*, 2009; Bae *et al.*, 2011) (Figure 3.4).
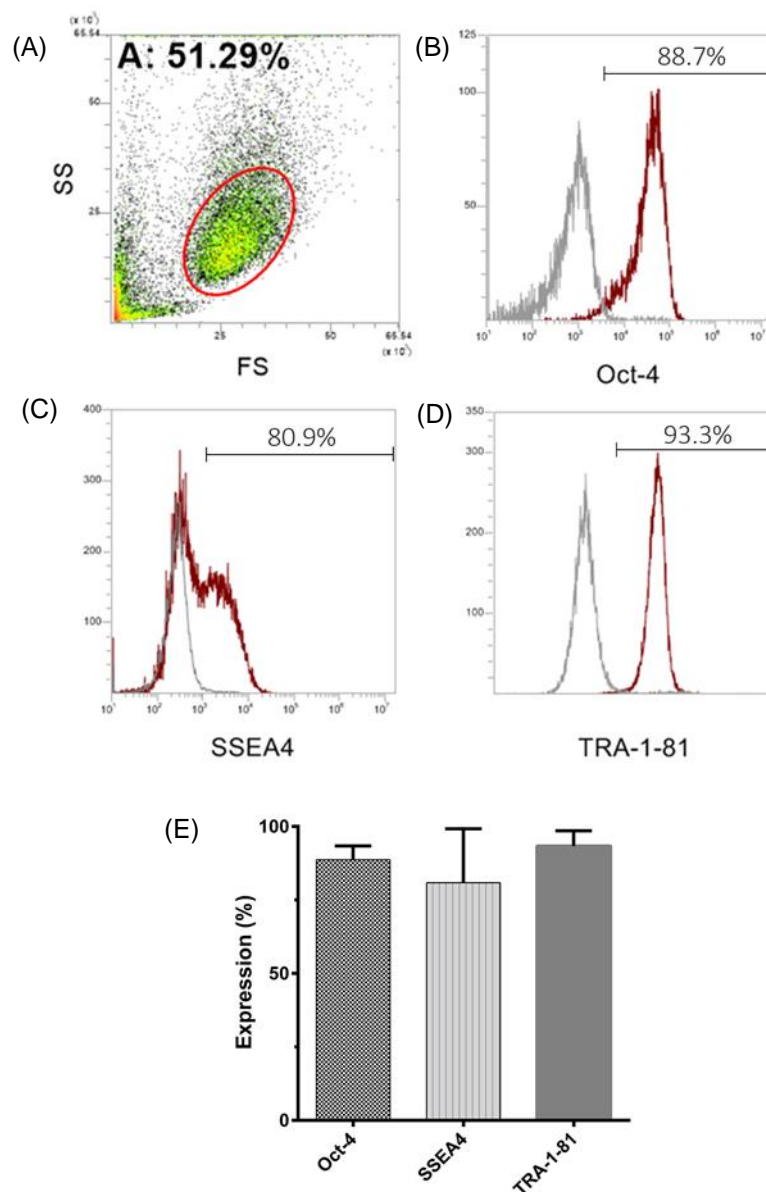
Figure 3.4 Flow cytometry analysis of pluripotency markers Oct-4, SSEA4 and TRA-1-81 for hESC line shef3. The gating strategy is detailed with a (A) SS v FS dot plot (gate A) to remove debris. (B-D) Each histogram then shows the negative population stained with an isotype control (grey) and the stained sample (red) with positive expression gated from the top 1% of the isotype control. (E) Bar chart of the expression found from the mean positive expression with 88.7%, 80.9% and 93.3% noted respectively in N=3, ±SD.

3.4 Initial Retinal Differentiation Protocol

The initial photoreceptor differentiation protocol chosen was from previous work as described in 2.3.1. This involved manually dissociated stem cells, before a two-day suspension culture step to form aggregated EBs. A cocktail of growth factors including DKK-1, Noggin and IGF-1 was used in the media. On day three, scraped EBs were plated onto Matrigel coated well plates with media changed every other day for 21 days. For the final week of differentiation, the media composition was changed to aid production of progenitor photoreceptors. This included the addition of Taurine, DAPT and retinoic acid, after the withdrawal of DKK-1, Noggin and IGF-1. The process has been diagrammatically detailed in Figure 3.5.
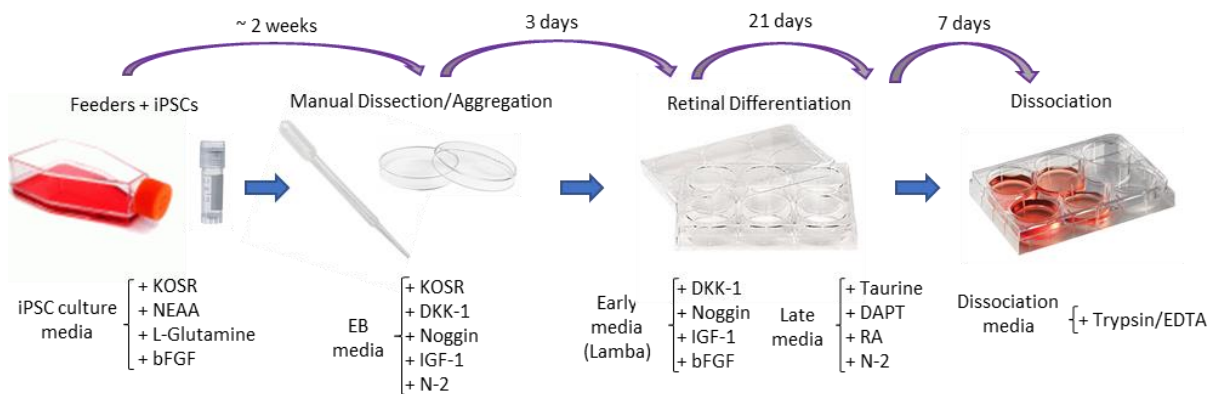
Figure 3.5 Initial retinal differentiation protocol for the production of human pluripotent stem cell derived- progenitor photoreceptors. iPSCs were manually dissociated into clumps, then cultured in suspension for 3 days in define retinal media. EBs were cultured adherently for a further 21 days, before a late-stage retinal growth factor mix was added for the final week. Retinal cultures were dissociated with T/E for characterisation.

3.4.1 Manual dissociation and aggregation

iPSC were manually dissociated from a T25 flask using a fine tipped pipette. The cell clumps in suspension were transferred to a bacterial grade, non-adherent dish for two days in retinal media to aggregate. EBs produced were polydispersed, with diameters ranging from 32µm to 190µm (Figure 3.6). There was also a significant amount of cell death noted, with many cells not forming EBs. EBs were more angular than expected, and many were broken up or had combined together with another aggregates to form much larger conglomerates.
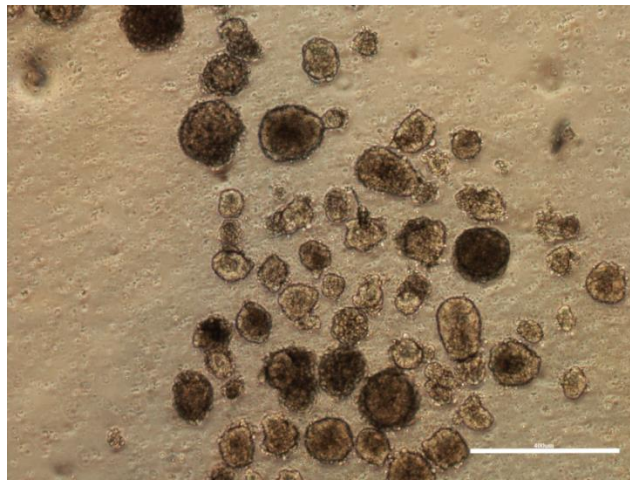
Figure 3.6 *Phase contrast microscopy image of scraped iPSC aggregate EBs in suspension on day 3 using the initial retinal differentiation protocol. Scale bar = 400µm.*

On day 3, scraped EBs were plated onto Matrigel coated 12 well plates at a density of 30 EBs per well. Adherent differentiation was then carried out according to the initial retinal protocol. At day 31, cells were analysed by flow cytometry to quantify progenitor photoreceptor production through CRX expression.
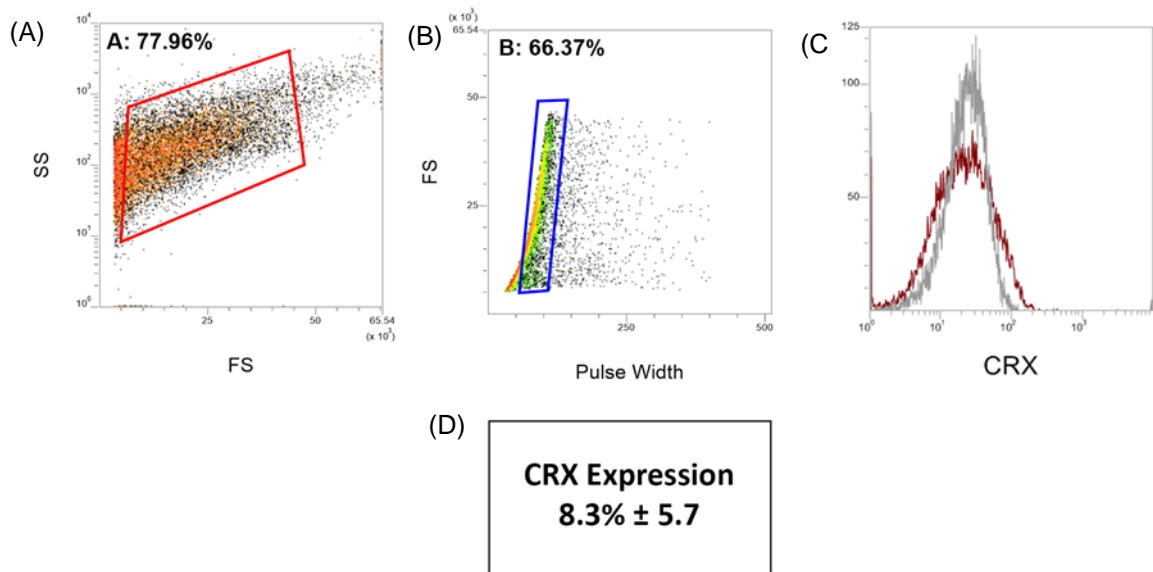
Figure 3.7 *Flow cytometry analysis of CRX expression in day 31 iPSC retinal differentiation cultures using the initial retinal differentiation protocol. The gating strategy is detailed with a (A) SS v SS dot plot (gate A) to remove debris and then (B) pulse width to remove doublets (gate B). (C) The histogram then shows the negative population stained with an isotype control (grey) and the CRX stained sample (red) with positive expression gated from the top 1% of the isotype control. (D) A mean of 8.3% expression was noted in N= 4 ± SD.*

Day 31 differentiated populations comprised of 8.3 ± 5.7% progenitors (mean ± standard deviation) with a coefficient of variation (CV) of 69% (Figure 3.7). The high standard deviation and CV indicates significant variability between differentiation runs. Improvements to the differentiation protocol must be made in order to investigate the impact of different purification technologies. Variation must be minimised and progenitor cell numbers increased to provide sufficient cell numbers for analysis.

3.5 Improved Retinal Differentiation Protocol

After several iterations, an improved retinal differentiation was established based on the original Lamba et al. protocol (Lamba *et al.*, 2006). Stem cell colonies were enzymatically dissociated with TrypLE, before being inoculated into AggreWell plates for cell aggregation. On day three, EBs were plated onto Matrigel coated plates and cultured for 28 days in a defined retinal media

which was changed every other day. The protocol has been diagrammatically represented in Figure 3.8.
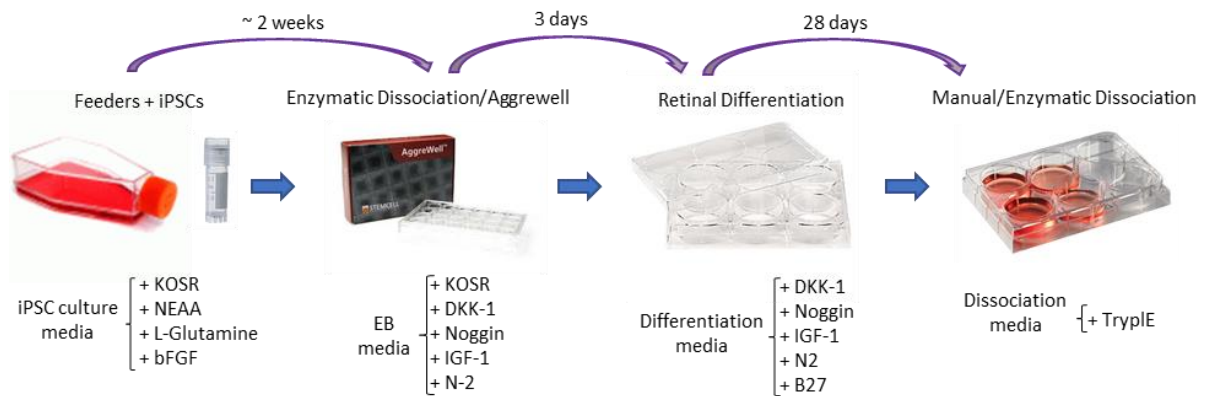
Figure 3.8 *Improved retinal differentiation protocol for the production of human pluripotent stem cell derived-progenitor photoreceptors. iPSCs were enzymatically dissociated and seeded into AggeWell plates at defined densities. EBs were cultured in suspension for 3 days in defined retinal media, then plated and grown adherently for 28 days before a mix of enzymatic and manual dissociation for characterisation.*

3.5.1 AggreWell EB formation

The first step to minimise variability from manual processing was by improving the aggregation step. To produce more spherical, consistently sized EBs, stem cell colonies were enzymatically dissociated with TrypLE into a single cell suspension for aggregation instead of using the manual scraping method (where heterogeneous clumps of cells with varied sizes and geometries were used).

The single cell suspension was seeded into an AggreWell 400Ex plate at an inoculation cell number to disperse 1000 cells per microwell. An AggreWell plate is a 6 well plate which contains approximately 4700 microwells per well. The hypothesis is that, after seeding a specific number of cells and centrifuging them to uniformly disperse cells across the well, each microwell will contain a fixed number of cells. Microwells are 400µm diameter inverse pyramid shapes which promote the formation of a single aggregate clumps; one per microwell (Figure 3.9). By

varying the total number of cells seeded into the whole well, EB size can be controlled. By forming a single EB in each separate microwell, the production of reproducible EBs can be scaled out.
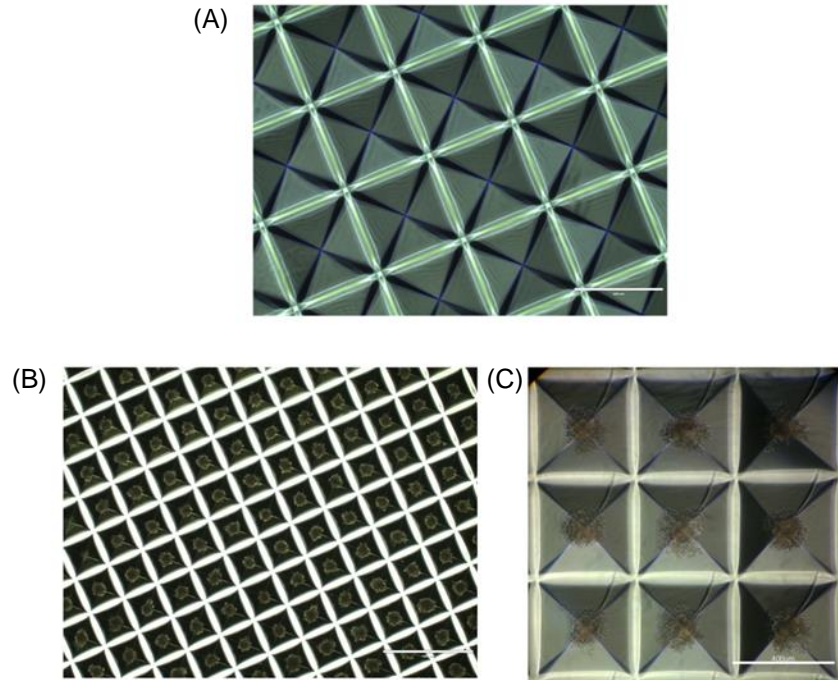
Figure 3.9 *Images of AggreWell plates. (A) An empty AggreWell plate to show the 'inverse pyramid' structure of individual microwells, an AggreWell plate with (B) Shef3 and (C) iPSC cells seeded at a density of 1000 cells per microwell to show how single aggregates form in each microwell. Scale bars are (A,C) 400μm or (B) 1000μm.*

To investigate the impact of enzymatically dissociating cells whilst using AggreWell-controlled EBs, early neuronal expression was assessed to ensure EBs were still being directed towards a retinal lineage. Flow cytometry analysis of OTX2 and Pax6 homeobox genes, seen in early human foetal retinal development 6 to 10 weeks after conception (Larsen *et al.*, 2009), was conducted. Additionally CRX, a marker of photoreceptor progenitors, and Oct-4, a marker associated with maintaining and re-gaining pluripotency (Shi and Jin, 2010), was examined.
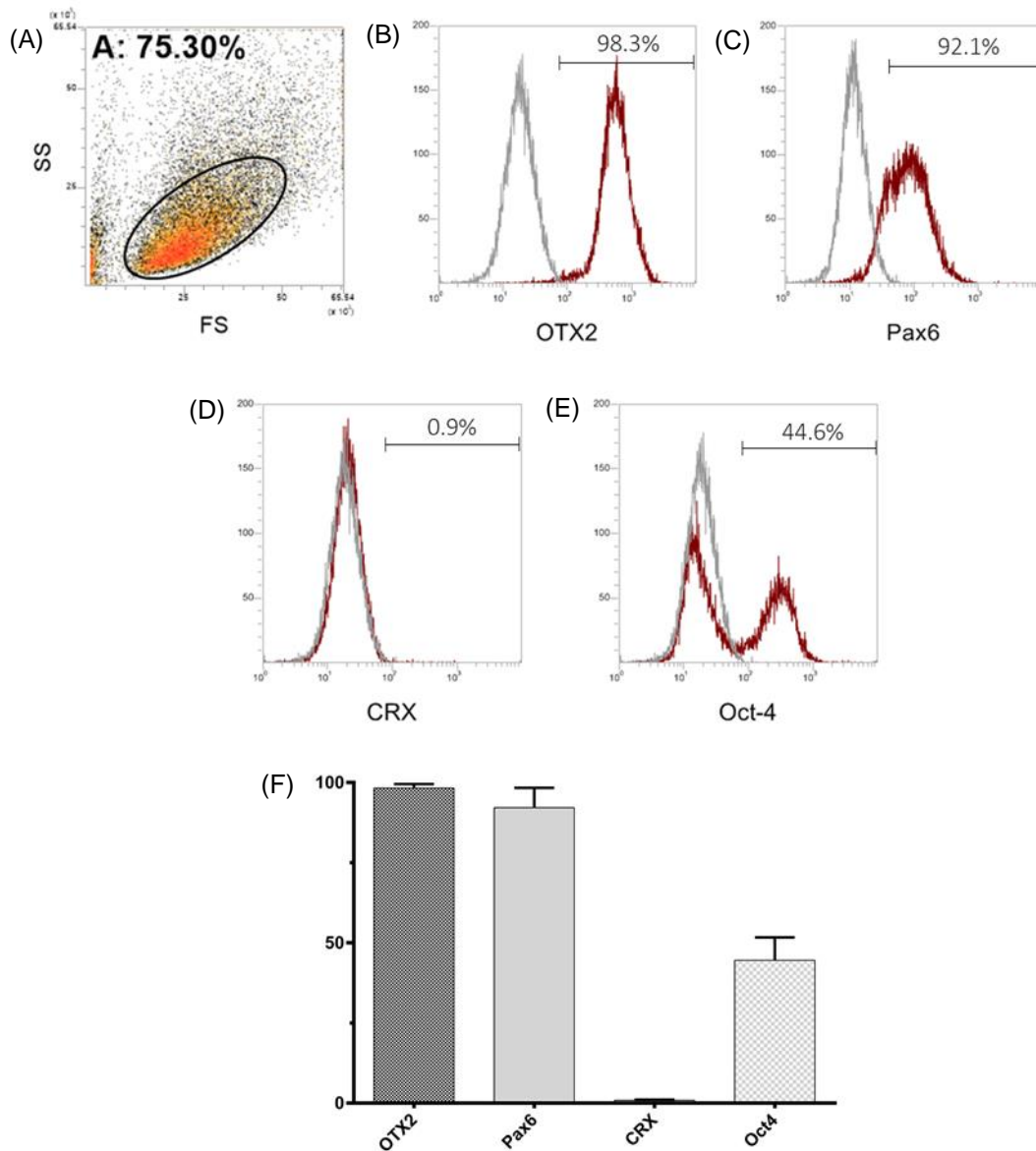
Figure 3.10 *Flow cytometry data of the early retinal markers OTX2 and Pax6, the photoreceptor marker CRX and a pluripotency marker Oct-4 after 1 week of adherent differentiation using AggreWell plated EBs with the improved retinal differentiation protocol. The gating strategy is detailed with a (A) SS v FS dot plot (gate A) to remove debris. (B-E) Each histogram then shows the negative population stained with an isotype control (grey) and the stained sample (red) with positive expression gated from the top 1% of the isotype control. (F) Bar chart of the expression found from the mean positive expression with 98.3%, 92.1%, 0.9% and 44.6% noted for OTX2, Pax6, CRX and Oct-4 in N=3 ± SD.*

High levels of OTX2 and Pax6 (98 and 92%) were noted showing cells are directed towards a retinal lineage (Figure 3.10). Low levels of CRX were as expected at this early of the differentiation, and around half the cell population still expressed the pluripotency marker Oct-4.

3.5.2 Dissociation of retinal differentiation

The dissociation step to produce a single cell suspension from day 31 retinal differentiation cultures was investigated further. The initial protocol tested detailed incubation with Trypsin/EDTA, however this was noted to leave large chunks of attached cellular material (Figure 3.11 A). Consequently, the use of TrypLE (Figure 3.11 B), or using a combination of manual scraping and enzymatic dissociation (Figure 3.11 C) was tested.
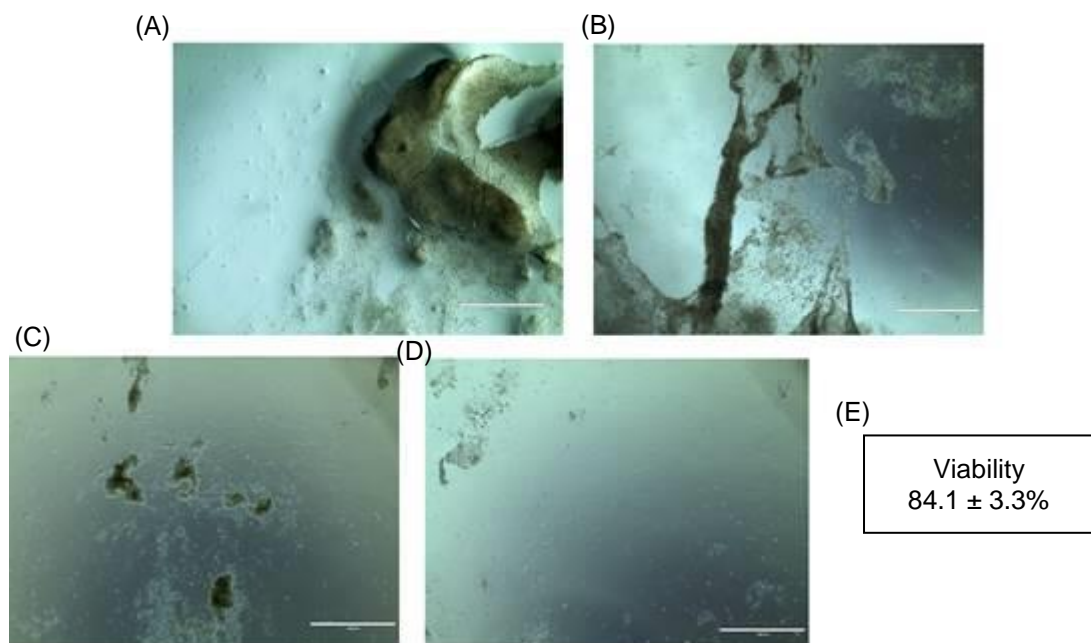
Figure 3.11 Dissociation of final week retinal differentiation culture by (A) 10 minutes in Trypsin/EDTA, (B) 10 minutes in TrypLE, (C) 20 minutes in TrypIE, or (D) a combination of TrypIE and manual scraping. (E) Cell viability after dissociating day 31 retinal differentiation cultures with a combination of TrypLE and manual scraping N = 10 ± SD.

Incubating cultures for 20 minutes in TrypLE detached more of the dense, multilayered material than with Trypsin, but a significant amount of cells remained attached. A combination of scraping using a fine tip pastette and TrypLE was then tested. Cultures were visibly more

thoroughly detached than with previous enzymatic only methods. Viability of the cell suspension was then assessed with trypan blue, and 84% of cells were viable after detachment.

As a further viability test, after dissociating retinal differentiation cultures, cells were counted and then re-seeded onto an adherent well plate (Figure 3.12). After approximately 24 hours, cells were trypsinised and viable cells counted. Viability was 97% and 75% of the cells seeded were recovered which suggests that cells maintain their viability. This is potentially an important finding for translation as progenitors must migrate and attach to a patient's damaged retina after injection into the sub-retinal space.
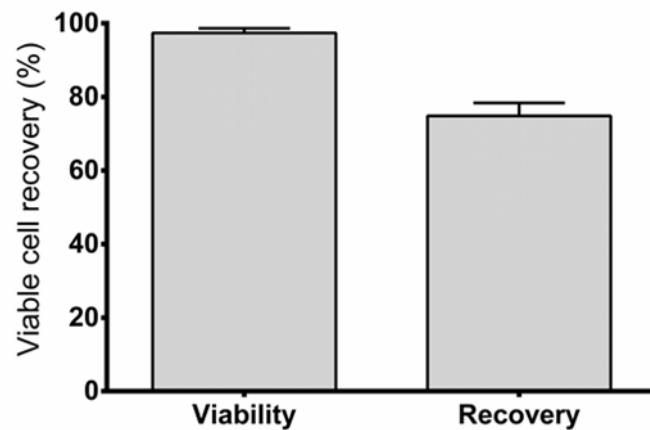
Figure 3.12 *Adherence test of dissociated day 31 iPSC retinal differentiation culture by counting, then re-plating cells for 24hours before viability and cell recovery was calculated. N = 5 ± SD.*

3.5.3 Improved photoreceptor production

While EBs are formed in AggreWell plates, the retinal induction media was changed daily until day three when EBs were plated onto Matrigel coated well plates and cultured adherently for a further 28 days.

To determine whether the improved protocol produced more progenitor photoreceptors than the initial protocol, CRX expression in the final population was evaluated. 35.7% of cells tested positive for the marker CRX, which calculates to over a 4-fold increase in comparison to the initial differentiation protocol (Figure 3.13). Additionally, with a standard deviation of 6 and a co-

efficient of variation at 19.5%, there is considerable lower variation between differentiation runs than previously noted.
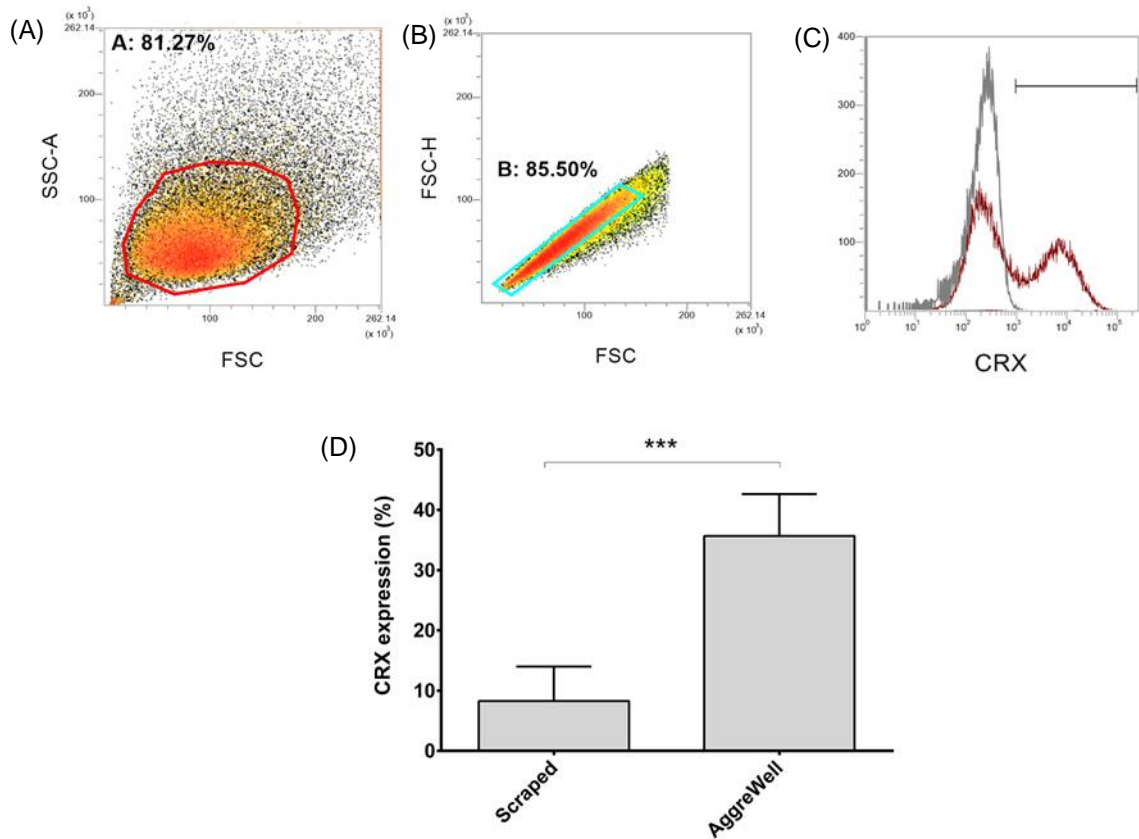
Figure 3.13 *Flow cytometry analysis of CRX expression from day 31 of the improved retinal differentiation protocol using AggreWell. The gating strategy is detailed with a (A) SS v FS scatter dot plot (gate A) to remove debris, and (B) FS height against area to remove doublets. (C) The histogram then shows the negative population stained with an isotype control (grey) and the CRX stained sample (red) with positive expression gated from the top 1% of the isotype control. (D) The bar chart is a comparison of CRX expression between the initial retinal scraped protocol vs the improved AggreWell differentiation protocol. A mean of 8.3% and 35.7% was noted in N = 4 and N = 6 ± SD for Scraped and AggreWell respectively. Significance was assessed through a two-tailed unpaired t test where P=0.0002.*

Although further optimisation could be possible through varying EB size, EB plating density or optimising the differentiation media composition, the current improvements are sufficient to

allow for progenitor photoreceptor cell sorting, which is the focus of this thesis. Future work may involve additional research into improving differentiation efficiency.

3.6 Scaling manufacture

To predict what manufacture scale is required for an autologous clinical therapy, an approximation of the final cell number is needed. From experimentally observed differentiation efficiencies and cell expansion, a starting pluripotent stem cell number can be estimated.

3.6.1 Clinical Scale

Currently, progenitor photoreceptor transplantation is in preclinical development and has shown much promise. As a result, an efficacious clinical dose size is still unknown but is an important consideration for translation. To estimate the scale, cell numbers of retinal pigment epithelium (RPE) from ongoing clinical trials can been used as a comparable therapy.

Table 3.1 *Assumptions and approximation of a clinical dosage (cell number) for transplantation*

Cell Type	Preclinical Dose Size (mouse models)	Clinical Dose Size
RPE	2.5×10^4 (Lu et al. 2009; Hambright et al. 2012)	2×10^5 (ClinicalTrials.gov Identifier: NCT02445612)
RPC	8×10^5 (MacLaren *et al.*, 2006)	6×10^6 (calculated)

The scale ratio between mouse and human dose size was estimated from the sub-retinal injection of RPE cells (Table 3.1). A ratio of 8 was noted and applied to preclinical retinal progenitor cell (RPC) transplantation, conducted by MacLaren et al. The result was an estimated scale of 6×10^6 cells per eye for injection.

Although there are many other factors affecting the dose size required for a progenitor photoreceptor treatment, such as the integration efficiency of cells (West *et al.*, 2012) or formulation and delivery method, a comparison to RPE clinical dose size can give an

approximation to determine the feasibility of scaling production. A more detailed analysis involving RP, such as what percentage of the human retina requires repopulating, may be necessary to improve processing assumptions. More recent studies detailing iPSC and ESC-derived retinal progenitor cells to restore visual function in mice (Barnea-Cramer *et al.*, 2016), and recent clinical data for iPSC-derived RPE transplantation (NCT02464956) will facilitate future work in this area.

3.6.2 Cell expansion

During the 31-day differentiation, cells will divide before they reach their post-mitotic state as progenitor photoreceptors. To quantify cell expansion, viable cell counts were conducted before and following differentiation and the difference calculated (Table 3.2).

Table 3.2 *Cell expansion during retinal differentiation in 12 well plates n = 23, ±SD.*

Starting iPSC/well	Final cells/well	Population Doubling
1.5×10^4	$5.6 \times 10^6 \pm 5.3 \times 10^5$	8.5 ± 0.14

A population doubling (PD) of 8.5 was found. Given that currently 35.7% of the final cell population express CRX (Figure 3.13), and approximately 6×10^6 cell are predicted for transplantation (Table 3.1), a starting iPSC population of around 2.4×10^4 would be required to produce 8.8×10^6 cells after differentiation. For this scale, a $75cm^2$ T-flask would facilitate manufacture of a single dose.

Although these differentiation calculations do not include additional cellular material for assays, variation of starting material – it's reprogramming or differentiation efficiency, or whether multiple doses would be required, it is still indicative to the scale required for a patient. In chapter 8 where an economic appraisal of the bioprocess is carried out, these additional considerations have been taken into account and discussed further.

3.6.3 Scaling progenitor production

In order to test the feasibility of scaling production, the retinal differentiation protocol was performed in 12-well plates, 6-well plates, T25 flasks and T75 flasks. Images were taken every other day during the full retinal differentiation, and morphological comparisons made at day 6, day 12, day 18 and day 24 in 12-well, 6-well and T75 flasks (microscopy images in Appendix B).

For each experiment, 1000 cell AggreWell-formed EBs were plated at a density of 7.5 EBs per cm^2 with 0.2ml of media per cm^2 (see Table 3.3). Media was changed on alternate days for all conditions using the improved retinal differentiation protocol. Although media was changed at the same time, it was noted that as evaporation rates varied with different surface areas, the volume of spent media removed fluctuated slightly depending on scale.

Table 3.3 *Seeding density and media volumes for retinal dissociation scale up experiments.*

	Area (cm^2)	EBs seeded	Media volume (ml)
12-well plate	4	30	0.8
6-well plate	9	68	2
T25 flask	25	188	5
T75 flask	75	563	15

Throughout differentiation, similar morphologies were observed for all tested scales. After plating, EBs spread in similar patterns to around 190µm at 6 days. At day 12, a monolayer covered the entire well or flask, and multi-layered structures spread from the core of initial plated EBs. From day 18, visually cell density appeared to increase comparably between each experiment, and similar spherical structures were formed.

Further work may include additional testing of different scales for comparability of CRX, NRL and other relevant marker expression. The specific growth rate at different scales could also be examined, with different initial EB seeding densities utilised. Finally, the use of different plastics or the positioning of EBs in well plates may have an impact on differentiation efficiency and could be tested.

3.7 Adherent differentiation Morphology

Cells were observed and imaged every other day during retinal differentiation. A time course analysis of the culture was created to investigate how cells grew and spread during adherent culture of EBs. Initially, EBs were plated at a density of 30 per well in a 12-well plate.
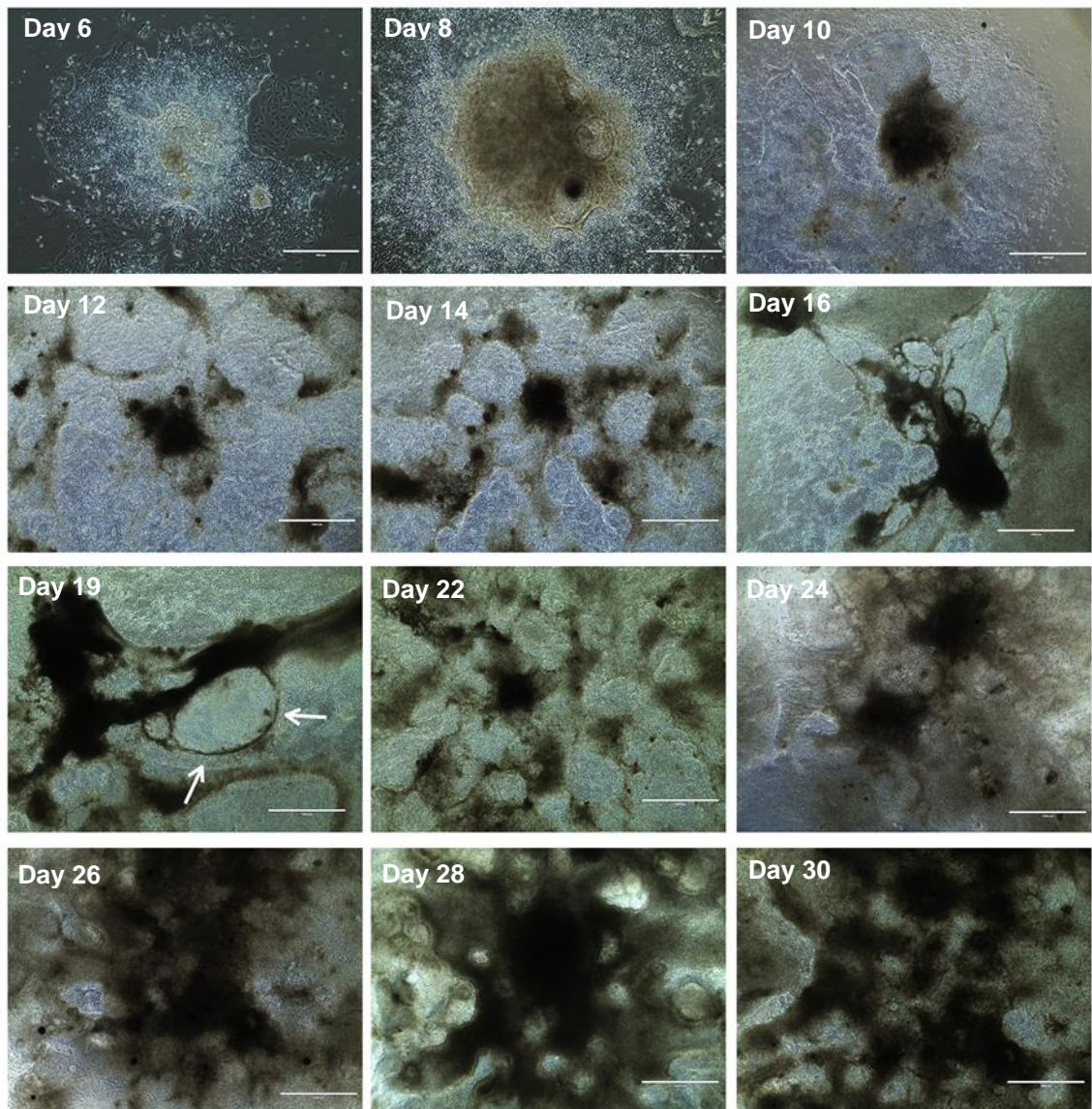
Figure 3.14 *Time course morphology analysis by microscopy of the adherent retinal differentiation of iPSC-derived 1000 cell EBs, processed with the improved retinal differentiation protocol. After plating EBs and commencing adherent culture on day 3, images were taken at*

day 6, 8, 10, 12, 14, 16, 19, 22, 24, 26, 28 and 30. The arrows highlight 'optic cup-like' structures. Scale bar = (A-B) 400µm or (C-L) 1000µm.

Once aggregates had settled and adhered, 1000 cell EBs spread to around 600µm in diameter. Over the 28-day adherent culture, a multi-layered dense cell network developed until the initial adhered EBs were almost indistinguishable. Additionally, similar morphologies to 'optic cup'-like structures with translucent zones surrounded by thin, circular bands were observed (as highlighted by the arrows in Figure 3.13). This may indicate the presence of surface ectoderm and lens fiber cell development (Hyer *et al.*, 2003; Wang *et al.*, 2010). However, further phenotype analysis would be required to conclude this.

3.8 Differentiation Product Analysis

By characterising the target cell population, it is possible to produce a more well define, safer product through a greater understanding of what the key process parameters are. When using stem cells as a source material, defining your product is even more importance due to potential tumorigenic material being present.

3.8.1 Visualising multilayer adherent cells

As seen in Figure 3.13, differentiation cultures on day 31 are dense, multi-layered formations which can be over 300µm thick. As standard microscopy, or even confocal microscopy, was unable to fully penetrate the opaquer areas, multiphoton microscopy was utilised to generate a three dimensional image of where CRX-positive cells were found within retinal differentiations.

The foremost observation was that CRX-positive cells were found in denser layers of the culture, specifically on the border between denser areas (where an EB had initially adhered) and spherical, 'optic cup'-like structures which appear around week 3 (as seen in Figure 3.14). Vertical bands of CRX-positive cells formed, running in waves through multiple layers from the base of the well up and across the culture (Figure 3.15).
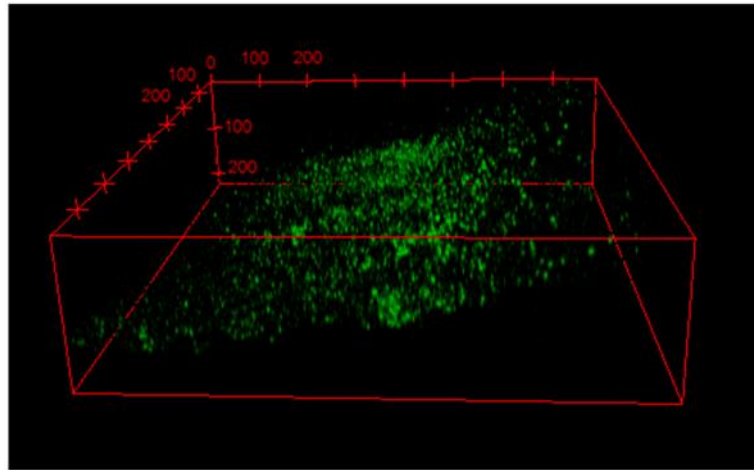
Figure 3.15 *Multiphoton confocal microscopy of immunostained CRX (green) in day 31 retinal differentiation cultures. 46 slices 5µm apart were taken through the culture and stacked together using ImageJ. The scale box is shown in red and is 800µm x 800µm x 225µm.*

By understanding how progenitor photoreceptors grow and the geographical environment within cultures that facilitates this, it may be possible to further optimise culture conditions and improve differentiation efficiency by examining surrounding cell types. Further characterising may lead to more knowledge over the microclimate that promotes the photoreceptor directed lineage.

3.8.2 Retention of pluripotency

A primary concern when using a pluripotent cell source is that the product may contain tumorigenic material. There are numerous reports evaluating the risk of tumour formation or other unwanted effects for medicinal products (Committee for Advanced Therapies (CAT), 2011; Herberts, Kwa and Hermsen, 2011). As such, it is important to know if pluripotent markers are still expressed at day 31 in the differentiation. Oct-4 is commonly associated with pluripotency with stem cell lines (Zhang *et al.*, 2014) and was tested on day 31 differentiation cultures. It is known to be one of the last pluripotency markers lost through differentiation (Karwacki-Neisius *et al.*, 2013) so is most likely to still be expressed.
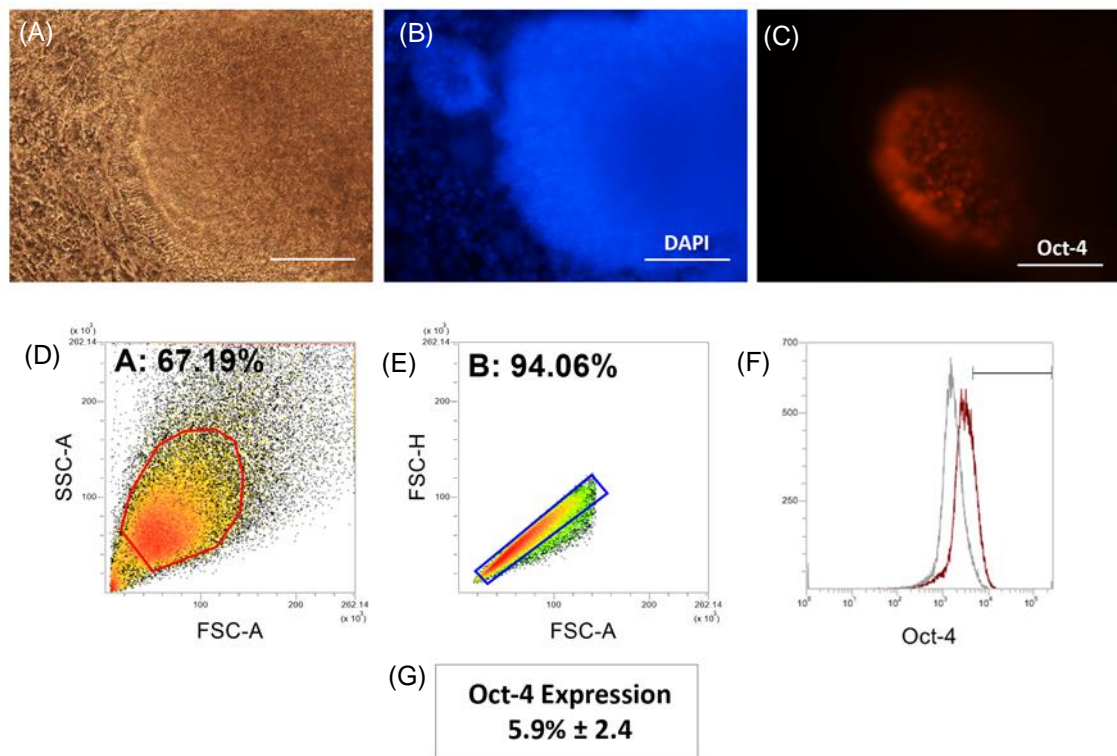
Figure 3.16 *Fluorescent microscopy of Oct-4 expression in day 31 retinal differentiation culture with (A) Phase contrast, (B) DAPI and (C) Oct-4 immunostaining. Scale bar = 50µm. Flow cytometry analysis was also used to quantify expression. The gating strategy is detailed with a (D) SS v FS dot plot (gate A) to remove debris then (E) FS height against area to remove doublets (gate B). (F) The histogram then shows the negative population stained with an isotype control (grey) and the Oct-4 stained sample (red) with positive expression gated from the top 1% of the isotype control. (G) A mean of 5.9% expression was noted in N = 10 ± SD.*

Positive staining for Oct-4 was observed in the majority of samples tested, which highlights the importance of purification before transplantation. Flow cytometry analysis was showed nearly 6% of cells expressed Oct-4 on day 31 (Figure 3.14). Although pluripotency cannot be linked to the expression of a single marker, noting Oct-4 expression is still a concern.

Further analysis may include broadening the panel of pluripotency markers tested, and assessing whether cells still possess the capacity for differentiation.

3.8.3 Defining the regenerative population

In addition to removing material that could differentiate into unwanted or dangerous cell types, it is important to positively isolate the regenerative population for improved efficacy. This is the progenitor photoreceptor population that, when transplanted into a damaged retina, can integrate and form a new functioning synaptic pathway to restore vision.

The definition of this population is currently limited by the expression of markers to distinguish one cell type from another. There are two commonly used transcription factors to identify these progenitors: CRX and NRL. The initial publication by MacLaren showing retinal repair used NRL to define the desired cell population for transplantation (MacLaren *et al.*, 2006). However, since then, many publications switch between CRX and NRL to select for progenitor photoreceptors (Lakowski *et al.*, 2010, 2011). Little analysis has been done to find the true regenerative population which can integrate into a retina and restore light sensitivity. What has been noted, however, is the variability of in vivo data using varied progenitor photoreceptor selection criteria (Tucker *et al.*, 2011; Zhou *et al.*, 2011; Klassen *et al.*, 2012; West *et al.*, 2012).
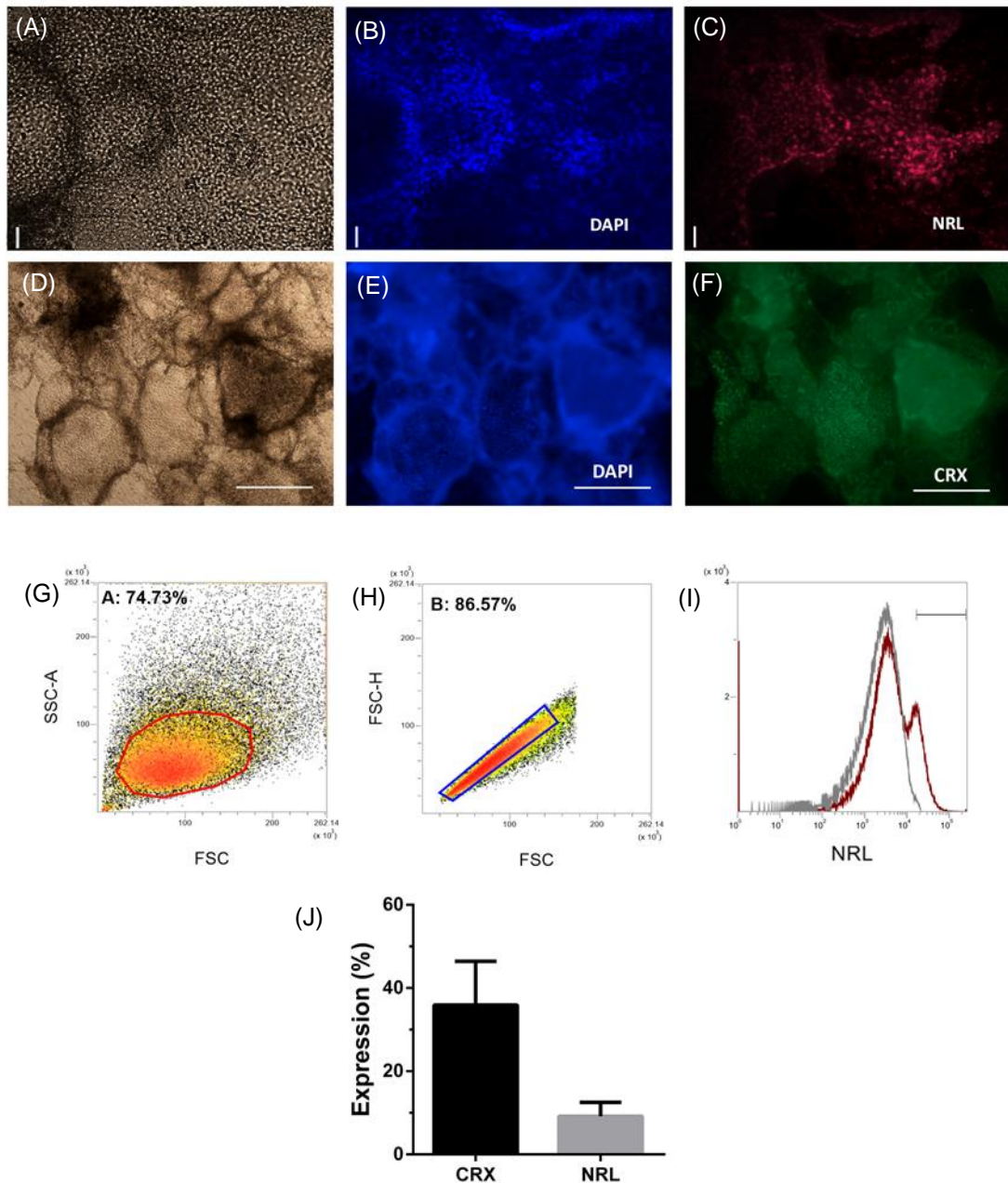
Figure 3.17 *Confocal microscopy of NRL expression in day31 retinal differentiation cultures with (A) Bright field, (B) DAPI and (C) NRL immunostaining. Scale bar = 56µm. Florescent microscopy of CRX expression immunostaining in day 31 retinal differentiation culture with (D) phase contrast, (E) DAPI and (F) CRX immunostaining. Scale bar = 250µm. Flow cytometry analysis of progenitor photoreceptor markers CRX and NRL in day 31 iPSC retinal differentiation cultures. The gating strategy is detailed with a (G) SS v FS dot plot (gate A) to remove debris then (H) FS height against area to remove doublets (gate B). (I) The histogram shows the negative population stained with an isotype control (grey) and the NRL stained*

sample (red) with positive expression gated from the top 1% of the isotype control. (J) Expression has been quantified and compared against CRX expression in a bar chart with a mean of 38.9 and 9.2 for CRX and NRL respectively. N = 11 (CRX) or 9 (NRL) ± SD.

Immunostaining of NRL and CRX showed positive expression of both markers in the final differentiated population (Figure 3.17), confirming the presence of progenitor photoreceptors. Again, to quantify expression levels, flow cytometry was chosen to determine what percentage of the target cell population was present at day 31. Interestingly, 38.9% of the population expressed CRX, while only 9.2% tested positive for NRL expression which correlates with previous literature findings (Lamba, Gust and Reh, 2009). This data also suggests that, based on progenitor selection criteria, different cell types would be isolated which will react differently in vivo (see previous literature references).

Co-expression analysis was also carried out on retinal differentiated cells. NRL was observed to almost unilaterally co-express CRX, whilst only 19% of CRX-positive cells co-expressed with NRL. This means that using NRL as a selection criterion would provide a specific sub-type of the CRX-positive population for transplantation (Figure 3.18).

(F)	CRX-positive population	
	NRL-positive (%)	NRL-negative (%)
	19.3	80.7
	28.4	71.6
	25.1	74.9
	Mean: 24.3	Mean: 75.7
	SD: 3.8	SD: 3.8

(G)	NRL-positive population	
	CRX-positive (%)	CRX-negative (%)
	99.8	0.2
	99.9	0.1
	99.9	0.1
	Mean: 99.9	Mean: 0.1
	SD: 0.1	SD: 0.1
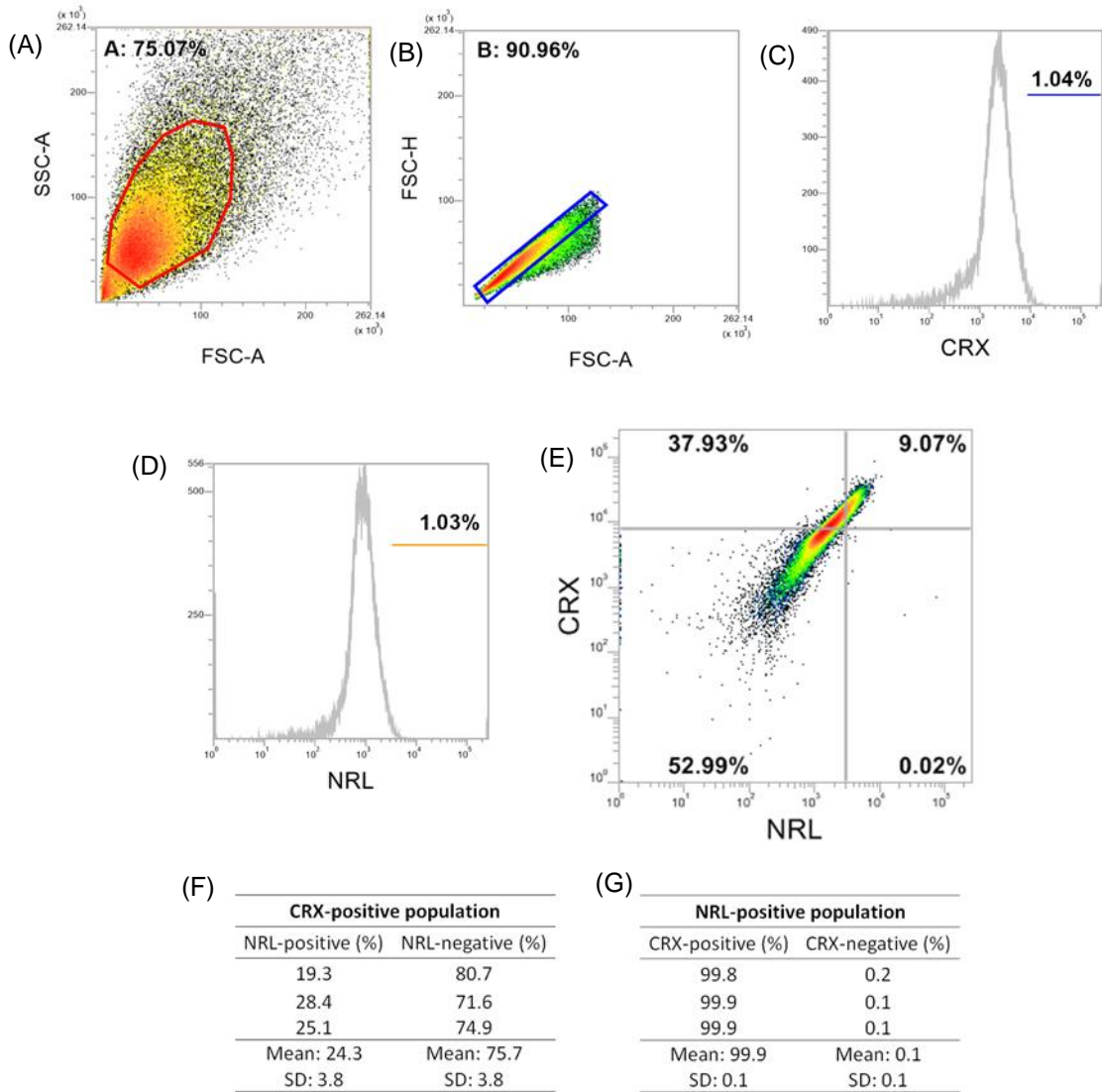
Figure 3.18 *Co-expression analysis of CRX and NRL in day 31 retinal differentiation cultures. The gating strategy is detailed with a (A) SS v FS dot plot (gate A) to remove debris then (B) FS height against area to remove doublets (gate B). (C,D) The histograms show the negative populations stained with an isotype control (grey) used to gated positive expression from the top 1% of the isotype control. (E) A dot plot showing co-expression of CRX and NRL, split into quadrants to illustrate positive/negative expression. The top right quadrant is CRX+/NRL+; the top left quadrant is CRX+/NRL-; the bottom left quadrant is CRX-/NRL-; and the bottom right quadrant is CRX-/NRL+. The Table inserts show a breakdown of the (F) CRX-positive cell population for NRL expression (+/-), and the (G) NRL-positive cell population for CRX expression (+/-) for N = 3, with each repeat shown as a separate row with the mean and SD below.*

There are three types of photoreceptors: rod and two types of cones, M and S. NRL is a basic motif-leucine zipper domain expressed in photoreceptors (Swaroop *et al.*, 1992; Swain *et al.*, 2001) and will dictate whether a rod or cone fate occurs. Low NRL expression produces either M or S cones, based on TRβ2 expression (Ng *et al.*, 2011). For rod cells, once a given threshold of NRL expression is reached, CRX will be expressed (Swaroop, Kim and Forrest, 2010) and these NRL-CRX cells will initiate rod differentiation. CRX is therefore expressed around 10.5 weeks after conception, and is critical for phototransduction (Furukawa *et al.*, 1999) and, with NRL, regulating rhodopsin transcription (Rehemtulla *et al.*, 1996; Mitton *et al.*, 2000). These biological distinctions within CRX and NRL development emphasise the difference in the cell type being selected for.

Although retinitis pigmentosa (RP) is associated with many different genetic mutations, autosomal dominant RP has been linked specifically to a novel mutation within the NRL gene (Bessant *et al.*, 1999; Martinez-Gimeno *et al.*, 2001). However, fifteen different mutations within the CRX gene have also been directly linked with retinal dystrophies (Bibb *et al.*, 2001). As a result, to select immature photoreceptors which will form functional photoreceptors after retinal integration, further research must be performed to distinguish the specific cell phenotype required. This may likely involve the use of multiple markers to select for the regenerative population – potentially a critical point for purification technologies which will be discussed later.

3.9 Shef3 differentiation

The production of progenitor photoreceptors was also investigated in a human embryonic cell line using Shef3. Prior work has demonstrated photoreceptors can be generated from Shef3 using the initial retinal protocol detailed in chapter 3.4, but has not been assessed using the improved retinal differentiation protocol, or in direct comparison to an iPSC bioprocess.

3.9.1 Differentiation Morphology

As with iPSC retinal differentiation, a time course analysis to observe morphological development throughout the adherent protocol was conducted. Cell cultures were imaged and images compiled together for Figure 3.19.
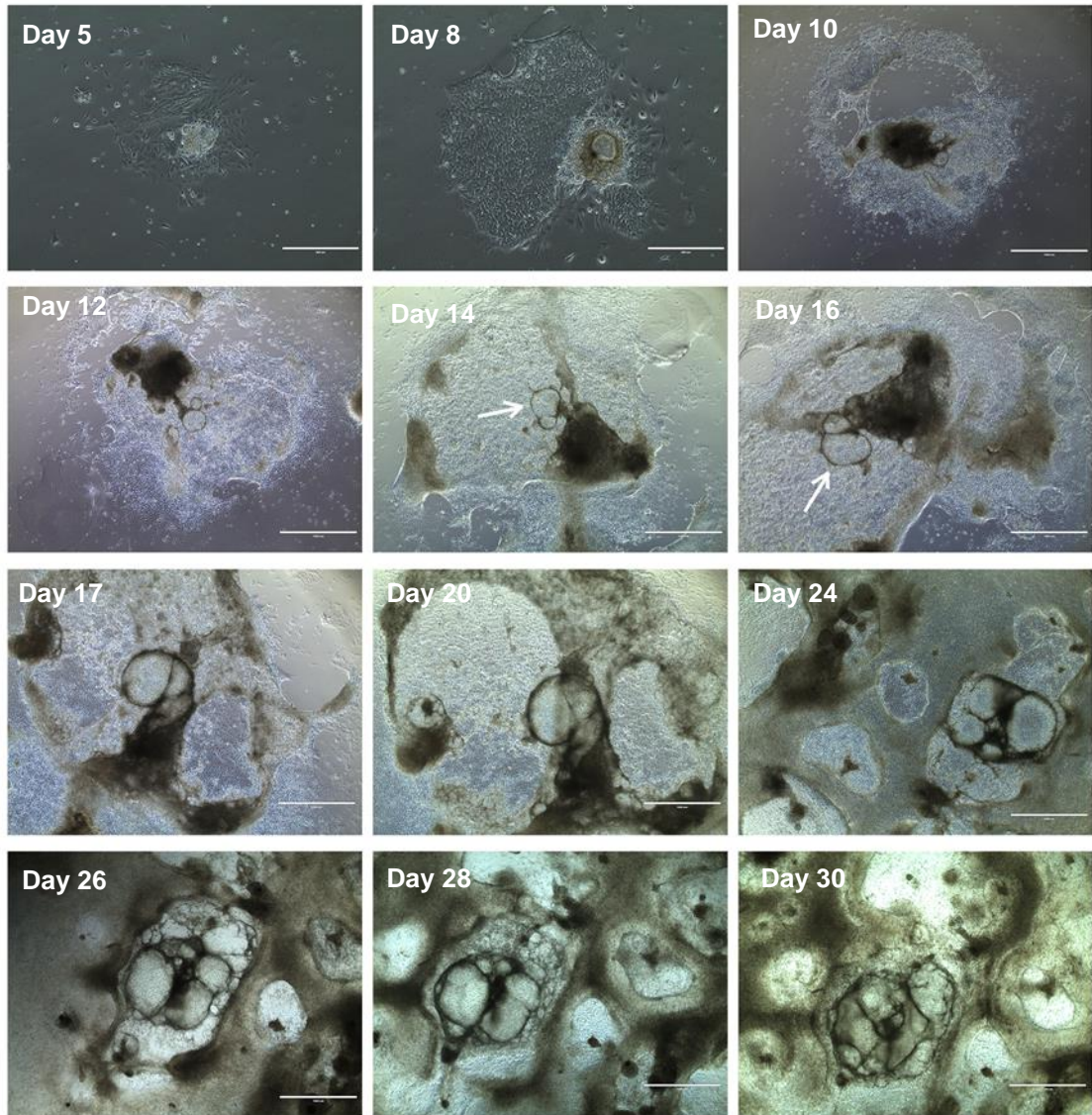
Figure 3.19 *Time course morphology analysis by microscopy of the adherent retinal differentiation of Shef3-derived 500 cell EBs processed with the improved retinal differentiation protocol. EBs were adherently cultured from day 3 and images taken on day 5, 8, 10, 12, 14, 16, 17, 20, 24, 26, 28 and 30. The arrows highlight optic cup-like structures. Scale bar = (A-B) 400µm or (C-L) 1000µm.*

Both 500 and 1000 cell EBs aggregated in AggreWell were tested. 1000 cell EBs after initial adherence spread to around 600µm in diameter, similarly to iPSC derived EBs. Over the retinal protocol, multi-layered dense cell populations were also noted, however, different morphological structures were observed. Spherical 'optic cup'-like formations occurred in week 2 compared to week 3 with iPSC (see arrows in Figure 3.19). On day 31, the final cell culture was not as uniformly, dense with more variation in cell density and structural formation. Further work may involve detailing the exact morphological and phenotypic variation between iPSC and hESC.

3.9.2 Differentiation Product analysis

The photoreceptor population on day 31 was also investigated in a same fashion as with iPSC retinal differentiation cultures. Flow cytometry analysis showed 20.9% CRX-positive cells present (Figure 3.20). Although slightly lower than with iPSC, there was no significant difference in expression as tested through a two-tailed unpaired t test. This result demonstrates firstly that photoreceptors can be reproducibly derived using the improved retinal protocol from two different pluripotent cell types, and secondly that significantly higher CRX-expression levels are noted than with Shef3 differentiation with the initial retinal protocol (Bae, 2011). As a result, the improved retinal differentiation protocol will be used to produce enough material to investigate downstream purification technologies.
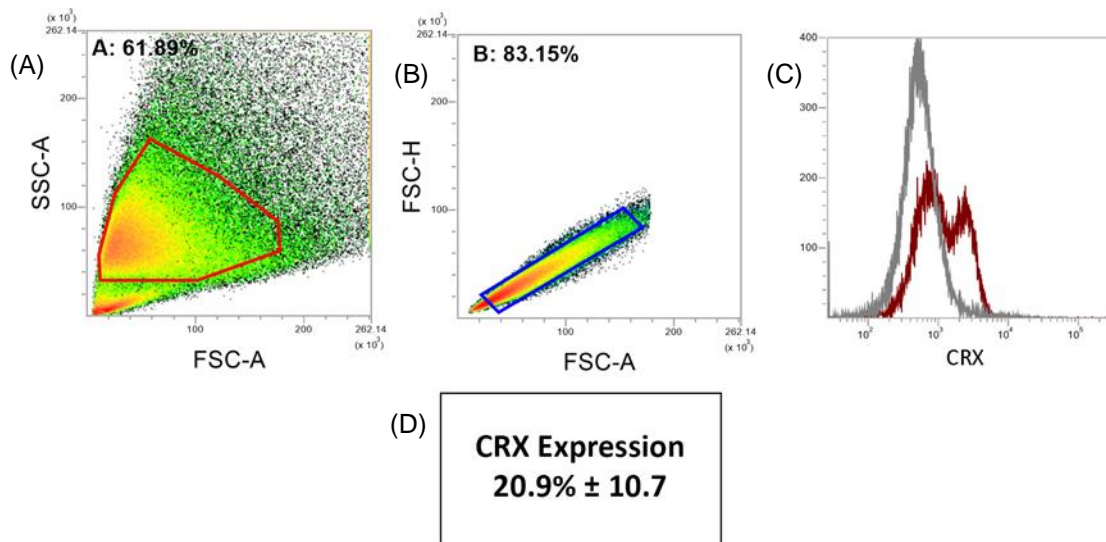
Figure 3.20 *Flow cytometry analysis of CRX in day 31 retinal differentiation cultures from Shef3 cells using the improved retinal differentiation protocol. The gating strategy is detailed with a (A) SS v FS dot plot (gate A) to remove debris then (B) FS height against area to remove doublets (gate B). (C) The histogram shows the negative population stained with an isotype control (grey) and the CRX stained sample (red) with positive expression gated from the top 1% of the isotype control. (D) A mean of 20.9% CRX positive cells was noted with N = 12 ± SD.*

3.10 Chapter Discussion

This chapter established a protocol for the retinal differentiation of progenitor photoreceptors from iPSCs to facilitate production of enough cellular material for downstream analysis. Improvements to the protocol focused on standardising aggregation and dissociation to improve differentiation efficiency.

The potential to derive progenitor photoreceptors from pluripotent stem cells provides an outlet from the limitations and complications associated with donor material for transplantation. Firstly, pluripotency within stem cell colonies was demonstrated and, using an initial retinal differentiation protocol from previous experience, the production of photoreceptors was confirmed. However, to be able to assess purification, a larger progenitor population is required. As a result, an improved retinal differentiation protocol was tested which utilised a controlled

aggregation step for EB formation using AggreWell plates. The improved protocol was found to produce 4-fold CRX-positive progenitors, and will therefore be used in continued experimentation to examine purification.

Scalability studies of the current bioprocess were also performed from well plates to T75 flasks. Similar morphological properties were exhibited at each scale, however a further assessment of differentiation efficiency and progenitor photoreceptor function would be required for validation. By approximating the number of cells required for an autologous human dose through comparisons with RPE clinical work, it was calculated that a T75 flask scale could derived enough photoreceptors for transplantation. This serves as an indication of the scaling challenges required for this autologous bioprocess, however there are other factors such as progenitor photoreceptor integration efficiency in vivo which also effect the required cell dose.

The importance of purification to the bioprocess was highlighted through selectivity of the regenerative populations, reviewing CRX and NRL as defining cellular markers and the removal of unwanted, potentially dangerous cell contaminants. From comparative data between NRL and CRX expression, it is evident that tighter definition of the regenerative population will be required to capture the true regenerative cells for transplantation.

The improved retinal differentiation protocol was also demonstrated using a human embryonic stem cell line, to ensure progenitor photoreceptors could be produced. Photoreceptors were produced, and with significantly higher CRX-positive cell numbers than observed with prior work using the initial retinal protocol.

The findings of this chapter confirm the successful manufacture of iPSC-derived progenitor photoreceptors at an experimentally relevant scale for downstream purification studies, and demonstrate that CRX can be used as a marker for sorting progenitor cells.

Chapter 4: Downstream Bioprocessing

4.1 Introduction

The production of progenitor photoreceptors has now been reproducibly demonstrated through the differentiation of hESC and iPSC pluripotent material. However, retinal differentiation results in a heterogeneous mixture of uncharacterised cell types that must be removed from a cellular product. Downstream processing is required to purify the regenerative target cells for transplantation.

4.1.1 Antibody-dependent purification

Currently, few clinically tested high resolution cell sorting methods exist which can isolate rare cell populations. Many cell therapies involve a low resolution apheresis step such as isolating white blood cells from blood by leukapheresis. However, if further purification is required to separate T-cells or haematopoietic progenitor cells for example, then either FACS or MACS will be used.

FACS and MACS are the current gold standard for affinity cell sorting (Wognum and Eaves, 2003; Wobus and Boheler, 2005). For FACS, target cells are labelled with a fluorescent tag that has been conjugated to a specific characteristic surface marker for the target population. Bound cells can then be isolated from heterogeneous suspensions by fluorescence (Figure 4.1A). Instead of a fluorescent marker, MACS uses 50nm paramagnetic beads as a method to bind and capture target cells. Once subjected to a magnetic field, target cells are held in place due to their bound paramagnetic beads (Figure 4.1B).
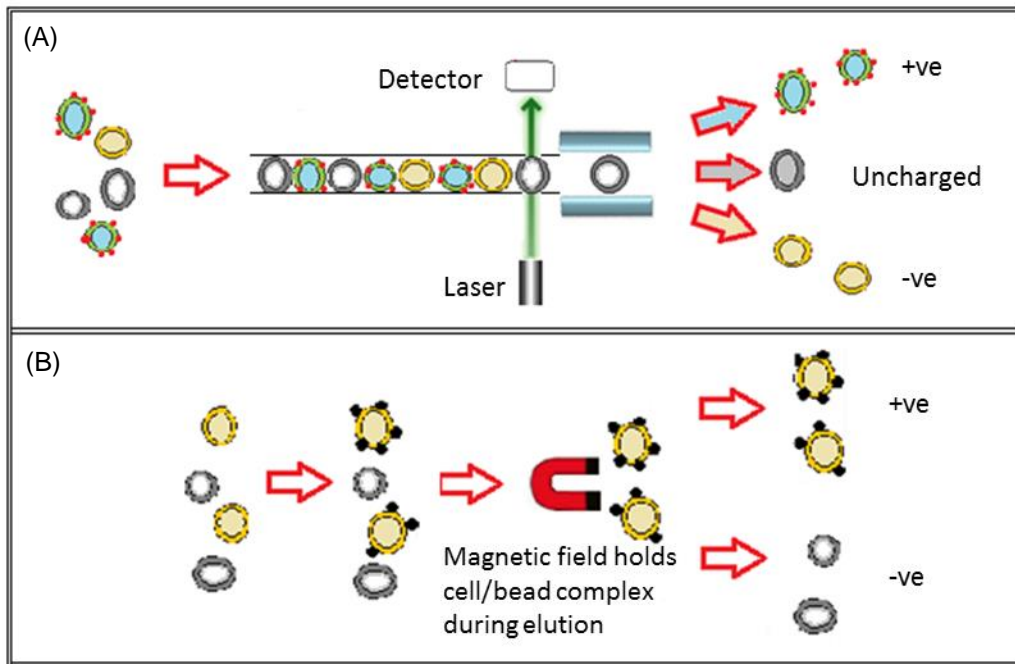
Figure 4.1 *Diagrammatic representation of antibody-dependent purification techniques. (A) FACS uses a fluorescent tag to identify target cells in a single cell interrogation system before sorting. (B) MACS requires paramagnetic beads to bind to target cells, which can then be held in place by a strong magnetic field for separation.*

Both FACS and MACS retain the purification-bound labels on the cellular product after sorting, which may present a problem for some clinical applications.

4.1.2 Selection markers

The specificity of antibody selection provides a method to separate precise cell types that are otherwise indistinguishable by their physiological attributes. However, this puts a lot of pressure on the selection marker (or markers) used to positively isolate target cells; especially for stem cell-derived products. These markers will define the cell population which is used as the final therapeutic product.

CRX and NRL are the two most common markers used to characterise progenitor photoreceptors (see chapter 1.9.2). Antibody-dependent purification methods have been used in a research setting by genetically altering cell lines to co-express a fluorescent protein with CRX and NRL to identify and sort progenitor photoreceptors (MacLaren *et al.*, 2006; Lakowski

et al., 2010). For a therapeutic application, however, transducing patient progenitor cells to fluoresce is impractical and adds significant cost and regulatory complications. Consequently, finding a surface marker which can distinguish progenitor photoreceptors is critical.

For progenitor photoreceptors, various markers have been tested, and one in particular – CD73 – has shown preliminary success (Koso *et al.*, 2009). Using CD73 to sort cell populations using either MACS (Eberle *et al.*, 2011) or FACS (Lakowski *et al.*, 2011) has selected positively for cells which can integrate into a retina.

4.1.3 CD73

CD73 is predominantly known for being a Mesenchymal Stem/Stromal Cell (MSC) marker, and is part of the International Society for Cellular Therapy (ISCT) criteria to define MSCs (Dominici *et al.*, 2006). CD73 is also expressed in fibroblastic cell types, endothelium and smooth muscle cells (See Figure 4.2).
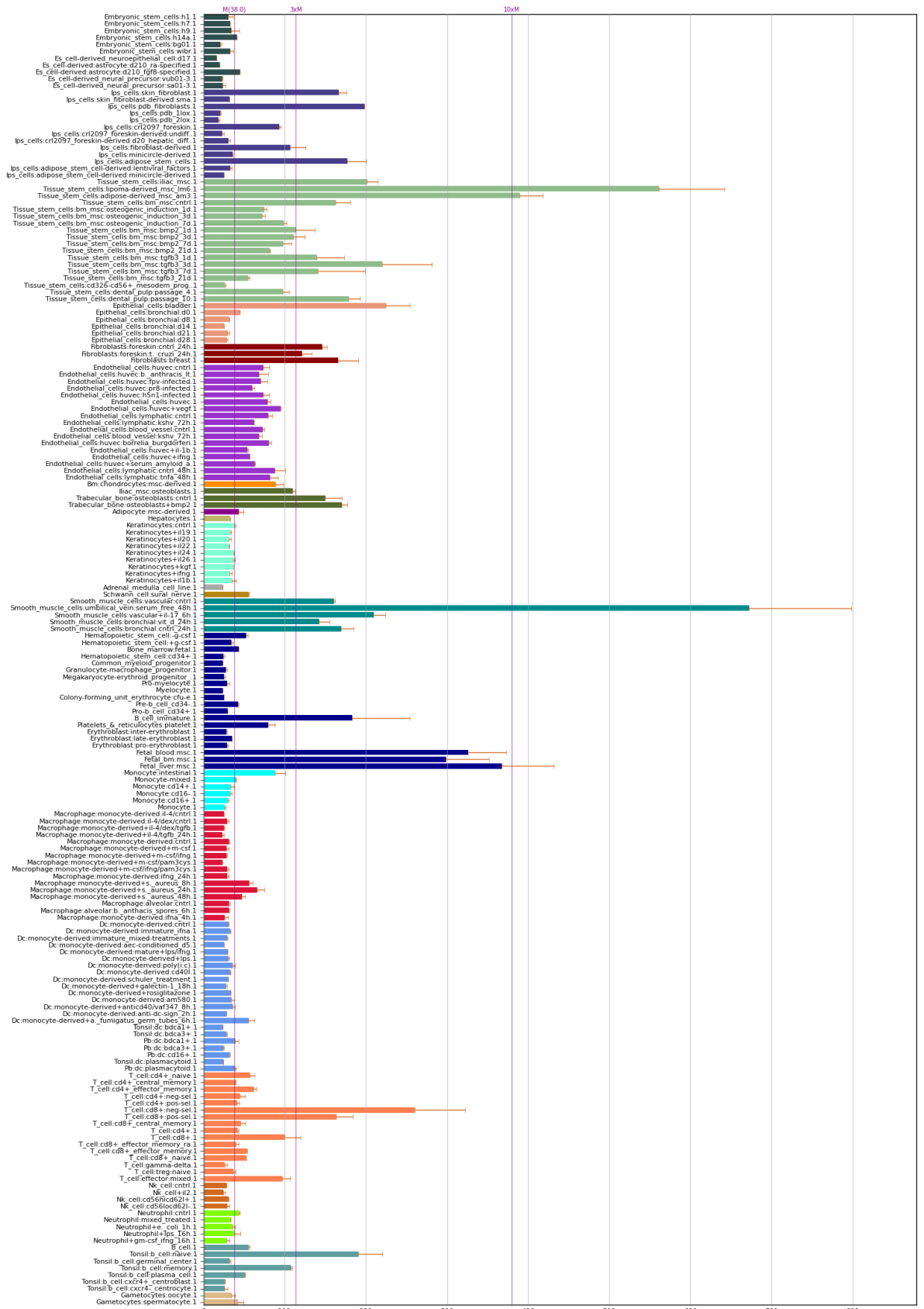
***Figure 4.2** Bar chart showing the different tissues and cells types related to CD73, as assessed using CD73 mRNA expression with high-density oligonucleotide arrays. The data set is from the Primary Cell Atlas, a meta dataset of 745 samples from different human primary cells studies. The figure is from BioGPS (BioGPS - Primary Cell Atlas, 2015).*

CD73 or NT5E is a 70-kDA glycosylphosphatidylinositol (GPI) anchored protein on the surface of cells that catalyses the conversion of 5'-adenosine monophosphate (AMP) to adenosine extracellularly (Zimmermann, 1992). Preliminary work has shown CD73 expression in cones-opsin mRNA from neonatal mice, but not in mature mice retinas (Koso *et al.*, 2009). As a result, it is hypothesised that CD73 is positioned genetically downstream of CRX and upstream of NRL in rod cell differentiation, and this is why it can be used as a marker for progenitor photoreceptors.

4.2 Aims and Hypotheses

4.2.1 Chapter Aim

Chapter 4 describes the characterisation and improvements made to downstream bioprocessing of the progenitor photoreceptor product. This involves the selection of a surface marker to identify and sort progenitor photoreceptors, and an evaluation of sorting characteristics and cell recovery using FACS and MACS affinity technology.

4.2.2 Hypotheses

Significant cell losses are predicted during sample preparation and cell sorting due to the number of processing steps, hold times and other limitations involved in current purification techniques. The sort purity is expected to be high for both FACS and MACS due to the specificity of antibody-dependent selection techniques.

4.3 CD73 expression

A common problem with isolating rare sub-populations is the method to identify target cells. In order to use CD73 as a selection marker to sort progenitor photoreceptors, expression in retinal differentiation cultures must be confirmed. To do this, immunostaining of day 31 retinal differentiation cultures was carried out. Confirming previously published data, CD73 positive expression was noted through fluorescent microscopy. Cultures were then co-stained with CRX or NRL to investigate the localisation of markers. Co-staining with CRX or NRL showed fluorescence grouped in the same areas as CD73 (Figure 4.3). Expression was seen in denser, multilayers zones throughout the differentiation culture.
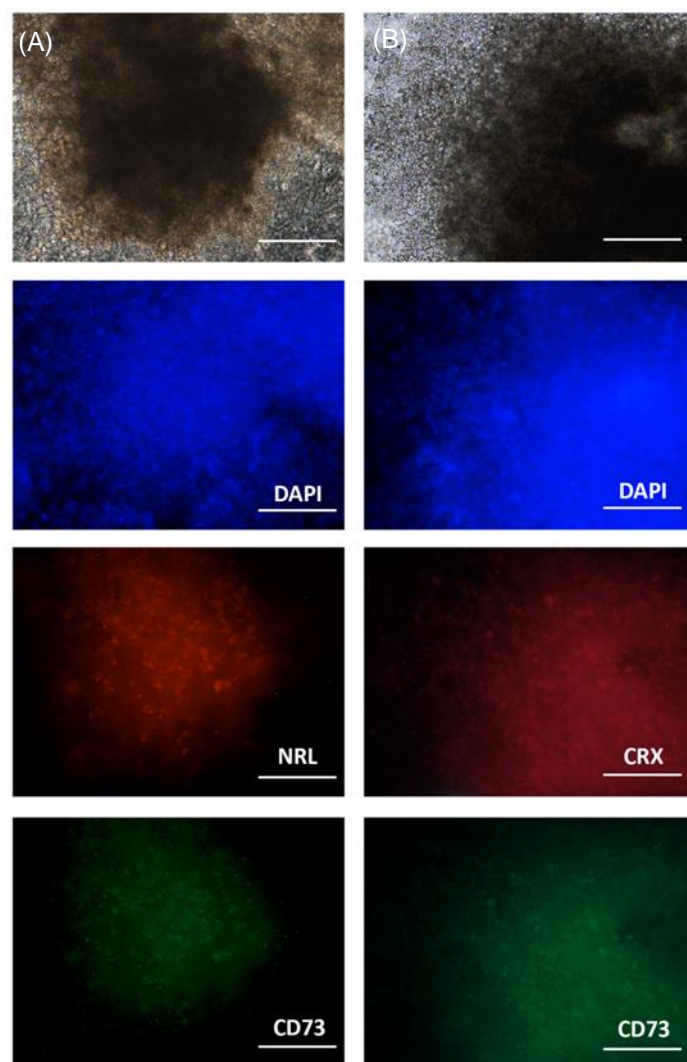
Figure 4.3 *Fluorescent microscopy of CD73 with a (A) NRL or (B) CRX co-stain in day 31 adherent differentiation cultures. Phase contrast, DAPI, CD73, NRL or CRX staining was performed. Scale bar = 50µm.*

Quantifying CD73 expression was performed with flow cytometry. While real time qPCR measures the amount of DNA or RNA present in a sample, flow cytometry will determine the percentage of a sample that expresses a target marker using protein expression. As antibody-dependent enrichment methods utilise surface proteins on a cell, this is the preferred form of analysis.

The initial retinal protocol and the improved differentiation protocol were both analysed for CD73 expression (Figure 4.4). A mean of 6.4% CD73-positive cells was found using the initial retinal differentiation protocol (comparable with 8.3% CRX expression in Figure 3.7), whilst a 5-fold increase was observed with the improved differentiation protocol: 32.2% (comparable to 35.7% CRX expression noted in Figure 3.15).
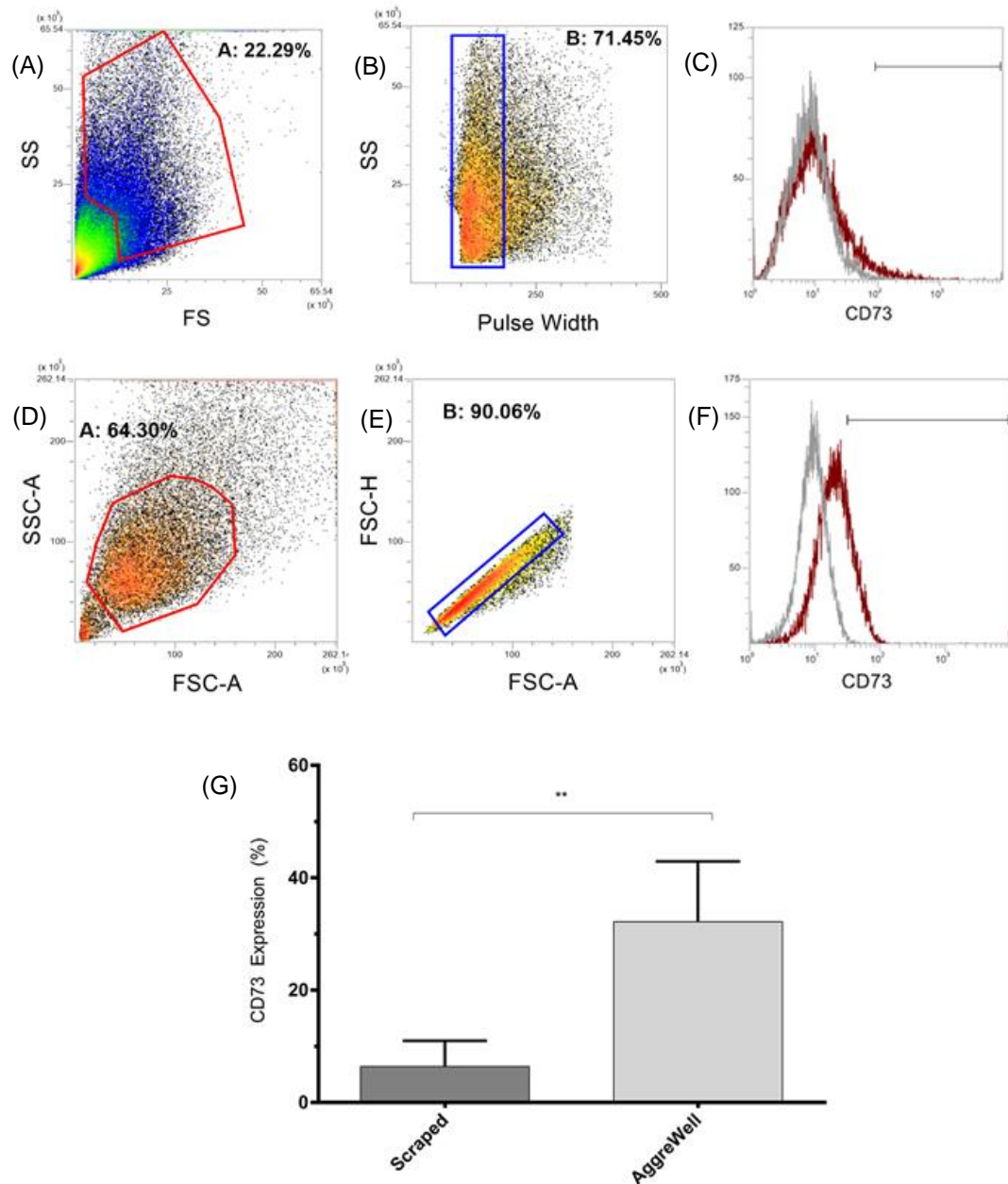
Figure 4.4 *Flow cytometry analysis of CD73 expression at day 31 of the initial retinal (Scraped) differentiation protocol and the improved (AggreWell) protocol. The gating strategies are detailed with (A, D) SS v FS dot plots (gates A) to remove debris then (B, E) pulse width or FS height against area to remove doublets (gates B). (C, F) The histograms show the negative population stained with an isotype control (grey) and the CD73 stained samples (red) with positive expression gated from the top 1% of the isotype controls. (G) Bar chart comparing CD73 expression from both protocols with a mean of 6.4% and 32.2% respectively. Significance was assessed through a two-tailed unpaired t test where P=0.0061 in N = 3 and N = 6 ± SD.*

This data confirms that CD73 is expressed in cells from the retinal differentiation, and improvements made to the differentiation protocol increase CD73 expression significantly. A similar percentage increase to the progenitor photoreceptor marker, CRX, suggests a correlation between both proteins.

4.4 Co-expression of CD73 in progenitor photoreceptors

To confirm that CD73 is associated with progenitor photoreceptors, an assessment of CD73 and CRX co-expression was carried out. Day 31 retinal differentiation cultures were sorted by FACS using CD73 as the selection marker, then the positively sorted populations stained for CRX to determine if both markers were co-expressed in cells. 94.6% of CD73-positive cells were found to express CRX (Figure 4.5). This confirms there is a strong link between two markers, as predicted from co-localisation observed through fluorescent microscopy. It therefore can be concluded that CD73 can be used as a cell surface marker for progenitor photoreceptor cells.
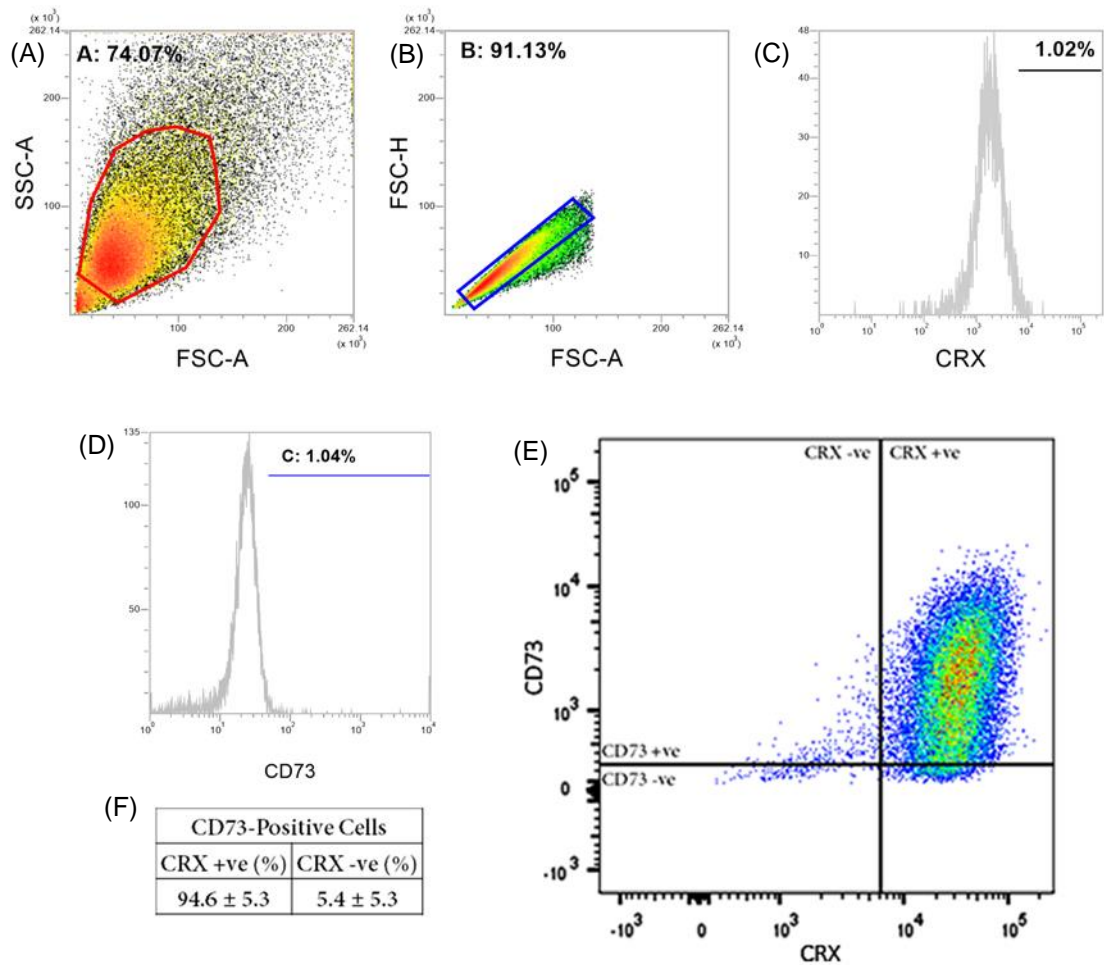
Figure 4.5 *Co-expression analysis of CRX and CD73 in day 31 retinal differentiation cultures. The gating strategy is detailed with a (A) SS v FS dot plot (gate A) to remove debris then (B) FS height against area to remove doublets (gate B). (C,D) The histograms show the negative populations stained with an isotype control (grey) used to gated positive expression from the top 1% of the isotype control. (E) A dot plot showing co-expression of CRX and CD73, split into quadrants to illustrate positive/negative expression. The top right quadrant is CD73+/CRX+; the top left quadrant is CD73+/CRX-; the bottom left quadrant is CD73-/CRX-; and the bottom right quadrant is CD73-/CRX+. (F) The Table insert show a breakdown of the CD73-positive cell population for CRX expression (+/-) for N = 6 ± SD.*

4.5 Evaluation of cell sorting

CD73 co-expression with CRX, is only the first key finding in assessing CD73's capacity for cell sorting. CD73 was used to positively sort progenitor photoreceptors, then feasibility assessed by flow cytometry. To determine if it can be used as a selection marker for progenitors, it must also be shown not to express on other undesired cell types.

4.5.1 CD73 sorting characteristics

An experiment was designed to investigate CD73 as a key marker to isolate progenitor photoreceptors, as shown in Figure 4.6. CRX was again utilised as the primary marker to identify target progenitor cells. Retinal differentiation cultures were sorted using CD73 as the selection marker by either FACS or MACS. The positively and negatively sorted cell populations (referred to henceforth as the 'cell product' and 'waste' streams) were then stained for CRX expression and analysed by flow cytometry.
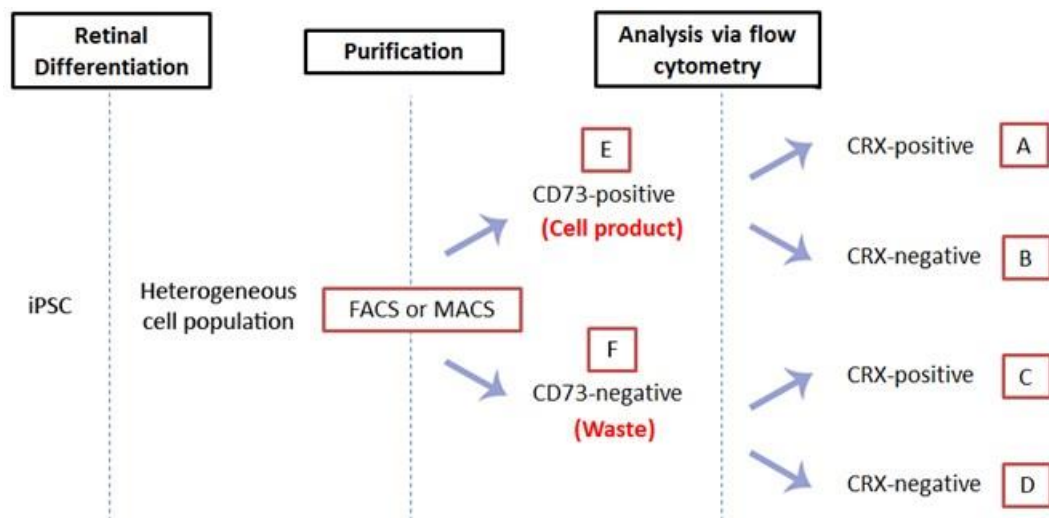
Figure 4.6 *Diagrammatic flowsheet detailing the experimental methods used to assess iPSC-derived CD73 sorted cell populations by FACS or MACS for CRX flow cytometry expression analysis.*

The data generated allowed the characteristics and efficiency of CD73 as a progenitor photoreceptor selection marker to be evaluated. By analysing the product and waste outputs, 93.4% and 94.6% of cells in the positive 'cell product' stream co-expressed CRX from MACS and FACS respectively (Figure 4.7). These values can define the sort purity, i.e. the number of

CRX-positive progenitors within the CD73-positive sorted population. As antibody-dependent separations have a high specificity towards their target antigen which minimises non-specific selection of unwanted cells, combined with the strong co-expression of CRX with CD73-positive cell populations (as shown in Figure 4.5), both purification methods tested performed as expected with high sort purities.
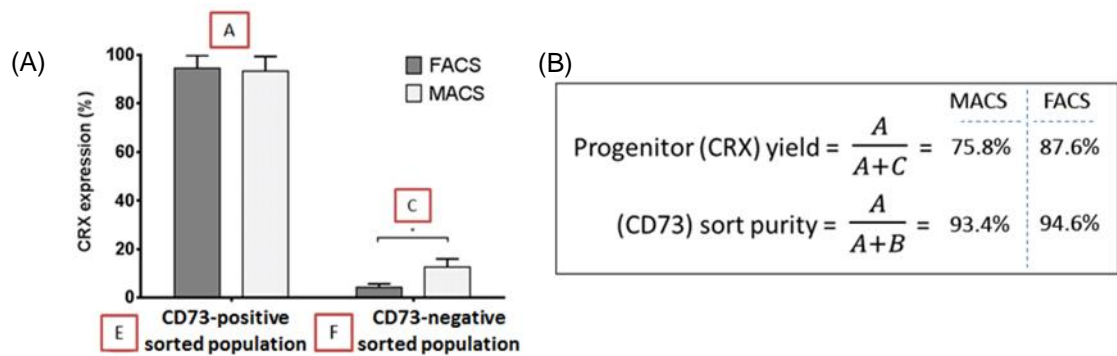
Figure 4.7 *CD73 cell sorting characteristics. (A) Bar chart comparing CRX-positive expression (%) following CD73 purification by FACS or MACS in the positively and negatively-sorted cell populations. Significance was assessed through a two-tailed unpaired t test where P ≤ 0.017 in N = 3 ± SD. The letters A to F refer to the experimental flowsheet in Figure 4.6. (B) The table insert is the equations and calculation of progenitor yield and sort purity for MACS and FACS. Progenitor yield is the percentage of CRX-positive photoreceptors recovered through a CD73-positive sort; sort purity is the percentage of cells within the CD73-positively sorted population which co-express CRX.*

However, a significant difference was observed in the percentage of CRX-positive cells in the negative 'waste' streams. 12.5% and 4.2% of the corresponding negative streams also co-express CRX in MACS and FACS (Figure 4.7A). These losses are due to a difference between cell populations expressing CD73 and CRX. When taking into account the cell numbers and quantifying this difference, a progenitor yield of 75.8% and 87.6% was calculated for MACS and FACS (Figure 4.7B). The progenitor yield describes the number of CRX-positive progenitor photoreceptors which are sorted by CD73.

MACS relies on a binary selection method where magnetically labelled cells are held in place within a powerful magnetic field, while remaining unlabelled cells are eluted as waste. As such, the degree of target protein expression is not a selection factor, and cell capture is dependent upon the induced paramagnetic force from attached MACS beads holding the cell in place. As FACS interrogates each event independently to assess cell size (forward scatter) and granularity (side scatter), a full spectrum of protein expression can be observed which permits very lowly expressing cells to be positively sorted. It is hypothesised that these low expressing CD73 cells result in FACS's higher progenitor yield.

The purity and yields observed through CD73 cell sorting also correspond with previously published data. Cell separations with MACS and FACS, predominantly using CD34, produce a consistently high purity over 90%, but yield fluctuates from 81% to 52%; comparable to the purity and yields presented here (Simmons and Torok-Storb, 1991; Handgretinger *et al.*, 1997; Bomberger *et al.*, 1998; Schumm *et al.*, 1999; Richel *et al.*, 2000; Martín-Henao *et al.*, 2001; Corsini *et al.*, 2002; Heß *et al.*, 2003; Tabilio *et al.*, 2004; Lang *et al.*, 2004; Ross *et al.*, 2009).

4.5.2 Cell recovery

As well as the progenitor photoreceptor yield through CD73 sorting, the final target cell population is also reduced from cells lost during processing. Through antibody staining, washing cells, and then running the sample through the sorter, cells are lost and apoptosis can be induced. The process to prepare and sort cells is detailed in Figure 4.8 B-C for FACS and MACS. Total viable cell number after cell sorting, as a percentage of the total starting cell number after dissociation, is termed the viable cell recovery.

(A)

(B) FACS Protocol
- Dissociate cells and count with trypan blue
- Quench
- Wash (centrifugation)
- Incubation with pre-conjugated antibody
- Wash
- Re-suspend in FACS buffer
- FACS sorting
- Cell count with trypan blue

(C) MACS Protocol
- Dissociate cells and count with trypan blue
- Quench
- Wash (centrifugation)
- Incubation with MACS beads
- Wash
- Re-suspend in MACS buffer
- Run through MACS column
- Cell count with trypan blue

Figure 4.8 *Viable cell recovery following FACS and MACS cell preparation and sorting of day 31 retinal differentiation cultures. (A) Bar chart showing the percentage of cells recovered after fluorophore or microbead binding and washing operations, then processing cells through a FACS machine or MACS column. A mean of 69.6% for FACS (N = 5 ± SD) and 58.7% for MACS (N = 4 ± SD) was found. The protocols for staining and processing (B) FACS and (C) MACS are shown in the table inserts.*

A low viable cell recovery of 58.7% and 69.6% was found for FACS and MACS following processing (Figure 4.8). This demonstrates that sample manipulation through labelling, washing and sorting results in substantial cell loss and correlates with published findings (Schmitz *et al.*, 1994; Gassei, Ehmcke and Schlatt, 2009). Additionally, although no significant difference was noted, the cell preparation and physical cell loss from processing cells through a FACS machine appears greater than MACS. Limited throughput of FACS due to single cell interrogations increase the processing time of samples, and will increase cell holding times. Additionally, low throughput limits operational feasibility at larger scales. The initial gating of samples, and to prevent air being injected into the machine, a small volume of cell suspension at the start and end of the process must be sacrificed. In comparison, MACS operates in a batch system where cell samples are separated in a column. Operational times are reduced and shear stress is minimal. However, the staining and washing of samples still results in high cell losses.

4.6 Validating CD73-positively sorted populations

As discussed previously, CD73 is also expressed on many other tissues, most commonly being associated with MSCs. Although co-expression with CRX is a strong indicator, to confirm that

incorrect cells are not being selected for, an MSC phenotyping kit was tested on CD73-positive cell populations after sorting. ISCT criteria specifies over 95% expression of CD105, CD73 and CD90 to classify as an MSC (Dominici *et al.*, 2006). CD73 FACS sorted day 31 retinal differentiation cultures were tested by flow cytometry for CD105 and CD90 expression and showed minimal expression. As a result, it was concluded that CD73 is an efficient cell surface marker to identify and isolate progenitor photoreceptors.

4.7 Chapter Discussion

As part of the bioprocess of cellular products, affinity purification provides a method to select for rare cell populations which otherwise may be morphologically of physically similar to other process impurities. This chapter investigated CD73 as a selection to identify and differentially isolate progenitor photoreceptors from a heterogeneous cell population, as well detailing the process characteristics and cell losses from FACS and MACS.

Progenitor photoreceptors are currently defined by transcription factors, found intracellularly within the nucleus. To enable separation using antibody-dependent cell sorting, a surface marker must be found which can differentially bind the target progenitors. CD73 was observed to be expressed within retinal differentiation cultures and be grouped with CRX and NRL expressing cells. Further investigation showed that 94.6% CD73-positive populations co-expressed with CRX suggesting a strong correlation with progenitor photoreceptors.

CD73 sorting with FACS and MACS was then assessed to determine the purity and yield. Both techniques produced a high purity above 90%, and similar but lower progenitor yields of 75.8% and 87.6% respectively. Due to the high selectivity of antibody binding and co-expression between CRX and CD73, a high purity was expected. The reduced progenitor yield highlights that a percentage of the target population does not express CD73. As a result, future analysis may involve the selection of multiple markers to define the target cell population. However, both MACS and FACS leaving cellular labels bound to target cells following purification which may complicate the bioprocess.

Viable cell recovery through MACS and FACS was also assessed, and a recovery of 69.6% for FACS and 58.7% for MACS noted. Due to the multiple processing steps required to label and wash cells via centrifugation pre-sorting, large cell losses were observed for both current purification methods. Being able to minimise cell processing and mitigate product manipulation by removing cell labelling would be a key advantage in relation to scalability, purification cost and cellular recovery. Combining the high purity of affinity binding whilst reducing the amount of cells lost through the bioprocess is beneficial.

Chapter 5: Affinity SpheriTech bead manufacture

5.1 Introduction

There are various translational challenges and operational limitations to FACS and MACS. These include the retention of cellular labels after purification which can cause cytotoxic effects (L'azou *et al.*, 2008), and processing challenges such as low viable cell recoveries and variable progenitor yields. As a result, a label-free novel affinity purification method was assessed with SpheriTech beads.

5.1.1 Polymer beads

SpheriTech beads are rigid lipophilic supports, created by crosslinking sebacic acid and poly-Ɛ-lysine. Crosslinking is the process of connecting two bonds together on a polymer chain. By controlling the amount of sebacic acid that links chains together, the flexibility and strength of the polymer can be controlled.

The cross-linked polymer is then mixed within an immiscible solvent before polymerisation. By adding the polymer to solvent, individual droplets can be created through agitation. Once the desired composition and size of droplets is achieved, the addition of a polymerising agent (EDCI) will initiate the reaction and form stable polymer beads.

For affinity purification, the beads are functionalised by converting surface free amine groups to carboxylic acids which activate the polymer to react with a protein, polyclonal or monoclonal antibody. This means that CD73 can be covalently immobilised onto the surface of beads to facilitate affinity cellular binding.

SpheriTech beads can be manufactured buoyant and/or paramagnetic. To create buoyant beads, hollow microparticles are mixed into the aqueous solution of poly-Ɛ-lysine before polymerisation. The ratio of hollow microparticles to polymer can be controlled to define the bead density required. To manufacture paramagnetic beads, superparamagnetic iron oxide nanoparticles are dispersed within the aqueous polymer mixture before polymerisation. Iron

oxide is homogeneously distributed through the beads; the amount added to the solution will control the strength of paramagnetism. These features allow the manipulation of beads via fluidic or magnetic forces. When dealing will cellular products, gentle external manipulation of beads could be a significant processing advantage.
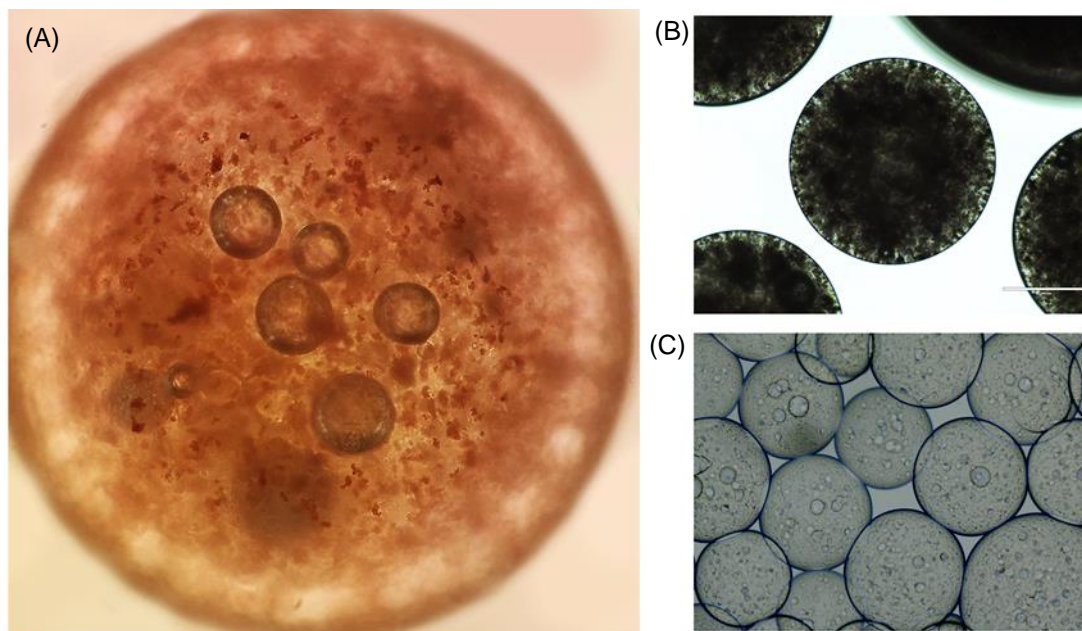
Figure 5.1 *Microscopy images of SpheriTech beads. (A) Bead with 1g iron oxide and hollow microballoons; (B) Beads with 2g iron oxide only; (C) Beads with hollow microballoons only.*

5.1.2 SpheriTech bead manufacture

To create polymer beads, an aqueous solution containing poly-Ɛ-lysine, sebacic acid, N-Methylmorpholine (to facilitate dissolving) and Span 80 (a detergent to aid droplet formation) is dissolved in water and mixed/dispersed within an immiscible solvent such as dichloromethane (DCM) or toluene. Agitation within the solvent creates droplets of the aqueous solution which form beads when polymerised. The rate of agitation, geometry of the vessel, and flowrate that the aqueous solution is added will impact the diameter and heterogeneity of the beads. The activating agent for polymerisation is EDCI and, similarly to the polymer, bead diameter and uniformity will be affected by how the powder is added and at what rate. To produce buoyant paramagnetic beads, hollow microballoons and iron oxide are added to the aqueous phase before dispersion in a solvent.

Before SpheriTech beads can be characterised and used for cell purification, the manufacture process must be assessed for reproducibility and feasibility.

5.1.3 Antibody immobilisation

By altering the surface chemistry of polymer beads, proteins or antibodies can be immobilised onto the bead's surface. For an affinity separation, bound antibodies are used to target specific cell surface receptors and separate desired cell types.
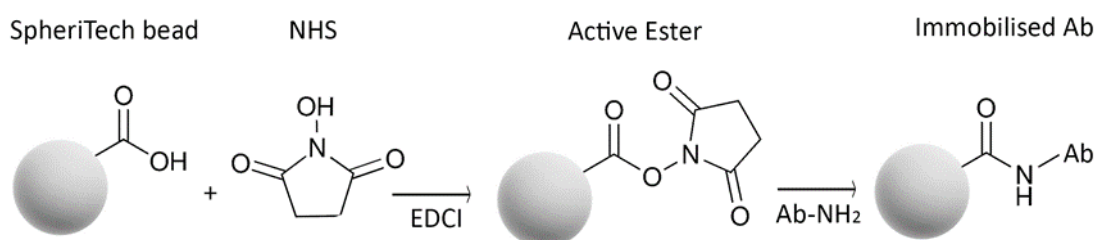
Figure 5.2 *Two-step carbodiimide reaction of antibody amine coupling to SpheriTech beads*

A carbodiimide reaction will couple poly-ε-lysine beads and antibody together through amine bonds. Carboxyl functional groups (-COOH) on the bead's surface are activated by EDCI to form an active O-acylisourea intermediate. NHS (N-hydroxysulfosuccinimide) is used to stabilise the intermediate and form an active ester. This then reacts with primary amines (-NH2) on the antibody to form a covalent bond (Figure 5.2).

CD73 monoclonal antibodies will be immobilised onto SpheriTech beads to allow binding of progenitor photoreceptors. Enough antibody must be immobilised to bind cells and maintain a connection during elution and washing steps to remove unwanted cell types. However, using too much antibody will increase the processing cost and may complicate the detachment of target cells after separation. Consequently, a balance is required to produce an economical and efficient binding process.

5.1.4 Iron oxide paramagnetism

The ability for materials to form an internal magnetic field when in contact with an external magnetic field is called paramagnetism. Paramagnetism provides a cheap and simple method to manipulate the movement of beads in situ, without the need for contact. By controlling the amount of iron oxide added into the aqueous polymer solution, the paramagnetism of beads can be varied. As with immobilising antibody, a balance between the addition of enough iron oxide to induce paramagnetism in beads, whilst not using excess to increase the chance of leachables or prevent bead buoyancy must be found.

5.1.5 Buoyancy

SpheriTech bead buoyancy is generated through the inclusion of hollow microballoons into the initial aqueous polymer solution. By controlling the amount of balloons, beads can be manufactured to float, sink or be held in suspension under a desired flowrate. Unlike expanded bed chromatography (EBA) where high flowrates are required to suspend beads, flowing against gravity to hold buoyant beads in suspension can be operated at much lower flowrates.

The combination of paramagnetism and buoyancy necessitates a controlled mix of both additives to produce the density and paramagnetism capabilities required. To assess this, both characteristics must be individually assessed, then their combined outputs investigated. Due to resource and time limitations involved in creating a homogeneous mixing regime for syringes, characterisation of buoyancy and paramagnetism was conducted on beads manufactured with the STR method that have been filtered to remove diameters outside the standard deviation.

5.2 Aims and Hypotheses

5.2.1 Chapter Aim

Chapter 5 introduces a novel purification technology with SpheriTech beads. The bead manufacture process is critiqued, and a novel production process created to improve uniformity of the beads generated. Additionally, a characterisation of SpheriTech beads is provided,

focussing on antibody immobilisation and the addition of iron oxide and hollow microballoons to induce buoyant and paramagnetic properties. The recommended antibody density to immobilise onto beads is assessed to prevent the waste of expensive protein. The individual and combined impact of paramagnetism and buoyancy is then evaluated through a variety of techniques.

5.2.2 Hypotheses

The initial bead manufacture process will produce heterogeneous batches of SpheriTech beads due to the lack of control over reagent addition and inadequate control of polymerisation. Uniform, homogeneous beads can be produced at high throughput by the creation of a continuous bead manufacture process using microfluidic technology and a greater degree of control over operating parameters. Paramagnetic and buoyant beads can be generated using polydispersed iron (III) oxide and hollow microballoons, added during manufacture.

5.3 Reactor manufacture

SpheriTech beads are produced by dispersing a water-soluble suspension within an immiscible solvent buffer to create droplets which can be polymerised. Beads were initially manufactured in a stirred tank reactor (STR) following a patent belonging to SpheriTech (SpheriTech, 2014). The reactor was filled with 0.5L of DCM and the aqueous polymer solution pumped in using a peristaltic pump. Agitation using an impeller formed immiscible droplets. Once these droplets are formed and the reactor equilibrated, EDCI as a powder was added to initiate polymerisation.

Throughout experimentation, various iterative improvements were made from this initial protocol:

1. Toluene is an insoluble mono-substituted benzene derived hydrocarbon, commonly used as a solvent for paints, adhesives and disinfectants. Different solvents are known to impact the nature of polymerisation such as activity, homogeneity and syndiospecificity (Volkis *et al.*, 2005), and as such, toluene was selected as the solvent

instead of DCM as aqueous droplets (before polymerisation) were more stable allowing more uniform, spherical beads to be produced.

2. Powders are comprised of heterogeneous angular clumps which are all different sizes with different surface areas to contact the aqueous phase. As such, it is not sufficient to create uniform aqueous droplets through the use of toluene, but initiate polymerisation in an uncontrolled method through the use of a powder. Consequently, the addition of the polymerisation activating agent (EDCI) was changed from scooping in a powder to dissolving EDCI in DCM and pumping the suspension into the reactor. This provided greater control over reaction kinetics by creating a uniform, constant concentration of EDCI to be inputted. Of note, EDCI is not soluble in toluene so DCM was used for to produce the suspension.

3. Mixing inside the reactor is critical to generate a homogeneous environment for polymerisation and, as a result, homogeneous polymer beads. Baffles are panels or intrusions inside a reactor to disrupt flow patterns and promote mixing of fluids. Baffles were added to the reactor to improve the mixing regime, and also the reactor geometry altered from spherical to a more typical stirred tank reactor design for the same purpose.

4. Additionally, to aid mixing, the single tier foldable Rushton impeller was changed to a Visco jet agitator. Rushton impellers promote radial mixing with incurred high shear stress. This is not ideal for bioreactors where axial flow is critical to maintain a homogeneous fluid. The geometry of the Visco jet impeller is designed to promote high-momentum mixing whilst operating at low laminar flowrates, through the cone's design to accelerate fluid and create turbulence at the exit through pressure build up at the cone's entrance. This provide short mix times with low motor power requirements for tanks with large volumes.

5. Previously undefined, an optimal impeller speed of 600rpm was determined through experimentation. This provide a quantitative measure of agitation which can be controlled and optimised for the desired mixing regime.

6. For paramagnetic beads, the <5 µm iron (II) oxide powder initially used was changed to iron (III) oxide with an APS of 20-40nm. This change in iron oxide will be discussed in

greater detail in chapter 5.6. Iron (III) oxide is non-toxic to cells and requires a lower mass of iron to produce the same paramagnetic effect as the iron (II) oxide used which further reduces risk.

7. Buoyant beads are generated through the addition of hollow microballoons. In order for the microballoons to integrate more efficiently into polymer beads, hollow microballoons were pre-treated with hydrochloric acid (HCL) making them more hydrophilic to facilitate polymer integration.

Characterisation data presented forthwith will use this updated reactor manufacture process with the improvements stated above. Further details of the manufacture process are described in Chapter 2.8.1 of materials and methods.

5.3.1 Size distribution

To characterise beads from STR production, bead diameter was measured as the primary output. A particle size analyser was used to determine bead diameter through laser diffraction. Light scattering and angular variation was used to calculate the volume of particles, then volume converted into an equivalent spherical diameter. Reactor manufacture produced beads from 251μm to 1386μm in diameter; a range of 1135 μm with a median of 435 μm (Figure 5.3).

A large number of bead fragments were also present after manufacture. High shear from the impeller and heterogeneity before and during polymerisation of aqueous droplets is believed to cause this. To validate the assumptions used in the particle size analyser, diameter measurements through microscopy were also tested. Beads were suspended in PBS in a single well dish, before phase contrast images were taken and processed using ImageJ to determine the Feret diameter and circularity.
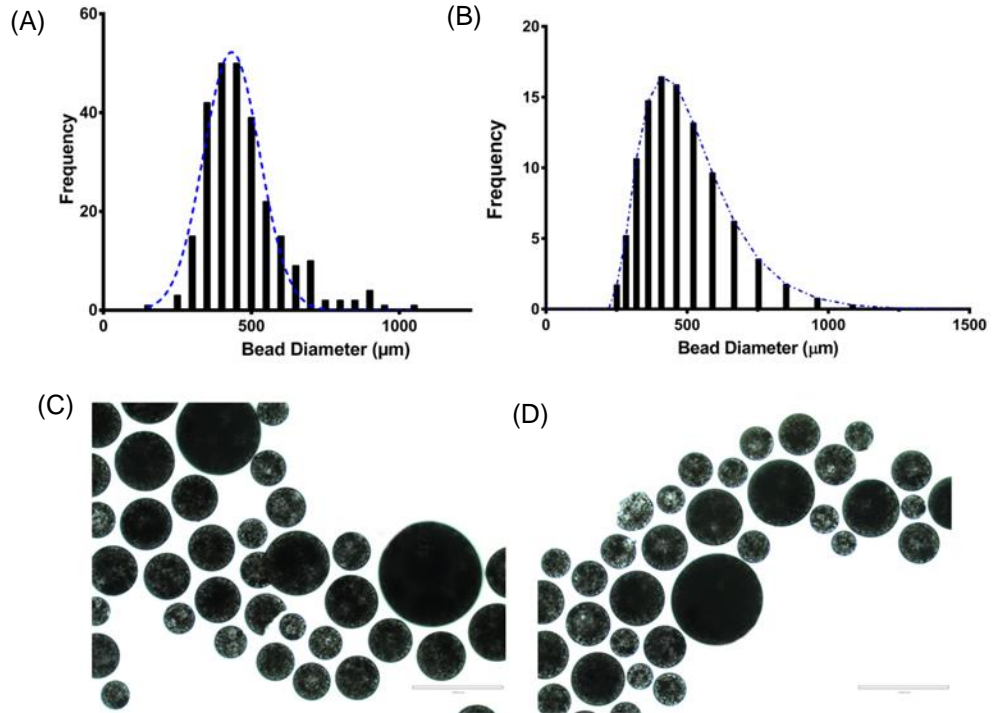
Figure 5.3 *Frequency particle size distributions of SpheriTech beads manufactured in a reactor. (A) Microscopy (N=268 beads) and a (B) particle size analyser (N=3 runs) was used to measure particle size. Phase contrast images of beads used in the (C) microscopy and (D) particle size analyser were taken. Scale bar = 1000 µm.*

Feret's diameter, or the caliper length, is the longest distance measured between two points along the region of interest (ROI) boundary. Bead diameters from 150µm to 1039µm, with a median of 448µm were found. The co-efficient of variation (CV), a comparative measure of dispersion within a frequency distribution (calculated from the ratio of the standard deviation to the mean - 113/471µm), was 28.2.

As a result, diameter measurements from both analysis methods are comparable, and produce similar ranges and median particle size measurements. Heterogeneity is visually noticeable in the range of bead sizes manufactured, as confirmed through these tests. Furthermore, a particle circularity of 0.83 ± 0.08 (N=72 ± SD) was noted when discounting broken or fragmented beads, however, this value dropped to 0.51 ± 0.39 (N=292 ± SD) with these included. This also suggests that, in addition to a large variation in bead size, there is also a high degree of fragmentation and damage occurring to beads during manufacture in a reactor.

In order to assess bead size in relation to cellular binding efficiency, a greater degree of control over the manufacture conditions and bead output is necessary. Consequently, a new production method for SpheriTech beads is required.

5.4 Microfluidic droplet generator

To create a more controlled manufacture process with a homogeneous bead output, the properties of microfluidic systems were utilised. A continuous process was opted for in comparison to the batch reactor method, to allow greater control over scale and process inputs. The microfluidic droplet generator was manufacture from Teflon to withstand the solvents used during processing. By utilising a T-junction design to make uniform droplets of aqueous polymer solution within a solvent, beads created can be reproducible with the potential for scale out if required.

The manufacture process consisted of two syringes, the microfluidic chip, and a stirred beaker filled with DCM and EDCI. One syringe was filled with the aqueous polymer phase (poly-Ɛ-lysine + sebacic acid + NMM + Span 80) and the other with the solvent phase (DCM + EDCI). They were placed into a syringe pump with low pulsation and connected to the microchip T-junction with a single outlet tube fed into a beaker containing DCM and EDCI. The beaker was continually mixed with a magnetic stirrer or overhead impeller. Droplets generated in the chip would commence polymerisation in the tubing, then complete the reaction in the stirred beaker. This microfluidic manufacture process is summarised in Figure 5.4.
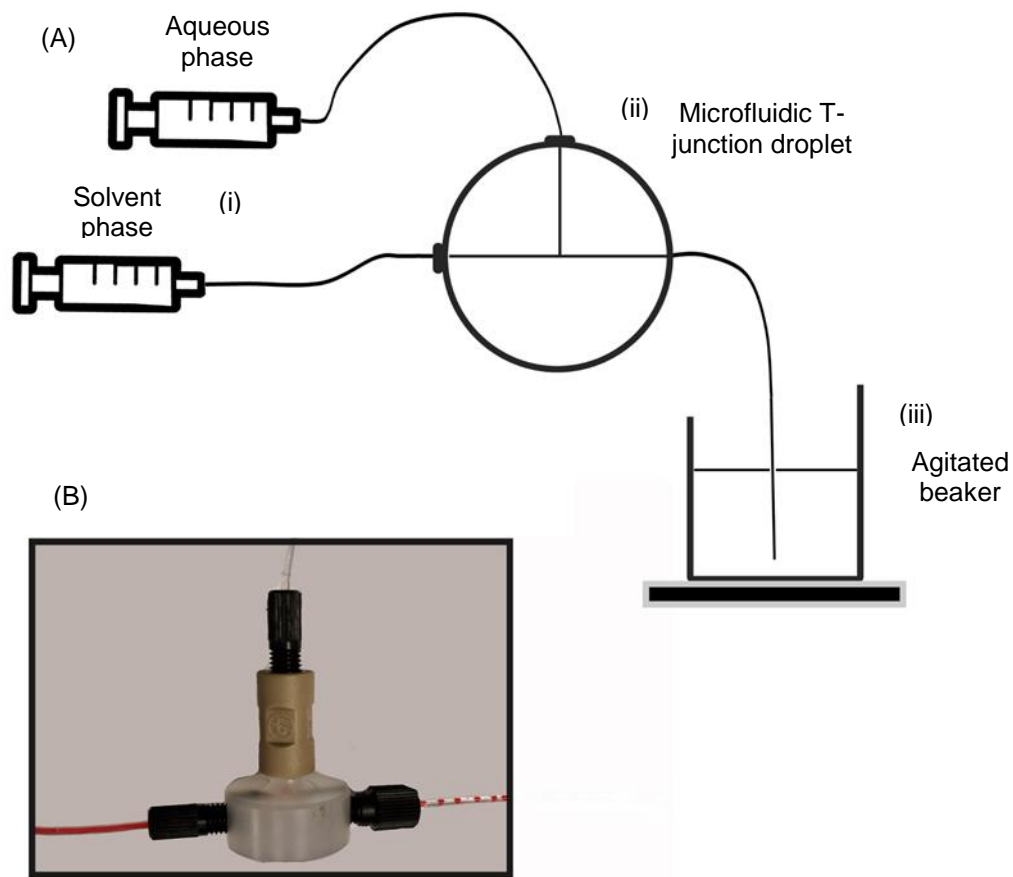
Figure 5.4 Microfluidic bead manufacture process. (A) Diagrammatic representation of the microfluidic SpheriTech bead manufacture process. (i) The aqueous polymer solution and solvent (with polymerisation activating agent)-filled syringes are pumped into the (ii) microfluidic T-junction to generate droplets of a defined size. Polymerisation commences in the tubing exiting the microchip, and is completed in a (iii) stirred beaker containing excess activating agent. (B) Droplet generation using red dye in heptane to illustrate the formation of droplets in the microchip.

There are four main manufacture variables in the system: composition of the aqueous phase, solvent phase and solution in the output beaker; the ratio between the aqueous and solvent input streams; the combined flowrate of both input streams; the chip's internal geometry and channel dimensions. Due to time and manufacture constraints, the same microfluidic chip was maintained throughout all experiments so geometry was unchanged.

5.4.1 Size distribution

As with STR production, diameter was experimentally determined by microscopy to determine the reliability and reproducibility of production. A frequency histogram was constructed to provide comparable analysis of heterogeneity (Figure 5.5).
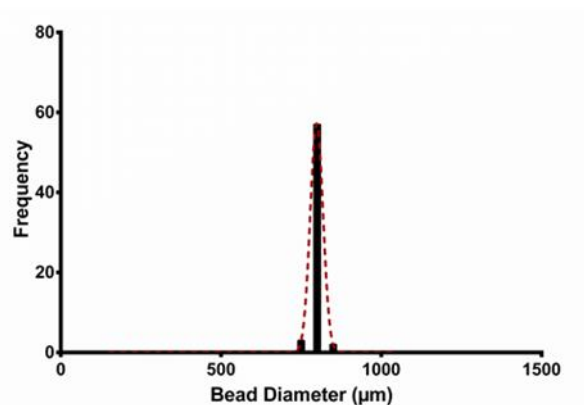
Figure 5.5 *Particle size distribution of SpheriTech beads manufactured in a microfluidic droplet generator at 1µl/s aqueous phase and 3µl/s solvent inputs (N=84).*

A bead diameter range of 77µm was observed with a standard deviation of 11 and CV of 1.5 (Figure 5.6) – significantly lower than that experienced with the reactor. Consequently, we can conclude that heterogeneity is considerably lower with the microfluidic chip than reactor manufacture. Additionally, as the system relies on laminar flow, there are minimal shear forces which break apart the beads minimising bead fragmentation.
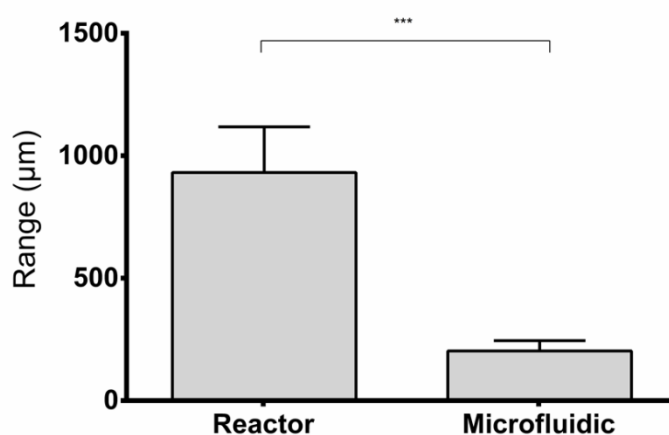
Figure 5.6 *Comparison of the homogeneity of beads manufactured from a reactor or microfluidic production method. The mean bead range (maximum – minimum diameter)*

produced from N=3 reactor batches ± SD and N=4 different flowrates within the microchip ± SD is plotted in a bar chart. Significance was determined using a two-tailed unpaired t test where P=0.0006.

While operating at higher flowrates and low input stream ratios, there were instances where droplets combined together before polymerisation. This would double the droplet volume (and consequently bead volume) and increase polydispersion. However, by controlling the flowrates of both input streams, these incidents can be mitigated.

5.4.2 Impact of flowrates

The diameter of droplets from the generator can be controlled by varying the ratio between the two inlet streams, and by the combined input flowrate of both streams together.

The combined input flowrate was calculated by:

$$combined\ flowrate\ (\mu l/s) = Aqueous\ phase\ flowrate\ (\mu l/s) + solvent\ flowrate\ (\mu l/s)$$

The ratio of input flowrates was calculated by:

$$ratio\ of\ input\ flowrates = \frac{Aqueous\ phase\ flowrate\ (\mu l/s)}{Solvent\ flowrate\ (\mu l/s)}$$

The combined flowrate was varied between 2.5 µl/s and 5 µl/s, while maintaining a fixed ratio between both inputs. The diameter of beads was measured using microscopy, as before, with a minimum of N=62 beads examined for all conditions. Although higher flowrates increase the production rate of beads, above 5 µl/s individual droplets did not form so this was set as the maximum flowrate. An inversely proportional trend was noted between flowrate and bead diameter, where increasing the combined flowrate decreased the diameter of beads produced (Figure 5.7).

The ratio between aqueous and solvent input flowrates was varied between 0.1 and 0.7, with the combined flowrate maintained throughout experimentation. A proportional trend was noted

between the input ratio and bead size, where using a higher ratio (approaching 1) produced larger beads.
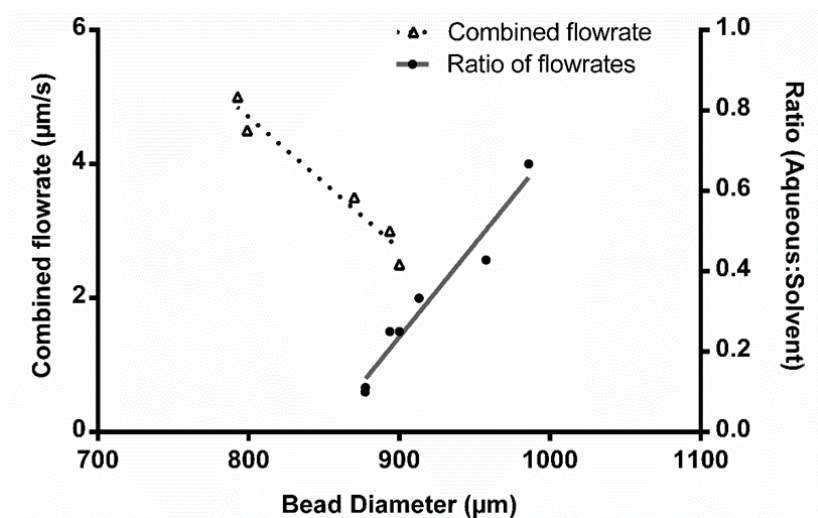
Figure 5.7 *Impact of combined flowrate and the ratio of input flowrates on bead manufacture. The combined flowrate (triangles with a dotted line on the left Y-axis) was measured with a fixed input stream ratio of 0.1 (aqueous:solvent). The ratio of the aqueous (polymer) to the solvent input flowrates (circles with a solid black line on the right Y-axis) was measured with a fixed combined flowrate of 2.5 µl/s. Bead diameter was measured through microscopy for both variables. A minimum of N=62 beads were measured at each data point.*

As a result, operating at a low ratio and high flowrate will result in the smallest bead size. Conversely, running at a high ratio and low flowrate will produce the largest beads. To further investigate how both parameters interacted together, a matrix was created to test a range of different parameters using bead diameter as the output. Combined flowrates between 2 µl/s and 5µl/s were tested, and input flowrate ratios between 0.2 and 1 (Figure 5.8).

The contour plot confirms that, at smaller ratios and higher combined flowrates, smaller beads are manufactured. Between 0.2 and 0.8 aqueous:solvent phase ratios, the combined flowrate and ratio of flowrates appear to have a comparable impact upon bead size. Maintaining one variable and changing the other will alter bead size in an almost linear fashion. Above a 0.8 ratio, bead size is observed to increase whilst decreasing the flowrate. This is due to the agglomeration of droplets at the T-junction, due to insignificant spacing between new droplets

being generated. A zone where droplets were not produced at all was found between a combined flowrate of 4 µl/s and ratio of 1, and a combined flowrate of 5 µl/s with a ratio of 0.3. In this operational zone, droplets did not form at the T-junction with longer, cylindrical polymeric tubes being produced which did not polymerise effectively because of their reduced surface area:volume.
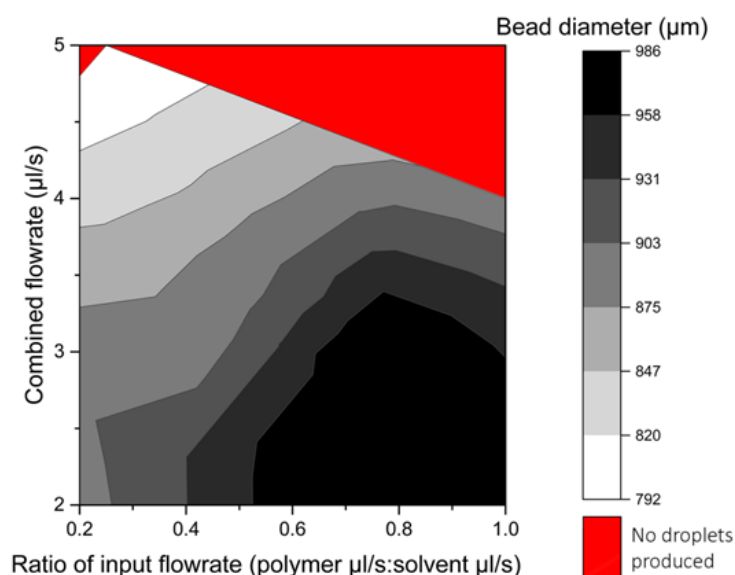
Figure 5.8 *Analysis of bead size from different manufacture conditions. By varying the ratio of the polymer:solvent phase between 0.2 and 1, and combined flowrate between 2µl/s and 5µl/s, the size of beads produced was measured and plotted on a contour plot. The area shaded in red is where no beads were formed due to agglomeration of droplets in the T-junction.*

As a result, to define the operating conditions required for different specifications of beads, both these factors must be controlled. An experimental design space between a flowrate ratio of 0.2 and 0.6, and combined flowrates between 3 µl/s and 4 µl/s is recommended for this microfluidic chip (Table 5.1).

Table 5.1 *Recommended experimental parameters for microfluidic manufacture of SpheriTech beads*

Combined flowrate (µl/s)	Aqueous:solvent phase
3 - 4	0.2-0.6

To produce smaller beads without designing a new chip, the amount of detergent (Span 80) in the aqueous phase was increased, and a second detergent (Tween) was added into the solvent phase. This allowed 400-600 μm beads to be produced using the same system. For cell binding studies, beads with a mean of 450 μm beads were utilised.

5.4.2 Bead heterogeneity vs flowrate

To investigate the impact flowrate has upon the heterogeneity of beads produced, the combined flowrate and flowrate ratio was given a ranking to allow both conditions to be assessed together. To do this, combined flowrate was split into 5 groups with a rank of 1 to 5 associated with each group; rank 1 being the slowest rate at 2-2.5 μl/s, and then incremental tiers of 0.5 μl/s up to rank 5 at 4.5-5 μl/s. The same process was applied to the ratio of input flowrates, with increasing rank (i.e. from 1 to 5) correlating to a 0.2 decrease in the ratio from 1.0 to 0.0. Consequently, each experimental run has an associated combined flowrate and input ratio rank. These two ranks were added together to provide a combined ranking; a higher ranking was correlated to conditions produced smaller beads, a lower ranking to larger.

Standard deviation from the mean bead diameter was calculated for every condition tested, and a scatter graph plotted of the combined rank against standard deviation (Figure 5.9).

(B)

Combined flowrate	Rank
2.0 - 2.5	1
2.5 - 3.0	2
3.0 - 3.5	3
3.5 - 4.0	4
4.5 - 5.0	5

(C)

Ratio of input flowrates	Rank
0.0 - 0.2	5
0.2 - 0.4	4
0.4 - 0.6	3
0.6 - 0.8	2
0.8 - 1.0	1
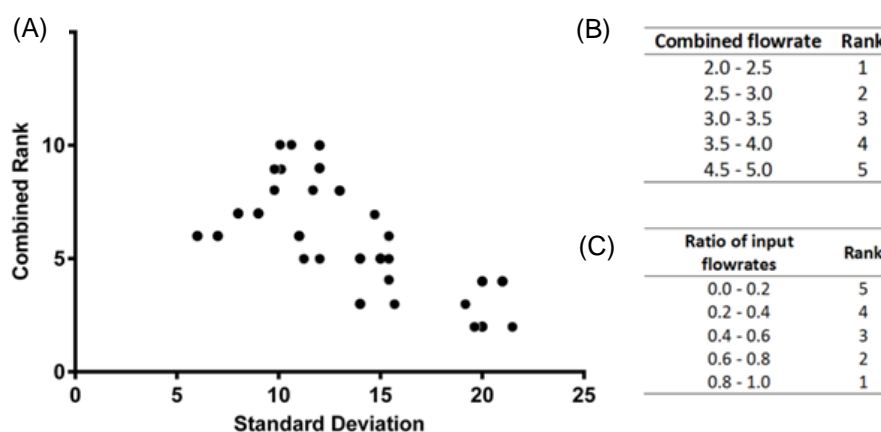
Figure 5.9 *Impact of flowrates upon bead heterogeneity. By grouping combined flowrates and flowrate ratios tested into 5 tiers, a rank could be applied to every condition tested. A high rank related to smaller beads and a low rank to larger beads. The 5 ranks for (B) combined flowrate*

and (C) the ratio of flowrates are detailed in the table inserts. (A) A scatterplot of the combined rank against standard deviation was then created from N=30 conditions.

Standard deviation was below 23 for all experimentally tested inputs, 5 fold lower than with STR manufacture, confirming the previous conclusion that microfluidic manufacture produces more uniform beads than an STR production method. Interestingly, a trend was also observed suggesting conditions with a higher combined rank (i.e. with smaller beads) produced a more homogeneous product than those with a lower combined rank (producing larger beads). This data agrees with visual observations that droplets can agglomerate together at higher ratios and lower flowrates, and that, at ratios of 0.8, decreasing the flowrate will increase bead size. Droplets combining together will increase the dispersity of bead diameters and consequently produce a less homogeneous bead population.

5.4.3 Production rate

The rate of bead manufacture through a microfluidic chip at different flowrates was also investigated. By creating a matrix and varying the aqueous volumetric flowrate from 0.1 to 1µl/s, the number of beads generated at different sizes can be determined. The theoretical number of beads per second generated was calculated and the data plotted on a contour plot for bead diameters between 300 µm and 600 µm (Figure 5.10).
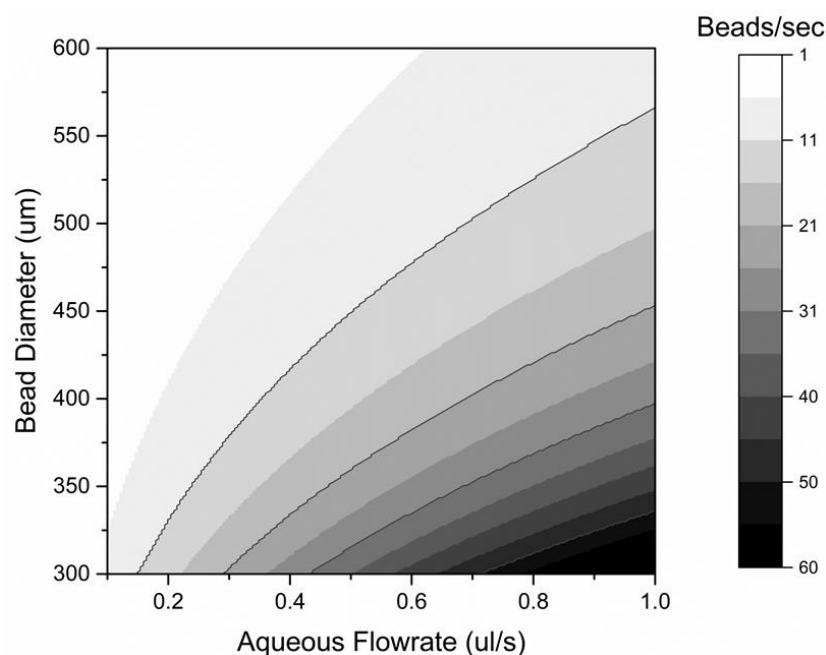
Figure 5.10 *Production rates of beads using the microfluidic chip. At a range of aqueous flowrates between 0.1 µl/s and 1µl/s, a contour plot illustrating the amount of droplets generated per second to produce different bead diameters is shown using a scale from 1-60 beads per second.*

The production rate of beads is dependent on the aqueous phase flowrate. Varying the ratio between the aqueous:solvent phase, as previously shown, can be used to alter the size of beads produced. Given the current microfluidic chip parameters, while operating with a combined flowrate under 5 µl/s, maximising the aqueous phase flowrate will increase the manufacture throughput which may be critical for larger scale production. The chip can also be scaled out to operate multiple fluidic chips in parallel to increase bead production.

5.5 Antibody immobilisation

Once a controlled, uniform product can be manufactured, SpheriTech beads must be characterised for their critical criteria to facilitate cell purification. Characterisation broadly falls into three categories: antibody immobilisation, paramagnetism and buoyancy.

5.5.1 Bead topology

To assess how SpheriTech beads appear at the macro and microscopic scale, electron microscopy (EM) was implemented to visualise the surface at different resolutions. Three different scales were observed (x1000, x20,000 and x50,000) to simulate the scale at which a cell, antibody and an operator would interact with the beads.
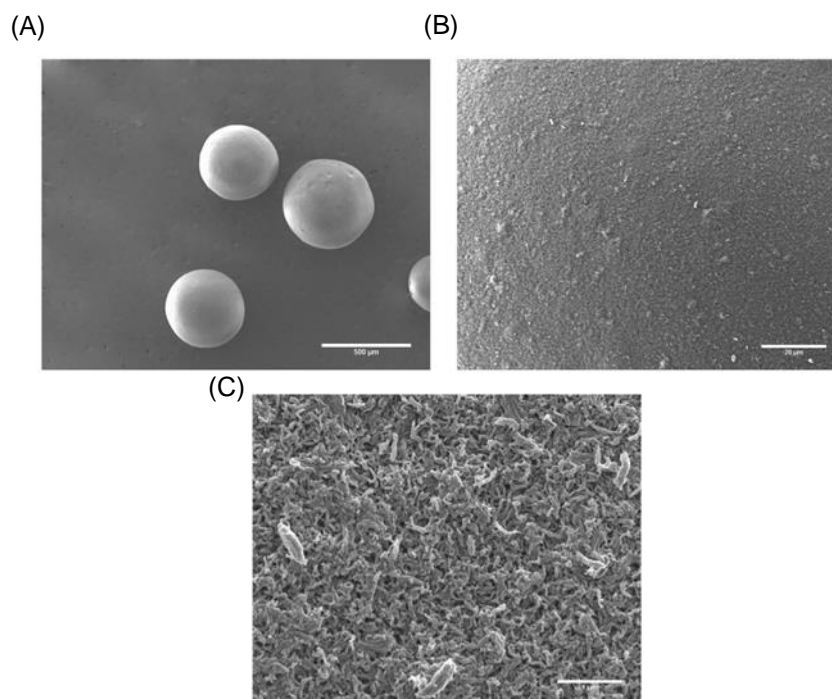
Figure 5.11 *EM of SpheriTech beads at (A) x1000, (B) x10,000 and (C) x20,000 magnifications. Scale bars are 500µm, 20µm and 1µm.*

The surface of polymer beads appear relatively smooth up to a magnification of x10,000, thus cell interaction will be with an almost planar, flat surface. Beads are not macroporous to permit cell entry, so cell binding will only occur on the surface. However, at a x20,000 scale the surface is microporous with visible apertures into the bead (Figure 5.11). As a result, there is a risk that antibody could permeate through the bead and not be immobilised exclusively on the surface. Due to the significant cost of antibody, any waste from diffusion into the bead must be minimised.

5.5.2 Antibody diffusion

To determine if antibody is lost through micropores, excess CD73 primary antibody was immobilised onto SpheriTech beads before cryosectioning the bead into 5µm slices. The slices

were then incubated with a secondary fluorophore-conjugated antibody, and compared against beads without immobilised CD73, to detect whether antibody had diffused into the bead.

(A)　　　　　　　　　　　　　　(B)
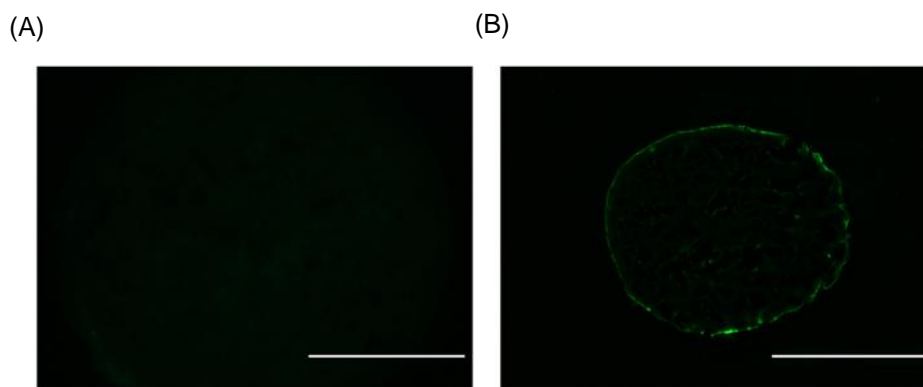
Figure 5.12 *Antibody diffusion into SpheriTech beads during immobilisation. (A) A control with no immobilised CD73 antibody and a (B) CD73 immobilised bead sample was cryosectioned into 5µm slices after staining with a secondary fluorophore-conjoined antibody. Scale bars = 200µm*

A band of positive fluorescence was observed around the perimeter of immobilised beads, with limited spots of fluorescence noted towards the core (Figure 5.12). This suggests that antibody diffusion during the incubation process is minimal, so antibody is not wasted by binding inside the core of the bead. As antibody is the primary cost of bead manufacture, this is an important finding for commercial feasibility.

5.5.3 Antibody and antigen density

Bound antibody can be observed by fluorescence, but for quantification the technique of gold immunostaining was utilised. Gold is used as a label due to its high electron density which gives the particles photoemissive properties to stand out from other unlabelled structures. Using a scanning electron microscope (SEM), individual gold particles can be observed with a theoretical 5nm resolution (compared to 200nm with the wavelength of light). By counting the gold bright spots in a given area, the density of immobilised antibody and distribution pattern

can be assessed. This method of staining can be used to measure both the density of antibody immobilised on beads, and surface antigen density on cells.

Excess CD73 antibody was first immobilised onto SpheriTech beads to fully saturate all available carboxyl functional groups. A secondary antibody conjugated to 20nm gold colloidal particles was incubated with the immobilised beads to bind to CD73. SEM revealed a mean of 15 CD73 antibodies immobilised per μm^2 of bead surface area (Figure 5.13). This corresponds to a maximum antibody capacity for SpheriTech beads, given the current manufacture parameters.

(A) (B)

Surface CD73 Antigens: 4.12 ± 2.79/um²   Immobilised CD73: 15.46 ± 2.48/um²
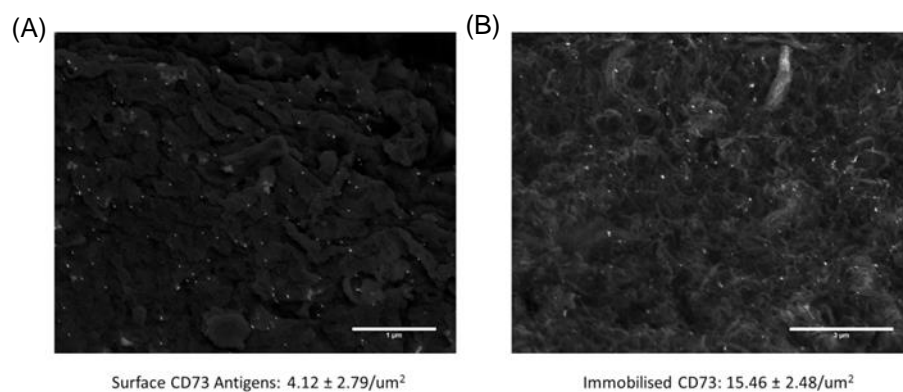
Figure 5.13 Gold immunostaining with SEM. (A) CD73 antigens on MRC-5 cells and (B) immobilised CD73 antibody on SpheriTech beads. A mean antigen density of 4 μm^{-2} and a mean antibody density of 15 μm^{-2} was observed for cells and beads respectively (N=11 images from 8 cells ± SD; N = 9 images from 7 beads from multiple production runs ± SD).

The same technique was applied with cells to assess the topography and surface density of surface CD73 antigens. MRC-5 cells were incubated with CD73 primary antibody, then the secondary gold-conjugated antibody for identification. Stained cells were compared against a control sample with no primary antibody. A density of 4 CD73 antigens per μm^2 of the cell's surface was observed, and antigens were fairly homogeneously dispersed in small clusters across the surface.

For cell binding studies, an approximate density of 4 CD73 antibodies per μm^2 of bead surface area will be used for antibody immobilisation. This equates to the available density of CD73 receptors on the cell surface. Although fundamental cell:bead binding studies will be performed with MRC-5 cells, future work should involve the confirmation of CD73 antigen density on progenitor photoreceptors.

5.6 Paramagnetism

Through the addition of iron oxide, it is possible to manufacture SpheriTech beads that can be manipulated with a magnetic field. Altering the amount of iron oxide added should control the strength of the induced paramagnetic force. Paramagnetism was characterised firstly through the ability to hold beads in place with a magnetic field, then further investigated for iron oxide homogeneity and the oxidative state within beads.

5.6.1 Magnetic field strength

A microfluidic chip was designed and manufactured to investigate bead paramagnetism. The PMMA chip consisted of a single linear 1.5 mm channel, with various incremental cut-outs either side for a magnet to be placed in. Two magnets were placed symmetrically either side of the central fluidic channel at defined distances from the centre, and SpheriTech beads with iron oxide in flowed along the channel at 2 µl/s. The beads were held between the magnets, confirming that the addition of iron oxide creates paramagnetic beads that can be manipulated under flow (Figure 5.14). When flowing control beads without iron oxide through the channel, and when magnets were placed into the furthest cut-outs (~1.2cm) from the channel, beads flowed directly through the chip and were not held.

An investigation into the impact of PMMA was carried out using a gaussmeter to measure magnetic field strength through two different diameters of thermoplastic. A microscope stage with 10 µm incremental movements was used to vary the distance of the gaussmeter from a fixed neodymium iron boron magnet. Magnetic field strength readings were taken, before a 1.5mm or 5mm thick PMMA block was placed in front of the magnet.
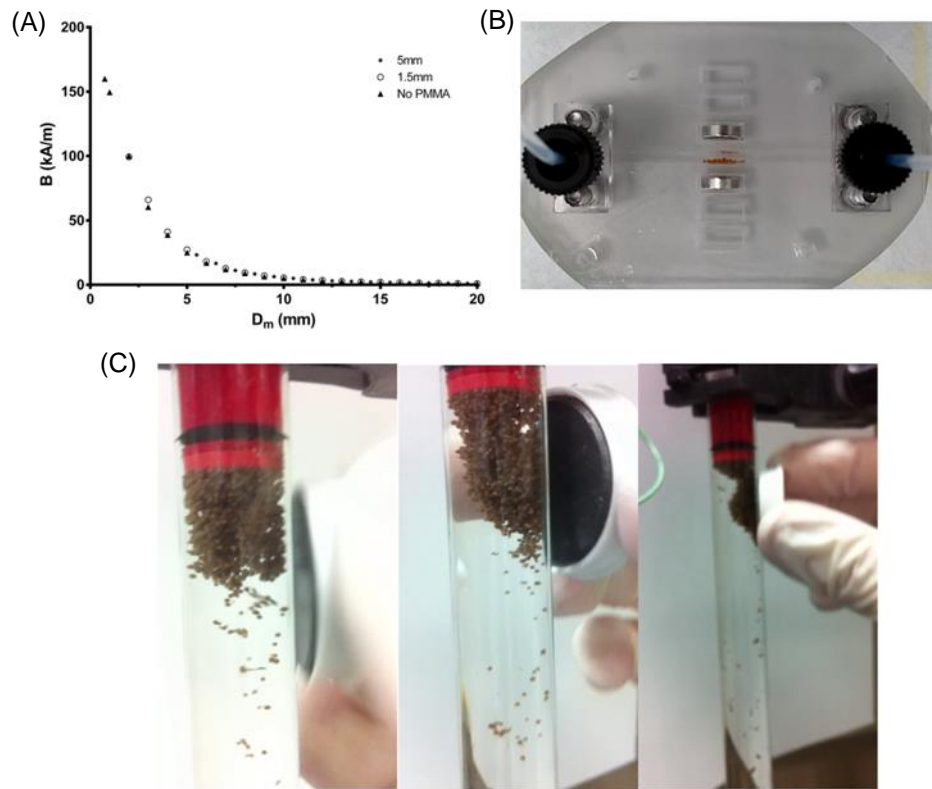
Figure 5.14 *Induced magnetism in beads and the effect of PMMA on magnetic field strength.*
(A) Scatter graph of magnetic field strength, B, against distance from the magnet, Dm, with no
PMMA (▲), 1.5mm PMMA (○) or 5mm PMMA (•). (B) Microfluidic chip with a 1.5 mm linear
channel with cut-out incremental holes either side showing captured beads under flow by
magnets with a 2 µl/s flowrate. (C) Buoyant paramagnetic beads floating and being manipulate
by a magnet in a 1cm diameter chromatography column to produce and inverted expanded bed.

A minimal reduction in magnetic field strength was recorded, with both the 1.5mm and 5mm
PMMA block producing comparable magnetic fields strengths to when no block was present.
This suggesting that up to 5mm of PMMA will not impact the capability to hold paramagnetic
beads within a channel. This result may be important for the design of a purification device,
where beads are held in place and manipulated through magnetism.

5.6.2 Magnetisation

Paramagnetic material will produce magnetisation in the direction of the applied field. This
means that paramagnetic SpheriTech beads are attracted towards a magnet (Figure 5.14C).

Magnetisation in ferromagnetic nanoparticles can flip direction dependent on temperature, so these materials are called superparamagnetic. This induced magnetic moment can be measured by a Superconducting Quantum Interference Device (SQUID).

SQUID was used as a magnetometer to measure the magnetisation of colloidal iron (iii) oxide dispersed within SpheriTech beads. If under a constant current, the voltage will oscillate depending on the magnetic flux which is called the (AC) Josephson Effect. By measuring these oscillations, the changes in magnetic flux can be determined for samples with very low amounts of magnetic material. SQUIDs can detect magnetic fields of 5×10^{-14} T using two parallel Josephson junction: two superconductors separated by thin, insulating barrier through which electrical current can flow without dissipating. Superconductors allowing current to flow in this manner is known as a supercurrent.

(A)
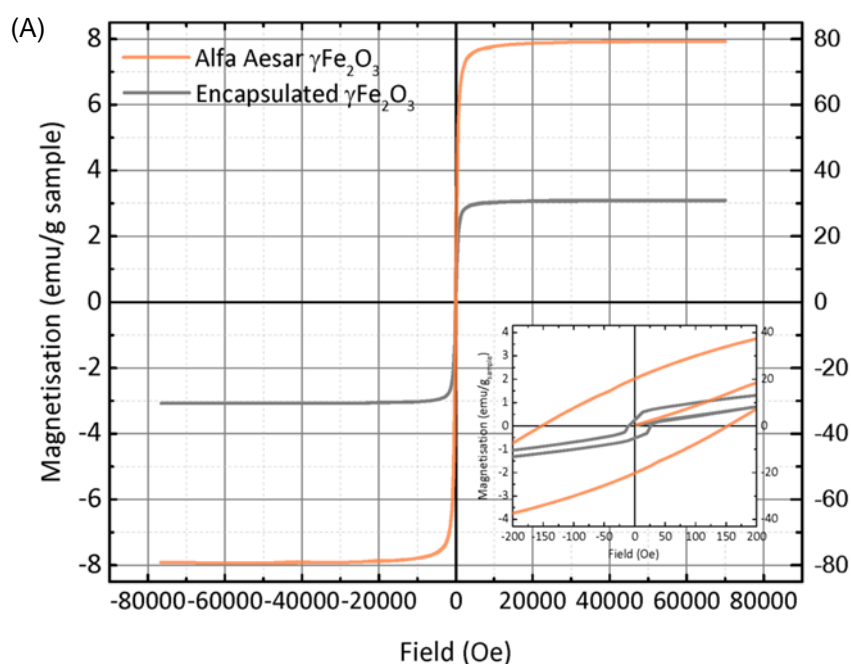
(B)

Material	Magnetisation ±SD (emu/g)
Alfa Aesar iron (iii) oxide	84.08 ± 2.6
SpheriTech beads	3.56 ± 0.47

Figure 5.15 *Magnetisation hysteresis loops of encapsulated and free iron oxide. (A) Alfa Aesar iron (iii) oxide (orange line, plotted on the right hand y-axis) and encapsulated iron (iii) oxide in dried SpheriTech beads (grey line, plotted on the left hand y-axis) was assessed using SQUID*

SQUID magnetometry was performed with Dr Lara Bogart at the Healthcare Biomagnetics Laboratory in The Royal Institution of Great Britain. Firstly, the magnetism of Alfa Aesar iron (iii) oxide, the ingredient mixed with poly-Ɛ-lysine to create paramagnetic beads, was tested. A magnetisation of 84.08 ± 2.6 emu/g of powder was measured which corresponds approximately to literature values and previous experience (Akbar *et al.*, 2004; Wu, He and Jiang, 2008).

Dried polymer bead samples between 2.2mg to 4.9mg were then tested and compared against the pure iron (iii) oxide ingredient. A magnetism of 3.56 ± 0.48 emu/g was noted between three batches of SpheriTech beads, which relates to a technical saturation of 4.2% (Figure 5.15). This suggesting a low concentration of magnetic material within the beads. Due to the low standard deviation between technical repeats, a fairly homogeneous mix of iron oxide is present within beads from the same batch (3.31 ± 0.08, 4.2 ± 0.16, 3.18 ± 0.21). However, beads from different batches which contained the same initial amount of iron (iii) oxide ingredient had a larger deviation from the mean, suggesting iron uptake during droplet formation and polymerisation may vary during production.

For material to be superparamagnetic it must display irreversibility of magnetisation. This is observed from a symmetrical hysteresis loop across positive to negative magnetic field strengths. With a scale from -200 to 200 Oe, it was clear that although the iron (iii) oxide used was superparamagnetic (the smooth orange curve on the graph insert in Figure 5.15), encapsulated iron oxide in beads could not be classed as superparamagnetic at 300 K. If superparamagnetism was needed, a higher concentration of iron oxide could be added during manufacture, however, for bead capture and manipulation within a magnetic field the paramagnetic effect displayed is sufficient.

For all batches of SpheriTech beads manufactured, beads were magnetically saturated at 1 Tesla. As a result, the maximum required magnetic field strength to hold them within a static field is 1 Tesla.

5.6.3 Iron oxidation

Iron oxide nanoparticles have many uses, from computer storage devices to magnetic resonance imaging (MRI) and other medical applications (Frey *et al.*, 2009; Kievit and Zhang, 2011). For therapeutics, addressing concerns over toxicity is paramount. As a result, there has been significant research into potential toxicological effects from iron oxide nanoparticles (Loeb, Asharani and Valiyaveettil, 2010; Soenen *et al.*, 2012).

Nanoparticles can contain magnetite (Fe_3O_4) and maghemite (Fe_2O_3) as a magnetic iron source. Magnetite nanoparticles have been shown to decrease ATP production and cell viability after exposure. Furthermore, they can damage mitochondria and endoplasmic reticulum (ER) which inhibits functionality and can lead to autophagic cell death (Zhang *et al.*, 2012; E.-J. Park *et al.*, 2014). However, maghemite nanoparticles have demonstrated a much lower toxicity compared to magnetite particles (E. J. Park *et al.*, 2014). Fe_2O_3 particles have been safely used in various therapeutic treatments, such as for dental hypersensitivity (Dabbagh *et al.*, 2014), colorectal cancer (da Paz *et al.*, 2012) and hypothermia (Kim, Xu and Lee, 2014). Consequently, to manufacture SpheriTech beads iron (iii) oxide is highly preferred.

Mössbauer spectroscopy was used to confirm the presence of maghemite from magnetite. The Mössbauer effect describes the resonance of nuclei when absorbing gamma radiation, and occurs when radiation has an identical transition energy to the nucleus which absorbs it. For spectroscopy, the radioactive source is oscillated at discrete velocity steps to produce the Doppler effect – the change in frequency from moving a source towards or away from a detector. [57]Fe is the most commonly used isotope due to its long excited state and low energy requirement to emit gamma radiation. When an emitted gamma-ray hits a receiving nucleus, the atoms will vibrate. If the energy profile aligns with the oscillating source, a resonant signal will be produced. The energy signals are termed hyperfine interactions and can be recorded

through spectroscopy. A peak will be observed at each time the radiation source and absorber nuclei energy is identical.

If there is a difference in electron fields such as with an isomer, there will be a shift in the resonance energy. This is identified by comparison to a known Mössbauer spectrum like ^{57}Fe. An isomer shift can be used to determine the electron configuration of ferrous (Fe^{2+}) or ferric ions (Fe^{3+}) which have a sextuplet or quintuplet spectrum respectively (Coey, Morrish and Sawatzky, 1971; Tuček, Zboril and Petridis, 2006). There are fewer s-electrons in ferrous ions which produce a larger isomer shift.
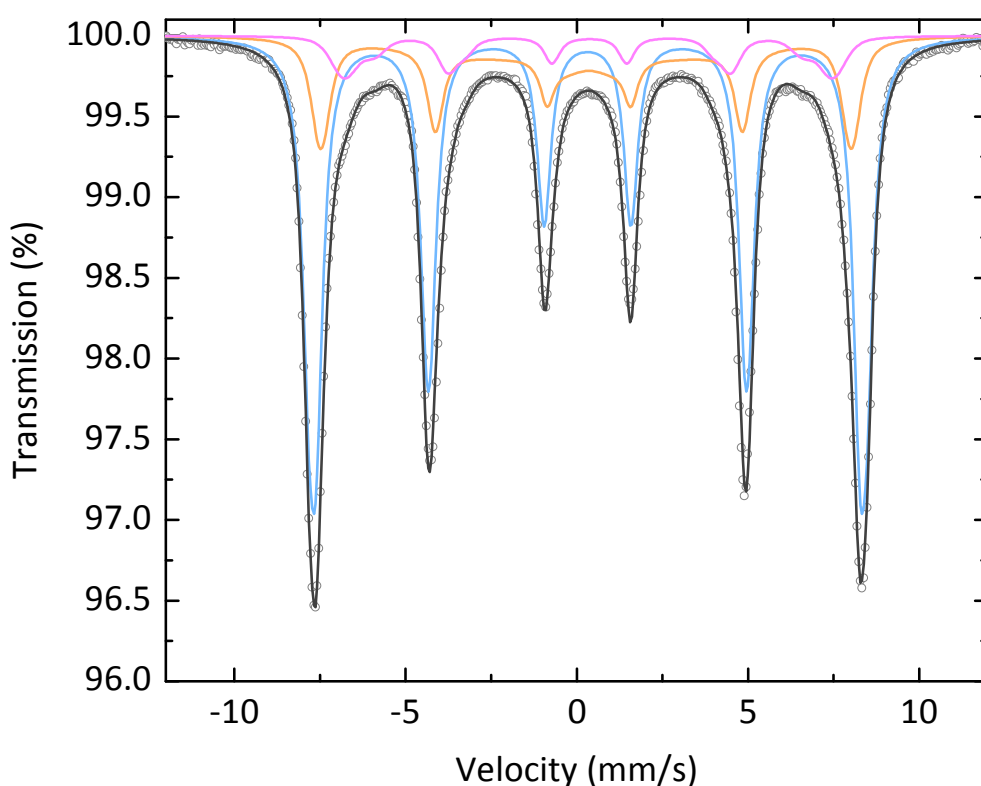
Figure 5.16 *Mössbauer spectrum of Alfa Aesar iron oxide. An ^{57}Fe radioactive source was oscillated by ±15mm/s at room temperature next to a sample of dried SpheriTech beads and the absorption (%transition through the sample) recorded for N=3 samples. Experimental data points are shown as circular dots (○), the fitted spectrum is the darm black line, the sub-spectra are the coloured lines.*

Mössbauer spectrometry was performed with Dr Lara Bogart at the Department of Chemistry at University College London. To determine the oxidation state of iron oxide used, a Mössbauer

spectrum was created for Alfa Aesar iron oxide and compared against the known isomer shift of iron (iii) oxide from previous experimentation (Ramos Guivar *et al.*, 2012). The gamma radioactive source was oscillated ±15 mm/s and produced an isomer shift of 0.32, 0.31 and 0.35 mm/s comparable to the reference material (Figure 5.16). Quadrupole splitting – the nuclear energy level of electron interactions caused by changes in the electric field - produced an asymmetrical sextuplet spectrum which is in keeping with maghemite. Comparable results were also found to iron (iii) oxide, suggesting no magnetite component is present. As such, the iron oxide selected is non-toxic and safe for use in SpheriTech beads.

More can be learnt about the Mössbauer effect and clinical applications in literature (Boyle and Hall, 1962; Mamani, Gamarra and Brito, 2014; Rümenapp, Wagner and Gleich, 2015).

5.7 Buoyancy

In addition to magnetism, the density of SpheriTech beads can be controlled through the addition of hollow microballoons. Altering the ratio of polymer to balloons will control the relative buoyancy of the beads.

Bead buoyancy was first demonstrated by leaving static beads in water, and observing whether they float or sink. Buoyancy under flow was then tested in a chromatography column. An 'inverted' expanded bed was created, utilising downwards flow against gravity with a bed forming at the top of the column through buoyancy. Pink dye was injected into the column to visualise the direction of flow (Figure 5.17).
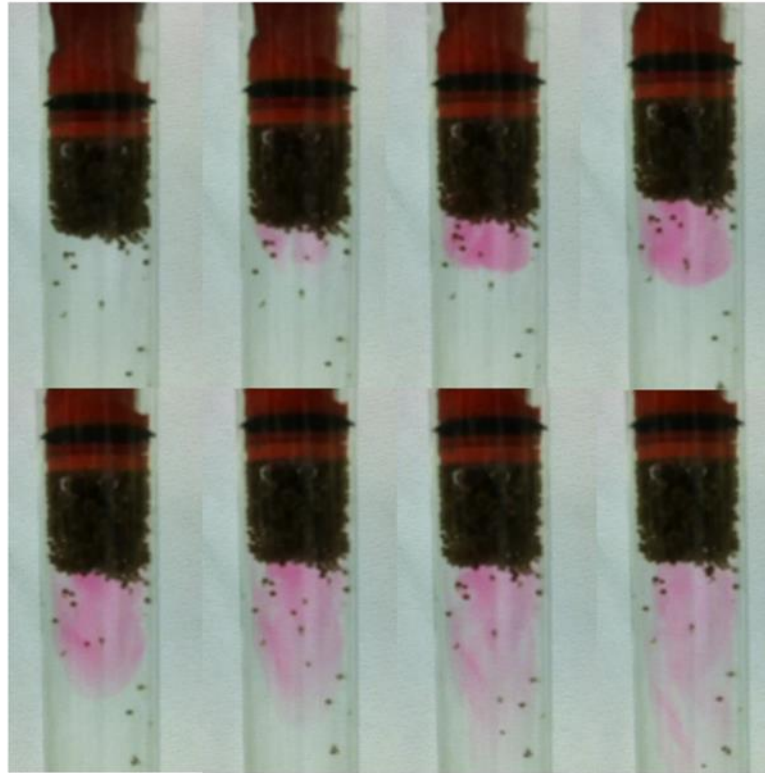
Figure 5.17 *Visualisation of buoyant beads under flow. SpheriTech beads forming a floating inverted expanded bed in a 1cm diameter chromatography column under downwards flowrate against gravity. A pink dye was injected into the PBS to visualise flow. Each image is 0.5 seconds apart.*

By increasing the flowrate, beads separated out and sunk to the bottom of the column. This suggests a distribution of hollow microbeads exist within the batch. For further work, polydispersity dispersity within a sample could be measured by incrementally increasing the flowrate and recording how many beads sink.

5.8 Combined bead characteristics

To produce buoyant paramagnetic beads, the impact of iron oxide and hollow microballoons must be assessed together. The mass of iron oxide within beads will alter the density of beads, varying bead buoyancy. Consequently, beads were manufactured with a range of values for both variables, and beads assessed for paramagnetism and buoyancy. A binary output was used to determine each characteristic: to confirm paramagnetism, beads must be held in place

within a microfluidic chip as tested in Figure 5.14 under a flowrate of 2 µl/s; to confirm buoyancy, beads were suspended in static PBS and assessed whether they floated or sunk.

Table 5.2 Manufacture conditions tested to produce paramagnetic or buoyant beads. The amount of iron oxide added (to 50ml aqueous polymer solution) and the ratio of polymer to hollow microballoons (as a % of polymer present) was varied, then bead output assessed for paramagnetism and buoyancy.

Manufacture conditions		Bead outputs	
Iron (III) oxide (g in 50ml solution)	Polymer:Microballoons (% polymer)	Paramagnetic	Buoyant
0	100	✕	✕
1	100	✓	✕
2	100	✓	✕
2	50	✓	✓
1	50	✓	✓

Above 1g of iron oxide (0.02 mg/µl of aqueous feed), beads were paramagnetic and captured within the microfluidic chip. With a 50:50 ratio of polymer to microballoons, buoyancy was also noted (Table 5.2). Due to the high demand of resources required to test a wide range of conditions, bead relative buoyancy to water was calculated through the density of poly-ε-lysine and hollow microbeads (Table 5.3).

Table 5.3 Mass of poly-ε-lysine, microballoons and iron oxide per µl of 50ml aqueous polymer solution with 1g of iron added.

Poly-ε-Lysine (mg/µl)	Hollow balloons (mg/µl)	Iron oxide (mg/µl)
0.21	0.03	0.02

Theoretical buoyancy could then be determined for a range of bead diameters, polymer:microballons and iron oxide additions by proportionally changing these parameters. A contour plot was created for 0 to 10g of iron oxide and for a 0 to 100 (%) ratio of polymer:hollow microballoons (Figure 5.18).
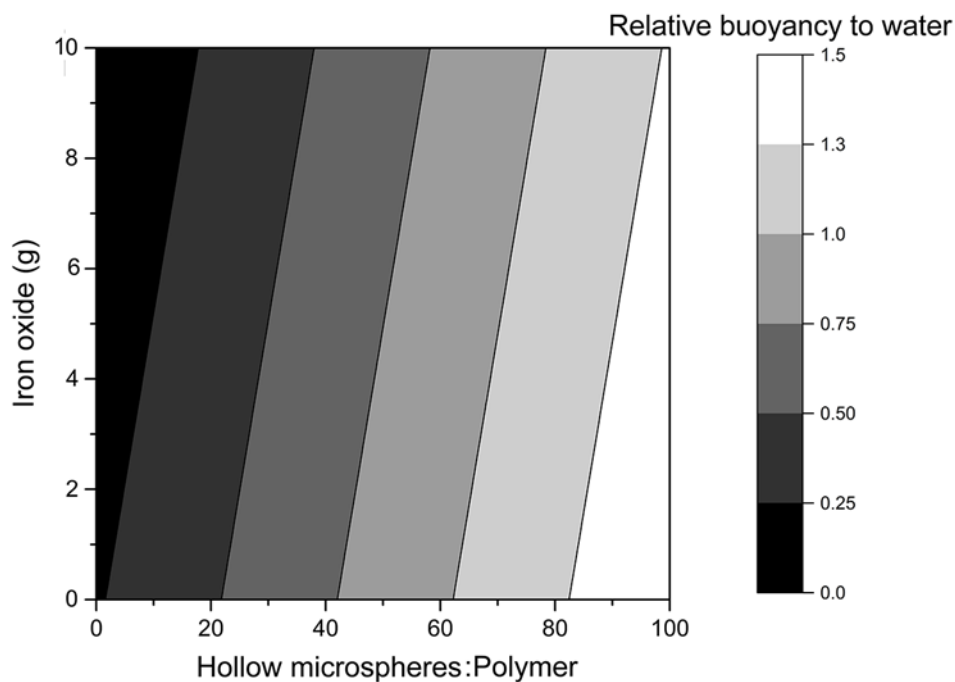
Figure 5.18 *Relative SpheriTech bead buoyancy to water for different manufacture conditions. Contour plot of the mass of iron oxide added (to a 50ml aqueous polymer phase) against the hollow balloons:ratio of polymer as a % of balloons present (where 100 = 100% microballoons and 0% polymer, and 0 = 0% hollow microspheres and 100% polymer). A scale of relative buoyancy from 0 to 1.5 has been used where 1.0 is an equal density to water, <1 means the beads will be buoyant, and >1 one means the beads will sink.*

This plot provides a range of operating conditions to manufacture specific bead densities. By controlling the iron oxide and polymer to microballoon ratio, bands of different density beads could be produced by pooling beads from different manufacture parameters. For example, the addition of 40% or 50% polymer:microballoon with 4g of iron oxide will both produce buoyant beads. However, the beads will have a relative density of 60% and 73% of water respectively. Two clear bands of beads could be produced by operating under a downwards flowrate against gravity. Consequently, in addition to manipulating beads via magnetic fields, flowrate could be used to control the separation and amalgamation of beads through controlled bead density.

5.9 Autofluorescence

During characterisation, it was noted that SpheriTech beads autofluoresce (Figure 5.19). It is still somewhat unclear why some polymers autofluoresce, but several intrinsically fluorescent structures such as polyurethanes and poly(phenylene ether) have been previously documented (Heckmann, 2005).
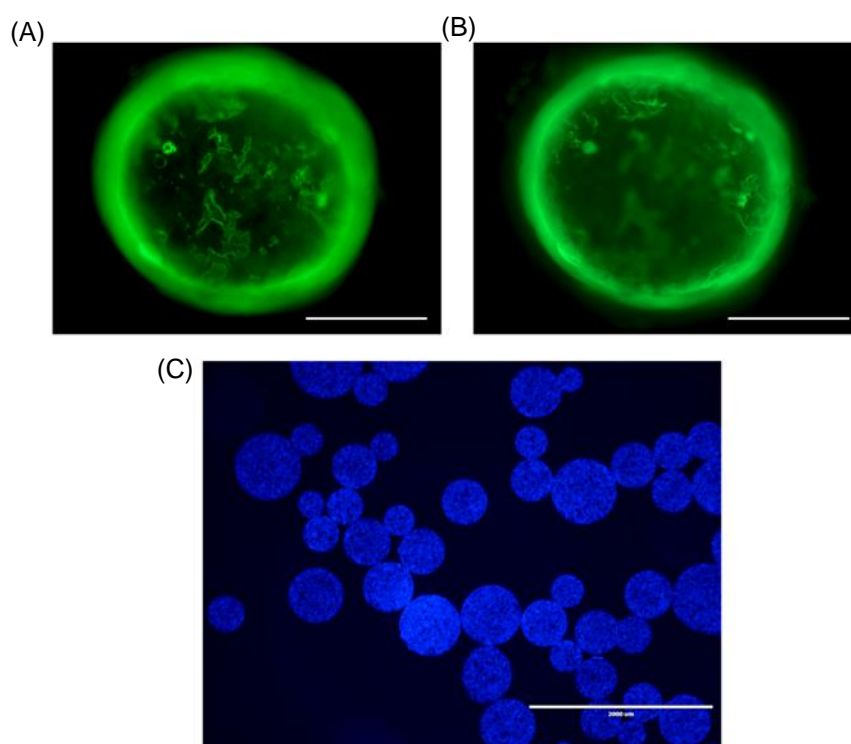
Figure 5.19 SpheriTech bead autofluorescence. (A-B) 470nm excitation and 525nm emission; (C) 360nm excitation and 447nm emission. Scale bar = (A-B) 250 µm or (C) 1000 µm.

For SpheriTech beads, autofluorescence is important as it could interfere with immunostaining and optical analysis techniques to identify bound cells. As a result, SpheriTech beads were tested with a range of excitation wavelengths to record excitation through relative fluorescence units (RFU). Although a large range of excitation wavelengths produced fluorescence, higher excitation wavelengths above 500 nm resulted in lower emission intensities (Figure 5.20). As a result, when beads are imaged for cell counts, antibodies with higher wavelengths or strong fluorescence will be utilised to minimise background bead fluorescence.
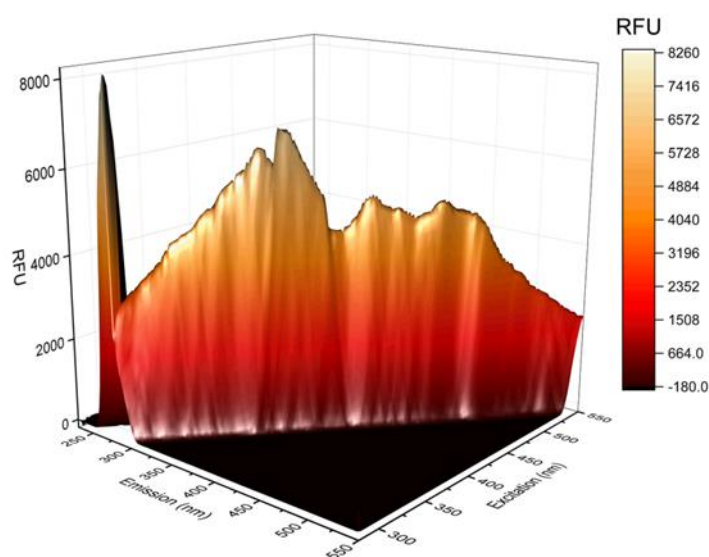
Figure 5.20 *Autofluorescence of SpheriTech beads. Fluorescence intensity was measured over across a range of 230-550nm excitation and 280-550 nm emission wavelengths with a step size of 2nm with SpheriTech beads in PBS. A RFU of 0 to 8200 was measured.*

5.10 Chapter Discussion

SpheriTech beads are poly-Ɛ-lysine spheroids, capable of being manufactured with different physical and chemical properties to facilitate a wide range of applications. By covalently immobilising antibody onto their surface, a novel affinity purification platform can be established for the isolation of target cell types. This chapter investigated the manufacture and physical properties of SpheriTech beads, as well as their potentially to purify CD73-positive.cells by affinity purification.

To test SpheriTech beads as a novel purification technology, first the manufacture process must be tried and tested for feasibility and reproducibility. Initially, manufacture was based off a patent by SpheriTech using an STR. Various iterative improvements were made to this process to minimise variability and improve mixing, such as the use of toluene to stability aqueous phase droplet formation and the controlled addition of EDTA to regulate polymerisation. Using bead size as an output, particle size distribution was assessed from 3 reactor runs using the improved STR manufacture. A large degree of polydispersion was noted with a bead diameter

range of 889µm due to the lack of control over polymerisation and homogeneity of aqueous droplet sizes, with many beads distorted or fragmented from shear.

Consequently, an alternative manufacture method was created to tackle these problems by utilising the properties of a microfluidic system to produce uniform droplets in a T-junction droplet generator. Droplet polymerisation begins in tubing connecting the microchip to a stirred beaker, then completed in a beaker containing excess polymerisation activating agent in suspension. The output bead diameter was found to be much more consistent, with very few bead fragments present. A range of 77µm was noted, nearly 4-fold lower than through STR manufacture.

The impact of the combined input flowrate, and the ratio between both input flowrates upon on the size of beads produced was investigated as critical process parameters which impact bead diameter. The two variables were tested independently, and increasing the combined flowrate and decreasing the ratio correspondingly reduced bead diameter. An assessment of both variables combined was then carried out to establish a recommended zone of operation from a contour plot. The homogeneity at different operational parameters was tested through standard deviation from the mean, and high flowrates with low input stream ratios produced the most homogeneous bead populations.

This data provides operational ranges to manufacture uniform beads within a given specification in a reproducible and scalable manner at minimal cost in a high throughput system. However tighter control over operational parameters will provide a greater understand of the bead population produced, and permits fine tuning of critical manufacture parameters to meet the specificity of beads required. However, in order to develop a novel purification technique, the basic technology and operational characteristics of SpheriTech beads must be understood. To do this, beads were evaluated for three key characteristics: the capacity to immobilise antibody on their surface to facilitate cell affinity purification; the ability to produce paramagnetic beads and manipulated them through a magnetic field; the production of buoyant beads by integration of hollow microballoons.

After confirming that antibody wasn't lost inside microporous cavities in beads, the density to immobilise antibody onto the surface was assessed.

Antibody immobilisation on beads was assess using gold immunostaining with SEM. However, before assessing the density of antibody bound, it was confirmed through fluorescence microscopy that antibody was not lost in microporous polymer bead structure but remained bound on the surface. This is an important finding as antibody lost inside the beads cannot bind to protein on cells, and antibody is the key cost driver for SpheriTech beads. By using SEM to visually determine the density and topography of CD73 antigens on the cells, a corresponding antibody density for the surface of beads was established. This density, 4 CD73 antigens/μm^2, will be immobilised onto beads for fundamental cell binding studies to follow. 4 CD73 antigens/$\mu m2$ represents the maximum capacity of protein, and therefore the maximum concentration required for bead binding while minimising waste.

Bead paramagnetism was confirmed by the capture of beads within a microfluidic channel using a magnetic field. PMMA was observed not to have an impact upon this manipulation, providing information for future purification device design. The amount of magnetic material within beads was then characterised using SQUID magnetometry. A magnetism of 3.56 emu/g was found, and beads observed to reach a technical saturated at 1 Tesla, providing the maximum magnetic field strength required to manipulate beads. Similarly, for development of a purification device, this data provides a basis for material selection and operational characteristics.

In addition to the magnetism, the oxidation state of iron oxide used was tested to ensure that no toxic magnetite was present within the formulation. Nanoparticles can contain magnetite (Fe_3O_4) and maghemite (Fe_2O_3) as a magnetic iron source, however the literature shows that magnetite negatively impacts the structure and functionality of cells. It was confirmed that no magnetite was present in production.

Buoyancy, through the addition of hollow microballoons, was then assessed in a reverse expanded bed chromatography column with downwards flow (against gravity). To investigate a range of operating conditions for the production of buoyant paramagnetic beads, an algorithm was created to determine the relative buoyancy of beads to water, giving a range of production

parameters to control bead buoyancy. A contour plot of 0 to 10g of iron oxide per gram of polymer, and 0 to 100 (%) ratio of polymer:hollow microballoons was created. A range of experimental conditions were then tested and showed comparable results to the calculated outcome of relative buoyancy to water. Using this plot, an assessment of the bead's physical characteristics can be made from different bead manufacture parameters.

Finally, during characterisation, autofluorescence of SpheriTech beads was noted. To minimise complications in further studies, autofluorescence intensity was assessed for a wide range of excitation and emission wavelengths. Lower fluorescence intensity was noted at higher excitation wavelengths, so these are recommended to minimise background fluorescence.

Chapter 6: Affinity bead binding studies

6.1 Introduction

In Chapter 6, SpheriTech beads were characterised to evaluate the key features they possess to support affinity purification operations. Given this broader understanding of the material and physical properties of beads, the functional binding of cells can now be investigated.

6.1.1 Bead separation

Due to limitations in current affinity technology (Table 6.1), there is still no universally accepted purification platform to separate rare cell types. As a result, there is demand for a novel purification technology which isn't limited by throughput or the necessity for a cellular label.

Table 6.1 *Key benefits and limitations of SpheriTech bead purification against FACS and MACS*

Advantages	Limitations
- No bead endocytosis	- No clinical precedence
- Label free, simple cell detachment	- Competing against established technology
- Reduced sample preparation	- No optimised device for the purification
- Ability to run multiple positive separations	
- Minimal operator training	
- Scalable platform	

Affinity SpheriTech beads with immobilised CD73 may offer a solution to this demand, offering scalable, label-free cell purification. However, their capacity for cell binding must first be investigated and compared against current affinity technologies.

6.2 Aims and Hypotheses

6.2.1 Chapter Aim

Chapter 7 offers a study into the fundamental binding between beads and cells, reviewing the impact of bead size, binding capacity and cell detachment. Differential binding of progenitor photoreceptors to SpheriTech beads was performed, and the findings compared to FACS and MACS.

6.2.2 Hypotheses

SpheriTech beads will differentially bind target cells with high sort purity, comparable to current affinity purification techniques. Additionally, the reduced processing of samples during preparation and cell sorting will produce significantly higher cell recoveries than FACS and MACS.

6.3 MRC-5 phenotyping

For fundamental bead binding studies, a convenient cell source was required before testing stem cell-derived progenitors. However, in order to use the same immobilisation protocol for affinity purification beads, a cell line expressing CD73 was needed.

MRC-5, a human fibroblast line, was cultured and then stained for CD73. Immunostaining showed the majority of cells to positively express the antigen (Figure 6.1).
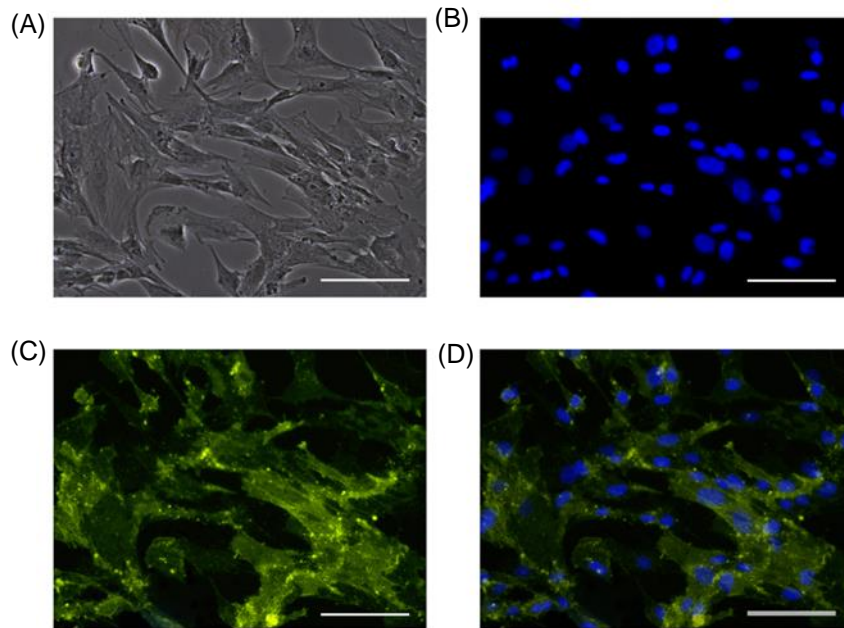
Figure 6.1 *Fluorescent microscopy of CD73 expression MRC-5 cells with (A) Phase contrast, (B) DAPI and (C) CD73 immunostaining and (D) a merged image. Scale bar = 50µm.*

To quantify expression, flow cytometry was used and over 99% of cells were found to be CD73-positive (Figure 6.2). As a result, MRC-5 will be used as a substitute for progenitor photoreceptors to investigate fundamental cell binding characteristics for affinity SpheriTech beads.
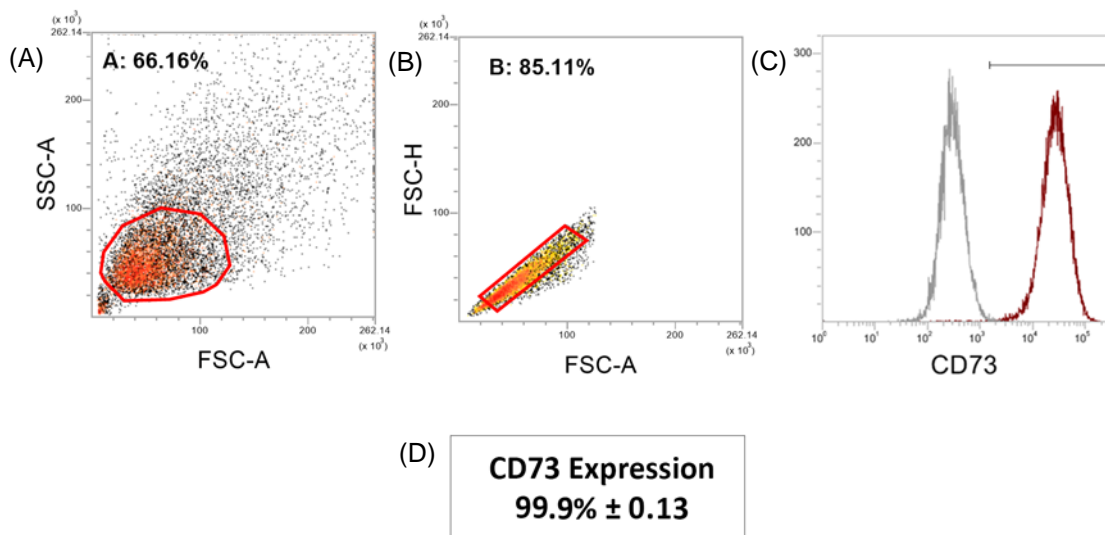
Figure 6.2 *Flow cytometry analysis to quantify CD73 expression in MRC-5 cells. The gating strategy is detailed with a (A) SS v FS dot plot (gate A) to remove debris then (B) FS height*

against area to remove doublets (gate B). (C) The histogram shows the negative population stained with an isotype control (grey) and the CD73 stained sample (red) with positive expression gated from the top 1% of the isotype control. (D) A mean of 99.9% expression was noted in N = 4 ± SD.

6.4 Non-specific binding

Polylysine is frequently used to promote attachment of adherent cells, with polylysine-treated tissue culture surfaces used in cell culture (Mazia, Schatten and Sale, 1975). As a result, it is a concern that proteins will stick to the cationic polymer beads and bind cells non-specifically.

For this reason, excess MRC-5 cells were stained with CellTracker green (CMFDA) fluorescent dye, then incubated with unmodified beads for 15 minutes at room temperature on a roller machine. The cell suspension was drained, before beads were washed with PBS and viewed under a fluorescent microscope. Numerous cells were observed to be bound onto beads, suggesting there is a high degree of non-specific binding (Figure 6.3).

(A) (B) (C)

Incubation   Post-wash, Untreated   Post-wash, Treated
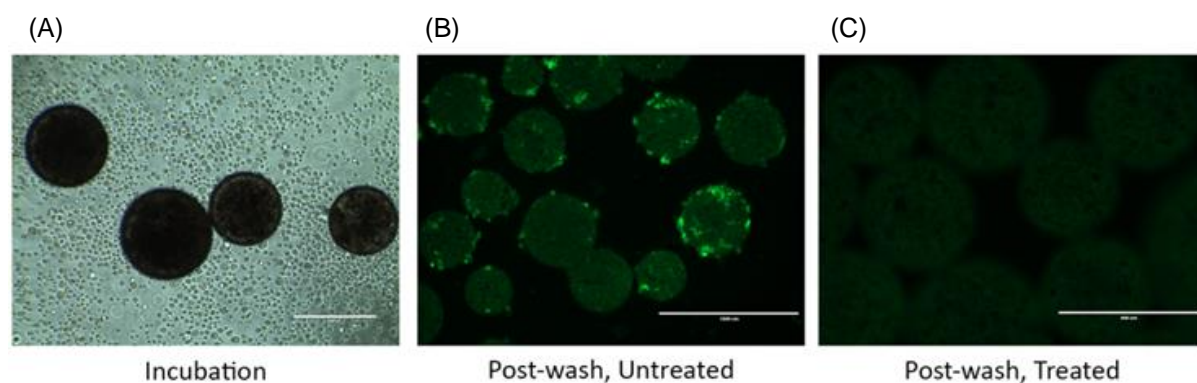
Figure 6.3 *Assessment of non-specific cell binding. (A) Cells were stained with CellTracker green fluorescent dye and incubated with a control of unmodified beads for 15 minutes on a roller machine. (B) After eluting the unbound suspension and washing with PBS, beads were imaged under a fluorescent microscope and non-specific cell binding was observed. (C) Beads pre-treated with ethanolamine were then incubated with stained cells, washed and imaged with fluorescent microscopy. No non-specific binding was observed with treated beads. Scale bars = (A, C) 400 µm or (B) 1000 µm.*

Protein binding to Poly-Ɛ-Lysine is facilitated by activated carboxyl groups on the surface of beads. Therefore, to prevent non-specific binding of cells, unreacted esters must be deactivated. Ethanolamine is a primary amine which binds to NHS-ester groups and prevents protein binding. Beads were therefore washed with 5%v/v ethanolamine to cap free carboxyls, then the same experiment incubating green fluorescently stained MRC-5 cells was carried out. After a PBS wash, the beads were imaged and no bound cells were noted.

As a result, treatment with ethanolamine has been shown to mitigate cells binding non-specifically to beads. This will allow selective binding through affinity interactions, by antibody immobilised onto the bead's surface binding to specific target cells in suspension.

6.5 Bound cell counts

Spheritech beads were immobilised with approximately 4 CD73 antibodies per cm^2 to produce affinity beads for purification (see Figure 5.14). In order to characterise their capacity to bind cells, the number of bound cells must be determined.

6.5.1 Supernatant-derived count

To assess cell binding, firstly the number of bound cells must be determined. By counting the number of unbound cells after incubation with affinity beads, a supernatant-derived bound cell count can be calculated. An initial viable cell count was recorded before incubation, then after elution and washing, the unbound cell suspension was counted and deducted from the initial cell count. To determine cells lost through handling samples, the experiment was run 5 times with no beads present during the incubation, and the average cell loss deducted from each supernatant-derived count.

An initial cell suspension of 2.4×10^5 per experiment was incubated with beads for 15 minutes. After eluting and washing, a cell count was performed on the supernatant suspension to find an average of 7.2×10^4 viable cells. As a result, the average number of cells bound to beads was derived to be 1.6×10^5 (Figure 6.4).
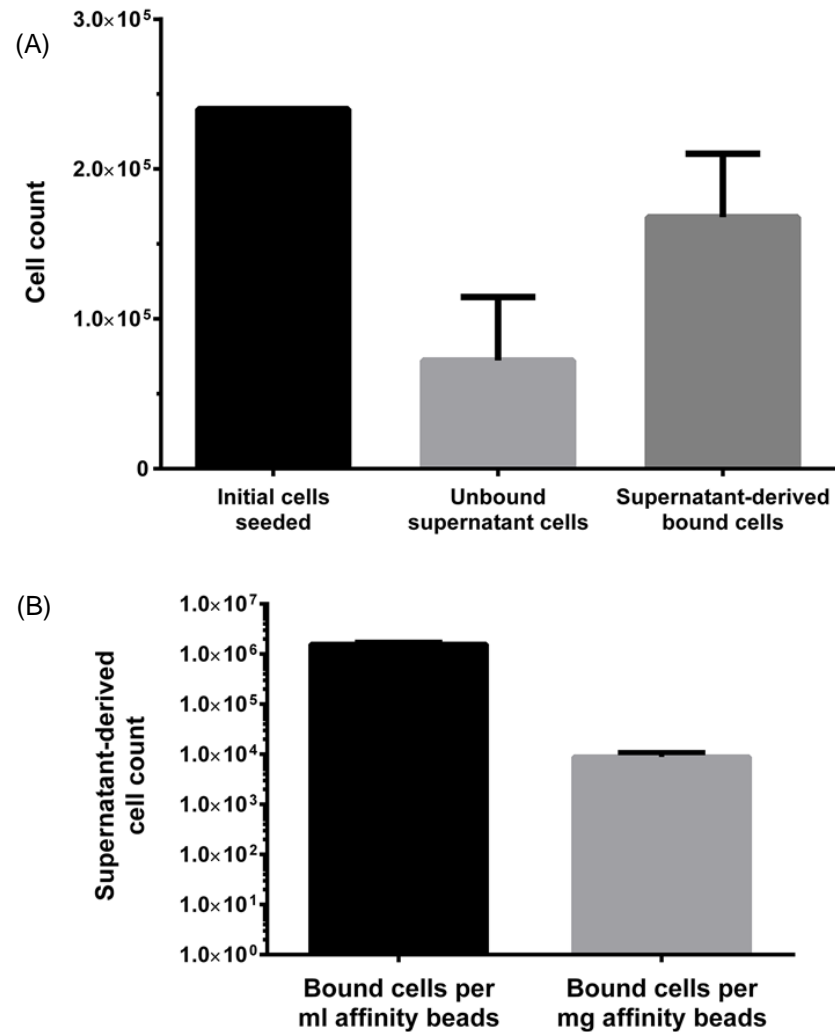
Figure 6.4 *Supernatant-derived cell counts for affinity bead separation. (A) Bar chart of the initial cell count, supernatant cell counts after incubation with SpheriTech beads and the derived cell number bound to beads for N = 5 ± SD. (B) Bar chart of supernatant-derived bound cells per ml or mg of affinity purification beads for N = 4 experiments ± SD.*

The standard deviation noted for supernatant-derived counts is likely due to variation in the number and size of affinity beads used. Consequently, to present cell binding in a manner which can be interpreted and assessed across multiple samples, the bound cells per ml and mg of affinity beads were calculated. The volume and mass of beads used in each experiment were determined by suspending beads into a known volume of PBS, and measuring the displacement and increase in mass. An average of 17 mg and 100ul of SpheriTech beads per

sample were tested, and found to bind 1.56×10^6 cells and 8.81×10^3 cells per ml and mg of affinity beads respectively.

From this, an approximation of the required beads to process an autologous dosage can be estimated (as discussed in Chapter 3.6). Assuming 8.8×10^6 cells are needed for a clinical dose, around 6ml or 1g of beads will be sufficient to separate this cell number. However, to further investigate bead binding and improve upon this initial calculation, the impact of bead size, cell recovery through capture and cell detachment, and validation of differential binding must be carried out.

6.5.1 Confocal-derived count

A second method of bound cell counts using confocal microscopy was developed to investigate the impact of bead size. For visual counts, MRC-5 cells were stained with a red fluorescent DNA dye before incubation with affinity purification beads for 15 minutes. Bead complexes were then washed and fixed with PFA for fluorescent confocal imaging (Figure 6.5). Cells were manually counted on the visible top hemisphere of a bead, and the number multiplied by two to give the total cell number per bead.
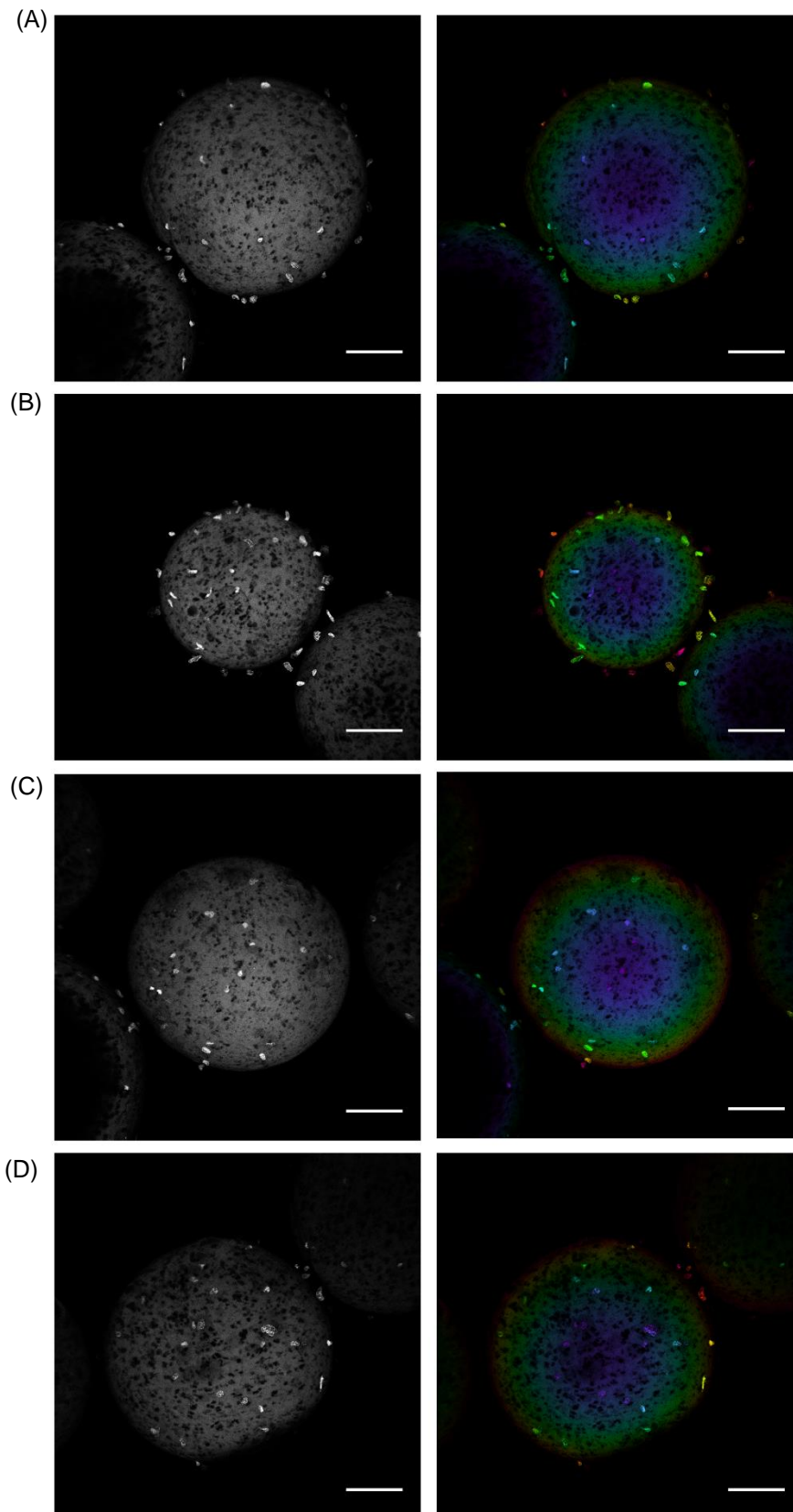
Figure 6.5 *Fluorescent confocal microscopy images of MRC-5 cells bound to affinity beads.*
CellTracker red fluorescent stained MRC-5 were incubated with SpheriTech beads for

15minutes before washing and eluting unbound cells. (A-D) Bound cells were then imaged on a confocal microscope with a greyscale and pseudo-3D colour depthmap image taken to aid in the visual count of bound cells. Scale bars = 85 μm.

As with supernatant counts, the raw cell counts gave a large cell binding range due to variation in bead size. However, given that individual beads were assessed, a greater variation was noted than with supernatant-derived sample counts. A range from 24 to 644 cells per bead was counted with a mean of 117, across a wide range of bead sizes (Figure 6.6). However, this counting technique permits the impact of bead size upon binding to be assessed by measuring bead diameter.
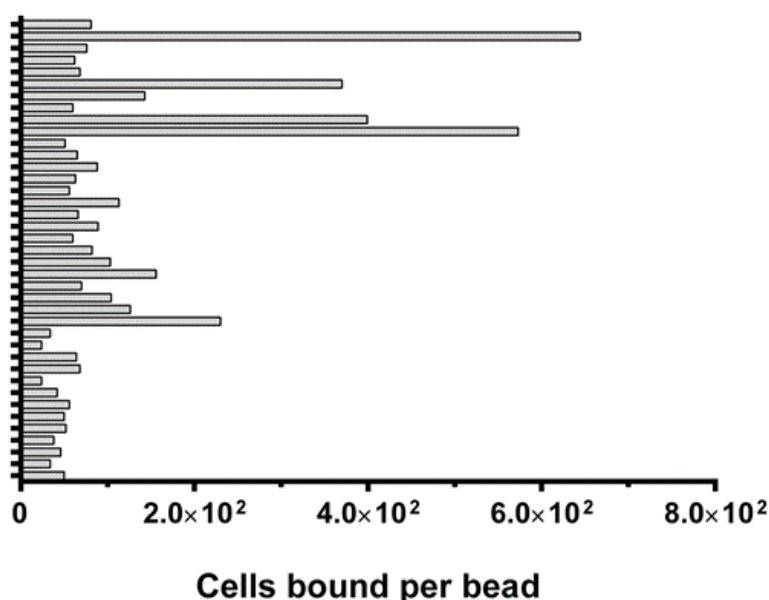
Figure 6.6 Cell binding from fluorescent confocal-derived cell counts. Bar chart showing the number of bound MRC-5 cells on individual beads, as derived through visual imaging counts.

6.6 Impact of bead size upon binding

6.6.1 Contact angle

Before looking at the impact of bead size, the angle of binding between cells and beads was analysed to determine a range of bead sizes to test. To assess this, an equation was used to calculate the contact angle between 10 μm and 20 μm diameter cells, and beads between 1 μm

and 1000 μm in diameter. For mathematical simplification, cells were assumed to be planar discs and beads to be spherical. The calculation for contact angle was:

$$A = [TAN (D_c/2)/(D_b/2)] * (180/\pi)$$

Where A is the contact angle (°), D_c is the cell diameter (μm) and D_b is the bead diameter (μm).
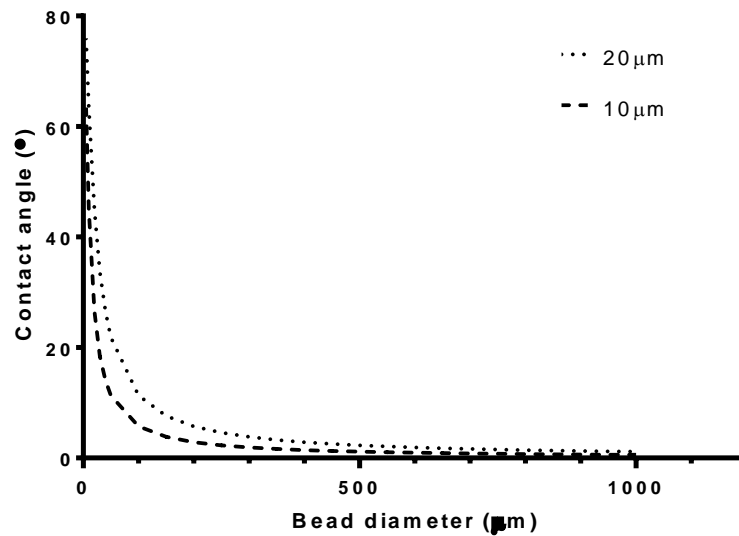
Figure 6.7 Contact angle of cell binding to beads. Line graph of the angle of cellular binding to beads for 10 μm (thick dotted line) and 20 μm (fine dotted line) diameter cells and beads between 1 μm and 1000 μm.

With a bead diameter above 200 μm, the contact angle with cells was observed to plateau towards an asymptote of 0° (Figure 6.7). Due to this phenomenon, for bead diameters greater than 200 μm there is negligible change in the angle of binding experienced by cells. As a result, to provide similar binding characteristics, a range from 200 μm to 1000 μm will be examined. The maximum bead diameter was implemented for testing due to impracticality over the surface area:volume ratio at this size.

6.6.2 Cell binding study

Affinity purification beads, within the aforementioned manufactured size range, were incubated with stained MRC-5 cells as previously detailed. The bound cells were then imaged under a fluorescent confocal microscope and, by measuring the diameter of affinity beads and assuming sphericity, cell binding per unit surface area was calculated.
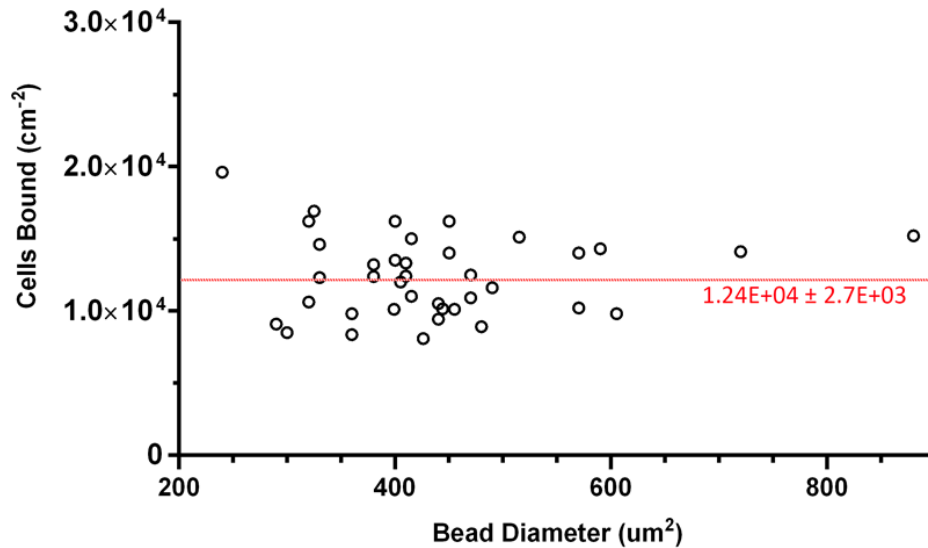
Figure 6.8 *Impact of affinity bead size upon cell binding. Scatter graph of cells bound per cm^2 against the diameter of beads (µm) as determined using confocal microscopy where each bead is a point on the graph. The red line is the mean bound cells/cm^2 ± SD.*

An average bead capacity of 1.2 x 10^4 cells per cm^2 was found across the examined diameter range (Figure 6.8). Importantly, only a small standard deviation of 2.7 x 10^3 was noted suggesting bead diameter did not have a significant impact upon cell binding. The hypothesis that contact angle may be a critical attribute cannot be confirmed, however, although a negligible change in contact angle produced consistent cell binding. Further work could involve testing bead diameters below 200 µm.

6.6.3 Bound cell coverage

To investigate the coverage of cells across a bead's surface, a few assumptions must be made. For the 200 µm to 1000 µm beads, possible surface area is in the order of 0.126 mm^2 to 3.14 mm^2. Cells usually have a diameter of approximately 20µm, so assuming binding in a planar

fashion with contact length equating to the cell diameter, a cell would take up 314 µm^2 of area. As a result, one bead could potentially bind from 100 to 10,000 cells with 100% of the available surface area covered. To compare this theoretical maximum binding capacity to the density of cells bound through experimentation, cells bound across a range of bead sizes were compared against the surface area available.

A cell density of 1.2×10^4 cells per cm^2 of bead surface area equates to around 4% of total bead coverage (Figure 6.9). Across the range of bead sizes tested, this results in 16 to 390 cells per bead.
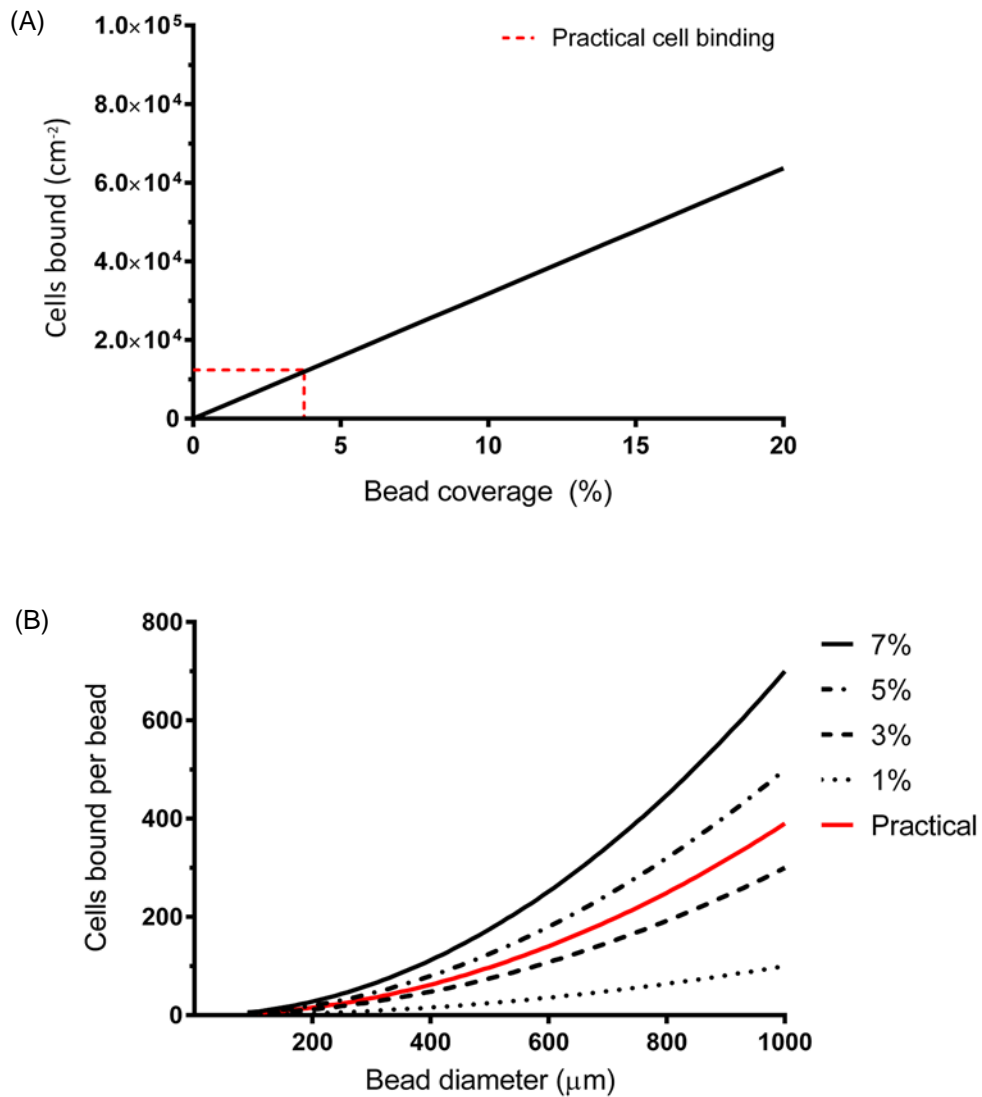
Figure 6.9 *Cell coverage of beads. (A) Line graph showing the relationship between bound cells density against the percentage of bead surface covered. The experimentally-derived cells*

bound per surface area is shown as a red line and correlates to 4% bead coverage. (B) Cells bound per bead was then plotted against bead diameter for different percentages of bead coverages: 1%, 3%, 5%, 7% and the experimentally derived bead surface coverage of 4%.

Although complete bead coverage is unrealistic when operating a dynamic system, 4% is lower than the expected binding density. This may be down to several factors. Firstly, interaction between cells during binding is little understood. At the point of contact between cell and bead, the impact velocity and rolling motion is unknown. A combination of the rotational and translational motion must be considered, based off the centre of mass and angular velocity. It is unknown whether the cell will be fixed at the point of contact, or if there is rolling or slipping of the cell across the bead surface. This may interfere with adjacent cell binding and reduce the possible coverage.

Secondly, the current purification system used is a batch system with an uncontrolled mixing regime. For affinity separation to function, it is critical for cells to contact beads and initiate binding. Therefore, ensuring that all cells have direct contact with beads is a priority when designing a device to perform purification.

Although low bead coverage was noted, the importance of optimising this interaction is based on the cost and scale of production required. If affinity beads can operate economically with favourable cell interactions at a 4% bead coverage, optimisation is shifted towards other operational characteristics. The necessity to differentially bind cells, then effectively detach target cells and acquire a high yield of viable cells must still be assessed.

6.7 Cell detachment

As well as the capture of cells, release of bound cells must be explored. For affinity beads with no cellular label, endocytosis or retention of a fluorescent tag is not a concern. However, detachment from beads must still be an efficient process and maintain cell viability.

To investigate detachment, enzymatic cell release with trypsinisation was tested. Cells were stained with CellTracker green fluorophore and captured by affinity beads. The unbound cell suspension was counted to calculate the supernatant-derived bound cell count, then (cell bound) beads incubated with Trypsin for 5 to 10 minutes. The suspension was quenched, then detached viable cells counted and the beads imaged.
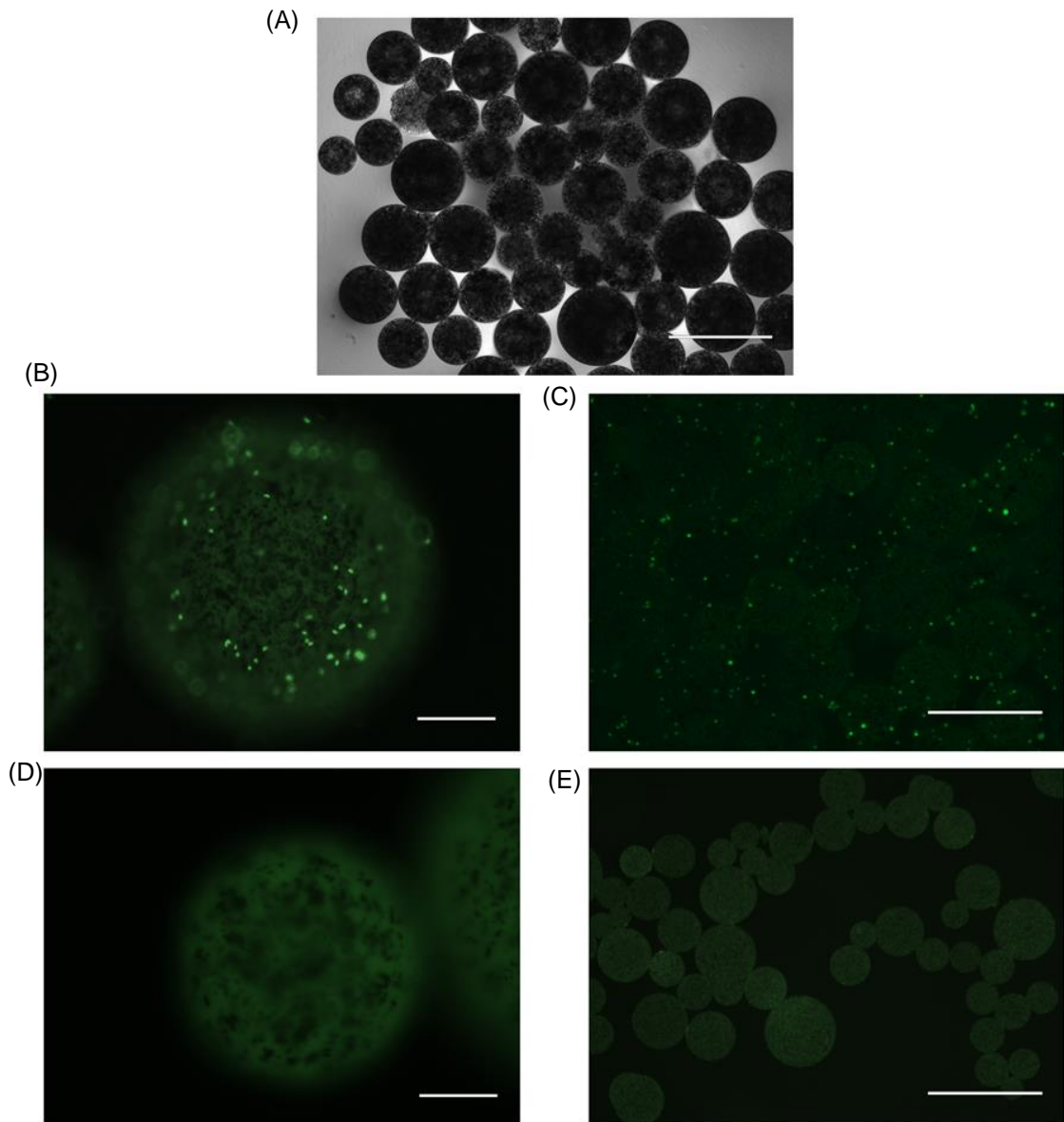
Figure 6.10 *Detachment of cells from affinity beads. (A) Beads were initially imaged by phase contrast before starting the purification. After staining with CellTracker green fluorophore, MRC-5 cells were incubated with affinity SpheriTech beads, and after washing, (B-C) bound cells were imaged using fluorescent microscopy. Cells were enzymatically detached from beads, and*

(D-E) the beads were imaged again to observe any remaining bound cells. Scale bar = (A, C-E) 1500 µm, (B-D) 200 µm.

In all samples tested, negligible cells were noted to be attached to the beads after release, demonstrating that enzymatic detachment is an effective strategy with regard to cellular recovery (Figure 6.10).

To further evaluate trypsinisation as a method to detach cells, supernatant-derived bound cell counts were compared against the viable cell count from detached cells. From this, cell recovery can be calculated. In 6 experiments using the previously detailed method, supernatant-derived bound cell counts were determined and compared against viable cell counts following the detachment of affinity bead-bound progenitor photoreceptors. A high cell recovery of 89% was found, confirming the visual observation that cells are efficiently detached by trypsinisation (Table 6.2).

Table 6.2 Cell detachment efficiency from affinity SpheriTech beads using progenitor photoreceptors.

Supernatant-derived bound cell count	Detached cell count	Cell detachment efficiency (%)
8.2×10^5	7.4×10^5	90
9.8×10^5	9.0×10^5	92
2.7×10^6	2.4×10^6	88
1.2×10^6	1.1×10^6	90
1.5×10^6	1.3×10^6	85
1.9×10^6	1.7×10^6	88
		Average: 89

The detached cells were re-plated overnight to ensure their capacity for adhesion had not been impaired through capture and release. Bead binding was shown to not impact the cells' ability to adhere to plastic, and minimal floating apoptotic cells were noted in the media. Capture and

release of cells from affinity beads has now been established, but the selective binding of target populations must still be assessed.

6.8 Differential binding of progenitor photoreceptors

To compare SpheriTech bead binding against FACS and MACS, the same methodology to assess purity, yield and viable cell recovery was assessed for progenitor photoreceptors derived from human pluripotent stem cells.

6.8.1 CD73 sorting characteristics

Again, co-expression with CRX was used as the key criterion to assess immobilised CD73 affinity beads' capacity for differential cell binding. As with FACS and MACS, after sorting cells with SpheriTech beads, the unbound cell population (waste stream) and the final purified (cell product) population after detachment were stained for CRX expression and assessed by flow cytometry. Again, as with the examination of current purification technology, the progenitor yield and sort purity were derived from expression data.

(A)
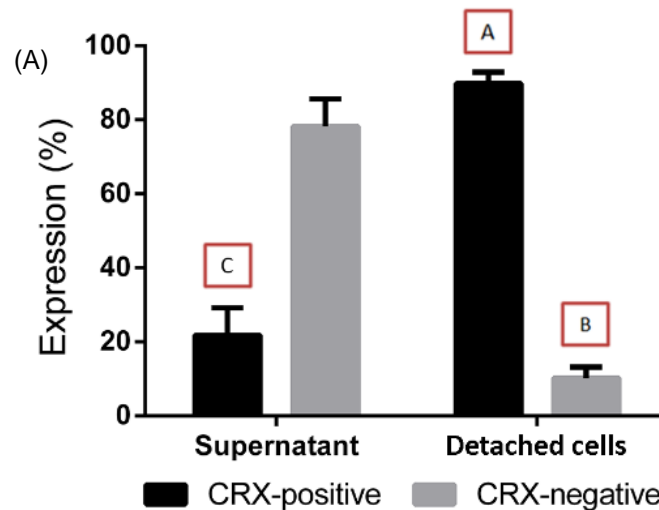
(B)

$$\text{Progenitor (CRX) yield} = \frac{A}{A+C} = 54.9 \pm 9.1\%$$

$$\text{(CD73) sort purity} = \frac{A}{A+B} = 89.8 \pm 3.3\%$$

Figure 6.11 *SpheriTech bead sorting characteristics. (A) Bar chart comparing the unbound supernatant and detached positively purified cell population for CRX expression. Black shaded columns show CRX-positive expression, and grey shaded columns are CRX-negative cells. N = 6 ± SD. (B) The table insert shows the equations and result of progenitor yield and sort purity for affinity beads. A to C refer to the letters highlighting columns in the bar chart. Progenitor yield is the percentage of CRX-positive photoreceptors recovered through a CD73-positive purification; sort purity is the percentage of cells within the CD73-positively sorted population which co-express CRX.*

As the same CD73 antibody was immobilised on SpheriTech beads as used for MACS and FACS, a similar specificity towards binding was expected. By analysing the detached cell suspension, 89.8% of cells expressed CRX which defined the sort purity – the number of CRX-positive progenitors within the CD73 affinity bead positively sorted cell population (Figure 6.11). This result is comparable to that observed with both previous techniques assessed.

However, the progenitor yield noted was significantly lower than that previously identified for MACS and FACS. 21.8% of the unbound supernatant tested positive for CRX expression, meaning the purified detached population contained only 54.9% of the total CRX positive cells. Comparatively, MACS and FACS previously boasted yields of 75.8% and 87.6%.

The difference is explained by the purification systems used. With the current, proof-of-principle system for SpheriTech bead binding, mixing is dependent on a roller machine for agitation. However, this is an inefficient method to ensure all cells interact with beads to promote binding. The low yield is likely due to target cells not contacting affinity beads, thereby preventing cell capture.

Further work should involve the design and manufacture of a purification device which prioritises cell and bead contact, whilst preventing clogging or blockages. This may involve a chromatography-style system which can utilise the buoyant and paramagnetic effect SpheriTech beads possess, to manipulate beads around the cell suspension. Whether a column

or chip design, deviation from incubating cells in a batch system is suggested to enable either re-circulation of the cell suspension or utilising the benefit of plug flow in a column.

6.8.2 Cell recovery

Cells lost through processing were again analysed as previously with FACS and MACS, calculating the difference between starting cells numbers and those recovered in the waste (unbound supernatant) and product (detached cell) outputs. The processing of cells for SpheriTech purification is detailed in Figure 6.12 B. The dissociated retinal differentiation suspension is washed and incubated with affinity beads for 15 minutes on a roller machine. After eluting the unbound cell suspension and washing the beads, target cells are detached enzymatically. The total viable cell number after cell sorting, as a percentage of the starting cell number, was then calculated.
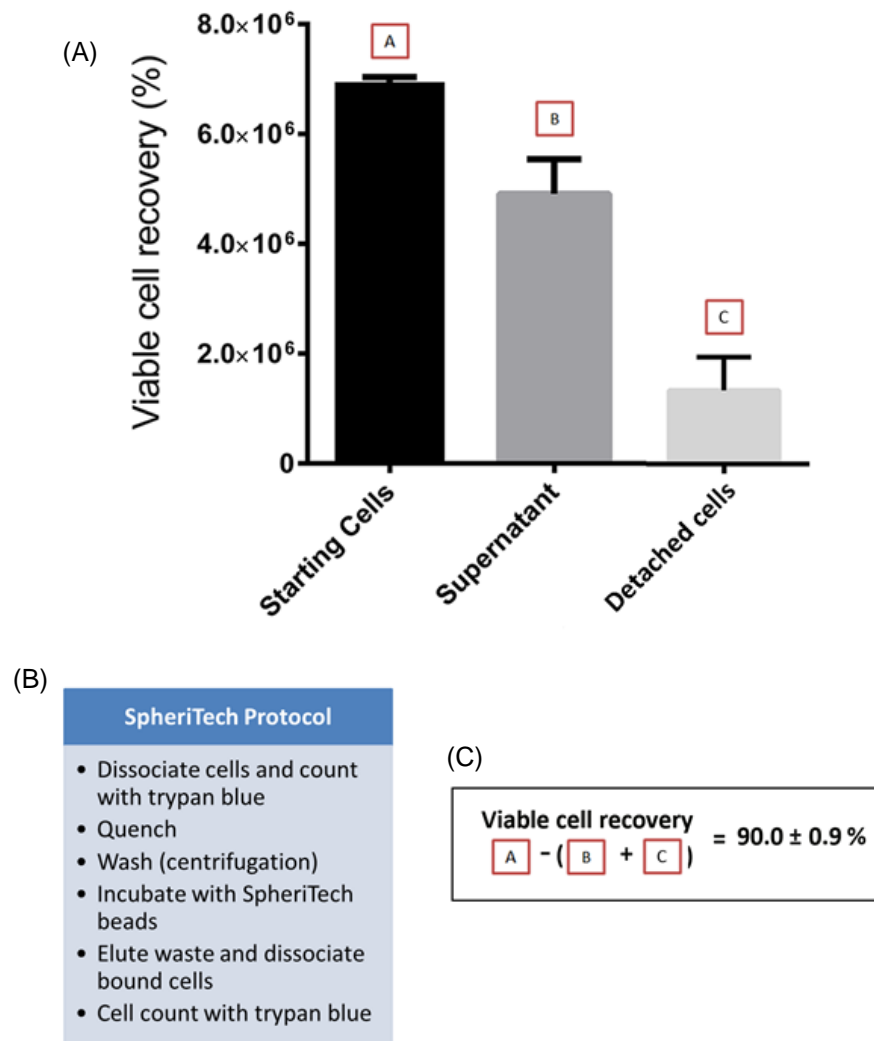
Figure 6.12 *Viable cell recovery following SpheriTech purification of day 31 retinal differentiation cultures. (A) Bar chart showing viable cell number for the starting retinal cell suspension, unbound supernatant and detached purified progenitor cells. A mean of 6.9 x 10^6, 4.9 x 10^6 and 1.3 x 10^6 respectively was noted (N=6). (B) The protocol for purification with SpheriTech beads is detailed in the table insert, (C) and the equation and calculation of viable cell recovery shown with A to C referring to the letters highlighting columns in the bar chart.*

Unlike current purification technology, cell labelling is not required for SpheriTech purification. FACS antibody staining or MACS bead incubation requires multiple centrifugation wash steps, each with an associated cell loss. There is no preparation or label required for SpheriTech beads as they are mixed directly with the cell suspension for target cell capture. Compared to the 69.6% and 58.7% viable cell recovery for FACS and MACS respectively, 90% of cells were

recovered through processing with affinity beads (Figure 6.12). This illustrates a significant reduction in cells lost through sample preparation and processing.

6.9 Chapter Discussion

Having developed a reproducible manufacture process and characterised the physical properties of affinity SpheriTech beads, this chapter evaluated bead potential to bind cell population and differentially separate a target cell population in comparison to current affinity techniques.

Initially non-specific binding of cells to beads was examined and found to occur with polymer beads which promote protein binding. As this would prevent selective cell binding, beads were incubated with ethanolamine after antibody immobilisation to cap any remaining free carboxyl groups on the surface. This short incubation prevented non-specific binding and allowed the beads to be utilised for further investigation.

The method to count bound cells bound to beads was then assessed through a supernatant and confocal-derived method. Deductive cell counts from unbound supernatant allowed the cellular binding per ml and mg of beads to be calculated as 1.56×10^6 cells and 8.81×10^3. This represents the binding capacity of affinity beads given their current chemical makeup and manufacture specifications. Through visual cell counts using fluorescent confocal microscopy, the impact of bead size could also be assessed. After modelling the contact angle of cell binding, a range of 200 µm to 1000 µm affinity beads was chosen for testing with MRC-5 cells that express CD73. This range was chosen because, due to the asymptotic nature of the binding angle, at diameters above 200 µm the binding angle of cells is negligibly affected; above 1000 µm, the surface area to volume ratio is detrimental to purification efficiency. Within this range, bead size was shown to be independent of cell binding per surface area. Further investigation at smaller diameters is necessary to demonstrate a relationship between binding angle and bead size.

Cell detachment was evaluated by using enzymatic cell release from beads, chosen due to processing simplicity without subjecting cells to harsh conditions such as with pH-mediated

release. Trypsinisation was shown to efficiently detach cells, recovering 89% of bound cells with high viability.

Cell binding, the capacity and detachment for a range of bead diameters, has been demonstrated. As with FACS and MACS, the purification of pluripotent stem cell-derived progenitor photoreceptors was characterised for SpheriTech beads. The purity and yield, based on CRX expression, within the unbound supernatant and detached final cellular product was evaluated. A comparable high purity was noted to current purification techniques, expect as the same antibody with high selectivity has been used in each technique. However, the progenitor yield for SpheriTech beads was lower than expected at 54.9%. This result may be due to inefficiency with the incubation of cells and beads, with the target cell population not contacting beads due to ineffective mixing in the current batch (proof-of-concept) system. Ensuring contact between all cells and beads is paramount for affinity separation, and the current purification system does not permit adequate cell mixing or bead manipulation to accomplish this. As such, development of a purification device to fulfil these needs is required.

The viable cell recovery from processing samples with SpheriTech beads was assessed as previously with FACS and MACS. As no product labelling is required, this greatly reduced the bioprocess complexity, risk and process duration. A significantly higher recovery of 90% was found due to the minimal processing of samples in comparison to current affinity technology, and no cellular label remained attached to the cell product after sorting. To truly understand how SpheriTech beads match up against current purification technology, and critically assess how experimentally-derived binding characteristics impact the overall bioprocess, an economic appraisal of the novel technology was carried out.

Chapter 7: Deterministic cost model for cell therapy purification

7.1 Introduction

By inputting the experimental characteristics of FACS, MACS and SpheriTech bead purification into a bioprocess economics tool, the associated cost of goods (COGs) can be evaluated and compared. The tool created provides a method to quantitatively assess novel purification strategies, and determine what critical developmental improvements must be made to compete against current affinity technology.

7.1.1 Deterministic tools

Decisional tools and economic approaches to bioprocess appraisal have been successfully applied to the biopharmaceutical sector (Farid *et al.*, 2000; Farid, Washbrook and Titchener-Hooker, 2005; Chhatre *et al.*, 2007; Stonier *et al.*, 2012; Pollock, Ho and Farid, 2013). Deterministic models possess the capacity to improve bioprocess design by identifying optimal cost-effective production or scaling strategies. Comparing different technologies across a range of manufacture scales and operational variables provides 'switch-points', where the most cost-effective bioprocess can be evaluated. This has previously been carried out for expansion and differentiation in allogeneic and autologous bioprocesses (Simaria *et al.*, 2014; Hassan *et al.*, 2015; Jenkins *et al.*, 2015), and iPSC-derived products (Darkins and Mandenius, 2013).

7.1.2 Integrated experimental and economic analysis

To date, most studies in this field have focussed on either an economic (Darkins and Mandenius, 2013; Jenkins *et al.*, 2015) or experimental approach (Gouras *et al.*, 1992; MacLaren *et al.*, 2006; Lamba, Gust and Reh, 2009; Lakowski *et al.*, 2011) towards bioprocess development in cell therapy. Here, an integrated experimental and economic appraisal of affinity

purification platforms has been created. The methodology and integrated techno-economic analysis used can be applied to other bioprocesses which utilise affinity purification.

Experimental data to populate the decisional tool was from Chapter 4, with base case model inputs detailed in Table 7.1. Purification yield, purity and differentiation efficiency were selected from experimental results, as was the turnaround time and throughput of MACS and FACS. Additional assumptions over costing are reviewed in Chapter 2.15 and in appendix A. The model was used to evaluate COG per dose for purification operations, as well as the bioprocess as a whole.

Table 7.1 *Process parameters for MACS and FACS purification technology based on experimental data from Chapter 4 and methodologies described in Chapter 2.*

	Yield	Purity	Throughput (cells/hr)	Turnaround (preparation & cleaning)	Differentiation Efficiency	Dose Size
MACS	75.0	94.6	3.6×10^7	2.5 hr		
					30%	10^7
FACS	87.6	93.4	1.2×10^8	3.9 hr		

Design and analysis with the bioprocess economic tool was conducted in collaboration with Michael Jenkins from UCL, Biochemical Engineering. More details about the

7.2 Aims and Hypotheses

7.2.1 Chapter Aim

Chapter 8 presents a techno-economic appraisal of affinity purification, assessing the COG per dose when utilising different cell purification strategies within a bioprocess. A breakdown of the key cost drivers was derived through sensitivity analysis, then multiple scenarios run to find the favoured purification strategies at different operating parameters. SpheriTech beads were then economically compared to FACS and MACS in the economic tool.

7.2.2 Hypotheses

Purification will play an important part in bioprocess COG per dose with antibody-associated costs as a key cost driver. The limited throughput of FACS purification will impact economic favourability at larger scales. The COG per dose using SpheriTech beads will be competitive to current technology due to the low antibody reagent costs and improved cell recoveries.

7.3 COG breakdown

The COG breakdown for individual components of purification, as well as the impact purification technology has upon the entire bioprocess, was assessed using the bioprocess economic tool. Autologous therapies require a scale-out, rather than scale-up strategy to be adopted for bioprocess design, and as a result, it is unlikely a single facility could deal with an annual demand in excess of 10,000 doses per year. Consequently, three different annual demands were initially trialled to evaluate economies of scale that could be achieved: 100, 1000 and 10,000.

When looking at the entire bioprocess, purification accounted for around 10 to 15% of the total COG, regardless of the purification technology used (Figure 7.1 A). The total COG per dose equated to between £30,000 and £40,000 depending on scale, with differentiation accounting for approximately 50% of this total.

An annual demand of 1000 doses was selected to perform cost breakdowns for each purification technique, due to negligible economics of scale noted above this. At base case inputs, both methods cost a little over £3000 per dose, and were dominated by antibody associated reagent costs. Purification cost 12% more with MACS in comparison to FACS purification (Figure 7.1 B), predominantly due to disposable costs that were 3.9-fold greater. Although MACS offers a reduction in indirect, labour, and media & reagents costs (39%, 20%, and 9% respectively), these savings did not outweigh the stated difference in disposables.
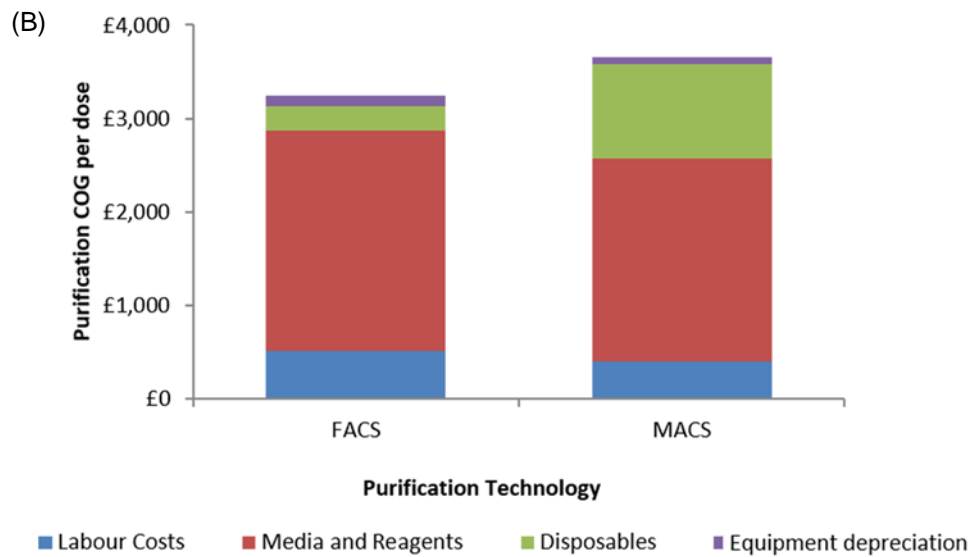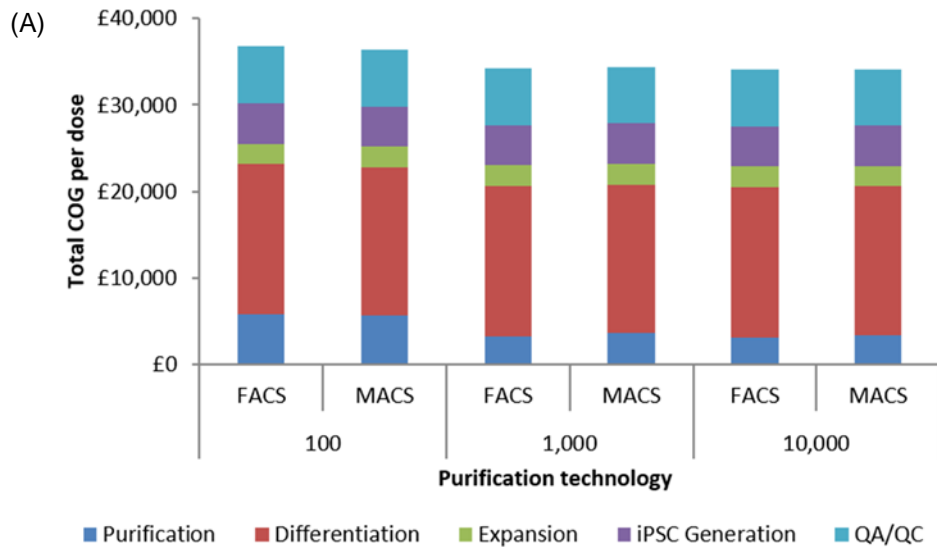
Figure 7.1 *COG analysis. (A) COG breakdown for the whole bioprocess by unit operation when FACS and MACS are employed as cell purification at annual demands of 100, 1000, and 10,000 doses. (B) Bar chart showing a breakdown of purification costs for the use of FACS and MACS when an annual demand of 1,000 doses is required.*

7.4 Sensitivity Analysis

To further evaluate how the choice of purification technology effects bioprocess COG, sensitivity analysis was conducted to find the key operating parameters. By varying every base-case input in the model by 15%, the top four parameters with the largest impact upon COG/dose were

determined (Figure 7.2). Regardless of purification technology used, the key economic drivers (i.e. factors which had the greatest impact on COG/dose) were all parameters that had a direct effect on the scale and cell number required for differentiation.
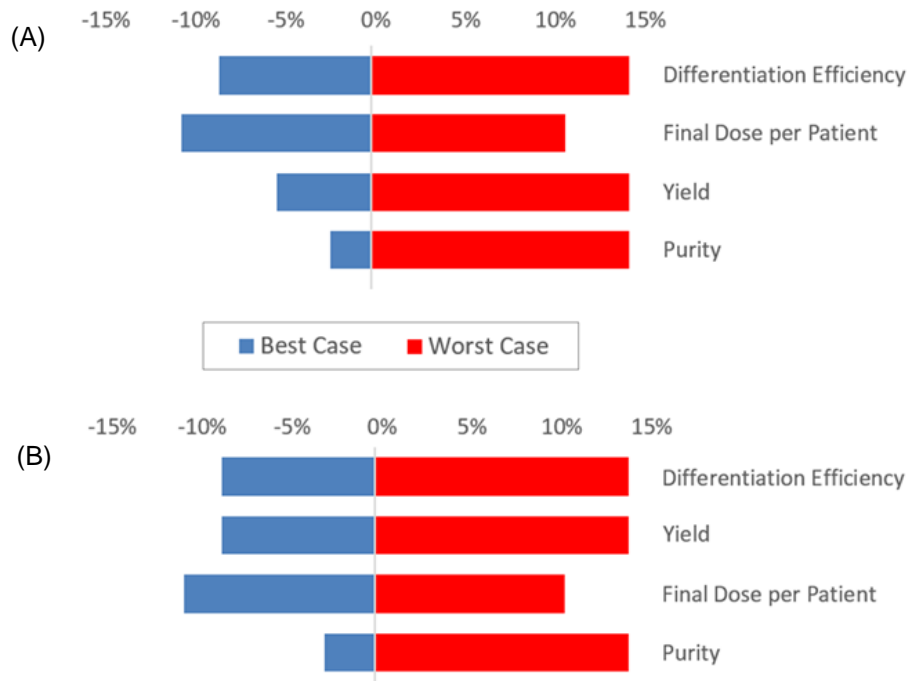
Figure 7.2 *Sensitivity analysis. Tornado charts showing the effects of varying key process parameters on bioprocess COG per dose when (A) FACS or (B) MACS is used for cell purification. Best case (blue) and worst case (red) values were calculated by adjusting each parameter by +/- 15% from the base case value given in Table 7.1, with an annual demand of 1,000 doses.*

Altering the progenitor yield and sort purity by 15% produced a 21% and 16% swing in COG/dose for MACS, and a 20% and 17% swing for FACS respectively. These results appear to confirm the hypothesis that, whilst purification is perceived to account for a relatively small percentage of the total COG, purification performance characteristics have a significant impact upon the COG associated with the bioprocess.

7.5 Scenario Analysis

Now that the key cost drivers were established, the economic model was used to evaluate the favoured purification technology across different scenarios.

7.5.1 Differentiation efficiency and Dose size

Currently, both dose size and differentiation efficiency are unknown variables as to date, progenitor photoreceptor transplantation has only been tested pre-clinically in animal studies. Identification of the 'true' regenerative population to transplant into a patient - cells which will integrate into a recipient's retina and form functional photoreceptors - is also still a heavily researched topic. Additionally, iPSC therapies may not be truly autologous: through HLA matching, there is potential to treat multiple patients from one donor, dramatically increasing the production scale required. This, in addition to variability regarding retinal integration efficiency (West et $al.$, 2012) and potentially increasing the cell number for quality assurance, will increase the cell numbers required per dose.

As a result, selecting a range for scenario analysis was principally based on current literature and existing clinical therapies. Operating at scales of 10^8 cells or more is likely to be a necessity. Dose size was varied from 10^7 to 2×10^8, whilst differentiation efficiency was assigned values between 30% and 80% to reflect the variation found in literature differentiation protocols (Lamba et $al.$, 2006; Osakada et $al.$, 2008; Boucherie, Sowden and Ali, 2011; Meyer et $al.$, 2011; Tucker et $al.$, 2011; Aizawa and Shoichet, 2012; Mellough et $al.$, 2012).

At a differentiation efficiency of 30% (meaning, after differentiation 30% of the heterogeneous cell population are progenitor photoreceptors), FACS is the more cost-effective technology up to a dose size of 2.9×10^7 (Figure 7.3). For efficiencies up to 80%, a maximum of 6.8×10^7 cells can be processed while still keeping FACS cost-effective. Exceeding these dosages will produce an operating window whereby $COG_{MACS} < COG_{FACS}$.

At dose sizes above 7×10^7 cells, multiple FACS machines would be required to process an individual sample in under 4 hours. Operating above this duration would significantly impact cell viability (Veraitch et $al.$, 2008), and as such it was assumed multiple machines would be required. Whilst the use of multiple FACS machines in parallel could theoretically be used to

purify an individual cell suspension (with samples pooled together after purification), it is unlikely to be employed in a clinical setting. As such, an operational window exists above 3×10^7 or 7×10^7, depending on differentiation efficiency, where FACS is not feasible.
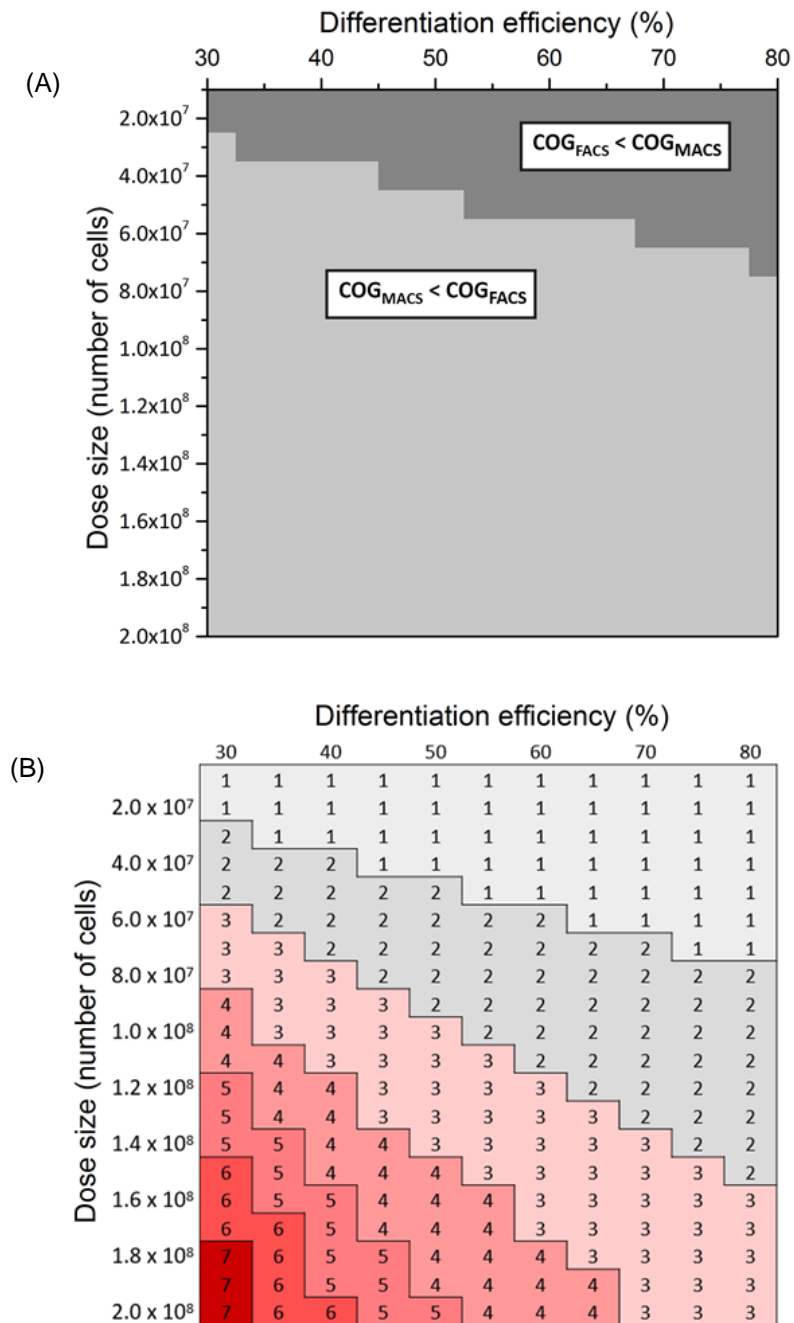
Figure 7.3 *Scenario analysis of key cost drivers showing the economically favoured purification technology. (A) Contour plot illustrating the effects of differentiation efficiency and dose size on FACS or MACS being the most cost-effective technology. Lightly-shaded areas indicate windows where FACS would prove more cost-effective than MACS. Darker-shaded areas*

indicate windows of operation whereby purification of target cells through MACS proves more cost-effective than FACS. (B) Matrix illustrating the impact of dose size and differentiation efficiency on the number of FACS machines required to process an individual patient sample within a 4-hour window. The numbers inside the matrix represent the number of FACS machines required to process the sample in each scenario.

As highlighted through this analysis, FACS is a relatively low throughput technology. For CD73 purification of progenitors, FACS was found to only be feasible when a final dose size in the magnitude of 10^7 or less cells are required. MACS is more suited to larger scales by operating in a batch system which reduces the duration of processing.

7.5.2 Yield and Purity

As sort purity and progenitor yield also have a significant impact upon bioprocess COG, variation within their operating parameters was assessed too. Purity and yield were assigned values between 60-100% and 85-100% respectively, and run through the deterministic model (Figure 7.4 A). When either parameter dropped below 80%, the COG for MACS ($COG_{MACS\ PUR}$) was found to be lower than FACS ($COG_{FACS\ PUR}$). Again, this is likely due to the limited throughput of FACS, eliciting the use of multiple machines when process duration exceeds 4 hours.

To further highlight the switch point between economic favourability, sort purity was fixed at 95% whilst progenitor yield was changed to either 75% or 85% (Figure 7.4 B). At a yield of 85%, FACS purification costs were lower than MACS due to savings in material and reagent costs. However, when progenitor yield is reduced down to 75%, FACS purification costs exceed MACS as a higher cell number is necessary to meet the final dose size.
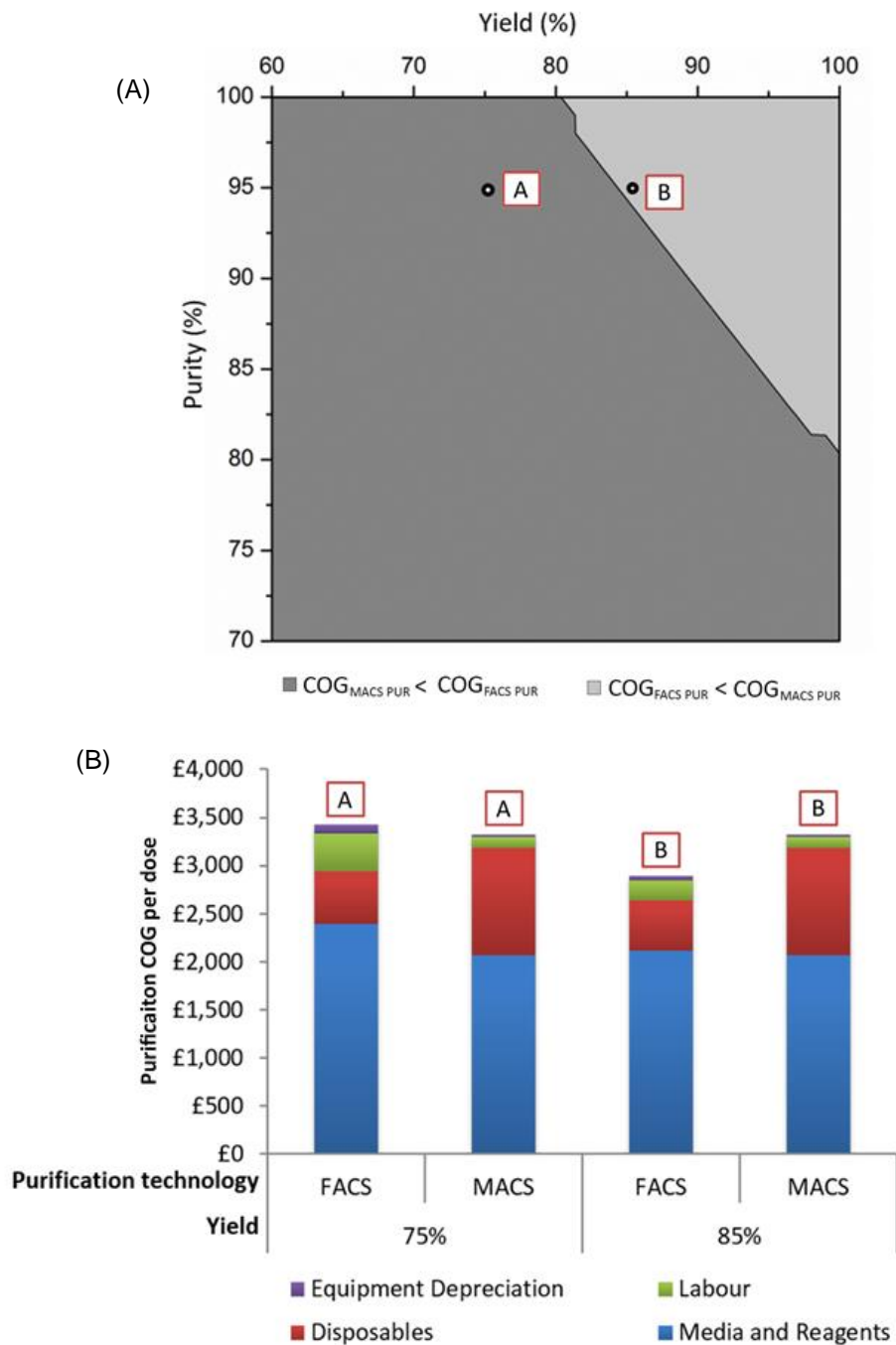
Figure 7.4 Impact of purity and yield on bioprocessing. (A) Contour plot illustrating the effect of varying sort purity and progenitor yield on whether FACS or MACS is the most cost-effective purification technology. A dose size of 10^7 and an annual demand of 1,000 doses was assumed. (B) Purification COG breakdown per dose for FACS and MACS purification when a yield of 75% (point A) or 85% (point B) is assumed, with a fixed purity of 95% for both techniques. These chosen points are labelled on the contour plot.

7.6 SpheriTech COG breakdown

So far, scale has been identified as the key factor to dictate choice of affinity purification. However, there are other limitations with current techniques which must be addressed. Both FACS and MACS result in the retention of a cellular label after purification. Either a fluorescent tag or an iron oxide nanoparticle remain bound to cells which may be unsuitable for transplantation (Alford *et al.*, 2009; Singh *et al.*, 2010; Szalay *et al.*, 2012; E. J. Park *et al.*, 2014). Furthermore, there is a concern that MACS beads may undergo endocytosis, or interfere if multiple positive purification steps are required.

As a result, affinity SpheriTech beads were also examined for their ability to leave purified cells label-free. For analysis, the same consumable demand per run was used for SpheriTech bead as with MACS operations, assuming similar clinical requirements for tubing and other plastic disposables.

Cost benefits from SpheriTech beads are predominantly due to the reduced antibody demand, as well as a higher viable cell recovery by minimising sample processing (see Chapter 6.8.2). As previously noted (Figure 7.1 B), antibody reagents are the primary cost driver for purification. Fluorophore conjugated antibodies must saturate cells to elicit excitation for target identification, with the amount of antibody required heavily impacted by the volume and number of cells processed. Similarly with MACS, the capture of cells is dependent upon the permanent binding MACS beads which have been coated in antibody. Due to their high surface area to volume ratio, a large amount of antibody must be fixed to MACS beads to facilitate binding with cells. Due to their size, the paramagnetic response from individual beads is negligible so a high number of MACS beads are required.

Contrastingly, the binding requirements for cells to SpheriTech beads are dependent solely on achieving enough force to temporarily capture cells. The maximum immobilised antibody capacity is based on antigen density observed from a cell's surface. This temporary bond to capture cells requires significantly less strength (and therefore antibody) than with current affinity techniques that use antibody-fixed labels as a method to identify target cells.

For FACS and MACS, 80% and 65% of operation's cost is due to antibody, and around 6% of the total bioprocess COG for both technologies (Table 7.2). The percentage COG associated with antibody for SpheriTech beads is a factor of 15 lower than current MACS and FACS. Antibody contributed to only 4% of the purification costs, and 0.15% of the total bioprocess COG with SpheriTech purification.

Table 7.2 *Comparison of antibody consumable costs per dose for different purification techniques, and as a percentage of the purification operation or total bioprocess COG.*

Purification Method	Antibody Cost per Dose	Percentage of Purification Cost (%)	Percentage of Total Cost (%)
FACS	£2,098	80	6.2
MACS	£2,065	65	6.0
SpheriTech beads	£49	4.2	0.15

However, reducing the economic gain from antibody requirements is the significantly lower progenitor yield found from SpheriTech purification compared with FACS and MACS (see Chapter 6.8.1). For the base case bioprocess, the total COG associated with SpheriTech is £36,000 per dose, 5% and 7% higher than the COG per dose for a MACS-based or FACS-based bioprocesses respectively (Figure 7.5 A). When using affinity beads, minimising the contact between cells and beads to ensure all the cells have direct contact during incubation is critical. As discussed previously, this limited yield is likely due to target cells not interacting with beads and consequently being eluted as unbound impurities.
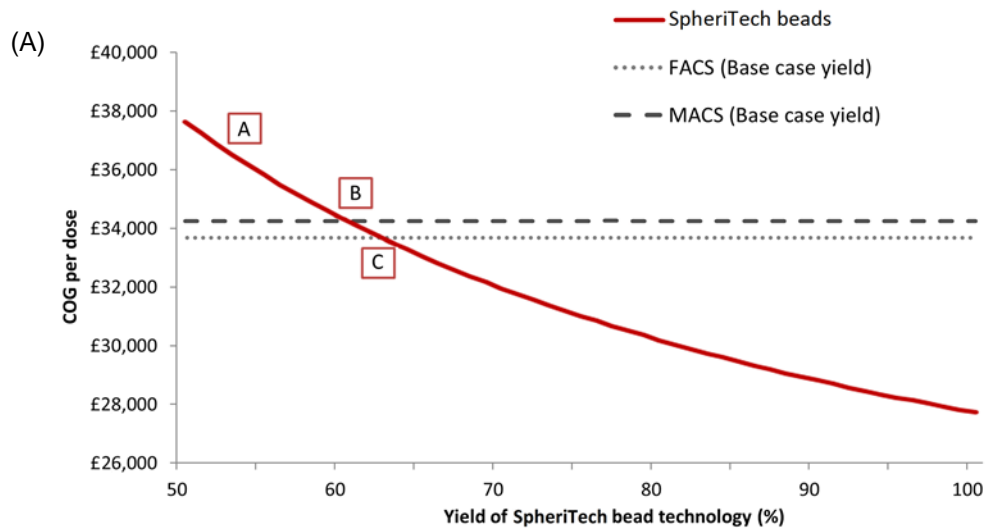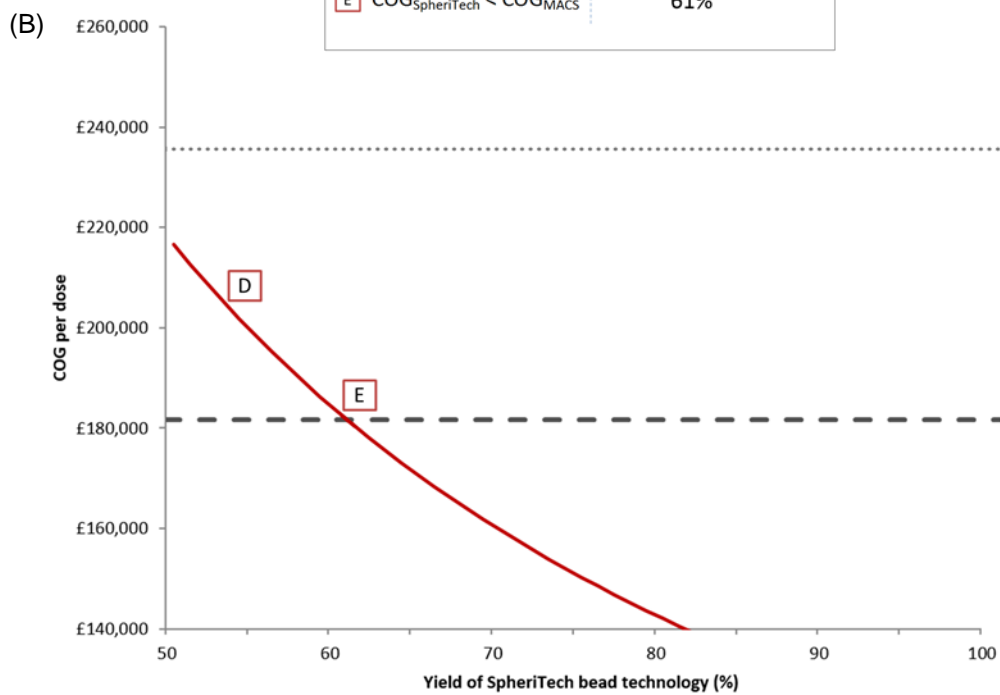
Figure 7.5 *Effect of SpheriTech purification yield on the overall bioprocess COG. Line graph of the COG per dose against yield at a dose size of (A) 10^7 and (B) 10^8. Point A and D represents the current SpheriTech bead yield. This is compared against the COG for MACS and FACS processes, given base case operating values (the dash and dotted horizontal lines). (C) The table insert shows the percentage yield that must be achieved using SpheriTech beads to be*

economically favoured against MACS and FACS technology (which occurs at point B and C respectively, and at point E for MACS at the higher dose size).

To quantify what improvement may be required to compete with current affinity technology, the economic tool was used to determine the progenitor yield required for SpheriTech to match the COG per dose of FACS and MACS at base case model inputs. The critical yield threshold for SpheriTech to compete with current affinity technologies was 63% (Figure 7.5 A). Given a final dose size of 10^7 cells with an annual demand of 1000 doses, the technologies ranked FACS, MACS, and then SpheriTech in order of economic preference. An 8 percentage point increase in the progenitor yield, from 55% to 63%, for SpheriTech beads is required to compete with MACS.

However, if a higher dose of 10^8 cells is required then MACS becomes the preferred technology, followed by SpheriTech and then FACS (Figure 7.5 B). At this dose, a critical yield of 60% was found, above which SpheriTech would beat the leading technology and become the economically favoured purification method. Again, this reduction in the favourability of FACS is due to limitations in process throughput.

These progenitor yield thresholds represent quantitative targets for the future process development of SpheriTech beads. By developing a purification system which can operate with a yield above 63%, SpheriTech purification becomes a real commercial opportunity to compete with current affinity technology.

7.7 Chapter Discussion

This chapter investigated the COG for current affinity purification and SpheriTech beads to identify the key cost drivers and determine critical process parameters which impact the bioprocess and purification costs. To compare purification characteristics and investigate their commercial potential, an economic bioprocess modelling tool was created. The tool permitted an economic appraisal of different purification technologies to evaluate their impact upon a complete bioprocess.

An annual dose of 100, 1000 and 10,000 was inputted into the model to determine the cost breakdown of each operation in the bioprocess, and observed whether economies of scale could be achieved through scale-out autologous production. Above 1000 doses per year, little benefit was noted so this was chosen as the base case demand in a single facility platform.

Although costs directly associated with purification comprise a small percentage of the total bioprocess COG, sensitivity analysis illustrated that performance characteristics which impact the dose size and cell population size will have a key impact upon upstream processing. As such, although differentiation costs dominate the bioprocess, operational characteristics for purification were found to significantly alter the COG per dose by changing the required cell number. Four key cost drivers (dose size, differentiation efficiency, purity and yield) were assessed across a range of scenarios to establish zones of operational favourability for FACS and MACS. At a dose size above $7x10^7$ MACS was the most economical choice, independent of differentiation efficiency. This was due to a maximum processing window of 4 hours for FACS, above which multiple machines must be purchased to meet the required throughput. As a result, equipment costs severely rose which produced this switch point. Similarly, a switch point was found when assessing purity and yield at base-case input values. Unless a very high purity and yield can be operated at, MACS was found to be the preferred system. FACS analysis was based on the MACSQuant Tyto which utilises disposable cartridges which contains the sorter microchip, collection chambers and fluidics. Issues with equipment cleaning after use, and the risk of droplet-based sorting are mitigated, however, limited throughput and cellular product labelling are still unchanged from traditional FACS systems.

Varying the key parameters which effect critical variables established economically favoured operational zones for each technology. To assess the economic feasibility of SpheriTech beads, the COG per dose was calculated using the economic model and compared against current technology. SpheriTech bioprocess costs were higher than MACS at both dose sizes tested due to lower progenitor yields. To ascertain a quantitative output to describe further development needed to compete with MACS and FACS economically, comparative COGs while varying the SpheriTech progenitor yield was reviewed against each technology. The yield must be improved to exceed 63% to ensure economic feasibility. However, due to simplification of the bioprocess

by mitigating cell labelling steps, and the resulting reduction in process risk and clinical feasibility of the product not being tagged, these advantages may have an impact on the current economic disparity.

Chapter 8: Summary and future work

8.1 Final words

Cell therapy is a rapidly growing market with an estimated increase in revenue of 1 billion USD per year (Mason *et al.*, 2012). Significant strives have been made towards the translation of therapies across a wide range of indications. However, technical challenges in ATMP bioprocesses inhibit the approval of novel treatments.

8.1.1 Key findings

Human pluripotent stem cells are a viable source of progenitor photoreceptors for transplantation. By implementing more control over aggregation, the efficiency and reproducibility of retinal differentiation can be dramatically improved. However, differentiation generates very heterogeneous cultures which containing potentially dangerous cellular impurities. As a result, purification is critical; not only to remove any harmful impurities, but to isolate the regenerative target cell population.

Current affinity purification technologies result in high purity separations due to the specificity of antibody binding, but variable yields have been noted with MACS. As FACS interrogates cells on a one-by-one basis, operational feasibility is limited by scale. As cell labelling is required for both FACS and MACS, the viable cell yield is reduced through additional manipulation steps which complicate the bioprocess, reducing clinical feasibility and increasing process risk.

SpheriTech beads produce a label-free alternative to current affinity steps with no labelling or washing steps necessary. They can be manufactured using microfluidic technology to produce homogeneous, controlled bead sizes and compositions. SpheriTech beads can be buoyant and paramagnetic through the addition of hollow microbeads and iron (III) oxide. They differentially bind cells with high purity, independent of bead size. However, to economically compete with current affinity technology, improvements to progenitor yield must be made.

8.1.2 Final Discussion

Photoreceptor dystrophies present a major unmet therapeutic challenge due to the diversity of genes, sites of mutation and mechanisms of inheritance involved. There are currently no treatments to prevent or reverse degradation.

For inherited retinal diseases that can be pinpointed to a specific genetic defect, such as with Leber's congenital amaurosis, preliminary clinical safety for in vivo gene therapy is promising (Maguire *et al.*, 2008). A recombinant AAV vector has been injected sub-retinally into patients to correct a gene defect preventing RPE function, producing no serious adverse effects (Bainbridge *et al.*, 2008). However, for most photoreceptor diseases, the integration of autologous iPSC-derived cells will likely present an effective method to limit degeneration (West *et al.*, 2009). This is especially true for RP, where genetic mutations in rod photoreceptors result in the slow death of both rods and cones leading to central blindness (Bovolenta and Cisneros, 2009).

Autologous treatment for a wider scope of retinal dystrophies may likely involve a combination of ex vivo, gene-corrected cell therapies in the future (Fields *et al.*, 2010; Cramer *et al.*, 2014). By modifying patients' cells to fix the underlying cause of non-functional phenotypes, corrected cells could be transplanted back into patients to rescue the damaged structural or functional defect (Bashar *et al.*, 2016). This technique of autologous ex vivo gene & cell therapy combination has recently showed much clinical promise with CAR-T products, (Pule *et al.*, 2008; Kalos *et al.*, 2011; Porter *et al.*, 2011; Brentjens *et al.*, 2013; Grupp *et al.*, 2013; Maude *et al.*, 2014; Lee *et al.*, 2015). Purification strategies for these clinical therapeutics involve a minimum of two sequential CliniMACS procedures with negative, then a positive cell selection (Liu *et al.*, 2016). As MACS beads remain bound to target cells, multiple positive selection steps cannot be used in series. Furthermore, whilst bulk selection is feasible, selection of rarer sub-populations with the correct phenotype has been limited by the process recovery of MACS (Schriebl *et al.*, 2010; Turtle *et al.*, 2016).

By switching to a cell purification technology like SpheriTech beads that does not share these technical limitations, various processing benefits are possible.

1) A more reproducible and defined product can be achieved from the addition of sequential, high recovery positive separation steps

2) Improving product specificity may improve the therapeutic efficacy, leading to a reduced cell dose size which decreases the cost and demand of the bioprocess

3) Increased product safety by mitigating any bound cellular label which can cause adverse clinical effects.

Whilst other label-free technologies are typically limited by throughput (Karumanchi and Doddamane, 2002; Lau, Lee and Chan, 2008; Vykoukal *et al.*, 2008; Tsukamoto *et al.*, 2009; Bhagat *et al.*, 2011; Choudhury *et al.*, 2012), SpheriTech bead purification could also help to unlock the potential of allogeneic therapies by providing a scalable platform to process much larger volumes than MACS. Due to the size of MACS beads, samples must be processed through small diameter columns to ensure the paramagnetic beads are captured within a strong magnetic field. Additionally, there is risk from depending on a single supplier when using MACS. Having a bioprocess wholly dependent upon one supplier results in a lack of control over financial and technical process considerations. If the supplier decides to change or discontinue the product, or the company goes into liquidation, there is no flexibility built into the bioprocess as manufacture will cease.

8.2 Future work

A key improvement for SpheriTech beads is increasing the progenitor yield from purification. To address this issue, a new device must be designed and manufactured that focuses on the current limitations of cell:bead contact during incubation.

When separating rare cell populations based of surface markers, it is critical that each cell contacts beads in a manner that can facilitate binding. Chromatography-based systems have shown some preliminary success (Olusanya, Bracewell and Veraitch, 2010), however column blockage has detrimentally impacted progress. As SpheriTech beads offer both buoyancy and paramagnetism, the design of a column utilising these features may help prevent blockage.

A second critical factor for affinity separations is definition of the target cell population. For photoreceptor dystrophies, targeting the regenerative population that will form new synaptic pathways after transplantation is critical. Definition of this population is currently limited to CRX and NRL, however further work could be carried out to further specify the desired cell phenotypes. This too must be carried out with a corresponding surface marker or markers. Although CD73 has shown high levels of co-expression with CRX, and has sorted cells which mature into photoreceptors in vivo, improving the marker selection can dramatically impact therapeutic efficacy.

As more information is learnt about the target cell type and its characteristics, the estimation of cell numbers required can be improved. The cell losses during cell manufacture, transplantation and integration into the damaged retina, can be better defined from recent clinical development. Following the emergence of new clinical data from RPE clinical trials, and more in depth preclinical photoreceptor studies, assumptions regarding cell number and process costs can be fed back into the economic tool to improve the COG predictions.

Finally, generating more data surround SpheriTech bead binding will be beneficial. Studying cell binding below 200 μm may help further understanding regarding the impact of contact angle. The kinetics of cell binding and thermodynamics should be studies to minimise the required incubation times and help design the purification device.

Studies into bead degradation should be assessed to determine the stability of SpheriTech beads in terms of polymer stability, buoyancy and paramagnetism maintenance. More detail over the characterisation of the materials involved in SpheriTech is necessary. A study of the leakage or cleavage of antibody during cell detachment would give more data regarding the life cycle analysis of SpheriTech beads and provide the shelf life of beads; whether they can be repeatedly used, whether fouling occurs or what the loss of paramagnetism or buoyancy is over time. Additionally, an investigation into immobilising antibody in a larger scale bulk system would facilitate commercialisation of the technology.

8.3 Final thesis conclusion

Purification technology remains a bottleneck in the expanding field of cell therapies. The retention of cellular labels, limited cell recovery and scalability of the current gold standard methods highlight the need for development of a new technology. This thesis has shown SpheriTech beads to be beneficial for the purification of progenitor photoreceptors. A reproducible manufacture process has been established to efficiently manufacture homogeneous beads, and the upstream manufacture of progenitor photoreceptors has been significantly improved to facilitate purification. SpheriTech beads have bioprocess advantages over current technologies by mitigating cell label and wash steps which result in cell loss, increased process duration and risk.

Bibliography

Aflatoonian, B., Ruban, L., Jones, M., Aflatoonian, R., Fazeli, A. and Moore, H. D. (2009) 'In vitro post-meiotic germ cell development from human embryonic stem cells.', *Human reproduction (Oxford, England)*, 24(12), pp. 3150–9. doi: 10.1093/humrep/dep334.

Aizawa, Y. and Shoichet, M. S. (2012) 'The role of endothelial cells in the retinal stem and progenitor cell niche within a 3D engineered hydrogel matrix.', *Biomaterials*. Elsevier Ltd, 33(21), pp. 5198–5205. doi: 10.1016/j.biomaterials.2012.03.062.

Akagi, T., Mandai, M., Ooto, S., Hirami, Y., Osakada, F., Kageyama, R., Yoshimura, N. and Takahashi, M. (2004) 'Otx2 homeobox gene induces photoreceptor-specific phenotypes in cells derived from adult iris and ciliary tissue.', *Investigative ophthalmology & visual science*, 45(12), pp. 4570–5. doi: 10.1167/iovs.04-0697.

Akbar, S., Hasanain, S. K., Azmat, N. and Nadeem, M. (2004) 'Synthesis of Fe2O3 nanoparticles by new Sol-Gel method and their structural and magnetic characterizations'.

Akimoto, M., Cheng, H., Zhu, D., Brzezinski, J. A., Khanna, R., Filippova, E., Oh, E. C. T., Jing, Y., Linares, J.-L., Brooks, M., Zareparsi, S., Mears, A. J., Hero, A., Glaser, T. and Swaroop, A. (2006) 'Targeting of GFP to newborn rods by Nrl promoter and temporal expression profiling of flow-sorted photoreceptors.', *Proceedings of the National Academy of Sciences of the United States of America*, 103(10), pp. 3890–5. doi: 10.1073/pnas.0508214103.

Alford, R., Simpson, H. M., Duberman, J., Craig Hill, G., Ogawa, M., Regino, C., Kobayashi, H. and Choyke, P. L. (2009) 'Toxicity of organic fluorophores used in molecular imaging: Literature review', *Molecular Imaging*, 8(6), pp. 341–354. doi: 10.2310/7290.2009.00031.

Amgen (2015) *Amgen and Kite Pharma Announce Strategic Cancer Immunotherapy Collaboration to Advance the Application of Novel Chimeric Antigen Receptor (CAR) T Cell Therapies - Press Release, Jan. 5, 2015*. Available at: http://investors.amgen.com/phoenix.zhtml?c=61656&p=irol-newsArticle&ID=2002967 (Accessed: 5 November 2015).

Amit, M., Carpenter, M. K., Inokuma, M. S., Chiu, C. P., Harris, C. P., Waknitz, M. a, Itskovitz-Eldor, J. and Thomson, J. a (2000) 'Clonally derived human embryonic stem cell lines maintain pluripotency and proliferative potential for prolonged periods of culture.', *Developmental biology*, 227(2), pp. 271–8. doi: 10.1006/dbio.2000.9912.

Amit, M. and Itskovitz-Eldor, J. (2012) 'Morphology of Human Embryonic and Induced Pluripotent Stem Cell Colonies Cultured with Feeders', in *Atlas of Human Pluripotent Stem Cells*. Totowa, NJ: Humana Press, pp. 15–39. doi: 10.1007/978-1-61779-548-0_2.

Andrews, P. W. (1987) 'Human teratocarcinoma stem cells: glycolipid antigen expression and modulation during differentiation.', *Journal of cellular biochemistry*, 35(4), pp. 321–32. doi: 10.1002/jcb.240350407.

Andrews, P. W., Banting, G., Damjanov, I., Arnaud, D. and Avner, P. (1984) 'Three monoclonal antibodies defining distinct differentiation antigens associated with different high molecular weight polypeptides on the surface of human embryonal carcinoma cells.', *Hybridoma*, 3(4), pp. 347–61. doi: 10.1089/hyb.1984.3.347.

Andrews, P. W., Damjanov, I., Simon, D., Banting, G. S., Carlin, C., Dracopoli, N. C. and Føgh, J. (1984) 'Pluripotent embryonal carcinoma clones derived from the human teratocarcinoma cell line Tera-2. Differentiation in vivo and in vitro.', *Laboratory investigation; a journal of technical methods and pathology*, 50(2), pp. 147–62. Available at:

http://www.ncbi.nlm.nih.gov/pubmed/6694356 (Accessed: 25 August 2016).

Arnhold, S., Klein, H., Semkova, I., Addicks, K. and Schraermeyer, U. (2004) 'Neurally selected embryonic stem cells induce tumor formation after long-term survival following engraftment into the subretinal space', *Investigative Ophthalmology and Visual Science*. The Association for Research in Vision and Ophthalmology, 45(12), pp. 4251–4255. doi: 10.1167/iovs.03-1108.

Athersys Inc. (2015) *Athersys Announces Results From Phase 2 Study of MultiStem(R) Cell Therapy for Ulcerative Colitis (NASDAQ:ATHX)*. Available at: http://www.athersys.com/releasedetail.cfm?ReleaseID=907107.

Bae, D. (2011) *Developing an efficient process for the production of retinal progenitor cells (RPCs) from human pluripotent stem cells using lowered oxygen tension*. University College London.

Bae, D., Mondragon-Teran, P., Hernandez, D., Ruban, L., Mason, C., Bhattacharya, S. S. and Veraitch, F. S. (2011) 'Hypoxia Enhances the Generation of Retinal Progenitor Cells from Human Induced Pluripotent and Embryonic Stem Cells.', *Stem cells and development*, 0(0). doi: 10.1089/scd.2011.0225.

Bainbridge, J. W. B., Smith, A. J., Barker, S. S., Robbie, S., Henderson, R., Balaggan, K., Viswanathan, A., Holder, G. E., Stockman, A., Tyler, N., Petersen-Jones, S., Bhattacharya, S. S., Thrasher, A. J., Fitzke, F. W., Carter, B. J., Rubin, G. S., Moore, A. T. and Ali, R. R. (2008) 'Effect of gene therapy on visual function in Leber's congenital amaurosis', *New England Journal of Medicine*, 358(21), pp. 2231–2239. doi: 10.1056/NEJMoa0802268.

Bannunah, A. M., Vllasaliu, D., Lord, J. and Stolnik, S. (2014) 'Mechanisms of Nanoparticle Internalization and Transport Across an Intestinal Epithelial Cell Model: Effect of Size and Surface Charge', *Molecular Pharmaceutics*, 11(12), pp. 4363–4373. doi: 10.1021/mp500439c.

Barnea-Cramer, A. O., Wang, W., Lu, S.-J., Singh, M. S., Luo, C., Huo, H., McClements, M. E., Barnard, A. R., MacLaren, R. E. and Lanza, R. (2016) 'Function of human pluripotent stem cell-derived photoreceptor progenitors in blind mice.', *Scientific reports*, 6, p. 29784. doi: 10.1038/srep29784.

Bashar, A. E., Metcalfe, A. L., Viringipurampeer, I. A., Yanai, A. and Gregory-evans, C. Y. (2016) 'An ex vivo gene therapy approach in X-linked retinoschisis', *Molecular vision*. Emory University, 22(March), pp. 718–733.

Beebe, D. C. (1986) 'Development of the ciliary body: a brief review.', *Transactions of the ophthalmological societies of the United Kingdom*, pp. 123–30. Available at: http://www.ncbi.nlm.nih.gov/pubmed/3541302 (Accessed: 28 August 2016).

Bersenev, A. (2016) *Crude versus defined CAR T-cell therapy product*. Available at: http://stemcellassays.com/2016/05/crude-versus-defined-car-t-cell-therapy-product/.

Berson, D. M., Dunn, F. A. and Takao, M. (2002) 'Phototransduction by retinal ganglion cells that set the circadian clock.', *Science (New York, N.Y.)*, 295(5557), pp. 1070–3. doi: 10.1126/science.1067262.

Bessant, D. A., Payne, A. M., Mitton, K. P., Wang, Q. L., Swain, P. K., Plant, C., Bird, A. C., Zack, D. J., Swaroop, A. and Bhattacharya, S. S. (1999) 'A mutation in NRL is associated with autosomal dominant retinitis pigmentosa.', *Nature genetics*, 21(4), pp. 355–6. doi: 10.1038/7678.

Bhagat, A. A. S., Hou, H. W., Li, L. D., Lim, C. T. and Han, J. (2011) 'Pinched flow coupled shear-modulated inertial microfluidics for high-throughput rare blood cell separation.', *Lab on a chip*, 11(11), pp. 1870–8. doi: 10.1039/c0lc00633e.

Bibb, L. C., Holt, J. K. L., Tarttelin, E. E., Hodges, M. D., Gregory-Evans, K., Rutherford, A., Lucas, R. J., Sowden, J. C. and Gregory-Evans, C. Y. (2001) 'Temporal and spatial expression patterns of the CRX transcription factor and its downstream targets. Critical differences during human and mouse eye development.', *Human Molecular Genetics*, 10(15), pp. 1571–1579. doi: 10.1093/hmg/10.15.1571.

BioGPS - Primary Cell Atlas (2015) *NT5E (5'-nucleotidase ecto)*. Available at: http://ds.biogps.org/?dataset=BDS_00013&gene=4907.

Boccaccio, C. (1999) '[Sorting CD34 antigens: objectives, biological and clinical results].', *Presse médicale (Paris, France : 1983)*, 28(31), pp. 1709–16.

Boland, M. J., Hazen, J. L., Nazor, K. L., Rodriguez, A. R., Gifford, W., Martin, G., Kupriyanov, S. and Baldwin, K. K. (2009) 'Adult mice generated from induced pluripotent stem cells.', *Nature*, 461(7260), pp. 91–4. doi: 10.1038/nature08310.

Bomberger, C., Singh-Jairam, M., Rodey, G., Guerriero, A., Yeager, A. M., Fleming, W. H., Holland, H. K. and Waller, E. K. (1998) 'Lymphoid reconstitution after autologous PBSC transplantation with FACS-sorted CD34+ hematopoietic progenitors.', *Blood*. American Society of Hematology, 91(7), pp. 2588–600. doi: 10.1016/0167-5699(95)80117-0.

Bonner, W. A., Hulett, H. R., Sweet, R. G. and Herzenberg, L. A. (1972) 'Fluorescence activated cell sorting.', *The Review of scientific instruments*, 43(3), pp. 404–9. Available at: http://www.ncbi.nlm.nih.gov/pubmed/5013444 (Accessed: 30 August 2016).

Borm, P. J. A. and Kreyling, W. (2004) 'Toxicological hazards of inhaled nanoparticles--potential implications for drug delivery.', *Journal of nanoscience and nanotechnology*, 4(5), pp. 521–31. Available at: http://www.ncbi.nlm.nih.gov/pubmed/15503438 (Accessed: 1 September 2016).

Boucherie, C., Sowden, J. C. and Ali, R. R. (2011) 'Induced pluripotent stem cell technology for generating photoreceptors.', *Regenerative medicine*, 6(4), pp. 469–79. doi: 10.2217/rme.11.37.

Bovolenta, P. and Cisneros, E. (2009) 'Retinitis pigmentosa: cone photoreceptors starving to death.', *Nature neuroscience*. Nature Publishing Group, 12(1), pp. 5–6. doi: 10.1038/nn0109-5.

Boyle, A. J. F. and Hall, H. E. (1962) 'The Mössbauer effect', *Reports on Progress in Physics*. IOP Publishing, 25(1), p. 311. doi: 10.1088/0034-4885/25/1/311.

Brentjens, R. J., Davila, M. L., Riviere, I., Park, J., Wang, X., Cowell, L. G., Bartido, S., Stefanski, J., Taylor, C., Olszewska, M., Borquez-Ojeda, O., Qu, J., Wasielewska, T., He, Q., Bernal, Y., Rijo, I. V, Hedvat, C., Kobos, R., Curran, K., Steinherz, P., Jurcic, J., Rosenblat, T., Maslak, P., Frattini, M. and Sadelain, M. (2013) 'CD19-targeted T cells rapidly induce molecular remissions in adults with chemotherapy-refractory acute lymphoblastic leukemia.', *Science translational medicine*. American Association for the Advancement of Science, 5(177), p. 177ra38. doi: 10.1126/scitranslmed.3005930.

Bryan, N., Lewis, F. C., Bond, D., Stanley, C. and Hunt, J. A. (2013) 'Evaluation of a Novel Non-Destructive Catch and Release Technology for Harvesting Autologous Adult Stem Cells', *PLoS ONE*. Edited by I. Kerkis. Public Library of Science, 8(1). doi: 10.1371/journal.pone.0053933.

Bundey, S. and Crews, S. J. (1984) 'A study of retinitis pigmentosa in the City of Birmingham. I Prevalence.', *Journal of medical genetics*, 21(6), pp. 417–20. Available at: http://www.ncbi.nlm.nih.gov/pubmed/6512829 (Accessed: 28 August 2016).

Carpenter, M. K., Rosler, E. and Rao, M. S. (2003) 'Characterization and differentiation of human embryonic stem cells.', *Cloning and stem cells*, 5(1), pp. 79–88. doi: 10.1089/153623003321512193.

Cattoglio, C., Facchini, G., Sartori, D., Antonelli, A., Miccio, A., Cassani, B., Schmidt, M., von

Kalle, C., Howe, S., Thrasher, A. J., Aiuti, A., Ferrari, G., Recchia, A. and Mavilio, F. (2007) 'Hot spots of retroviral integration in human CD34+ hematopoietic cells.', *Blood*, 110(6), pp. 1770–8. doi: 10.1182/blood-2007-01-068759.

Chambers, S. M., Fasano, C. a, Papapetrou, E. P., Tomishima, M., Sadelain, M. and Studer, L. (2009) 'Highly efficient neural conversion of human ES and iPS cells by dual inhibition of SMAD signaling.', *Nature biotechnology*, 27(3), pp. 275–80. doi: 10.1038/nbt.1529.

Chen, H.-H., Chien, C.-C., Petibois, C., Wang, C.-L., Chu, Y. S., Lai, S.-F., Hua, T.-E., Chen, Y.-Y., Cai, X., Kempson, I. M., Hwu, Y. and Margaritondo, G. (2011) 'Quantitative analysis of nanoparticle internalization in mammalian cells by high resolution X-ray microscopy.', *Journal of nanobiotechnology*, 9, p. 14. doi: 10.1186/1477-3155-9-14.

Chen, S., Wang, Q. L., Nie, Z., Sun, H., Lennon, G., Copeland, N. G., Gilbert, D. J., Jenkins, N. A. and Zack, D. J. (1997) 'Crx, a novel Otx-like paired-homeodomain protein, binds to and transactivates photoreceptor cell-specific genes.', *Neuron*, 19(5), pp. 1017–30. Available at: http://www.ncbi.nlm.nih.gov/pubmed/9390516 (Accessed: 28 August 2016).

Chen, X., Wang, C., Yin, J., Xu, J., Wei, J. and Zhang, Y. (2015) 'Efficacy of Mesenchymal Stem Cell Therapy for Steroid-Refractory Acute Graft-Versus-Host Disease following Allogeneic Hematopoietic Stem Cell Transplantation: A Systematic Review and Meta-Analysis.', *PloS one*, 10(8), p. e0136991. doi: 10.1371/journal.pone.0136991.

Chhatre, S., Francis, R., O'Donovan, K., Titchener-Hooker, N. J., Newcombe, A. R. and Keshavarz-Moore, E. (2007) 'A prototype software methodology for the rapid evaluation of biomanufacturing process options', *Biotechnology and Applied Biochemistry*, 48(2), pp. 65–78. doi: 10.1042/BA20070018.

Choudhury, D., Ramsay, W. T., Kiss, R., Willoughby, N. A., Paterson, L. and Kar, A. K. (2012) 'A 3D mammalian cell separator biochip.', *Lab on a chip*, 12(5), pp. 948–53. doi: 10.1039/c2lc20939j.

Chung, Y., Klimanskaya, I., Becker, S., Li, T., Maserati, M., Lu, S.-J., Zdravkovic, T., Ilic, D., Genbacev, O., Fisher, S., Krtolica, A., Lanza, R. (2008) 'Human Embryonic Stem Cell Lines Generated without Embryo Destruction', *Cell Stem Cell*. Elsevier, 2(2), pp. 113–117. doi: 10.1016/j.stem.2007.12.013.

Churchill, J. D., Bowne, S. J., Sullivan, L. S., Lewis, R. A., Wheaton, D. K., Birch, D. G., Branham, K. E., Heckenlively, J. R. and Daiger, S. P. (2013) 'Mutations in the X-linked retinitis pigmentosa genes RPGR and RP2 found in 8.5% of families with a provisional diagnosis of autosomal dominant retinitis pigmentosa.', *Investigative ophthalmology & visual science*, 54(2), pp. 1411–6. doi: 10.1167/iovs.12-11541.

Clark, G., Stockinger, H., Balderas, R., van Zelm, M. C., Zola, H., Hart, D. and Engel, P. (2016) 'Nomenclature of CD molecules from the Tenth Human Leucocyte Differentiation Antigen Workshop.', *Clinical & translational immunology*. Nature Publishing Group, 5(1), p. e57. doi: 10.1038/cti.2015.38.

Coey, J. M. D., Morrish, A. H. and Sawatzky, G. A. (1971) 'A Mössbauer study of conduction in Magnetite', *Le Journal de Physique Colloques*. EDP Sciences, 32(C1), pp. C1-271-C1-273. doi: 10.1051/jphyscol:1971190.

Committee for Advanced Therapies (CAT) (2011) *Reflection paper on stem cell-based medicinal products.* doi: EMA/CAT/571134/2009.

Corsini, C., Bertolini, F., Mancuso, P., Cinieri, S., Peccatori, F. and Martinelli, G. (2002) 'Short- and long-term safety of the 2 x 106 CD34+ cells/kg threshold for hematopoietic reconstitution after high-dose chemotherapy and peripheral blood progenitor cell support', *Annals of Oncology*. Oxford University Press, 13(6), pp. 983–985. doi: 10.1093/annonc/mdf181.

Cowan, C. A., Klimanskaya, I., McMahon, J., Atienza, J., Witmyer, J., Zucker, J. P., Wang, S., Morton, C. C., McMahon, A. P., Powers, D. and Melton, D. A. (2004) 'Derivation of Embryonic Stem-Cell Lines from Human Blastocysts', *New England Journal of Medicine*. Massachusetts Medical Society , 350(13), pp. 1353–1356. doi: 10.1056/NEJMsr040330.

Cramer, A. O. and MacLaren, R. E. (2013) 'Translating induced pluripotent stem cells from bench to bedside: application to retinal diseases.', *Current gene therapy*. Europe PMC Funders, 13(2), pp. 139–51. Available at: http://www.ncbi.nlm.nih.gov/pubmed/23320477 (Accessed: 2 September 2016).

Cramer, A. O., Singh, M. S., McClements, M. and MacLaren, R. E. (2014) 'Transplantation of Ex-Vivo Genetically Modified Photoreceptor Precursors', *Investigative Ophthalmology & Visual Science*, 55(13), pp. 1446–1446.

Crook, J. M., Peura, T. T., Kravets, L., Bosman, A. G., Buzzard, J. J., Horne, R., Hentze, H., Dunn, N. R., Zweigerdt, R., Chua, F., Upshall, A., Colman, A. (2007) 'The Generation of Six Clinical-Grade Human Embryonic Stem Cell Lines', *Cell Stem Cell*. Elsevier, 1(5), pp. 490–494. doi: 10.1016/j.stem.2007.10.004.

Dabbagh, A., Abu Kasim, N. H., Bakri, M. M., Wakily, H., Ramasindarum, C. and Abdullah, B. J. J. (2014) *Polyethylene-glycol coated maghemite nanoparticles for treatment of dental hypersensitivity*, *Materials Letters*. doi: 10.1016/j.matlet.2014.01.120.

Darkins, C. L. and Mandenius, C.-F. (2013) 'Design of large-scale manufacturing of induced pluripotent stem cell derived cardiomyocytes', *Chemical Engineering Research and Design*. Institution of Chemical Engineers, 92(August), pp. 1–11. doi: 10.1016/j.cherd.2013.08.021.

Davis, A. A., Matzuk, M. M. and Reh, T. A. (2000) 'Activin A promotes progenitor differentiation into photoreceptors in rodent retina.', *Molecular and cellular neurosciences*, 15(1), pp. 11–21. doi: 10.1006/mcne.1999.0806.

Decembrini, S., Koch, U., Radtke, F., Moulin, A. and Arsenijevic, Y. (2014) 'Derivation of traceable and transplantable photoreceptors from mouse embryonic stem cells.', *Stem cell reports*, 2(6), pp. 853–65. doi: 10.1016/j.stemcr.2014.04.010.

Dhandayuthapani, B., Yoshida, Y., Maekawa, T., Kumar, D. S., Dhandayuthapani, B., Yoshida, Y., Maekawa, T. and Kumar, D. S. (2011) 'Polymeric Scaffolds in Tissue Engineering Application: A Review', *International Journal of Polymer Science*. Hindawi Publishing Corporation, 2011, pp. 1–19. doi: 10.1155/2011/290602.

Dominici, M., Le Blanc, K., Mueller, I., Slaper-Cortenbach, I., Marini, F., Krause, D., Deans, R., Keating, A., Prockop, D. and Horwitz, E. (2006) 'Minimal criteria for defining multipotent mesenchymal stromal cells. The International Society for Cellular Therapy position statement.', *Cytotherapy*, 8(4), pp. 315–7. doi: 10.1080/14653240600855905.

Dykes, J. H., Toporski, J., Juliusson, G., Békássy, A. N., Lenhoff, S., Lindmark, A. and Scheding, S. (2007) 'Rapid and effective CD3 T-cell depletion with a magnetic cell sorting program to produce peripheral blood progenitor cell products for haploidentical transplantation in children and adults.', *Transfusion*, 47(11), pp. 2134–42. doi: 10.1111/j.1537-2995.2007.01438.x.

Eberle, D., Schubert, S., Postel, K., Corbeil, D. and Ader, M. (2011) 'Increased Integration of Transplanted CD73-Positive Photoreceptor Precursors into Adult Mouse Retina.', *Investigative ophthalmology & visual science*, 52(9), pp. 6462–71. doi: 10.1167/iovs.11-7399.

Elder, A. and Oberdörster, G. (2006) 'Translocation and effects of ultrafine particles outside of the lung.', *Clinics in occupational and environmental medicine*, 5(4), pp. 785–96. doi: 10.1016/j.coem.2006.07.003.

van den Engh, G., Trask, B. and Visser, J. (1981) 'Surface antigens of pluripotent and committed haemopoietic stem cells.', *Haematology and blood transfusion*, 26, pp. 305–8. Available at: http://www.ncbi.nlm.nih.gov/pubmed/7033069 (Accessed: 29 August 2016).

Enver, T., Soneji, S., Joshi, C., Brown, J., Iborra, F., Orntoft, T., Thykjaer, T., Maltby, E., Smith, K., Dawud, R. A., Jones, M., Matin, M., Gokhale, P., Draper, J. and Andrews, P. W. (2005) 'Cellular differentiation hierarchies in normal and culture-adapted human embryonic stem cells', *Human Molecular Genetics*. Oxford University Press, 14(21), pp. 3129–3140. doi: 10.1093/hmg/ddi345.

Evans, M. J. and Kaufman, M. H. (1981) 'Establishment in culture of pluripotential cells from mouse embryos', *Nature*. Nature Publishing Group, 292(5819), pp. 154–156. doi: 10.1038/292154a0.

Fahim, A. T., Daiger, S. P. and Weleber, R. G. (1993) *Retinitis Pigmentosa Overview*, *GeneReviews(®)*. Available at: http://www.ncbi.nlm.nih.gov/pubmed/20301590 (Accessed: 28 August 2016).

Farid, S. S., Novais, J. L., Karri, S., Washbrook, J. and Titchener-Hooker, N. J. (2000) 'A tool for modeling strategic decisions in cell culture manufacturing', *Biotechnology Progress*, 16(5), pp. 829–836. doi: 10.1021/bp0001056.

Farid, S. S., Washbrook, J. and Titchener-Hooker, N. J. (2005) 'Decision-support tool for assessing biomanufacturing strategies under uncertainty: Stainless steel versus disposable equipment for clinical trial material preparation', *Biotechnology Progress*, 21(2), pp. 486–497. doi: 10.1021/bp049692b.

Feng, Q., Lu, S.-J., Klimanskaya, I., Gomes, I., Kim, D., Chung, Y., Honig, G. R., Kim, K.-S. and Lanza, R. (2010) 'Hemangioblastic derivatives from human induced pluripotent stem cells exhibit limited expansion and early senescence.', *Stem cells (Dayton, Ohio)*, 28(4), pp. 704–12. doi: 10.1002/stem.321.

Ferrer, M., Corneo, B., Davis, J., Wan, Q., Miyagishima, K. J., King, R., Maminishkis, A., Marugan, J., Sharma, R., Shure, M., Temple, S., Miller, S. and Bharti, K. (2014) 'A multiplex high-throughput gene expression assay to simultaneously detect disease and functional markers in induced pluripotent stem cell-derived retinal pigment epithelium.', *Stem cells translational medicine*, 3(8), pp. 911–22. doi: 10.5966/sctm.2013-0192.

Fields, M. A., Vickers, L., Cai, H., Gong, J., Tsang, S. and Priore, L. Del (2010) 'Ex Vivo Gene Expression of Retinal Differentiation Transcription Factors Induces a Photoreceptor Phenotype in Mouse Neural and Embryonic Stem Cells', *Investigative Ophthalmology & Visual Science*. The Association for Research in Vision and Ophthalmology, 51(13), pp. 2661–2661.

Freund, C. L., Gregory-Evans, C. Y., Furukawa, T., Papaioannou, M., Looser, J., Ploder, L., Bellingham, J., Ng, D., Herbrick, J. A., Duncan, A., Scherer, S. W., Tsui, L. C., Loutradis-Anagnostou, A., Jacobson, S. G., Cepko, C. L., Bhattacharya, S. S. and McInnes, R. R. (1997) 'Cone-rod dystrophy due to mutations in a novel photoreceptor-specific homeobox gene (CRX) essential for maintenance of the photoreceptor.', *Cell*, 91(4), pp. 543–53. Available at: http://www.ncbi.nlm.nih.gov/pubmed/9390563 (Accessed: 28 August 2016).

Frey, N. A., Peng, S., Cheng, K. and Sun, S. (2009) 'Magnetic nanoparticles: synthesis, functionalization, and applications in bioimaging and magnetic energy storage.', *Chemical Society reviews*, 38(9), pp. 2532–42. doi: 10.1039/b815548h.

Frick, K. D., Roebuck, M. C., Feldstein, J. I., McCarty, C. A. and Grover, L. L. (2012) 'Health services utilization and cost of retinitis pigmentosa.', *Archives of ophthalmology (Chicago, Ill. : 1960)*, 130(5), pp. 629–34. doi: 10.1001/archophthalmol.2011.2820.

Furukawa, T., Cepko, C. L., Morrow, E. M., Li, T. and Davis, F. C. (1999) 'Retinopathy and

attenuated circadian entrainment in Crx-deficientmice', *Nature Genetics*. Nature Publishing Group, 23(4), pp. 466–470. doi: 10.1038/70591.

Furukawa, T., Morrow, E. M. and Cepko, C. L. (1997) 'Crx, a novel otx-like homeobox gene, shows photoreceptor-specific expression and regulates photoreceptor differentiation.', *Cell*, 91(4), pp. 531–41. Available at: http://www.ncbi.nlm.nih.gov/pubmed/9390562.

Gallagher, A. G., Alorabi, J. A., Wellings, D. A., Lace, R., Horsburgh, M. J. and Williams, R. L. (2016) 'A Novel Peptide Hydrogel for an Antimicrobial Bandage Contact Lens.', *Advanced healthcare materials*, 5(16), pp. 2013–8. doi: 10.1002/adhm.201600258.

Gandini, A. (2010) 'Monomers and Macromonomers from Renewable Resources', in *Biocatalysis in Polymer Chemistry*. Weinheim, Germany: Wiley-VCH Verlag GmbH & Co. KGaA, pp. 1–33. doi: 10.1002/9783527632534.ch1.

Gassei, K., Ehmcke, J. and Schlatt, S. (2009) 'Efficient enrichment of undifferentiated GFR alpha 1+ spermatogonia from immature rat testis by magnetic activated cell sorting', *Cell and Tissue Research*. Springer-Verlag, 337(1), pp. 177–183. doi: 10.1007/s00441-009-0799-5.

Gearhart, J. (1998) 'New potential for human embryonic stem cells.', *Science (New York, N.Y.)*. American Association for the Advancement of Science, 282(5391), pp. 1061–2. doi: 10.1126/science.282.5391.1061.

Geruschat, D. R., Turano, K. A. and Stahl, J. W. (1998) 'Traditional measures of mobility performance and retinitis pigmentosa.', *Optometry and vision science : official publication of the American Academy of Optometry*, 75(7), pp. 525–37. Available at: http://www.ncbi.nlm.nih.gov/pubmed/9703042 (Accessed: 29 August 2016).

Glinka, A., Wu, W., Delius, H., Monaghan, A. P., Blumenstock, C. and Niehrs, C. (1998) 'Dickkopf-1 is a member of a new family of secreted proteins and functions in head induction.', *Nature*, 391(6665), pp. 357–62. doi: 10.1038/34848.

Gouras, P., Du, J., Kjeldbye, H., Yamamoto, S. and Zack, D. J. (1992) 'Reconstruction of degenerate rd mouse retina by transplantation of transgenic photoreceptors', *Investigative Ophthalmology and Visual Science*. The Association for Research in Vision and Ophthalmology, 33(9), pp. 2579–86.

Gouras, P., Du, J., Kjeldbye, H., Yamamoto, S. and Zack, D. J. (1994) 'Long-term photoreceptor transplants in dystrophic and normal mouse retina', *Investigative Ophthalmology and Visual Science*. The Association for Research in Vision and Ophthalmology, 35(8), pp. 3145–3153.

Govers, C., Berrevoets, C., Treffers-Westerlaken, E., Broertjes, M. and Debets, R. (2012) 'Magnetic-activated cell sorting of TCR-engineered T cells, using tCD34 as a gene marker, but not peptide-MHC multimers, results in significant numbers of functional CD4+ and CD8+ T cells.', *Human gene therapy methods*, 23(3), pp. 213–24. doi: 10.1089/hgtb.2012.074.

Grupp, S. A., Kalos, M., Barrett, D., Aplenc, R., Porter, D. L., Rheingold, S. R., Teachey, D. T., Chew, A., Hauck, B., Wright, J. F., Milone, M. C., Levine, B. L. and June, C. H. (2013) 'Chimeric antigen receptor-modified T cells for acute lymphoid leukemia', *N Engl J Med*. Massachusetts Medical Society, 368(16), pp. 1509–1518. doi: 10.1056/NEJMoa1215134.

Haim, M. (2008) 'Retinitis pigmentosa: problems associated with genetic classification', *Clinical Genetics*, 44(2), pp. 62–70. Available at: http://doi.wiley.com/10.1111/j.1399-0004.1993.tb03848.x (Accessed: 3 August 2012).

Hambright, D., Park, K.-Y., Brooks, M., McKay, R., Swaroop, A. and Nasonkin, I. O. (2012) 'Long-term survival and differentiation of retinal neurons derived from human embryonic stem cell lines in un-immunosuppressed mouse retina.', *Molecular vision*, 18(July 2011), pp. 920–36. Available at:

http://www.pubmedcentral.nih.gov/articlerender.fcgi?artid=3335781&tool=pmcentrez&rendertyp e=abstract.

Handgretinger, R., Greil, J., Schürmann, U., Lang, P., Gonzalez-Ramella, O., Schmidt, I., Führer, R., Niethammer, D. and Klingebiel, T. (1997) *Positive selection and transplantation of peripheral CD34+ progenitor cells: feasibility and purging efficacy in pediatric patients with neuroblastoma.*, *Journal Of Hematotherapy*.

Hanna, J., Wernig, M., Markoulaki, S., Sun, C.-W., Meissner, A., Cassady, J. P., Beard, C., Brambrink, T., Wu, L.-C., Townes, T. M. and Jaenisch, R. (2007) 'Treatment of sickle cell anemia mouse model with iPS cells generated from autologous skin.', *Science (New York, N.Y.)*, 318(5858), pp. 1920–3. doi: 10.1126/science.1152092.

Harrop, J. S., Hashimoto, R., Norvell, D., Raich, A., Aarabi, B., Grossman, R. G., Guest, J. D., Tator, C. H., Chapman, J. and Fehlings, M. G. (2012) 'Evaluation of clinical experience using cell-based therapies in patients with spinal cord injury: a systematic review', *Journal of Neurosurgery: Spine.* American Association of Neurological Surgeons, 17(Suppl1), pp. 230– 246. doi: 10.3171/2012.5.AOSPINE12115.

Haruta, M., Kosaka, M., Kanegae, Y., Saito, I., Inoue, T., Kageyama, R., Nishida, A., Honda, Y. and Takahashi, M. (2001) 'Induction of photoreceptor-specific phenotypes in adult mammalian iris tissue.', *Nature neuroscience*, 4(12), pp. 1163–4. doi: 10.1038/nn762.

Hassan, S., Simaria, A. S., Varadaraju, H., Gupta, S., Warren, K. and Farid, S. S. (2015) 'Allogeneic cell therapy bioprocess economics and optimization: downstream processing decisions.', *Regenerative medicine.* Future Medicine Ltd London, UK, 10(5), pp. 591–609. doi: 10.2217/rme.15.29.

He, X., Hahn, P., Iacovelli, J., Wong, R., King, C., Bhisitkul, R., Massaro-Giordano, M. and Dunaief, J. L. (2007) 'Iron homeostasis and toxicity in retinal degeneration.', *Progress in retinal and eye research*, 26(6), pp. 649–73. doi: 10.1016/j.preteyeres.2007.07.004.

Heckmann, W. (2005) 'Characterization of Polymer Materials by Fluorescence Imaging', *Microscopy and Microanalysis*, 11(S02). doi: 10.1017/S1431927605501508.

Herberts, C. A., Kwa, M. S. G. and Hermsen, H. P. H. (2011) 'Risk factors in the development of stem cell therapy.', *Journal of translational medicine*, 9, p. 29. doi: 10.1186/1479-5876-9-29.

Heß, G., Flohr, T., Huber, C., Kolbe, K., Derigs, H.-G. and Fischer, T. (2003) 'Safety and feasibility of CHOP/rituximab induction treatment followed by high-dose chemo/radiotherapy and autologous PBSC-transplantation in patients with previously untreated mantle cell or indolent B-cell-non-Hodgkin's lymphoma', *Bone Marrow Transplantation.* Nature Publishing Group, 31(9), pp. 775–782. doi: 10.1038/sj.bmt.1703925.

Hirami, Y., Osakada, F., Takahashi, K., Okita, K., Yamanaka, S., Ikeda, H., Yoshimura, N. and Takahashi, M. (2009) 'Generation of retinal cells from mouse and human induced pluripotent stem cells.', *Neuroscience letters*, 458(3), pp. 126–31. doi: 10.1016/j.neulet.2009.04.035.

Hu, B.-Y., Weick, J. P., Yu, J., Ma, L.-X., Zhang, X.-Q., Thomson, J. A. and Zhang, S.-C. (2010) 'Neural differentiation of human induced pluripotent stem cells follows developmental principles but with variable potency.', *Proceedings of the National Academy of Sciences of the United States of America*, 107(9), pp. 4335–40. doi: 10.1073/pnas.0910012107.

Hubbell, W. L. and Bownds, M. D. (1979) 'Visual transduction in vertebrate photoreceptors.', *Annual review of neuroscience*, 2, pp. 17–34. doi: 10.1146/annurev.ne.02.030179.000313.

Hyer, J., Kuhlman, J., Afif, E. and Mikawa, T. (2003) 'Optic cup morphogenesis requires pre-lens ectoderm but not lens differentiation', *Developmental Biology*, 259(2), pp. 351–363. doi: 10.1016/S0012-1606(03)00205-7.

Hyldgaard, M., Mygind, T., Vad, B. S., Stenvang, M., Otzen, D. E. and Meyer, R. L. (2014) 'The Antimicrobial Mechanism of Action of Epsilon-Poly-L-Lysine', *Applied and Environmental Microbiology*, 80(24), pp. 7758–7770. doi: 10.1128/AEM.02204-14.

Intrexon Corporation (2015) *Intrexon And Merck Serono Announce Agreement For The Development And Commercialization Of CAR-T Therapy*.

Itsykson, P., Ilouz, N., Turetsky, T., Goldstein, R. S., Pera, M. F., Fishbein, I., Segal, M. and Reubinoff, B. E. (2005) 'Derivation of neural precursors from human embryonic stem cells in the presence of noggin.', *Molecular and cellular neurosciences*, 30(1), pp. 24–36. doi: 10.1016/j.mcn.2005.05.004.

Jakob, H., Boon, T., Gaillard, J., Nicolas, J. and Jacob, F. (1973) '[Teratocarcinoma of the mouse: isolation, culture and properties of pluripotential cells].', *Annales de microbiologie*, 124(3), pp. 269–82. Available at: http://www.ncbi.nlm.nih.gov/pubmed/4599372 (Accessed: 29 August 2016).

Jayakody, S. A., Gonzalez-Cordero, A., Ali, R. R. and Pearson, R. A. (2015) 'Cellular strategies for retinal repair by photoreceptor replacement.', *Progress in retinal and eye research*, 46, pp. 31–66. doi: 10.1016/j.preteyeres.2015.01.003.

Jayasinghe, S. M., Wunderlich, J., McKee, A., Newkirk, H., Pope, S., Zhang, J., Staehling-Hampton, K., Li, L. and Haug, J. S. (2006) 'Sterile and disposable fluidic subsystem suitable for clinical high speed fluorescence-activated cell sorting.', *Cytometry. Part B, Clinical cytometry*, 70(5), pp. 344–54. doi: 10.1002/cyto.b.20111.

Jenkins, M., Bilsland, J., Allsopp, T. E., Ho, S. V. and Farid, S. S. (2015) 'Patient-specific hiPSC bioprocessing for drug screening: Bioprocess economics and optimisation', *Biochemical Engineering Journal*. doi: 10.1016/j.bej.2015.09.024.

Jin, Z.-B., Okamoto, S., Xiang, P. and Takahashi, M. (2012) 'Integration-free induced pluripotent stem cells derived from retinitis pigmentosa patient for disease modeling.', *Stem cells translational medicine*. AlphaMed Press, 1(6), pp. 503–9. doi: 10.5966/sctm.2012-0005.

Jomary, C. and Jones, S. E. (2008) 'Induction of functional photoreceptor phenotype by exogenous Crx expression in mouse retinal stem cells.', *Investigative ophthalmology & visual science*, 49(1), pp. 429–37. doi: 10.1167/iovs.07-0812.

Julius, M. H., Masuda, T. and Herzenberg, L. A. (1972) 'Demonstration that antigen-binding cells are precursors of antibody-producing cells after purification with a fluorescence-activated cell sorter.', *Proceedings of the National Academy of Sciences of the United States of America*, 69(7), pp. 1934–8. Available at: http://www.ncbi.nlm.nih.gov/pubmed/4114858 (Accessed: 30 August 2016).

Kahan, B. W. and Ephrussi, B. (1970) 'Developmental potentialities of clonal in vitro cultures of mouse testicular teratoma.', *Journal of the National Cancer Institute*, 44(5), pp. 1015–36. Available at: http://www.ncbi.nlm.nih.gov/pubmed/5514468 (Accessed: 29 August 2016).

Kalos, M., Levine, B. L., Porter, D. L., Katz, S., Grupp, S. A., Bagg, A. and June, C. H. (2011) 'T cells with chimeric antigen receptors have potent antitumor effects and can establish memory in patients with advanced leukemia.', *Science translational medicine*. American Association for the Advancement of Science, 3(95), p. 95ra73. doi: 10.1126/scitranslmed.3002842.

Kanemura, H., Go, M. J., Shikamura, M., Nishishita, N., Sakai, N., Kamao, H., Mandai, M., Morinaga, C., Takahashi, M. and Kawamata, S. (2014) 'Tumorigenicity studies of induced pluripotent stem cell (iPSC)-derived retinal pigment epithelium (RPE) for the treatment of age-related macular degeneration.', *PloS one*. Public Library of Science, 9(1), p. e85336. doi: 10.1371/journal.pone.0085336.

Kang, L., Wang, J., Zhang, Y., Kou, Z. and Gao, S. (2009) 'iPS Cells Can Support Full-Term Development of Tetraploid Blastocyst-Complemented Embryos', *Cell Stem Cell*, pp. 135–138. doi: 10.1016/j.stem.2009.07.001.

Karumanchi, R. and Doddamane, S. (2002) 'Field-assisted extraction of cells, particles and macromolecules', *TRENDS in*. Available at: http://www.sciencedirect.com/science/article/pii/S0167779901018479 (Accessed: 3 May 2012).

Karwacki-Neisius, V., Göke, J., Osorno, R., Halbritter, F., Ng, J. H., Weiße, A. Y., Wong, F. C. K., Gagliardi, A., Mullin, N. P., Festuccia, N., Colby, D., Tomlinson, S. R., Ng, H.-H. and Chambers, I., (2013) 'Reduced Oct4 Expression Directs a Robust Pluripotent State with Distinct Signaling Activity and Increased Enhancer Occupancy by Oct4 and Nanog', *Cell Stem Cell*. Elsevier, 12(5), pp. 531–545. doi: 10.1016/j.stem.2013.04.023.

Keegan, D. J., Kenna, P., Humphries, M. M., Humphries, P., Flitcroft, D. I., Coffey, P. J., Lund, R. D. and Lawrence, J. M. (2003) 'Transplantation of syngeneic Schwann cells to the retina of the rhodopsin knockout (rho-/-) mouse', *Investigative Ophthalmology and Visual Science*. The Association for Research in Vision and Ophthalmology, 44(8), pp. 3526–3532. doi: 10.1167/iovs.02-0097.

Kelley, M. W., Turner, J. K. and Reh, T. A. (1995) 'Regulation of proliferation and photoreceptor differentiation in fetal human retinal cell cultures.', *Investigative ophthalmology & visual science*, 36(7), pp. 1280–9. Available at: http://www.ncbi.nlm.nih.gov/pubmed/7775105 (Accessed: 1 September 2016).

Kettler, K., Veltman, K., van de Meent, D., van Wezel, A. and Hendriks, A. J. (2014) 'Cellular uptake of nanoparticles as determined by particle properties, experimental conditions, and cell type.', *Environmental toxicology and chemistry / SETAC*, 33(3), pp. 481–92. doi: 10.1002/etc.2470.

Khan, I. F., Hirata, R. K., Wang, P.-R., Li, Y., Kho, J., Nelson, A., Huo, Y., Zavaljevski, M., Ware, C. and Russell, D. W. (2010) 'Engineering of human pluripotent stem cells by AAV-mediated gene targeting.', *Molecular therapy : the journal of the American Society of Gene Therapy*. Nature Publishing Group, 18(6), pp. 1192–9. doi: 10.1038/mt.2010.55.

Khanna, H., Akimoto, M., Siffroi-Fernandez, S., Friedman, J. S., Hicks, D. and Swaroop, A. (2006) 'Retinoic acid regulates the expression of photoreceptor transcription factor NRL.', *The Journal of biological chemistry*, 281(37), pp. 27327–34. Available at: http://www.jbc.org/cgi/content/abstract/281/37/27327 (Accessed: 16 July 2012).

Kievit, F. M. and Zhang, M. (2011) 'Surface engineering of iron oxide nanoparticles for targeted cancer therapy.', *Accounts of chemical research*, 44(10), pp. 853–62. doi: 10.1021/ar2000277.

Kim, C.-Y., Xu, L. and Lee, E.-H. (2014) 'Self-heating of Magnetite Nanoparticles for a Potential Hyperthermia Application', *Journal of the Korean Physical Society*, 65(2), pp. 261–266. doi: 10.3938/jkps.65.261.

Kim, D., Kim, C.-H., Moon, J.-I., Chung, Y.-G., Chang, M.-Y., Han, B.-S., Ko, S., Yang, E., Cha, K. Y., Lanza, R. and Kim, K.-S. (2009) 'Generation of human induced pluripotent stem cells by direct delivery of reprogramming proteins.', *Cell stem cell*. NIH Public Access, 4(6), pp. 472–6. doi: 10.1016/j.stem.2009.05.005.

Kim, K., Doi, A., Wen, B., Ng, K., Zhao, R., Cahan, P., Kim, J., Aryee, M. J., Ji, H., Ehrlich, L. I. R., Yabuuchi, A., Takeuchi, A., Cunniff, K. C., Hongguang, H., Naveiras, O., Yoon, T. J., Irizarry, R. A. (2010) 'Epigenetic memory in induced pluripotent stem cells.', *Nature*. NIH Public Access, 467(7313), pp. 285–90. doi: 10.1038/nature09342.

Klassen, H., Kiilgaard, J. F., Warfvinge, K., Samuel, M. S., Prather, R. S., Wong, F., Petters, R. M., Cour, M., Young, M. J., la Cour, M. and Young, M. J. (2012) 'Photoreceptor Differentiation

following Transplantation of Allogeneic Retinal Progenitor Cells to the Dystrophic Rhodopsin Pro347Leu Transgenic Pig', *Stem cells international*, 2012, p. 939801. doi: 10.1155/2012/939801.

Kodituwakku, A. P., Jessup, C., Zola, H. and Roberton, D. M. (2003) 'Isolation of antigen-specific B cells', *Immunology and Cell Biology*. Nature Publishing Group, 81(3), pp. 163–170. doi: 10.1046/j.1440-1711.2003.01152.x.

Kokkinopoulos, I., Pearson, R. A., Macneil, A., Dhomen, N. S., MacLaren, R. E., Ali, R. R. and Sowden, J. C. (2008) 'Isolation and characterisation of neural progenitor cells from the adult Chx10(orJ/orJ) central neural retina.', *Molecular and cellular neurosciences*, 38(3), pp. 359–73. doi: 10.1016/j.mcn.2008.03.008.

Koso, H., Minami, C., Tabata, Y., Inoue, M., Sasaki, E., Satoh, S. and Watanabe, S. (2009) 'CD73, a novel cell surface antigen that characterizes retinal photoreceptor precursor cells.', *Investigative ophthalmology & visual science*, 50(11), pp. 5411–8. doi: 10.1167/iovs.08-3246.

Kwan, A. S. L., Wang, S. and Lund, R. D. (1999) 'Photoreceptor Layer Reconstruction in a Rodent Model of Retinal Degeneration', *Experimental Neurology*, 159(1), pp. 21–33. doi: 10.1006/exnr.1999.7157.

L'azou, B., Jorly, J., On, D., Sellier, E., Moisan, F., Fleury-Feith, J., Cambar, J., Brochard, P. and Ohayon-Courtès, C. (2008) 'In vitro effects of nanoparticles on renal cells.', *Particle and fibre toxicology*, 5, p. 22. doi: 10.1186/1743-8977-5-22.

Lakowski, J., Baron, M., Bainbridge, J., Barber, a C., Pearson, R. a, Ali, R. R. and Sowden, J. C. (2010) 'Cone and rod photoreceptor transplantation in models of the childhood retinopathy Leber congenital amaurosis using flow-sorted Crx-positive donor cells.', *Human molecular genetics*, 19(23), pp. 4545–59. doi: 10.1093/hmg/ddq378.

Lakowski, J., Han, Y. T., Pearson, R., Gonzalez-Cordero, A., West, E., Gualdoni, S., Barber, A., Hubank, M., Ali, R. and Sowden, J. (2011) 'Effective Transplantation of Photoreceptor Precursor Cells Selected via Cell Surface Antigen Expression', *STEM CELLS*. Wiley Online Library, 29(9), pp. 1391–1404. doi: 10.1634/stem.694.

Lalu, M. M., McIntyre, L., Pugliese, C., Fergusson, D., Winston, B. W., Marshall, J. C., Granton, J., Stewart, D. J. (2012) 'Safety of Cell Therapy with Mesenchymal Stromal Cells (SafeCell): A Systematic Review and Meta-Analysis of Clinical Trials', *PLoS ONE*. Edited by A. P. Beltrami. Public Library of Science, 7(10), p. e47559. doi: 10.1371/journal.pone.0047559.

Lamba, D. A., Gust, J. and Reh, T. A. (2009) 'Transplantation of human embryonic stem cell-derived photoreceptors restores some visual function in Crx-deficient mice', *Cell Stem Cell*. Elsevier Inc., 4(1), pp. 73–79. doi: 10.1016/j.stem.2008.10.015.

Lamba, D. A., McUsic, A., Hirata, R. K., Wang, P.-R., Russell, D. and Reh, T. A. (2010) 'Generation, purification and transplantation of photoreceptors derived from human induced pluripotent stem cells.', *PloS one*. Edited by R. Linden. Public Library of Science, 5(1), p. e8763. doi: 10.1371/journal.pone.0008763.

Lamba, D. a, Karl, M. O., Ware, C. B. and Reh, T. a (2006) 'Efficient generation of retinal progenitor cells from human embryonic stem cells.', *Proceedings of the National Academy of Sciences of the United States of America*, 103(34), pp. 12769–74. doi: 10.1073/pnas.0601990103.

Lang, P., Bader, P., Schumm, M., Feuchtinger, T., Einsele, H., Fuhrer, M., Weinstock, C., Handgretinger, R., Kuci, S., Martin, D., Niethammer, D. and Greil, J. (2004) 'Transplantation of a combination of CD133+ and CD34+ selected progenitor cells from alternative donors', *British Journal of Haematology*. Blackwell Science Ltd, 124(1), pp. 72–79. doi: 10.1046/j.1365-2141.2003.04747.x.

Larsen, K. B., Lutterodt, M., Rath, M. F. and Møller, M. (2009) 'Expression of the homeobox genes PAX6, OTX2, and OTX1 in the early human fetal retina', *International Journal of Developmental Neuroscience*, 27(5), pp. 485–492. doi: 10.1016/j.ijdevneu.2009.04.004.

Lau, A. Y., Lee, L. P. and Chan, J. W. (2008) 'An integrated optofluidic platform for Raman-activated cell sorting.', *Lab on a chip*, 8(7), pp. 1116–20. Available at: http://www.ncbi.nlm.nih.gov/pubmed/18584087 (Accessed: 7 August 2012).

LaVail, M. M., Yasumura, D., Matthes, M. T., Lau-Villacorta, C., Unoki, K., Sung, C. H. and Steinberg, R. H. (1998) 'Protection of mouse photoreceptors by survival factors in retinal degenerations.', *Investigative ophthalmology & visual science*, 39(3), pp. 592–602. Available at: http://www.ncbi.nlm.nih.gov/pubmed/9501871 (Accessed: 29 August 2016).

Lawrence, J. M., Keegan, D. J., Muir, E. M., Coffey, P. J., Rogers, J. H., Wilby, M. J., Fawcett, J. W. and Lund, R. D. (2004) 'Transplantation of Schwann Cell Line Clones Secreting GDNF or BDNF into the Retinas of Dystrophic Royal College of Surgeons Rats', *Investigative Ophthalmology and Visual Science*. The Association for Research in Vision and Ophthalmology, 45(1), pp. 267–274. doi: 10.1167/iovs.03-0093.

Lawrence, S. (2016) *Celgene affirms Juno CAR-T deal as key to long-term growth | FierceBiotech*, *2016-07-28*. Available at: http://www.fiercebiotech.com/biotech/celgene-affirms-juno-car-t-deal-as-key-to-long-term-growth (Accessed: 29 July 2016).

Lee, D. W., Kochenderfer, J. N., Stetler-Stevenson, M., Cui, Y. K., Delbrook, C., Feldman, S. A., Fry, T. J., Orentas, R., Sabatino, M., Shah, N. N., Steinberg, S. M., Stroncek, D., Tschernia, N., Yuan, C., Zhang, H., Zhang, L., Rosenberg, S. A., Wayne, A. S. and Mackall, C. L. (2015) 'T cells expressing CD19 chimeric antigen receptors for acute lymphoblastic leukaemia in children and young adults: A phase 1 dose-escalation trial', *The Lancet*. Elsevier, 385(9967), pp. 517–528. doi: 10.1016/S0140-6736(14)61403-3.

Levine, E. M., Fuhrmann, S. and Reh, T. A. (2000) 'Soluble factors and the development of rod photoreceptors.', *Cellular and molecular life sciences : CMLS*, 57(2), pp. 224–34. doi: 10.1007/PL00000686.

Liang, F. Q., Dejneka, N. S., Cohen, D. R., Krasnoperova, N. V, Lem, J., Maguire, a M., Dudus, L., Fisher, K. J. and Bennett, J. (2001) 'AAV-mediated delivery of ciliary neurotrophic factor prolongs photoreceptor survival in the rhodopsin knockout mouse.', *Molecular therapy : the journal of the American Society of Gene Therapy*, 3(2), pp. 241–8. doi: 10.1006/mthe.2000.0252.

Liang, Y.-C., Svec, F. and Fréchet, J. M. J. (1995) 'Monodisperse polymer beads as packing material for high-performance liquid chromatography. Preparation of macroporous poly(2,3-epoxypropyl vinylbenzyl ether-co-divinylbenzene) beads, their properties, and application to HPLC separations', *Journal of Polymer Science Part A: Polymer Chemistry*. John Wiley & Sons, Inc., 33(15), pp. 2639–2646. doi: 10.1002/pola.1995.080331510.

Liu, L., Sommermeyer, D., Cabanov, A., Kosasih, P., Hill, T. and Riddell, S. R. (2016) 'Inclusion of Strep-tag II in design of antigen receptors for T-cell immunotherapy.', *Nature biotechnology*. Nature Research, 34(4), pp. 430–4. doi: 10.1038/nbt.3461.

Loeb, S., Asharani, P. and Valiyaveettil, S. (2010) 'Investigating the toxicity of iron (III) oxide nanoparticles, zinc (II) oxide nanorods and multi-walled carbon nanotubes on red blood cells', *… At: Http://Www. Nus. Edu. Sg/ …*, (Iii), pp. 1–4. Available at: http://www.nus.edu.sg/nurop/2010/Proceedings/FoS/Chemistry/Stephanie Katharine Loeb_NT081367E.pdf.

Lu, B., Malcuit, C., Wang, S., Girman, S., Francis, P., Lemieux, L., Lanza, R. and Lund, R. (2009) 'Long-term safety and function of RPE from human embryonic stem cells in preclinical models of macular degeneration.', *Stem cells (Dayton, Ohio)*, 27(9), pp. 2126–35. doi:

10.1002/stem.149.

Lumelsky, N., Blondel, O., Laeng, P., Velasco, I., Ravin, R. and McKay, R. (2001) 'Differentiation of embryonic stem cells to insulin-secreting structures similar to pancreatic islets.', *Science (New York, N.Y.)*, 292(5520), pp. 1389–94. doi: 10.1126/science.1058866.

MacLaren, R. E., Pearson, R. a, MacNeil, a, Douglas, R. H., Salt, T. E., Akimoto, M., Swaroop, a, Sowden, J. C. and Ali, R. R. (2006) 'Retinal repair by transplantation of photoreceptor precursors.', *Nature*, 444(7116), pp. 203–7. doi: 10.1038/nature05161.

MacNeil, A., Pearson, R. A., MacLaren, R. E., Smith, A. J., Sowden, J. C. and Ali, R. R. (2007) 'Comparative analysis of progenitor cells isolated from the iris, pars plana, and ciliary body of the adult porcine eye.', *Stem cells (Dayton, Ohio)*, 25(10), pp. 2430–8. doi: 10.1634/stemcells.2007-0035.

Maguire, A. M., Simonelli, F., Pierce, E. A., Pugh, E. N., Mingozzi, F., Bennicelli, J., Banfi, S., Marshall, K. A., Testa, F., Surace, E. M., Rossi, S., Lyubarsky, A., Arruda, V. R., Konkle, B., Stone, E., Sun, J., Jacobs, J., Dell'Osso, L., Hertle, R., Ma, J., Redmond, T. M., Zhu, X., Hauck, B., Zelenaia, O., Shindler, K. S., Maguire, M. G., Wright, J. F., Volpe, N. J., McDonnell, J. W., Auricchio, A., High, K. A. and Bennett, J. (2008) 'Safety and efficacy of gene transfer for Leber's congenital amaurosis.', *The New England journal of medicine*, 358(21), pp. 2240–8. doi: 10.1056/NEJMoa0802315.

Majors, R. E. (2008) 'The Role of Polymers in Solid-Phase Extraction and Sample Preparation', *LCGC North America*, 26(11), pp. 1074–1090.

Mamani, J. B., Gamarra, L. F. and Brito, G. E. de S. (2014) 'Synthesis and characterization of Fe3O4 nanoparticles with perspectives in biomedical applications', *Materials Research*. Materials Research, 17(3), pp. 542–549. doi: 10.1590/S1516-14392014005000050.

Martin, G. R. (1981) 'Isolation of a pluripotent cell line from early mouse embryos cultured in medium conditioned by teratocarcinoma stem cells.', *Proceedings of the National Academy of Sciences of the United States of America*, 78(12), pp. 7634–7638. doi: 10.1073/pnas.78.12.7634.

Martinez-Gimeno, M., Maseras, M., Baiget, M., Beneito, M., Antiñolo, G., Ayuso, C. and Carballo, M. (2001) 'Mutations P51U and G122E in retinal transcription factor NRL associated with autosomal dominant and sporadic retinitis pigmentosa.', *Human mutation*, 17(6), p. 520. doi: 10.1002/humu.1135.

Martín-Henao, G. A., Picón, M., Amill, B., Querol, S., Ferrà, C., Grañena, A. and García, J. (2001) 'Combined positive and negative cell selection from allogeneic peripheral blood progenitor cells (PBPC) by use of immunomagnetic methods.', *Bone Marrow Transplantation*, 27(7), pp. 683–687.

Masland, R. H. (2001) 'The fundamental plan of the retina', *Nature Neuroscience*. Nature Publishing Group, 4(9), pp. 877–886. doi: 10.1038/nn0901-877.

Mason, C., McCall, M. J., Culme-Seymour, E. J., Suthasan, S., Edwards-Parton, S., Bonfiglio, G. A. and Reeve, B. C. (2012) 'The Global Cell Therapy Industry Continues to Rise during the Second and Third Quarters of 2012', *Cell Stem Cell*. Elsevier, 11(6), pp. 735–739. doi: 10.1016/j.stem.2012.11.013.

Mastri, M., Lin, H. and Lee, T. (2014) 'Enhancing the efficacy of mesenchymal stem cell therapy.', *World journal of stem cells*, 6(2), pp. 82–93. doi: 10.4252/wjsc.v6.i2.82.

Maude, S. L., Frey, N., Shaw, P. A., Aplenc, R., Barrett, D. M., Bunin, N. J., Chew, A., Gonzalez, V. E., Zheng, Z., Lacey, S. F., Mahnke, Y. D., Melenhorst, J. J., Rheingold, S. R., Shen, A., Teachey, D. T., Levine, B. L., June, C. H., Porter, D. L. and Grupp, S. A. (2014)

'Chimeric Antigen Receptor T Cells for Sustained Remissions in Leukemia', *New England Journal of Medicine*. Massachusetts Medical Society, 371(16), pp. 1507–1517. doi: 10.1056/NEJMoa1407222.

Mazia, D., Schatten, G. and Sale, W. (1975) 'Adhesion of cells to surfaces coated with polylysine. Applications to electron microscopy', *The Journal of Cell Biology*. Rockefeller University Press, 66(1), pp. 198–200. doi: 10.1083/jcb.66.1.198.

Mcintyre, C. A., Flyg, B. T. and Fong, T. C. (2010) 'Fluorescence-Activated Cell Sorting for CGMP Processing of Therapeutic Cells', *BioProcess International*, pp. 44–53.

McLaren, A. (2001) 'Ethical and social considerations of stem cell research', *Nature*. Nature Publishing Group, 414(6859), pp. 129–131. doi: 10.1038/35102194.

Mellough, C., Sernagor, E., Moreno-Gimeno, I., Steel, D. and Lako, M. (2012) 'Efficient Stage Specific Differentiation of Human Pluripotent Stem Cells Towards Retinal Photoreceptor Cells', *STEM CELLS*, 44(0). doi: 10.1002/stem.1037.

Meyer, J. S., Howden, S. E., Wallace, K. A., Verhoeven, A. D., Wright, L. S., Capowski, E. E., Pinilla, I., Martin, J. M., Tian, S., Stewart, R., Pattnaik, B., Thomson, J. A. and Gamm, D. M. (2011) 'Optic vesicle-like structures derived from human pluripotent stem cells facilitate a customized approach to retinal disease treatment.', *Stem cells (Dayton, Ohio)*, 29(8), pp. 1206–18. doi: 10.1002/stem.674.

Mitalipova, M. M., Rao, R. R., Hoyer, D. M., Johnson, J. A., Meisner, L. F., Jones, K. L., Dalton, S. and Stice, S. L. (2005) 'Preserving the genetic integrity of human embryonic stem cells', *Nature Biotechnology*. Nature Publishing Group, 23(1), pp. 19–20. doi: 10.1038/nbt0105-19.

Mitton, K. P., Swain, P. K., Chen, S., Xu, S., Zack, D. J. and Swaroop, A. (2000) 'The leucine zipper of NRL interacts with the CRX homeodomain. A possible mechanism of transcriptional synergy in rhodopsin regulation.', *The Journal of biological chemistry*, 275(38), pp. 29794–9. doi: 10.1074/jbc.M003658200.

Mukhopadhyay, M., Shtrom, S., Rodriguez-Esteban, C., Chen, L., Tsukui, T., Gomer, L., Dorward, D. W., Glinka, A., Grinberg, A., Huang, S. P., Niehrs, C., Izpisúa Belmonte, J. C. and Westphal, H. (2001) 'Dickkopf1 is required for embryonic head induction and limb morphogenesis in the mouse.', *Developmental cell*, 1(3), pp. 423–34. Available at: http://www.ncbi.nlm.nih.gov/pubmed/11702953 (Accessed: 1 September 2016).

Muñoz-Sanjuán, I. and Brivanlou, A. H. (2002) 'Neural induction, the default model and embryonic stem cells', *Nature Reviews Neuroscience*. Nature Publishing Group, 3(4), pp. 271–280. doi: 10.1038/nrn786.

Nakano, T., Ando, S., Takata, N., Kawada, M., Muguruma, K., Sekiguchi, K., Saito, K., Yonemura, S., Eiraku, M. and Sasai, Y. (2012) 'Self-formation of optic cups and storable stratified neural retina from human ESCs.', *Cell stem cell*, 10(6), pp. 771–85. doi: 10.1016/j.stem.2012.05.009.

Nemmar, A., Hoet, P. H. M., Vanquickenborne, B., Dinsdale, D., Thomeer, M., Hoylaerts, M. F., Vanbilloen, H., Mortelmans, L. and Nemery, B. (2002) 'Passage of inhaled particles into the blood circulation in humans.', *Circulation*, 105(4), pp. 411–4. Available at: http://www.ncbi.nlm.nih.gov/pubmed/11815420 (Accessed: 1 September 2016).

Neubert, J., Wagner, S., Kiwit, J., Bräuer, A. U. and Glumm, J. (2015) 'New findings about iron oxide nanoparticles and their different effects on murine primary brain cells.', *International journal of nanomedicine*, 10, pp. 2033–49. doi: 10.2147/IJN.S74404.

Ng, L., Lu, A., Swaroop, A. A., Sharlin, D. S., Swaroop, A. A. and Forrest, D. (2011) 'Two transcription factors can direct three photoreceptor outcomes from rod precursor cells in mouse

retinal development', *The Journal of neuroscience : the official journal of the Society for Neuroscience*, 31(31), pp. 11118–25. doi: 10.1523/JNEUROSCI.1709-11.2011.

Nichols, J., Zevnik, B., Anastassiadis, K., Niwa, H., Klewe-Nebenius, D., Chambers, I., Schöler, H. and Smith, A. (1998) 'Formation of pluripotent stem cells in the mammalian embryo depends on the POU transcription factor Oct4.', *Cell*, 95(3), pp. 379–91. Available at: http://www.ncbi.nlm.nih.gov/pubmed/9814708 (Accessed: 25 August 2016).

Nistor, G., Seiler, M. M. J., Yan, F., Ferguson, D. and Keirstead, H. S. (2010) 'Three-dimensional early retinal progenitor 3D tissue constructs derived from human embryonic stem cells', *Journal of neuroscience*. Elsevier B.V., 190(1), pp. 63–70. doi: 10.1016/j.jneumeth.2010.04.025.

O'Brien, K. M. B., Schulte, D. and Hendrickson, A. E. (2003) 'Expression of photoreceptor-associated molecules during human fetal eye development.', *Molecular vision*, 9(August), pp. 401–9. Available at: http://www.ncbi.nlm.nih.gov/pubmed/17121018.

O'Rahilly, R. (1975) 'The prenatal development of the human eye', *Experimental Eye Research*, 21(2), pp. 93–112. doi: 10.1016/0014-4835(75)90075-5.

Oberdörster, G. (2001) 'Pulmonary effects of inhaled ultrafine particles.', *International archives of occupational and environmental health*, 74(1), pp. 1–8. Available at: http://www.ncbi.nlm.nih.gov/pubmed/11196075 (Accessed: 1 September 2016).

Oh, S. K., Choi, K. H., Yoo, J. Y., Kim, D. Y., Kim, S. J. and Jeon, S. R. (2016) 'A Phase III Clinical Trial Showing Limited Efficacy of Autologous Mesenchymal Stem Cell Therapy for Spinal Cord Injury.', *Neurosurgery*, 78(3), p. 436–47; discussion 447. doi: 10.1227/NEU.0000000000001056.

Ohmine, S., Dietz, A. B., Deeds, M. C., Hartjes, K. A., Miller, D. R., Thatava, T., Sakuma, T., Kudva, Y. C. and Ikeda, Y. (2011) 'Induced pluripotent stem cells from GMP-grade hematopoietic progenitor cells and mononuclear myeloid cells', *Stem Cell Research & Therapy*. BioMed Central, 2(6), p. 46. doi: 10.1186/scrt87.

Okita, K., Nakagawa, M., Hyenjong, H., Ichisaka, T. and Yamanaka, S. (2008) 'Generation of mouse induced pluripotent stem cells without viral vectors.', *Science (New York, N.Y.)*, 322(5903), pp. 949–53. doi: 10.1126/science.1164270.

Olusanya, O., Bracewell, D. and Veraitch, F. S. (2010) 'Hydrophobic Interaction Chromatography for the Downstream Processing of Embryonic Stem Cell-Derived Cell Therapies', in *Poster seesion presented at: SBE's 2nd International Conference on Stem Cell Engineering 2010.* Boston, MA.

Osakada, F., Ikeda, H., Mandai, M., Wataya, T., Watanabe, K., Yoshimura, N., Akaike, A. A., Akaike, A. A., Sasai, Y. and Takahashi, M. (2008) 'Toward the generation of rod and cone photoreceptors from mouse, monkey and human embryonic stem cells.', *Nature biotechnology*. Nature Publishing Group, 26(2), pp. 215–24. doi: 10.1038/nbt1384.

Osakada, F., Ikeda, H., Sasai, Y. and Takahashi, M. (2009) 'Stepwise differentiation of pluripotent stem cells into retinal cells.', *Nature protocols*, 4(6), pp. 811–24. doi: 10.1038/nprot.2009.51.

Osakada, F., Jin, Z.-B., Hirami, Y., Ikeda, H., Danjyo, T., Watanabe, K., Sasai, Y. and Takahashi, M. (2009) 'In vitro differentiation of retinal cells from human pluripotent stem cells by small-molecule induction.', *Journal of cell science*, 122(Pt 17), pp. 3169–79. doi: 10.1242/jcs.050393.

Park, E. J., Umh, H. N., Choi, D. H., Cho, M. H., Choi, W., Kim, S. W., Kim, Y. and Kim, J. H. (2014) 'Magnetite- and maghemite-induced different toxicity in murine alveolar macrophage

cells', *Archives of Toxicology*, 88(8), pp. 1607–1618. doi: 10.1007/s00204-014-1210-1.

Park, E.-J., Umh, H. N., Kim, S.-W., Cho, M.-H., Kim, J.-H. and Kim, Y. (2014) 'ERK pathway is activated in bare-FeNPs-induced autophagy.', *Archives of toxicology*, 88(2), pp. 323–36. doi: 10.1007/s00204-013-1134-1.

Park, I.-H., Zhao, R., West, J. A., Yabuuchi, A., Huo, H., Ince, T. A., Lerou, P. H., Lensch, M. W. and Daley, G. Q. (2008) 'Reprogramming of human somatic cells to pluripotency with defined factors', *Nature*, 451(7175), pp. 141–6. doi: 10.1038/nature06534.

da Paz, M. C., Santos, M. de F. M. A., Santos, C. M. B., da Silva, S. W., de Souza, L. B., Lima, E. C. D., Silva, R. C., Lucci, C. M., Morais, P. C., Azevedo, R. B. and Lacava, Z. G. M. (2012) 'Anti-CEA loaded maghemite nanoparticles as a theragnostic device for colorectal cancer.', *International journal of nanomedicine*, 7, pp. 5271–82. doi: 10.2147/IJN.S32139.

Pearson, R. a., Barber, a. C., Rizzi, M., Hippert, C., Xue, T., West, E. L., Duran, Y., Smith, a. J., Chuang, J. Z., Azam, S. a., Luhmann, U. F. O., Benucci, a., Sung, C. H., Bainbridge, J. W., Carandini, M., Yau, K.-W., Sowden, J. C. and Ali, R. R. (2012) 'Restoration of vision after transplantation of photoreceptors', *Nature*. Nature Publishing Group, 486(7396), pp. 1–5. doi: 10.1038/nature10997.

Pei, Y. F. and Rhodin, J. A. G. (1970) 'The prenatal development of the mouse eye', *The Anatomical Record*. Wiley Subscription Services, Inc., A Wiley Company, 168(1), pp. 105–125. doi: 10.1002/ar.1091680109.

Pfizer (2014) *Pfizer And Cellectis Enter Into Global Strategic Cancer Immunotherapy Collaboration | Pfizer: One of the world's premier biopharmaceutical companies*, *June 18, 2014*. Available at: http://www.pfizer.com/news/press-release/press-release-detail/pfizer_and_cellectis_enter_into_global_strategic_cancer_immunotherapy_collaboration.

Pollock, J., Ho, S. V and Farid, S. S. (2013) 'Fed-batch and perfusion culture processes: economic, environmental, and operational feasibility under uncertainty.', *Biotechnology and bioengineering*, 110(1), pp. 206–19. doi: 10.1002/bit.24608.

Porter, D. L., Levine, B. L., Kalos, M., Bagg, A. and June, C. H. (2011) 'Chimeric antigen receptor-modified T cells in chronic lymphoid leukemia.', *The New England journal of medicine*. Massachusetts Medical Society, 365(8), pp. 725–33. doi: 10.1056/NEJMoa1103849.

Pule, M. A., Savoldo, B., Myers, G. D., Rossig, C., Russell, H. V, Dotti, G., Huls, M. H., Liu, E., Gee, A. P., Mei, Z., Yvon, E., Weiss, H. L., Liu, H., Rooney, C. M., Heslop, H. E. and Brenner, M. K. (2008) 'Virus-specific T cells engineered to coexpress tumor-specific receptors: persistence and antitumor activity in individuals with neuroblastoma.', *Nature medicine*. Nature Publishing Group, 14(11), pp. 1264–70. doi: 10.1038/nm.1882.

Ramos Guivar, J. A., Bustamante, A., Flores, J., Mejía Santillan, M., Osorio, A. M., Martínez, A. I., De Los Santos Valladares, L., W Barnes, C. H. and Ramos Guivar, J. (2012) 'Mössbauer study of intermediate superparamagnetic relaxation of maghemite (γ-Fe 2 O 3) nanoparticles', pp. 11–16. doi: 10.1007/s10751-013-0864-z.

Rehemtulla, A., Warwar, R., Kumar, R., Ji, X., Zack, D. J. and Swaroop, A. (1996) 'The basic motif-leucine zipper transcription factor Nrl can positively regulate rhodopsin gene expression.', *Proceedings of the National Academy of Sciences of the United States of America*, 93(1), pp. 191–5. Available at: http://www.pubmedcentral.nih.gov/articlerender.fcgi?artid=40204&tool=pmcentrez&rendertype=abstract (Accessed: 17 August 2012).

Retina International (2014) *Retina International Databases: Mutation Database*. Available at: http://www.retina-international.org/sci-news/databases/mutation-database/.

Riazifar, H., Jia, Y., Chen, J., Lynch, G. and Huang, T. (2014) 'Chemically induced specification of retinal ganglion cells from human embryonic and induced pluripotent stem cells.', *Stem cells translational medicine*, 3(4), pp. 424–32. doi: 10.5966/sctm.2013-0147.

Richel, D. J., Johnsen, H. E., Canon, J., Guillaume, T., Schaafsma, M. R., Schenkeveld, C., Hansen, S. W., McNiece, I., Gringeri, A. J., Briddell, R., Ewen, C., Davies, R., Freeman, J., Miltenyi, S. and Symann, M. (2000) 'Highly purified CD34+ cells isolated using magnetically activated cell selection provide rapid engraftment following high-dose chemotherapy in breast cancer patients', *Bone Marrow Transplantation*. Nature Publishing Group, 25(3), pp. 243–249. doi: 10.1038/sj.bmt.1702136.

Riera, M., Fontrodona, L., Albert, S., Ramirez, D. M., Seriola, A., Salas, A., Muñoz, Y., Ramos, D., Villegas-Perez, M. P., Zapata, M. A., Raya, A., Ruberte, J., Veiga, A. and Garcia-Arumi, J. (2016) 'Comparative study of human embryonic stem cells (hESC) and human induced pluripotent stem cells (hiPSC) as a treatment for retinal dystrophies', *Molecular Therapy — Methods & Clinical Development*. Nature Publishing Group, 3, p. 16010. doi: 10.1038/mtm.2016.10.

Rosner, M. H., Vigano, M. A., Ozato, K., Timmons, P. M., Poirier, F., Rigby, P. W. and Staudt, L. M. (1990) 'A POU-domain transcription factor in early stem cells and germ cells of the mammalian embryo.', *Nature*, 345(6277), pp. 686–92. doi: 10.1038/345686a0.

Ross, C., Vandergaw, A., Carr, K. and Helm, K. (2009) 'Comparison of Sorting Capabilities of Beckman Coulter MoFlo™ XDP and Becton Dickinson FACSAria™ I and II', *White Paper*.

Ruether, K. and Kellner, U. (1998) 'Inner retinal function in hereditary retinal dystrophies.', *Acta anatomica*, 162(2–3), pp. 169–77. Available at: http://www.ncbi.nlm.nih.gov/pubmed/9831765 (Accessed: 28 August 2016).

Rümenapp, C., Wagner, F. E. and Gleich, B. (2015) 'Monitoring of the aging of magnetic nanoparticles using Mössbauer spectroscopy', *Journal of Magnetism and Magnetic Materials*, 380, pp. 241–245. doi: 10.1016/j.jmmm.2014.09.071.

Sakuma, R., Ohnishi Yi, Y., Meno, C., Fujii, H., Juan, H., Takeuchi, J., Ogura, T., Li, E., Miyazono, K. and Hamada, H. (2002) 'Inhibition of Nodal signalling by Lefty mediated through interaction with common receptors and efficient diffusion.', *Genes to cells : devoted to molecular & cellular mechanisms*, 7(4), pp. 401–12. Available at: http://www.ncbi.nlm.nih.gov/pubmed/11952836 (Accessed: 1 September 2016).

Sanftner, L. H., Abel, H., Hauswirth, W. W. and Flannery, J. G. (2001) 'Glial Cell Line Derived Neurotrophic Factor Delays Photoreceptor Degeneration in a Transgenic Rat Model of Retinitis Pigmentosa', *Mol Ther*, 4(6), p. 622–629. doi: 10.1006/mthe.2001.0498.

Schmitz, B., Radbruch, A., Kümmel, T., Wickenhauser, C., Korb, H., Hansmann, M. L., Thiele, J. and Fischer, R. (1994) 'Magnetic activated cell sorting (MACS)--a new immunomagnetic method for megakaryocytic cell isolation: comparison of different separation techniques.', *European journal of haematology*, 52(5), pp. 267–75.

Schriebl, K., Lim, S., Choo, A., Tscheliessnig, A. and Jungbauer, A. (2010) 'Stem cell separation: a bottleneck in stem cell therapy.', *Biotechnology journal*, 5(1), pp. 50–61. doi: 10.1002/biot.200900115.

Schumm, M., Lang, P., Taylor, G., Kuçi, S., Klingebiel, T., Bühring, H. J., Geiselhart, A., Niethammer, D. and Handgretinger, R. (1999) 'Isolation of highly purified autologous and allogeneic peripheral CD34+ cells using the CliniMACS device.', *Journal Of Hematotherapy*, 8(2), pp. 209–218. Available at: http://www.ncbi.nlm.nih.gov/pubmed/10349915.

Schuster, S. J., Svoboda, J., Nasta, S. D., Porter, D. L., Chong, E. A., Landsburg, D. J., Mato, A. R., Lacey, S. F., Melenhorst, J. J., Chew, A., Hasskarl, J., Shah, G. D., Wasik, M. A.,

Marcucci, K. T., Zheng, Z., Levine, B. L. and June, C. H. (2015) 'Sustained remissions following chimeric antigen receptor modified T cells directed against CD19 (CTL019) in patients with relapsed or refractory CD19+ lymphomas', *Blood*. American Society of Hematology, 126(23), p. 183.

Semmler, M., Seitz, J., Erbe, F., Mayer, P., Heyder, J., Oberdörster, G. and Kreyling, W. G. (2004) 'Long-term clearance kinetics of inhaled ultrafine insoluble iridium particles from the rat lung, including transient translocation into secondary organs.', *Inhalation toxicology*, 16(6–7), pp. 453–9. doi: 10.1080/08958370490439650.

Sheridan, S. D., Surampudi, V. and Rao, R. R. (2012) 'Analysis of embryoid bodies derived from human induced pluripotent stem cells as a means to assess pluripotency', *Stem Cells International*. Hindawi Publishing Corporation, pp. 1–9. doi: 10.1155/2012/738910.

Shi, G. and Jin, Y. (2010) 'Role of Oct4 in maintaining and regaining stem cell pluripotency.', *Stem cell research & therapy*, 1(5), p. 39. doi: 10.1186/scrt39.

Shima, S. and Sakai, H. (1977) 'Polylysine Produced by *Streptomyces*', *Agricultural and Biological Chemistry*, 41(9), pp. 1807–1809. doi: 10.1080/00021369.1977.10862764.

Siena, S., Schiavo, R., Pedrazzoli, P. and Carlo-Stella, C. (2000) 'Therapeutic relevance of CD34 cell dose in blood cell transplantation for cancer therapy.', *Journal of clinical oncology : official journal of the American Society of Clinical Oncology*, 18(6), pp. 1360–77.

Simara, P., Motl, J. A. and Kaufman, D. S. (2013) 'Pluripotent stem cells and gene therapy', *Translational Research*, 161(4), pp. 284–292. doi: 10.1016/j.trsl.2013.01.001.

Simaria, A. S., Hassan, S., Varadaraju, H., Rowley, J., Warren, K., Vanek, P. and Farid, S. S. (2014) 'Allogeneic cell therapy bioprocess economics and optimization: Single-use cell expansion technologies', *Biotechnology and Bioengineering*, 111(1), pp. 69–83. doi: 10.1002/bit.25008.

Simmons, P. J. and Torok-Storb, B. (1991) 'CD34 expression by stromal precursors in normal human adult bone marrow.', *Blood*. American Society of Hematology, 78(11), pp. 2848–53. Available at: http://www.ncbi.nlm.nih.gov/pubmed/1720038 (Accessed: 16 July 2016).

Singh, N., Jenkins, G. J. S. S., Asadi, R. and Doak, S. H. (2010) 'Potential toxicity of superparamagnetic iron oxide nanoparticles (SPION)', *Nano Reviews*, 1(0), pp. 1–15. doi: 10.3402/nano.v1i0.5358.

Singh, S. and Nalwa, H. S. (2007) 'Nanotechnology and health safety--toxicity and risk assessments of nanostructured materials on human health.', *Journal of nanoscience and nanotechnology*, 7(9), pp. 3048–70. Available at: http://www.ncbi.nlm.nih.gov/pubmed/18019130 (Accessed: 12 April 2016).

Si-Tayeb, K., Noto, F. K., Sepac, A., Sedlic, F., Bosnjak, Z. J., Lough, J. W. and Duncan, S. A. (2010) 'Generation of human induced pluripotent stem cells by simple transient transfection of plasmid DNA encoding reprogramming factors.', *BMC developmental biology*. BioMed Central, 10, p. 81. doi: 10.1186/1471-213X-10-81.

Soenen, S. J., De Cuyper, M., De Smedt, S. C. and Braeckmans, K. (2012) 'Investigating the toxic effects of iron oxide nanoparticles.', *Methods in enzymology*, 509, pp. 195–224. doi: 10.1016/B978-0-12-391858-1.00011-3.

Van Soest, S., Westerveld, A., De Jong, P. T. V. M., Bleeker-Wagemakers, E. M. and Bergen, A. A. B. (1999) 'Retinitis pigmentosa: Defined from a molecular point of view', *Survey of Ophthalmology*, 43(4), pp. 321–334. doi: 10.1016/S0039-6257(98)00046-0.

Sommermeyer, D., Hudecek, M., Kosasih, P. L., Gogishvili, T., Maloney, D. G., Turtle, C. J. and

Riddell, S. R. (2015) 'Chimeric antigen receptor-modified T cells derived from defined CD8+ and CD4+ subsets confer superior antitumor reactivity in vivo', *Leukemia*. Nature Publishing Group, 30(2), p. 492. doi: 10.1038/leu.2015.247.

Sorrentino, F. S., Gallenga, C. E., Bonifazzi, C. and Perri, P. (2016) 'A challenge to the striking genotypic heterogeneity of retinitis pigmentosa: a better understanding of the pathophysiology using the newest genetic strategies.', *Eye (London, England)*. doi: 10.1038/eye.2016.197.

SpheriTech (2014) 'Cross-linked poly-e-lysine non-particulate support. WO/2013/041250'. Europe: WIPO. doi: WO/2013/041250.

Stevens, L. C. (1967) 'Origin of testicular teratomas from primordial germ cells in mice.', *Journal of the National Cancer Institute*, 38(4), pp. 549–52. Available at: http://www.ncbi.nlm.nih.gov/pubmed/6025005 (Accessed: 29 August 2016).

Stonier, A., Simaria, A. S., Smith, M. and Farid, S. S. (2012) 'Decisional tool to assess current and future process robustness in an antibody purification facility', *Biotechnology Progress*, 28(4), pp. 1019–1028. doi: 10.1002/btpr.1569.

Suemori, H., Yasuchika, K., Hasegawa, K., Fujioka, T., Tsuneyoshi, N. and Nakatsuji, N. (2006) 'Efficient establishment of human embryonic stem cell lines and long-term maintenance with stable karyotype by enzymatic bulk passage.', *Biochemical and biophysical research communications*, 345(3), pp. 926–32. doi: 10.1016/j.bbrc.2006.04.135.

Sugita, Y., Suzuki, H. and Tasaki, K. (1989) 'Human rods are acting in the light and cones are inhibited in the dark.', *The Tohoku journal of experimental medicine*, 157(4), pp. 365–72. Available at: http://www.ncbi.nlm.nih.gov/pubmed/2741172 (Accessed: 28 August 2016).

Swain, P. K., Hicks, D., Mears, A. J., Apel, I. J., Smith, J. E., John, S. K., Hendrickson, A., Milam, A. H. and Swaroop, A. (2001) 'Multiple phosphorylated isoforms of NRL are expressed in rod photoreceptors.', *The Journal of biological chemistry*, 276(39), pp. 36824–30. doi: 10.1074/jbc.M105855200.

Swaroop, A., Kim, D. and Forrest, D. (2010) 'Transcriptional regulation of photoreceptor development and homeostasis in the mammalian retina', *Nature Reviews Neuroscience*. Nature Publishing Group, 11(8), pp. 563–576. doi: 10.1038/nrn2880.

Swaroop, A., Xu, J. Z., Pawar, H., Jackson, A., Skolnick, C. and Agarwal, N. (1992) 'A conserved retina-specific gene encodes a basic motif/leucine zipper domain.', *Proceedings of the National Academy of Sciences of the United States of America*, 89(1), pp. 266–70. Available at: http://www.ncbi.nlm.nih.gov/pubmed/1729696 (Accessed: 9 June 2016).

Szalay, B., Tátrai, E., Nyírő, G., Vezér, T. and Dura, G. (2012) 'Potential toxic effects of iron oxide nanoparticles in in vivo and in vitro experiments.', *Journal of applied toxicology : JAT*, 32(6), pp. 446–53. doi: 10.1002/jat.1779.

Tabilio, A., Falzetti, F., Zei, T., De Ioanni, M., Bonifacio, E., Battelli, F., Iacucci Ostini, R., Ballanti, S., Cimminiello, M., Capponi, M., Silvani, C., Minelli, O., Fettucciari, K., Marconi, P., Rosati, E., Santucci, A., Di Ianni, M., Aversa, F. and Martelli, M. F. (2004) 'Graft engineering for allogeneic haploidentical stem cell transplantation', *Blood Cells, Molecules, and Diseases*, 33(3), pp. 274–280. doi: 10.1016/j.bcmd.2004.08.016.

Takahashi, K., Tanabe, K., Ohnuki, M., Narita, M., Ichisaka, T., Tomoda, K. and Yamanaka, S. (2007) 'Induction of Pluripotent Stem Cells from Adult Human Fibroblasts by Defined Factors', *Cell*, 131(5), pp. 861–72. doi: 10.1016/j.cell.2007.11.019.

Taylor, C. J., Bolton, E. M., Pocock, S., Sharples, L. D., Pedersen, R. A. and Bradley, J. A. (2005) 'Banking on human embryonic stem cells: estimating the number of donor cell lines needed for HLA matching.', *Lancet (London, England)*, 366(9502), pp. 2019–25. doi:

10.1016/S0140-6736(05)67813-0.

Taylor, C. J. and Dyer, P. A. (1995) 'Histocompatibility antigens', *Eye*. Nature Publishing Group, 9(2), pp. 173–179. doi: 10.1038/eye.1995.35.

Taylor, C. J., Peacock, S., Chaudhry, A. N., Bradley, J. A. and Bolton, E. M. (2012) 'Generating an iPSC bank for HLA-matched tissue transplantation based on known donor and recipient HLA types.', *Cell stem cell*, 11(2), pp. 147–52. doi: 10.1016/j.stem.2012.07.014.

Thomson, J. A., Itskovitz-Eldor, J., Shapiro, S. S., Waknitz, M. A., Swiergiel, J. J., Marshall, V. S. and Jones, J. M. (1998) 'Embryonic stem cell lines derived from human blastocysts.', *Science (New York, N.Y.)*. American Association for the Advancement of Science, 282(5391), pp. 1145–7. doi: 10.1126/science.282.5391.1145.

Thomson, J. A., Kalishman, J., Golos, T. G., Durning, M., Harris, C. P. and Hearn, J. P. (1996) 'Pluripotent cell lines derived from common marmoset (Callithrix jacchus) blastocysts.', *Biology of reproduction*, 55(2), pp. 254–9. Available at: http://www.ncbi.nlm.nih.gov/pubmed/8828827 (Accessed: 25 August 2016).

Thomson, J. A. and Marshall, V. S. (1998) 'Primate embryonic stem cells.', *Current topics in developmental biology*, 38, pp. 133–65. Available at: http://www.ncbi.nlm.nih.gov/pubmed/9399078 (Accessed: 29 August 2016).

Tsukamoto, M., Taira, S., Yamamura, S., Morita, Y., Nagatani, N., Takamura, Y. and Tamiya, E. (2009) 'Cell separation by an aqueous two-phase system in a microfluidic device.', *The Analyst*, 134(10), pp. 1994–8. doi: 10.1039/b909597g.

Tuček, J., Zboril, R. and Petridis, D. (2006) 'Maghemite Nanoparticles by View of Mössbauer Spectroscopy', *Journal of Nanoscience and Nanotechnology*, 6(4), pp. 926–947. doi: 10.1166/jnn.2006.183.

Tucker, B. a, Park, I.-H., Qi, S. D., Klassen, H. J., Jiang, C., Yao, J., Redenti, S., Daley, G. Q. and Young, M. J. (2011) 'Transplantation of adult mouse iPS cell-derived photoreceptor precursors restores retinal structure and function in degenerative mice.', *PloS one*, 6(4), p. e18992. doi: 10.1371/journal.pone.0018992.

Turtle, C. J., Hanafi, L.-A., Berger, C., Gooley, T. A., Cherian, S., Hudecek, M., Sommermeyer, D., Melville, K., Pender, B., Budiarto, T. M., Robinson, E., Steevens, N. N., Chaney, C., Soma, L., Chen, X., Yeung, C., Wood, B., Li, D., Cao, J., Heimfeld, S., Jensen, M. C., Riddell, S. R. and Maloney, D. G. (2016) 'CD19 CAR-T cells of defined CD4+:CD8+ composition in adult B cell ALL patients.', *The Journal of clinical investigation*. American Society for Clinical Investigation, 126(6), pp. 1–16. doi: 10.1172/JCI85309.

Valle, O., Erkkilä, H. and Raitta, C. (1981) 'Dominant progressive cone-rod dystrophy.', *Acta ophthalmologica*, 59(5), pp. 695–706. Available at: http://www.ncbi.nlm.nih.gov/pubmed/7315224 (Accessed: 28 August 2016).

Veraitch, F. S., Scott, R., Wong, J.-W., Lye, G. J. and Mason, C. (2008) 'The impact of manual processing on the expansion and directed differentiation of embryonic stem cells.', *Biotechnology and bioengineering*, 99(5), pp. 1216–29. doi: 10.1002/bit.21673.

Vogel, W., Scheding, S., Kanz, L. and Brugger, W. (2000) 'Clinical applications of CD34(+) peripheral blood progenitor cells (PBPC).', *Stem cells (Dayton, Ohio)*, 18(2), pp. 87–92. doi: 10.1634/stemcells.18-2-87.

Volkis, V., Smolensky, E., Lisovskii, A. and Eisen, M. S. (2005) 'Solvent effects in the polymerization of propylene catalyzed by octahedral complexes', *Journal of Polymer Science Part A: Polymer Chemistry*. Wiley Subscription Services, Inc., A Wiley Company, 43(19), pp. 4505–4516. doi: 10.1002/pola.20915.

Vykoukal, J., Vykoukal, D. M., Freyberg, S., Alt, E. U. and Gascoyne, P. R. C. (2008) 'Enrichment of putative stem cells from adipose tissue using dielectrophoretic field-flow fractionation.', *Lab on a chip*, 8(8), pp. 1386–93. doi: 10.1039/b717043b.

Wang, W.-L., Li, Q., Xu, J. and Cvekl, A. (2010) 'Lens fiber cell differentiation and denucleation are disrupted through expression of the N-terminal nuclear receptor box of NCOA6 and result in p53-dependent and p53-independent apoptosis.', *Molecular biology of the cell*. American Society for Cell Biology, 21(14), pp. 2453–68. doi: 10.1091/mbc.E09-12-1031.

Wang, X., Popplewell, L. L., Wagner, J. R., Naranjo, A., Blanchard, M. S., Mott, M. R., Norris, A. P., Wong, C. W., Urak, R. Z., Chang, W.-C., Khaled, S. K., Siddiqi, T., Budde, L. E., Xu, J., Chang, B., Gidwaney, N., Thomas, S. H., Cooper, L. J. N., Riddell, S. R., Brown, C. E., Jensen, M. C. and Forman, S. J. (2016) 'Phase 1 studies of central memory-derived CD19 CAR T-cell therapy following autologous HSCT in patients with B-cell NHL.', *Blood*. American Society of Hematology, 127(24), pp. 2980–90. doi: 10.1182/blood-2015-12-686725.

Watanabe, K., Kamiya, D., Nishiyama, A., Katayama, T., Nozaki, S., Kawasaki, H., Watanabe, Y., Mizuseki, K. and Sasai, Y. (2005) 'Directed differentiation of telencephalic precursors from embryonic stem cells', *Nat Neurosci*, 8(3), pp. 288–296. doi: 10.1038/nn1402.

Watanabe, K., Ueno, M., Kamiya, D., Nishiyama, A., Matsumura, M., Wataya, T., Takahashi, J. B., Nishikawa, S. S., Nishikawa, S. S., Muguruma, K. and Sasai, Y. (2007) 'A ROCK inhibitor permits survival of dissociated human embryonic stem cells', *Nature biotechnology*. Nature Publishing Group, 25(6), pp. 681–6. doi: 10.1038/nbt1310.

Webster, A. (2011) *Regenerative medicine in Europe: emerging needs and challenges in a global context*.

Weil, B. and Veraitch, F. (2014) 'Bioprocessing Challenges Associated with the Purification of Cellular Therapies', in Al-Rubeai, M. and Naciri, M. (eds) *Stem Cells and Cell Therapy SE - 6*. Springer Netherlands (Cell Engineering), p. 129–156 LA–English. doi: 10.1007/978-94-007-7196-3_6.

Welsbie, D. S., Yang, Z., Ge, Y., Mitchell, K. L., Zhou, X., Martin, S. E., Berlinicke, C. A., Hackler, L., Fuller, J., Fu, J., Cao, L., Han, B., Auld, D., Xue, T., Hirai, S., Germain, L., Simard-Bisson, C., Blouin, R., Nguyen, J. V, Davis, C. O., Enke, R. A., Boye, S. L., Merbs, S. L., Marsh-Armstrong, N., Hauswirth, W. W., DiAntonio, A., Nickells, R. W., Inglese, J., Hanes, J., Yau, K.-W., Quigley, H. A. and Zack, D. J. (2013) 'Functional genomic screening identifies dual leucine zipper kinase as a key mediator of retinal ganglion cell death.', *Proceedings of the National Academy of Sciences of the United States of America*, 110(10), pp. 4045–50. doi: 10.1073/pnas.1211284110.

West, E. L., Gonzalez-Cordero, A., Hippert, C., Osakada, F., Martinez-Barbera, J. P., Pearson, R. a, Sowden, J. C., Takahashi, M. and Ali, R. R. (2012) 'Defining the Integration Capacity of ES Cell-Derived Photoreceptor Precursors.', *Stem cells (Dayton, Ohio)*. doi: 10.1002/stem.1123.

West, E. L., Pearson, R. A., MacLaren, R. E., Sowden, J. C. and Ali, R. R. (2009) 'Cell transplantation strategies for retinal repair', *Progress in Brain Research*, pp. 3–21. doi: 10.1016/S0079-6123(09)17501-5.

Van Winkle, A. P., Gates, I. D. and Kallos, M. S. (2012) 'Mass transfer limitations in embryoid bodies during human embryonic stem cell differentiation.', *Cells, tissues, organs*, 196(1), pp. 34–47. doi: 10.1159/000330691.

Wobus, A. M. and Boheler, K. R. (2005) 'Embryonic Stem Cells : Prospects for Developmental Biology and Cell Therapy', *In Vitro*, pp. 635–678. doi: 10.1152/physrev.00054.2003.

Wobus, A. M., Holzhausen, H., Jäkel, P. and Schöneich, J. (1984) 'Characterization of a pluripotent stem cell line derived from a mouse embryo.', *Experimental cell research*, 152(1), pp.

212–9. Available at: http://www.ncbi.nlm.nih.gov/pubmed/6714319 (Accessed: 17 August 2012).

Wognum, A. and Eaves, A. (2003) 'Identification and isolation of hematopoietic stem cells', *Archives of medical research*. Available at: http://www.sciencedirect.com/science/article/pii/S0188440903001292 (Accessed: 3 May 2012).

Wright, L. S., Phillips, M. J., Pinilla, I., Hei, D. and Gamm, D. M. (2014) 'Induced pluripotent stem cells as custom therapeutics for retinal repair: Progress and rationale', *Experimental Eye Research*, 123, pp. 161–172. doi: 10.1016/j.exer.2013.12.001.

Wu, W., He, Q. and Jiang, C. (2008) 'Magnetic iron oxide nanoparticles: synthesis and surface functionalization strategies.', *Nanoscale research letters*, 3(11), pp. 397–415. doi: 10.1007/s11671-008-9174-9.

Xu, C., Inokuma, M. S., Denham, J., Golds, K., Kundu, P., Gold, J. D. and Carpenter, M. K. (2001) 'Feeder-free growth of undifferentiated human embryonic stem cells.', *Nature biotechnology*, 19(10), pp. 971–4. doi: 10.1038/nbt1001-971.

Xu, C., Police, S., Rao, N. and Carpenter, M. K. (2002) 'Characterization and enrichment of cardiomyocytes derived from human embryonic stem cells.', *Circulation research*, 91(6), pp. 501–8. Available at: http://www.ncbi.nlm.nih.gov/pubmed/12242268 (Accessed: 31 August 2016).

Yeom, Y. I., Fuhrmann, G., Ovitt, C. E., Brehm, A., Ohbo, K., Gross, M., Hübner, K. and Schöler, H. R. (1996) 'Germline regulatory element of Oct-4 specific for the totipotent cycle of embryonal cells.', *Development (Cambridge, England)*, 122(3), pp. 881–94. Available at: http://www.ncbi.nlm.nih.gov/pubmed/8631266 (Accessed: 25 August 2016).

Yoshida, T., Ozawa, Y., Suzuki, K., Yuki, K., Ohyama, M., Akamatsu, W., Matsuzaki, Y., Shimmura, S., Mitani, K., Tsubota, K. and Okano, H. (2014) 'The use of induced pluripotent stem cells to reveal pathogenic gene mutations and explore treatments for retinitis pigmentosa.', *Molecular brain*, 7, p. 45. doi: 10.1186/1756-6606-7-45.

Young, R. W. (1985) 'Cell differentiation in the retina of the mouse.', *The Anatomical record*, 212(2), pp. 199–205. doi: 10.1002/ar.1092120215.

Yu, J., Vodyanik, M. A., Smuga-Otto, K., Antosiewicz-Bourget, J., Frane, J. L., Tian, S., Nie, J., Jonsdottir, G. A., Ruotti, V., Stewart, R., Slukvin, I. I. and Thomson, J. A. (2007) 'Induced pluripotent stem cell lines derived from human somatic cells.', *Science (New York, N.Y.)*. American Association for the Advancement of Science, 318(5858), pp. 1917–20. doi: 10.1126/science.1151526.

Zhang, R., Piao, M. J., Kim, K. C., Kim, A. D., Choi, J.-Y., Choi, J. and Hyun, J. W. (2012) 'Endoplasmic reticulum stress signaling is involved in silver nanoparticles-induced apoptosis.', *The international journal of biochemistry & cell biology*, 44(1), pp. 224–32. doi: 10.1016/j.biocel.2011.10.019.

Zhang, Z.-N., Chung, S.-K., Xu, Z. and Xu, Y. (2014) 'Oct4 maintains the pluripotency of human embryonic stem cells by inactivating p53 through Sirt1-mediated deacetylation.', *Stem cells (Dayton, Ohio)*, 32(1), pp. 157–65. doi: 10.1002/stem.1532.

Zhao, X., Li, W., Lv, Z., Liu, L., Tong, M., Hai, T., Hao, J., Guo, C., Ma, Q., Wang, L., Zeng, F. and Zhou, Q. (2009) 'iPS cells produce viable mice through tetraploid complementation.', *Nature*, 461(7260), pp. 86–90. doi: 10.1038/nature08267.

Zheng, A., Li, Y. and Tsang, S. H. (2015) 'Personalized therapeutic strategies for patients with retinitis pigmentosa.', *Expert opinion on biological therapy*, 15(3), pp. 391–402. doi: 10.1517/14712598.2015.1006192.

Zhou, L., Wang, W., Liu, Y., de Castro, J. F., Ezashi, T., Telugu, B. P. V. L., Roberts, R. M., Kaplan, H. J. and Dean, D. C. (2011) 'Differentiation of induced pluripotent stem cells of Swine into rod photoreceptors and their integration into the retina.', *Stem cells (Dayton, Ohio)*, 29(6), pp. 972–80. doi: 10.1002/stem.637.

Zhou, W. and Freed, C. R. (2009) 'Adenoviral gene delivery can reprogram human fibroblasts to induced pluripotent stem cells.', *Stem cells (Dayton, Ohio)*, 27(11), pp. 2667–74. doi: 10.1002/stem.201.

Zimmermann, H. (1992) '5'-Nucleotidase: molecular structure and functional aspects', *Biochem. J*, 285, pp. 345–365.

Zrenner, E., Bartz-Schmidt, K. U., Benav, H., Besch, D., Bruckmann, A., Gabel, V.-P., Gekeler, F., Greppmaier, U., Harscher, A., Kibbel, S., Koch, J., Kusnyerik, A., Peters, T., Stingl, K., Sachs, H., Stett, A., Szurman, P., Wilhelm, B. and Wilke, R. (2011) 'Subretinal electronic chips allow blind patients to read letters and combine them to words.', *Proceedings. Biological sciences / The Royal Society*, 278(1711), pp. 1489–97. doi: 10.1098/rspb.2010.1747.

Appendix

A) Cost assumptions associated with different purification technologies, upstream processing, and miscellaneous components of the bioprocess. Where possible, values have been obtained directly. from vendors.

Parameter	Item (unit)	Cost per unit
MACS costs		
Consumable Costs		
	Consumable costs (per run)	£3,179
	Tubing Set	£1,178
	Tubing Rack	£81
Media & Reagents		
	CliniMACS Buffer (per L)	£1,423
	CliniMACS reagent (per mL)	£320
Fixed Equipment		
	CliniMACS Plus Cell Separator	£29,999
Labour		
	Operator wage (per annum)	£46,000
FACS costs		
Consumable Costs		
	Microfluidic Chip	£260
	Tubing set	£16
	Cell Strainer	£1.50
Media & Reagents		
	FACS reagent costs (per 100 tests)	£1,720
	PBS buffer (per L)	£800
	Accutase (per L)	£2,920

	Staining Buffer (FBS) (per L)	£2,302
	Staining Buffer (BSA) (per L)	£287
Fixed Equipment		
	SH800	£129,617
Labour		
	Operators wage (per annum)	£57,500
Upstream process costs		
	Reprogramming costs (per patient)	£4,700
	iPSC culture costs (per patient)	£2,360
	Differentiation costs (per 10^7 cells)	£2,226
Miscellaneous		
Fixed Equipment		
	Biosafety Cabinet (BSC)	£17,100
	Incubator	£17,835
QC & QA Costs	Per dose	£3,250

B) iPSC retinal differentiation in 12-well plates, 6-well plates, T25 flasks and T75 flasks. Images were taken every other day during the full retinal differentiation, and morphological comparisons made at day 6, day 12, day 18 and day 24.